Dissertation

submitted to the

Combined Faculty of Natural Sciences and Mathematics

of the Ruperto Carola University Heidelberg, Germany

for the degree of

Doctor of Natural Sciences

Presented by

M.Sc. Bettina Gudrun Bohl

Born in: Coburg

Oral examination: 22nd June 2021

Deciphering a regulatory function of endolysosomes
in asymmetric cell division of human neural stem cells
via the Notch signalling pathway

Referees: Prof. Dr. Gudrun Rappold
Prof. Dr. Philipp Koch

Table of Content

List of Figures

List of Tables

List of Abbreviations

%	percent	ILV	intraluminal vesicle
(v/v)	volume percent	Insc	Inscuteable
(w/v)	weight percent	iPSC	induced pluripotent stem cell
°C	degree Celsius	JAG	Jagged like
1X	single concentrated	l	litre
2D	two-dimensional	LAMP	lysosomal-associated membrane protein
3D	three-dimensional	Leu	Leupeptin
6xHis	6xHistidine tag	m	milli-
α	anti-	M	molar
ADAM	a disintegrin and metalloproteinase	min	minute
ANOVA	analysis of variance	mRNA	messenger RNA
ASCL	acheate-scute like	Mud	mushroom body-defective
aPKC	atypical protein kinase C	MVB	multivesicular body
BafA	BafilomycinA	µ	micro-
BMP	bone morphogenic protein	N/A	not applicable
bHLH	basic helix-loop-helix	n.s.	not significant
bp	base pair	n	nano-
Cas9	CRISPR associated protein 9	N-Cadherin	neural Cadherin
CBF	C promoter-binding factor	NB	neuroblast
CD	Cluster of differentiation	Nbl	Numblike
cDNA	complementary DNA	NES	neuroepithelial stem
CME	Clathrin-mediated endocytosis	Neur	Neuralized
CNS	central nervous system	NGN	Neurogenin
CP	cortical plate	NLS	nuclear localization sequence
CRB	Crumbs	NSC	neural stem cell
CRISPR	Clustered regulatory interspaced palindromic repeats	p	significance level
CSL	CBF1/RBPJk-Su(H)-LAG1	PAGE	polyacrylamid gel electrophoresis
Ct	treshold cycle	PAR(D)	partition defective homolog
CTB	Choleratoxin subunit B	PAX	Paired box
Ctrl	control	PBS	phosphate buffered saline
D. melanogaster	*Drosophila melanogaster*	PCP	planar cell polarity
DAPI	4,6-diamidino-2-phenylindole	PCR	polymerase chain reaction
DAPT	N-[N-(3,5.Difluorophenacetyl)-L-alanyl]-S-phenylglycine t-butyl ester	PEST	proline-glutamic acid-serine-threonine
ddH2O	double-distilled water	PFA	paraformaldehyde
DEPC	diethyl pyrocarbonate	Pins	partner of Insc
DLL	Delta like	PIP	phosphatidylinositol phosphate
DMSO	dimethyl sulfoxide	PKC	protein kinase C
DNA	desoxyribonucleic acid	qPCR	quantitative PCR

dNTP	desoxynucleotide triphosphate	RA	retinoic acid
DSL	Delta/Serrate/LAG-2	Rab	Ras-related in brain
DTX	deltex	RBP-J	recombination signal sequence-binding protein Jκ
e.g.	*exempli gratia* (for example)	RGC	radial glia cell
E8	Essential 8 medium	RNA	ribonucleic acid
EB	embryoid body	ROI	region of interest
ECD	extracellular domain	RT-PCR	reverse transcriptase PCR
EEA	early endosome antigene	RT	room temperature
EGF	epidermal growth factor	Sara	Smad ancor for receptor activation
ER	endoplasmic reticulum	SCRIB	Scribble
ESC	embryonic stem cell	sec	second
ESCRT	endosomal sorting complexes required for transport	SEM	standard error of the mean
et al.	*et alia* (and others)	SDS	sodium dodecyl sulphate
FBS	fetal bovine serum	Shh	sonic hedgehog
FGF	fibroblast growth factor	SM-NSC	small molecule NSC
FOX	forkhead box	SMAD	small mothers against decapentaplegic
FYVE	Fab1-YOTB-Vac1-EEA1	SNP	single nucleotide polymorphism
g	gram	SOP	sensory organ precursor
GFAP	glial fibrillary protein	SOX	sex-determining region Y box
GMC	ganglion mother cell	SSEA	stage-specific embryonic antigen
gRNA	guide RNA	Stau	Staufen
h	hour	tdTomato	tandem dimer Tomato
HDR	homology-directed repair	TM	transmembrane
HES	Hairy/Enhancer of split	TUBB3	βIII tubulin
HEY	Hairy Ears, Y-linked	v-ATPase	vacuolar ATPase
HOX	homeobox	VZ	ventricular-like zone
ICD	intracellular domain	Wnt	wingless/integrated
IF	immunofluorescence	x g	times gravity

1 Abstract

Stem cells are defined by their ability to both self-renew as well as to produce cells that differentiate to somatic cells. The switch between symmetric and asymmetric cell divisions is the conserved strategy by which stem cells can accomplish these two tasks. In this thesis, human induced pluripotent stem cell (iPSC)-derived neural stem cells (NSCs) were used to identify intracellular determinants that influence the cell fate of daughter cells during asymmetric cell division. Amongst various analysed vesicular compartments, LAMP1/2$^+$ and CD63$^+$ vesicles were identified as potential asymmetry factors. These represent late stages within the endolysosomal pathway. Withdrawal of growth factors from the culture medium increased the occurrence of asymmetrically segregated LAMP1$^+$ vesicles during cell division, linking asymmetric vesicle distribution to neuronal differentiation of NSCs. Further, Notch1/2 receptors, as well-known stem cell fate determinants, were found to be present in these LAMP1$^+$ vesicles. The intracellular transport of Notch receptors was dependent on Dynamin and coincided with the internalization of recombinant Notch receptor ligands. Inhibition of vesicular acidification led to decreased Notch cleavage and reduced expression of Notch target genes underlining the potential function of endolysosomal vesicles as signalling hubs for the activation of Notch receptors. Establishing a reporter cell line expressing tdTomato under the endogenous *HES1* promoter, Notch pathway activity was studied in actively dividing NSCs. The analysis of HES1 expression dynamics uncovered a link between high endolysosome content within a daughter cell during mitosis and a higher HES1 expression after cell division. This endolysosome-mediated bias in Notch signalling activity can be the basis for the decision of neuronal differentiation versus NSC fate maintenance. This is finally supported by the finding obtained in 3D forebrain organoids, that neurogenic cell divisions were associated with an accumulation of LAMP1$^+$ vesicles as well as Notch1 receptors in the remaining NSC.

Taken together, a putative, so far unrecognized function of LAMP1$^+$ vesicles as signalling hubs for Notch receptors during asymmetric cell division of human NSCs was discovered. Endocytosis and the increasingly acidic environment thereafter facilitates receptor cleavage and hence activation of the pathway. The active shuttling of endolysosomes to one daughter cell during mitosis leads to a biased Notch signalling activity potentially influencing the cell fate of the respective daughter cells.

2 Zusammenfassung

Die zwei wichtigsten Eigenschaften von Stammzellen sind auf der einen Seite ihre Fähigkeit zur Selbsterneuerung und auf der anderen Seite die gezielte Differenzierung in somatische Zellen. Die konservierte Strategie, um diese beiden Funktionen sicherzustellen, ist die Entscheidung zwischen symmetrischer und asymmetrischer Zellteilung. In dieser Arbeit werden neuronale Stammzellen herangezogen, welche aus humanen, induziert pluripotenten Stammzellen gewonnen wurden, um intrazelluläre Faktoren zu identifizieren, die die zelluläre Identität während einer asymmetrischen Zellteilung beeinflussen. Unter den verschiedenen analysierten vesikulären Kompartimenten wurden LAMP1/2^{+}- und CD63^{+}-Vesikel als potenzielle Asymmetriefaktoren identifiziert, welche die späteren Stufen des endolysosomalen Wegs darstellen. Nach dem Entzug von Wachstumsfaktoren aus dem Zellkulturmedium wurden LAMP1^{+}-Vesikel während der Zellteilung vermehrt asymmetrisch verteilt, was diese Vesikelasymmetrie mit der Differenzierung der neuronalen Stammzellen in Zusammenhang bringt. Im Weiteren konnten Notch1/2-Rezeptoren, welche nachweislich die Stammzellidentität sicherstellen können, innerhalb dieser endolysosomalen Vesikel nachgewiesen werden. Es wurde festgestellt, dass der intrazelluläre Transport der Notch-Rezeptoren abhängig von Dynamin ist und einhergeht mit der Internalisierung von rekombinanten Notch-Rezeptor-liganden. Wurde die Ansäuerung der Vesikel inhibiert, führte dies zu einer verringerten Spaltung von Notch-Rezeptoren und zu einer geringeren Expression von Notch-Zielgenen, was eine mögliche Funktion dieser Vesikel als Knotenpunkt für die Aktivierung des Notch-Signalwegs unterstreicht. Mit der Etablierung einer Reporter-Zelllinie, welche tdTomato unter dem endogenen HES1-Promotor exprimiert, wurde die Aktivität des Notch-Signalweges in sich aktiv teilenden neuronalen Stammzellen untersucht. Die Analyse der HES1-Expressionsdynamik deckte einen Zusammenhang zwischen einem höheren Endolysosomen-Gehalt in einer Tochterzelle während der Mitose und einer erhöhten HES1-Expression nach der Zellteilung auf. Es wurde gefolgert, dass die durch Endolysosomen vermittelte einseitige Aktivierung des Notch-Signalweges die Entscheidung zwischen neuronaler Differenzierung und dem Erhalt der neuronalen Stammzellidentität bedingen kann. Dies konnte schließlich in 3D Vorderhirn-Organoiden untermauert werden. In diesem System gingen neurogene Zellteilungen einher mit einer Anreicherung von LAMP1^{+}-Vesikeln und Notch1-Rezeptoren in der verbleibenden Stammzelle.

Zusammenfassend wird die Hypothese aufgestellt, dass LAMP1^{+}-Vesikel als bisher unbekannte Signalknotenpunkte für Notch-Rezeptoren während der asymmetrischen Zellteilung von neuronalen Stammzellen fungieren. Die Endozytose und die anschließende Ansäuerung der Vesikel bedingt die Spaltung der Rezeptoren und damit die Aktivierung des Signalwegs. Der aktive Transport der Endolysosomen in Richtung einer Tochterzellen während der Mitose führt daher zu einer einseitigen Aktivierung des Notch-Signalwegs, was die zelluläre Identität der entsprechenden Tochterzelle beeinflussen kann.

3 Introduction

3.1 Neural stem cells and neurodevelopment

The central nervous system (CNS) is one of the most complicated organ systems within the human body, orchestrating aspects from basic physiological to higher cognitive functions. The proper development, especially of the brain as the control centre, is a delicate process and any mistake or malformation can have detrimental consequences. Despite the unique morphology, size and cellular composition of the human brain, the coordination of developmental processes is strikingly conserved throughout evolution. Therefore, much of our current knowledge about human neurodevelopment has been adapted from studying model organisms, ranging from worms and flies to mice and primates. The human-specific increase in proliferative capacity of neural stem cells (NSCs) is the main reason for the unique expansion of the human brain not only in size, but also in capacities.

Therefore, the regulation of human NSC proliferation as well as the spatiotemporal regulation of NSC differentiation into neurons and glia cells is a very interesting field of research, which itself is constantly changing and developing. Catching a glimpse at a new either human-specific or evolutionary conserved molecular mechanisms controlling NSC function is the endeavour tackled in this thesis.

3.1.1 Mammalian neurodevelopment *in vivo*

The nervous system is developed as a part of the neuroectodermal germ layer, one of the three germ layers beside the endoderm forming internal organs and the mesoderm forming the skeletal and muscle system. The initial separation of the three germ layers is facilitated by morphogens, including fibroblast growth factors (FGFs), Wingless/Integrated (Wnt), bone morphogenic proteins (BMPs) and Nodal/Activin. High levels of BMP and Nodal push cells towards the two inner germ layers, mesoderm and endoderm [Kimelman and Kirschner, 1987; Smith et al., 1990; Köster et al., 1991; Zhou et al., 1993; Weber et al., 1996], whereas the ectoderm is specified by low Nodal signalling [Lowe et al., 2001] (Figure 1A). The additional secretion of BMP and Nodal inhibitors by the Spemann's organizer region, also called node in mammals, induces ectodermal cells to switch to a neuroepithelial cell fate generating the neural plate [Spemann and Mangold, 1924; Piccolo et al., 1996; Zimmerman et al., 1996; Piccolo et al., 1999; Bachiller et al., 2000]. Within this specialized region of the ectoderm, highly proliferating neuroepithelial stem (NES) cells lead to the thickening of the neural plate which finally invaginates and forms the neural tube.

As these NES cells need to generate the enormous variety of neuronal and glial subtypes constituting the nervous system, a well-defined regional patterning of the stem cell population is the basis for the correct organisation and the formation of functional neuronal networks. Patterning along the neural tube is established by defined regulatory regions secreting specific morphogens. The interplay between these morphogens is both able to form gradients of cell fates as well as sharp boundaries between compartments.

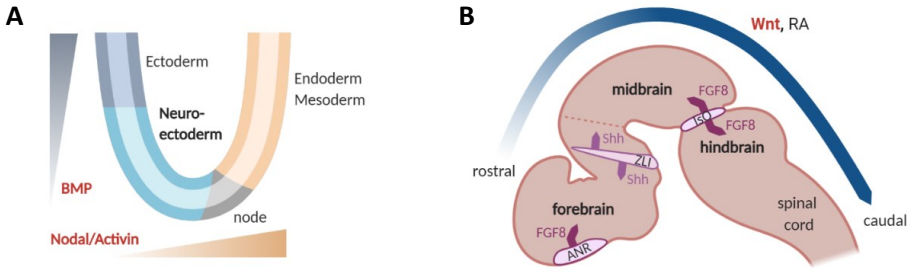

Figure 1: Tissue patterning during mammalian neurodevelopment.
Morphogen gradients and pattering centres for germ layer specification (A) and rostral-caudal neural tube patterning (B). Indicated in red are the signalling pathways adapted for the neural induction of pluripotent stem cells *in vitro*. (A) Germ layers are specified during the primitive-streak stage in mammalian embryogenesis. Neuroectodermal fate is defined by low BMP and low Nodal/Activin signalling mediated by the node region. (B) Initial rostral-caudal patterning is based on RA and Wnt signalling gradients. In later stages, the midbrain-hindbrain boundary is consolidated by FGF8 secretion from the IsO, whereas forebrain identity is established by FGF8 secreted from the ANR. The ZLI defines caudal forebrain and midbrain areas by providing Shh. ANR – anterior neural ridge, IsO – isthmic organizer, ZLI – zona limitans intrathalamica.

The initial rostral-caudal patterning along the neural tube is based on a gradient in Wnt signalling activity [Kiecker and Niehrs, 2001; Nordström et al., 2002], with high levels of Wnt secreted in caudal areas [McGrew et al., 1995; McGrew et al., 1997] and Wnt antagonist expression in rostral areas [Kazanskaya et al., 2000; Houart et al., 2002] (Figure 1B). Combining this gradient with additional morphogens, such as FGF8 [Crossley et al., 1996; Houart et al., 1998; Shanmugalingam et al., 2000; Fukuchi-Shimogori and Grove, 2001; Sato et al., 2001; Walshe and Mason, 2003] and Sonic hedgehog (Shh) [Zeltser et al., 2001; Kiecker and Lumsden, 2004], secreted by secondary organizer regions specifies the regional identity of adjacent compartments and corroborates the localization of boundaries between brain regions. Another morphogen important, but less well understood is retinoic acid (RA) which is secreted in the caudal area [Diez del Corral and Storey, 2004]. It is counteracted by the expression of RA-degrading enzymes in the rostral part [Sakai et al., 2001; Hernandez et al., 2007].

Beside the rostral-caudal patterning, cellular identities are further specified along the dorsal-ventral axis by two opposing morphogen gradients. On the ventral side, the floor plate of the neural tube together with the notochord secrets high levels of Shh. On the dorsal side, cellular identities are influenced by the neighbouring epithelial cells, which secrete both BMP and Wnt.

During neural tube formation and regional patterning NES cells mainly divide symmetrically to increase the stem cell pool. Around the onset of neurogenesis (embryonic day 10-12 in mouse [Hartfuss et al., 2001; Noctor et al., 2002], and gestational week 10-12 in humans [Choi and Lapham, 1978]), stem cells switch to asymmetric cell division and are termed radial glia cells (RGCs) from there on. RGCs are characterized by a radial morphology spanning the whole neural tissue from the apical lining around the ventricles to the basal pial surface and the expression of glial marker proteins, like glial fibrillary protein (GFAP) and brain lipid binding protein (BLBP) [Levitt and Rakic, 1980; Choi, 1981; Feng et al., 1994; Kurtz et al., 1994]. The switch from NES cell fate to a RGC fate is facilitated by the activation of several signalling pathways, including FGF and Notch signalling [Gaiano et al., 2000; Yoon et al., 2004; Sahara and O'Leary, 2009]. The switch to asymmetric cell division and the importance of Notch signalling for brain development is discussed further in chapters 3.3.3 and 3.2.3, respectively.

3.1.2 Modelling human neurodevelopment *in vitro*

Studying human-specific brain development used to be nearly impossible due to the inaccessibility of appropriate tissue samples or model systems. The possibility to cultivate, expand and differentiate human embryonic stem cells (ESCs) *in vitro* lay the ground for the first human model systems for early embryonic development [Thomson et al., 1998; Amit et al., 2000; Itskovitz-Eldor et al., 2000], including neurodevelopment [Pera et al., 2004; Gerrard et al., 2005; Itsykson et al., 2005]. Ethical concerns over the use of ESCs derived from human blastocysts were overcome by the generation of the first induced pluripotent stem cells (iPSCs). Forced expression of pluripotency factors in fully differentiated somatic cells overwrites their given cell fate reprogramming cells to a pluripotent stage [Takahashi and Yamanaka, 2006; Takahashi et al., 2007]. Similar to ESCs, iPSCs show a broad differentiation capacity *in vitro* enabling the generation of well-defined stem cell and progenitor pools and the differentiation of almost any somatic cell type.

The established signalling pathways involved in germ layer patterning and neurodevelopment *in vivo* are adapted to direct ESCs and/or iPSC differentiation (Figure 1). The meanwhile most widely used protocol to generate NSCs from pluripotent cells is based on the so called dual-small mothers against decapentaplegic (dual-SMAD) inhibition [Chambers et al., 2009]. SMAD signalling is usually activated by different anaplastic lymphoma kinase (ALK) receptor subtypes binding, amongst others, BMPs and Nodal/Activin. By inhibiting the BMP/Nodal/Activin-ALK-SMAD pathway using small molecules, like LDN193189 [Cuny et al., 2008] and A83-01 [Tojo et al., 2005], the mesodermal and endodermal differentiation of pluripotent cells is blocked and cells adapt a neuroectodermal fate. Additionally, the caudalization during neural induction can

be diminished by adding a Wnt signalling inhibitor, e.g. XAV939 [Watanabe et al., 2005; Kadoshima et al., 2013]. After this initial neural induction phase, cells typically express NSC marker proteins, like Nestin and Paired box 6 (PAX6) and can be differentiated into a variety of neuronal subtypes [Chambers et al., 2009].

For a scalable expansion of NSC populations before neuronal differentiation, a plethora of protocols were established in the last two decades. The self-renewal of NSCs can be triggered either by activation of proliferation-promoting pathways, e.g. Wnt and Shh [Reinhardt et al., 2013], or by supplementation of growth factors [Koch et al., 2009; Falk et al., 2012]. The former can be achieved by direct activation of the pathways with small molecules, e.g. CHIR99021 as a Glycogen synthase kinase 3 (GSK3) inhibitor for Wnt activation [Bain et al., 2007] and Purmorphamine as a Smoothened (Smo) receptor agonist for Shh activation [Sinha and Chen, 2006]. The cell population generated under these conditions are termed small molecule-NSCs (SM-NSCs) and grow in small, dense, highly proliferative cell colonies. A change from Wnt/Shh-activation to the treatment with growth factors, namely FGF2 and epidermal growth factor (EGF), induces a morphological shift of NSCs to form neural rosettes. In comparison to SM-NSCs, this second NSC population, called rosette-type NSCs from here on, exhibit a clear internal apical-basal polarization, signs of interkinetic nuclear migration and response to additional patterning cues during neuronal differentiation [Zhang et al., 2001; Elkabetz et al., 2008; Koch et al., 2009; Falk et al., 2012; Reinhardt et al., 2013]. Therefore, rosette-type NSCs are thought to represent a NSC population similar to NES cells and/or RGCs during early stages of neurodevelopment *in vivo*.

Beside this two-dimensional (2D) model for neurodevelopment, another field of iPSC-derived cell culture models boomed in the last years, the organoid system. In this three-dimensional (3D) setting, the self-organizing ability of stem and progenitor cells is utilized to mimic structural and spatial aspects of development. Therefore, iPSCs are aggregated into cellular spheres, called embryoid bodies (EBs), which are cultivated in suspension. After neural induction, developing brain organoids self-organize forming neural rosettes, which develop into loop-like structures [Eiraku et al., 2008; Kadoshima et al., 2013; Lancaster et al., 2013]. These structures are characterized by a ventricle surrounded by an apical membrane and a ventricular-like zone (VZ) comprised of NSCs. Comparable to the *in vivo* situation, NSCs in organoids span the VZ from apical to basal and divide directly adjacent to the ventricular lining. In later stages, a cortical plate-like zone (CP) is formed by the developing neurons outside the VZ, which can resemble all six layers of the human cortex [Qian et al., 2016]. Some evidence even show that organoids can model human-specific characteristics of neurodevelopment, e.g. the generation of outer RGCs [Kadoshima et al., 2013; Lancaster et al., 2013] and the induction of gyrification [Li et al., 2017;

Karzbrun et al., 2018]. Similar to the 2D system, the regional identity of the organoids can be further restricted by additional patterning cues, like Wnt- and Shh-inhibition to form forebrain- or neocortex-specific structures [Kadoshima et al., 2013; Iefremova et al., 2017; Xiang et al., 2017; Krefft et al., 2018].

Taken together, iPSC-derived NSCs in 2D and 3D are a powerful model system to study molecular, cell biological and structural aspects of human embryonic neurodevelopment.

3.2 Notch signalling pathway

As briefly mentioned in chapter 3.1.1, Notch signalling was described to be important for RGC fate specification in mouse around the turn of the 21th century [Gaiano et al., 2000]. The initial phenotypic characterization of the Notch locus, however, dates back over 100 years, when specific *Drosophila melanogaster* (*D. melanogaster*) mutants with "notched" wings were described [Dexter, 1914; Morgan, 1917]. The gene responsible for the phenotype was hence termed Notch and was later characterized as coding for a transmembrane receptor [Wharton et al., 1985; Kidd et al., 1986; Fehon et al., 1990] and the starting point for the Notch signalling pathway. Functionally, Notch was soon associated with neurogenic phenotypes in *D. melanogaster* [Metz and Bridges, 1917; Poulson, 1937] and later found to be also crucial for mammalian neurodevelopment, especially NSC maintenance and differentiation [Hatakeyama et al., 2004].

Canonically, the Notch signalling pathway is activated by cell-cell-contact, between a signal receiving cell expressing Notch receptors on its cell surface and a signal sending cell expressing the respective ligands from the Delta/Serrate/LAG-2 (DSL) family [Henderson et al., 1994; Mello et al., 1994; Tax et al., 1994]. In contrast to many other signalling pathways, an incoming Notch signal is not further amplified within the cell. Instead, ligand binding leads to the release of the intracellular domain (ICD) from the receptor, which directly regulates target gene expression. Despite the apparent simplicity of this pathway, Notch signalling is regulating a multitude of developmental processes in different cell types and tissues at different developmental stages. In addition to this simple, linear signalling from a cell-cell-contact to a change in gene expression, there are several layers of regulatory processes. To establish the spatiotemporal specificity of Notch signalling, many of these regulators act in a cell type-, context- and/or time-dependent manner. This makes Notch signalling one of the most interesting, but also most challenging signalling pathway to study.

3.2.1 Notch receptors and Notch ligands

In mammals, four Notch receptor isoforms are described [Maine et al., 1995]: Notch1 and Notch2 are structurally very similar and functionally equivalent [Liu et al., 2015] (Figure 2A). Notch3 exhibits a more restricted expression pattern, e.g. in vascular smooth muscle [Joutel et al., 2000], CNS [Lardelli et al., 1994] and pancreas [Apelqvist et al., 1999], and a limited property to activate transcription [Beatus et al., 2001]. Notch4 is the least understood isoform, but is thought to inhibit the signalling of other Notch isoforms [James et al., 2014].

All Notch receptors are expressed as a pro-form, which is translated at the endoplasmic reticulum (ER) as a single-pass transmembrane protein (Figure 2C). In the ER and later in the Golgi apparatus, Notch proteins undergo the first post-translational modification, namely O-glycosylation. Mediated by a variety of enzymes (Pofut family, Fringe family and Rumi) the addition of different O-glycans regulates Notch-ligand specificity [Brückner et al., 2000; Hicks et al., 2000; Moloney et al., 2000; Okajima and Irvine, 2002; Okajima et al., 2003; Kakuda and Haltiwanger, 2017; Luca et al., 2017; Schneider et al., 2018] and facilitates the cleavage of Notch receptors after ligand binding [Acar et al., 2008]. Within the trans-Golgi network the Notch pro-

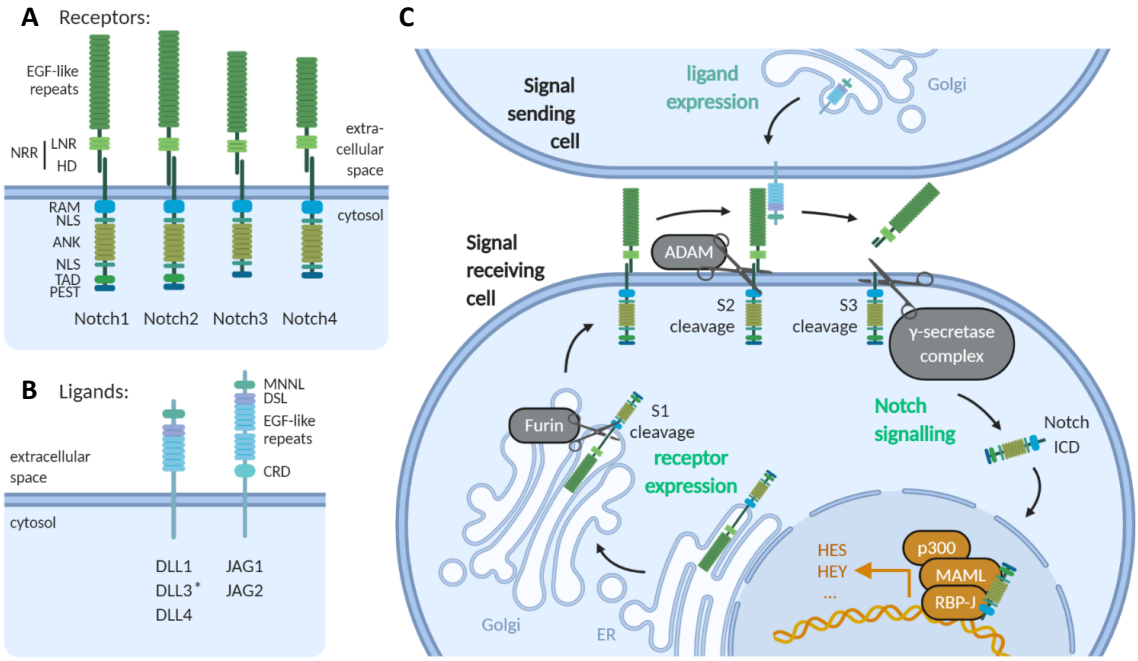

Figure 2: The Notch signalling pathway.
(A-B) Domain structure of human Notch receptor isoforms (Notch1-4) and Notch ligands (DLL1/3/4, JAG1/2). In comparison to the other Notch ligands, DLL3 only acts as a cis-inhibitor and cannot activate Notch signalling (*) [Ladi et al., 2005]. Indicated are intra- and extracellular domains: ANK – ankyrin repeats, CRD – Cysteine-rich domain, DSL – Delta/Serrate/LAG-2, HD – heterodimerization domain, LNR – LIN-12-Notch repeats, MNNL – module at the N-terminus of Notch ligands, NLS – nuclear localization signal, NRR – negative regulatory region, PEST – Proline-Glutamate-Serine-Threonine domain, RAM – RBP-J-associated module, TAD – transcription activation domain. (C) Schematic representation of Notch receptor processing during receptor expression (S1 cleavage by Furin) and activation (S2 and S3 cleavage by ADAM and γ-secretase, respectively). Release of the Notch intracellular domain (ICD) after the last cleavage, triggers its translocation to the nucleus and activation of downstream target genes (e.g. HES and HEY family genes).

forms are also cleaved for the first time by the Furin-like convertase (S1 cleavage) [Logeat et al., 1998] (Figure 2C). This leads to the assembly of the bipartite receptor heterodimers by the non-covalent binding of the Notch extracellular domain (ECD) and the Notch transmembrane (TM)-intracellular domain (ICD) [Sanchez-Irizarry et al., 2004].

The heterodimerization of Notch receptors serves to prevent ligand-independent activation of the receptor. The hydrophobic heterodimerization domain (HD) and the adjacent LIN12-Notch repeats (LNR) form the negative regulatory region (NRR) and sterically block the access to the S2 cleavage site within the HD [Sanchez-Irizarry et al., 2004; Gordon et al., 2007]. This blockage can be overcome by the binding of Notch receptors to its respective ligands, DLL1/3/4 and JAG1/2 in mammals, which are also single-pass transmembrane proteins [Lissemore and Starmer, 1999] (Figure 2B). The interaction is mediated by the module at the N-terminus of Notch ligands (MNNL), DSL domain and EGF-like repeats on the ligand side [Cordle et al., 2008; Andrawes et al., 2013] and the large arrays of EGF-like repeats on the receptor side [Rebay et al., 1991].

3.2.2 Notch signal transduction

Upon the binding between Notch receptors and ligands, the receptors undergo a series of proteolytic cleavages, finally releasing the Notch ICD into the cytosol. The soluble Notch ICD then mediates the signal transduction from the cell surface to the nucleus (Figure 2C).

The first step in this process is the release from the autoinhibition by the NRR. This is thought to be either overcome by simple conformational change upon ligand binding [Tiyanont et al., 2011] or by a pulling force applied by the internalization of the ligand into the signal sending cell [Parks et al., 2000; Nichols et al., 2007; Gordon et al., 2015; Lovendahl et al., 2018]. The S2 cleavage site can then be recognized by transmembrane metalloproteases from the A disintegrin and metalloprotease (ADAM) family [Brou et al., 2000; Mumm et al., 2000; Nichols et al., 2007]. After S2 cleavage, the intramembranous S3 cleavage site is available for the γ-secretase complex. This complex consists of Presenilin 1/2, Nicastrin, anterior pharynx-defective 1 (APH1) and presenilin enhancer 2 (PEN2), where Presenilin 1 facilitates the protease activity [Wolfe, 2006]. S3 cleavage releases the Notch ICD from the membrane into the cytosol [Kopan et al., 1996; Schroeter et al., 1998; Strooper et al., 1999], which is then bound by Importin α via its nuclear localization signals (NLS) [Huenniger et al., 2010]. This mediates the translocation of the ICD into the nucleus, where it triggers expression of Notch target genes [Schroeter et al., 1998; Struhl and Adachi, 1998].

DNA binding and transcriptional regulation by the Notch ICD is mediated by association with recombination signal sequence-binding protein Jκ (RBP-J), also called C promoter-binding factor 1 (CBF1), which belongs to the CBF/Suppressor of hairless/LAG-1 (CSL) family [Lecourtois and

Schweisguth, 1998; Schroeter et al., 1998; Struhl and Adachi, 1998]. RBP-J binds to a weak consensus sequence (C/tGTGGGAA) [Del Bianco et al., 2010] in the promoter region of target genes [Kovall and Hendrickson, 2004; Nam et al., 2006; Friedmann and Kovall, 2010] as well as in distal super-enhancer regions [Wang et al., 2014]. In the absence of Notch ICD, RBP-J recruits several transcriptional repressors, including epigenetic regulators like histone deacetylases, actively inhibiting expression of Notch target genes [Dou et al., 1994; Waltzer et al., 1995; Kao et al., 1998]. Upon translocation to the nucleus, the Notch ICD binds to RBP-J via its RBP-J-associated module (RAM) domain [Tamura et al., 1995]. In complex with RBP-J, the Notch ICD recruits the transcriptional coactivator Mastermind-like 1 (MAML1) via its ankyrin repeats (ANK) [Petcherski and Kimble, 2000; Wu et al., 2000; Nam et al., 2003; Nam et al., 2006]. This complex can, in turn, replace the inhibitory CSL complexes and recruits further transcriptional coactivators, like the histone acetyltransferase p300 [Yatim et al., 2012]. In addition to the recruited transcription activators, two of the four mammalian Notch isoforms (Notch1 and Notch2) contain an internal transcription activation domain (TAD) directly amplifying transcription of downstream target genes [Kurooka et al., 1998; Beatus et al., 2001; Liu et al., 2015].

3.2.3 Notch downstream signalling and cell fate determination

The group of Notch target genes is quite limited, with the main targets being members of the hairy/enhancer of split (HES) family and the HES related with YRPW motif (HEY) family [Jarriault et al., 1995; Maier and Gessler, 2000]. These proteins are themselves transcription factors with a basic helix-loop-helix structure and bind as homo- or heterodimers to N box (CACNAG) and class C site(CACG(C/A)G) DNA sequences [Sasai et al., 1992; Ohsako et al., 1994; Iso et al., 2001]. In combination with additional coregulators, this small group of Notch targets can facilitate various cell fate decisions both during embryonic development and during adult tissue maintenance. The main mechanisms involved in cell fate decision by Notch signalling include (1) maintenance of stem cell fate e.g. in embryonic myogenesis [Kopan et al., 1994; Mayeuf-Louchart et al., 2014] and the regeneration of the gut [Korinek et al., 1998; van Es et al., 2005], (2) induction of terminal differentiation, e.g. in the skin [Lowell et al., 2000; Estrach et al., 2008], and (3) regulation of fate decisions between cell lineages, e.g. during development of the hematopoietic system [Pui et al., 1999; Radtke et al., 1999; Han et al., 2002; Tanigaki et al., 2002; Saito et al., 2003; Hozumi et al., 2004]. The best understood function of Notch as a cell fate determinant, however, is its role during the development of the nervous system. Due to the scope of this thesis, I will concentrate on this “neurogenic” function of Notch in the following paragraphs.

Similar to the initial studies in *D. melanogaster*, the Notch-HES/HEY-axis was found to be crucial for the maintenance of the mammalian NSC pool during neurodevelopment [Ishibashi et al., 1994; Ohtsuka et al., 2001; Hatakeyama et al., 2004; Kageyama et al., 2008; Shimojo et al., 2008]. This is facilitated by the HES/HEY-dependent repression of proneuronal factors, such as acheate-scute like 1 (ASCL1), Neurogenin 1 and 2 (NGN1/2) on a transcriptional level [Chen et al., 1997; Cau et al., 2000; Hatakeyama et al., 2004; Imayoshi et al., 2008] and on a functional level [Sasai et al., 1992; Giagtzoglou et al., 2003]. Additional studies, however, revealed a more complicated picture, especially for the function of HES1: whereas a sustained HES1 activation rather triggers the cell cycle exit of NSCs [Baek et al., 2006], an oscillating HES1 expression seems to be beneficial for NSC maintenance [Shimojo et al., 2008]. This oscillation can be explained by an autoinhibitory feedback loop of HES1 [Takebayashi et al., 1994; Hirata et al., 2002] and induces an opposing oscillation of ASCL1 and NGN2. ASCL1, in this setting, does not function as a proneuronal factor, but promotes cell cycle progression and NSC proliferation [Castro et al., 2011]. The second typically considered proneuronal factor, NGN2, induces the expression of DLL1 in cycling NSCs [Castro et al., 2006; Hindley et al., 2012], whereas the NGN2-promoted neurogenic program is diminished during this HES1-induced oscillation [Ali et al., 2011]. The oscillating expression of DLL1 is thought to trigger the mutual activation of Notch signalling in a cluster of adjacent undifferentiated NSCs contributing to the corroboration of HES1 oscillation and stem cell maintenance [Kageyama et al., 2008; Shimojo et al., 2016].

When NSCs divide asymmetrically, Notch activity and hence HES/HEY expression is constantly reduced in one of the daughter cells (for more detail on asymmetric cell division see chapter 3.3). In turn, the sustained expression of proneuronal factors induces neurogenesis [Shimojo et al., 2008; Imayoshi et al., 2013]. The induction of DLL1 in the differentiating, immature neurons facilitates activation of Notch signalling in the adjacent NSC and hence the maintenance of its NSC fate, a process termed lateral inhibition [Kageyama and Ohtsuka, 1999; Kawaguchi et al., 2013]. An elegant, but experimentally not yet confirmed mechanism, suggests that a stepwise accumulation/decline of downstream effectors with each HES1 oscillation cycle can even explain the temporal shift in the cellular identity of the neuronal progeny: from deep layer neurons during early stages to superficial layer neurons and finally to astrocytes during late stages of development (reviewed in Kageyama et al., 2015). Whereas this gradual shift is so far speculative, the importance of Notch signalling for the switch from neurogenesis to astrogenesis is long established [Nakashima et al., 2001; Ohtsuka et al., 2001; Grandbarbe et al., 2003].

3.2.4 Regulation of the Notch signalling pathway

The impact of Notch signalling on this huge variety of crucial developmental decisions, not only in neurodevelopment, makes it necessary to strictly regulate its activity in a spatiotemporal manner. Meanwhile, a large range of processes are described to regulate Notch receptor signalling, which are partially universal and partially highly dependent on the identity of the involved cell types and the developmental stage.

First, Notch receptor-ligand interaction can have a variety of outcomes dependent on the combination of receptor and ligand isoforms as well as on the cellular identity. Ligand-specificity can be restricted or altered by O-glycosylation of the Notch ECD before its transport to the cell surface [Brückner et al., 2000; Hicks et al., 2000; Moloney et al., 2000; Okajima and Irvine, 2002; Okajima et al., 2003; Kakuda and Haltiwanger, 2017; Luca et al., 2017; Schneider et al., 2018]. Specific ligands in specific cell-types can even have an inhibitory effect on Notch signalling in the receiving cell, e.g. JAG1 inhibits Notch1 activation during angiogenesis [Hicks et al., 2000; Benedito et al., 2009]. Beside the so far discussed trans-interactions between receptors and ligands on neighbouring cells, also interactions within the same cell (cis-interaction) are involved in Notch signalling regulation. Both cis-inhibition [Fiuza et al., 2010; Sprinzak et al., 2010] as well as cis-activation have been described [Formosa-Jordan and Ibañes, 2014; Nandagopal et al., 2019].

As a second important regulatory mechanism, the degradation of Notch receptors as well as the turnover of the Notch ICD has to be mentioned. The latter is dependent on the C-terminal proline-glutamate-serine-threonine (PEST) domain [Fryer et al., 2004], which targets the ICD for proteolytic cleavage [Rogers et al., 1986]. The half-life can be further influenced by several post-translational modifications, including acetylation, phosphorylation and ubiquitination [Oberg et al., 2001; Fryer et al., 2004; Guarani et al., 2011]. Degradation of the transmembrane receptors is dependent on internalization from the plasma membrane and lysosomal degradation. Two of the first negative Notch regulators identified in *D. melanogaster*, Numb and Deltex (in mammals Numb/Numb-like and DTX1, respectively), are both involved in this process. Numb ubiquitinates Notch receptors, which become endocytosed and degraded [McGill and McGlade, 2003; McGill et al., 2009]. Deltex links Notch receptors to β-arrestin promoting its lysosomal degradation [Mukherjee et al., 2005; Puca et al., 2013]. Besides, there are also evidence that Notch receptor availability at the cell surface can be adapted under starvation conditions by targeting of receptors for autophagic degradation [Wu et al., 2016; Tao et al., 2018].

Ligands also undergo internalization which represents the third major regulatory mechanism. In contrast to receptor internalization, these processes are usually required for the activation of Notch signalling rather than to reduced ligand availability on the cell surface. The endocytosis of

Delta ligand into the signal sending cell can be induced by ubiquitination catalysed by the E3 ligases Neutralized (Neur) and Mindbomb (Mib) [Deblandre et al., 2001; Lai et al., 2001; Pavlopoulos et al., 2001; Itoh et al., 2003]. There are two mechanisms that are suggested to induce Notch activation by ligand internalization. The first one suggests, that ligands are internalized upon binding to the ECD of the receptor, which applies a pulling force on the receptor heterodimer promoting S2 cleavage [Meloty-Kapella et al., 2012; Gordon et al., 2015] (also discussed in chapter 3.2.2). The second mechanism suggests maturation of the ligand by endocytosis and recycling to the plasma membrane to be necessary for inducing Notch receptor interaction and downstream signalling [Wang and Struhl, 2004; Nichols et al., 2007].
Another level of regulation is based on the activity of the proteases processing Notch receptors, ADAM family proteases and the γ-secretase complex. For both, proteolytic activity was found to be regulated by the pH and the internalization into endolysosomes [McLendon et al., 2000; Bagshaw et al., 2003; Pasternak et al., 2003; Carey et al., 2005; Carey et al., 2011]. This suggests that the S2/S3 cleavage might not only take place at the cell surface, but that Notch processing is more efficient in endocytic and/or endolysosomal vesicles [Gupta-Rossi et al., 2004; Vaccari et al., 2008; Windler and Bilder, 2010; Chastagner et al., 2017]. Therefore, internalization and intracellular trafficking of receptors add even another layer of regulation to the Notch signalling pathway. Two mechanisms that involve the segregation of Notch-containing vesicles were described to be essential for asymmetric cell division in *D. melanogaster* and are discussed in detail in chapter 3.3.4.

3.3 Asymmetric cell division, cell fate decision and cellular polarity

As all stem cell populations, NSCs face two major challenges: maintaining the stem cell pool by self-renewal and orchestrating the differentiation into somatic cells. The major tool to facilitate these very contradicting processes is the cell division in an either symmetric or asymmetric fashion. In this context, a symmetric cell division is often defined as a mitotic event which generates two daughter cells with an identical cell fate. Whereas asymmetric cell divisions generate daughter cells with different cell fates. In a stricter definition, however, asymmetric cell divisions are characterized by a differential segregation of asymmetry factors during mitosis (Figure 3). These asymmetry factors can be individual molecules, including mRNAs [Kusek et al., 2012], whole protein complexes or even subcellular compartments, such as vesicles or mitochondria [Murke et al., 2015; Loeffler et al., 2019]. The asymmetric segregation of these factors can bias activation of signalling pathways, subcellular composition, epigenetic as well as metabolic states between daughter cells. Hence, asymmetry factors can act directly or indirectly

as cell fate determinants in the daughter cells. This links the narrower molecular definition of asymmetric cell division to the broader definition mentioned above.

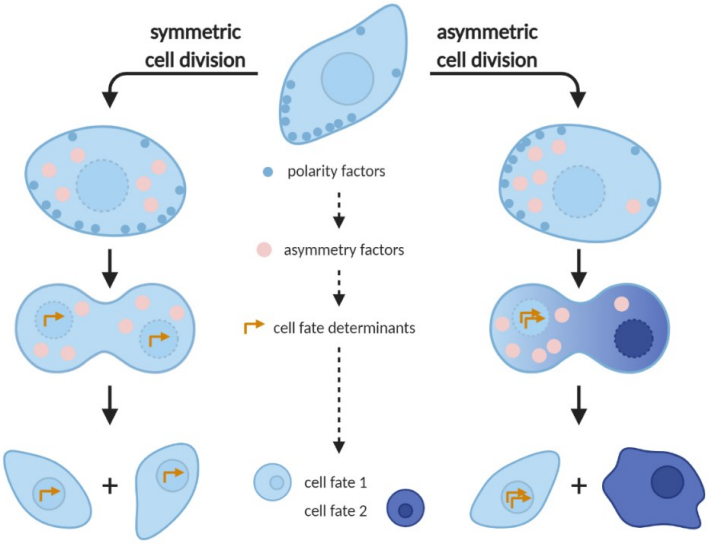

Figure 3: Symmetric and asymmetric cell division. Stem cells can divide symmetrically or asymmetrically depending on the distribution of polarity factors, which is independent of and maintained throughout the cell cycle. At the beginning of mitosis, polarity factors direct the trafficking of asymmetry factors, which are as a consequence either symmetrically or asymmetrically segregated. Asymmetry factors, in turn, influence the localization, recruitment or expression of cell fate determinants. Therefore, asymmetry factors can decide over the cell fate of the two daughter cells after mitosis.

The decision between symmetric and asymmetric cell division can be either made cell intrinsically or in response to external cues from a surrounding stem cell niche. The latter is more important in the regulation of adult stem cells, as the stem cell niche itself needs to be developed first. The external regulation of asymmetric cell division provides more precise and more variable regulatory options than the intrinsic pathway. This is important to maintain the limited pool of adult stem cells, while retaining the ability to react to differentiation stimuli (e.g. wounding, lesions). However, the focus in this study is on early embryonic neurodevelopment, that is why asymmetric cell division from here on is defined by the intrinsic mechanism, which is based on internal cell polarisation.

3.3.1 Apical-basal polarity and planar cell polarity (PCP) in (neuro-)epithelial cells

The basis for cell polarity is the intracellular sorting of polarity factors either in a plane perpendicular to the tissue plane (apical-basal polarity) or parallel to the tissue plane (planar cell polarity, PCP). Polarity factors are, hereby, not to be confused with asymmetry factors, as the former are asymmetrically distributed within the cell independent of the cell cycle phase. Cell polarity is a conserved mechanism that is especially prominent in all epithelial tissues, including neuroepithelial cells (Figure 4).

The core regulators of apical-basal polarity are the partitioning defect (PAR), Crumbs (CRB) and Scribble (SCRIB) protein complexes. They serve as signalling centres at defined membrane domains and influence a whole variety of cellular processes, including cytoskeletal dynamics

[Martin-Belmonte et al., 2007; Chartier et al., 2011], subcellular trafficking [Lock and Stow, 2005; Roeth et al., 2009; Vreede et al., 2014] and maintenance of intercellular junctions [Chen and Macara, 2005; Fogg et al., 2005]. The CRB complex is located at the apical membrane [Laprise et al., 2006; Li et al., 2008] and establishes the apical domain together with the PAR complex. The latter is recruited apically by its interaction with the apical junction complex formed by tight and adherens junctions [Itoh et al., 2001; Takekuni et al., 2003; Harris and Peifer, 2005; Morais-de-Sá et al., 2010]. The PAR complex consists of PARD3, PARD6 and isoforms of atypical protein kinase C (aPKC), PKCλ and PKCζ [Kemphues et al., 1988; Atwood et al., 2007]. Localization of PAR and CRB complexes to the apical side excludes the accumulation of components of the third polarity complex, the basal SCRIB complex [Bilder et al., 2000], from this intracellular domain and vice versa [Benton and Johnston, 2003; Bilder et al., 2003; Tanentzapf and Tepass, 2003; Hutterer et al., 2004]. This constant antagonism of the polarity complexes stabilizes the apical and basal membrane domains and facilitates polarized intracellular signalling.

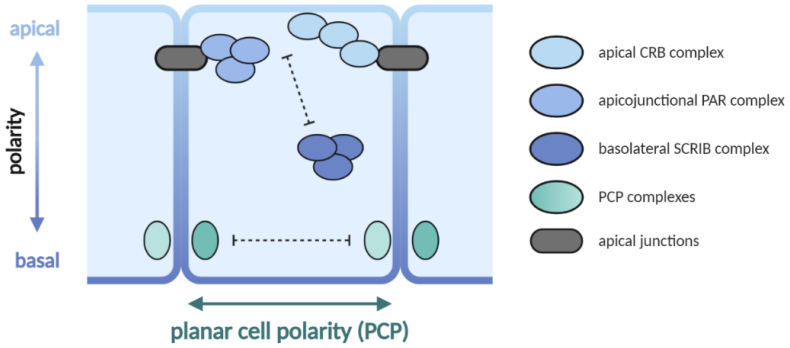

Figure 4: Establishment of cellular polarity in (neuro-)epithelial cells.
Apical-basal cell polarity is mediated by a complex interplay between three protein complexes (CRB, PAR and SCRIB complex) and apical cell-cell junctions (tight and adherens junctions). The apical localization of CRB and PAR complexes counteracts the assembly of SCRIB complex, facilitating the basal localization of this complex. Planar-cell polarity (PCP) complexes form around the transmembrane receptor CELSR and antagonize each other. CELSR – Cadherin EGF LAG seven-pass G-type receptor, CRB – Crumbs, PAR – partitioning defect, SCRIB – Scribble.

PCP is mediated by the heterophilic interaction of two antagonizing protein complexes at cell-cell contact points. Both complexes form around the transmembrane protein Cadherin EGF LAG seven-pass G-type receptor 1-3 (CELSR1-3) [Usui et al., 1999; Shimada et al., 2001], which is thought to homodimerize on the cell surface of neighbouring cells. The interaction with either Frizzled 3/6 (FZD3/6)-Dishevelled 1-3 (DVL1-3) or Van Gogh-like 1/2 (VANGL1/2)-Prickle 1-4 (PK1-4) is opposing each other within one cell as well as in the adjacent cell [Vinson and Adler, 1987; Tree et al., 2002; Jenny et al., 2005; Wang et al., 2006]. Thereby, the assembly of PCP complexes can spread through the whole tissue generating a uniform patterning. Whereas the apical-basal polarity is mostly triggered and maintained by cell intrinsic processes, the

establishment of PCP is thought to be based on extrinsic clues, such as mechanical forces and/or morphogen gradients [Hakanen et al., 2019; Li et al., 2021].

3.3.2 Asymmetric cell division in the *D. melanogaster* nervous system

Asymmetric cell division in *D. melanogaster* can be triggered by both of the described polarity mechanisms. Apical-basal polarity is the basis for asymmetric cell division of neuroblasts (NBs) in the developing CNS, whereas PCP induces asymmetry in dividing sensory organ precursor (SOP) cells of the peripheral nervous system.

Polarized NBs can divide symmetrically to increase the number of stem cells in the pool or asymmetrically to form an apical daughter cell, which retains the stem cell-like character, and a more restricted basal progenitor, termed ganglion mother cell (GMC) [Hartenstein et al., 1987; Boone and Doe, 2008; Bowman et al., 2008] (Figure 5A). Asymmetric division is induced upon delamination of the NBs from the polarized neuroectoderm [Kuchinke et al., 1998; Siegrist and Doe, 2006]. The switch to asymmetric cell division is thereby facilitated by Inscuteable (Insc), which recruits partner of Insc (Pins), the G proteins Gαi and mushroom body-defective (Mud) to the apical PAR complex [Schaefer et al., 2000; Wodarz et al., 2000; Bowman et al., 2006; Izumi et al., 2006; Siller et al., 2006]. In turn, microtubules and centrosomes are shifted to the apical pole inducing the mitotic spindle to orient parallel to the apical-basal axis. Beside this shift in spindle orientation, the PAR complex also triggers the accumulation of cell fate determinants at the basal domain by the activity of aPKC. Among these cell fate determinants are the Miranda (Mira)-Staufen (Stau)-Prospero (Pros)-Brain tumor (Brat) complex [Ikeshima-Kataoka et al., 1997; Shen et al., 1997; Matsuzaki et al., 1998; Lee et al., 2006; Wirtz-Peitz et al., 2008; Atwood and Prehoda, 2009], which triggers e.g. cell cycle exit [Betschinger et al., 2006], and Numb. As discussed in chapter 3.2.4, Numb inhibits Notch signalling and thereby induces the basal daughter cell to lose its stem cell fate and differentiating into the GMC [Lu et al., 1998; Smith et al., 2007; Wirtz-Peitz et al., 2008].

In the peripheral nervous system, the asymmetric cell division of SOP cells is dependent on the planar polarization of the cells in an anterior-posterior manner (Figure 5B). Due to a lack in Insc expression, the Pins-Gαi-Mud complex is not linked to the PAR complex in SOP cells and the orientation of the mitotic spindle is instead determined by PCP signalling [Lu et al., 1999; Bellaïche et al., 2001; Bellaïche et al., 2004; Ségalen et al., 2010]. Similar to NBs, however, the distribution of cell fate determinants is based on the accumulation of the PAR complex at the posterior side [Bellaïche et al., 2001; Schaefer et al., 2001]. Cell fate determination in the pIIa-daughter cells (pIIa and pIIb) is again highly dependent on Notch signalling. The Notch signalling bias between daughter cells is achieved by several different mechanisms, including asymmetric

localization of Numb and Neur to the anterior pIIb cell. These factors inhibit Notch signalling in the pIIb cell and activate Notch signalling on the adjacent pIIa, respectively [Lai et al., 2001; Berdnik et al., 2002; Le Borgne and Schweisguth, 2003; Hutterer and Knoblich, 2005; Couturier et al., 2013] (see also chapter 3.2.4). Two additional processes to bias Notch signalling during SOP cell division involve the directed segregation and accumulation of two specified

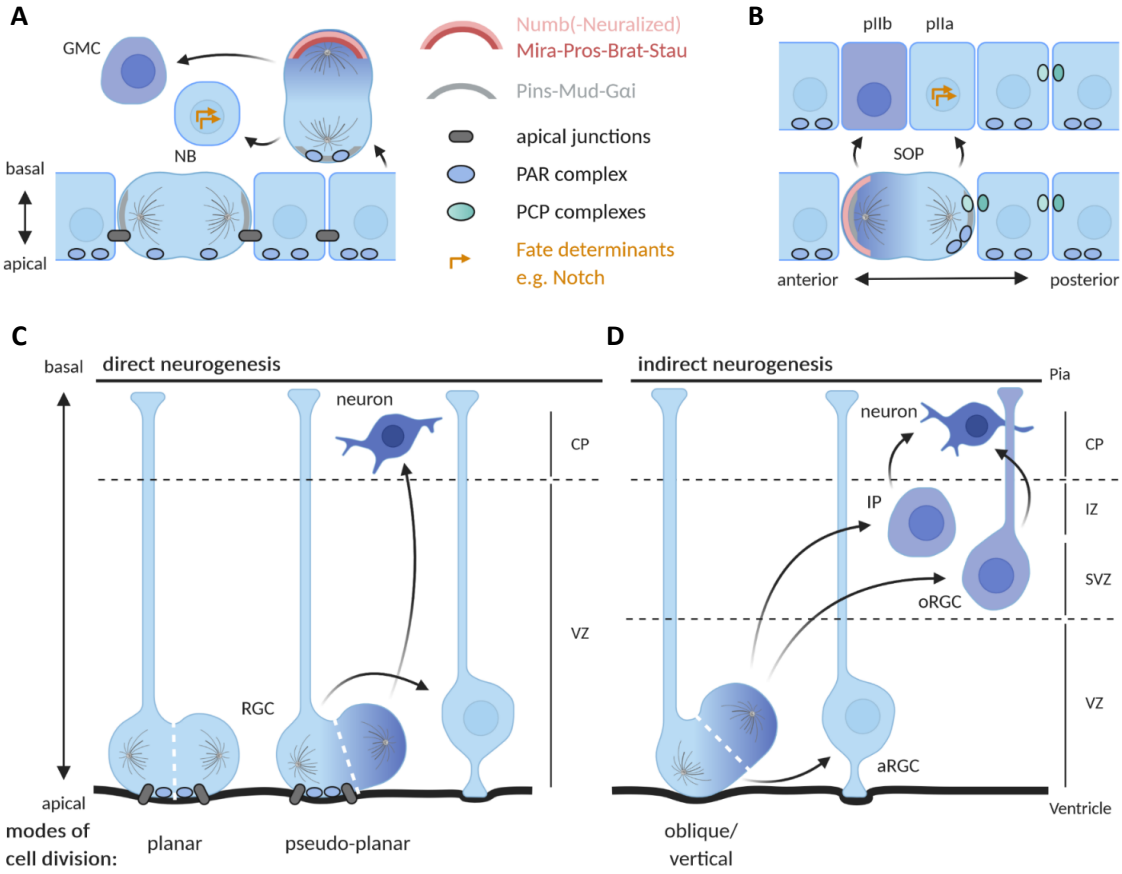

Figure 5: Asymmetric cell division in neurodevelopment.
(A-B) Asymmetry mechanisms in *D. melanogaster* neuroblasts (NBs) (A) and sensory organs precursor (SOP) cells (B). Neuroblasts divide symmetrically within the neuroectodermal layer by orienting the mitotic spindle perpendicular to the apical-basal axis by the Pins-Mud-Gαi complex. Upon delamination from the neuroectoderm, the spindle apparatus is anchored via Insc to the PAR complex at the apical site and therefore the cleavage plane forms parallel to the apical-basal axis. The basal accumulation of cell fate determinants (Numb and Mira-Pros-Brat-Stau) and the downstream regulation of e.g. Notch, leads to the asymmetric division into one NB and one more restricted ganglion mother cell (GMC). (B) In SOP cells spindle orientation is determined by PCP complexes triggering a plane of cell division parallel to the anterior-posterior axis. Cell fate determinants (Numb-Neuralized) localize to the anterior pole by the activity of the PAR complex, which is located posterior during cell division. Therefore, the anterior pIIb daughter cells show reduced level of Notch signalling, whereas Notch is activated in the posterior pIIa daughter cell.
(C-D) In mammals, radial glia cells (RGCs) represent the pool of neurogenic NSCs. (C) In early stages of neurogenesis, RGCs shift there mode of cell division from symmetric, planar division to asymmetric cell division, generating one RGC and one neuron. As the plane of cell division is only tilted slightly, divisions are termed pseudo-planar. Due to the spatially restricted apical membrane, this facilitates asymmetric inheritance of polarity factors influencing the cell fate of the daughter cells. (D) During later stages of development, apical RGCs (aRGCs) undergo indirect neurogenesis via intermediate progenitors (IPs) or outer RGCs (oRGCs). Here, the cell fate of the daughter cells is highly dependent on the plane of cell division and aRGCs regularly divide in a oblique or vertical manner.
CP – cortical plate, IZ – intermediate zone, SVZ – subventricular zone, VZ – ventricular zone.

subpopulations of intracellular vesicles. These will be discussed in detail in chapter 3.3.4 dealing with vesicles as asymmetry factors.

3.3.3 Polarity and asymmetric cell division in mammalian neurodevelopment

Similar to *D. melanogaster* NBs, mammalian NSCs, from NES cells to RGCs, adopt a clear apical-basal polarization, which is not only maintained throughout development, but is even crucial for the maturation and functionality of differentiating neurons [Nishimura et al., 2004; Shi et al., 2004; Zhang and Macara, 2008; Chen et al., 2013; Duman et al., 2013]. Whereas the influence of PCP in mammals is poorly understood, it seems to be important for neural tube closure and deficiencies of PCP lead to severe developmental defects [Lake and Sokol, 2009; Allache et al., 2012; Robinson et al., 2012].

The apical-basal polarity of NSCs is defined by the attachment of the cells on the one hand to the apical membrane around the ventricles and on the other hand to the basement membrane at the pial surface. The apical membrane domain is characterized by the accumulation of ubiquitously expressed polarity factors, such as the PAR complex [Manabe et al., 2002; Cappello et al., 2006; Kim et al., 2010], and junctional proteins, such as ZO-1 [Stevenson et al., 1986], as well as neural-specific isoforms, such as neural Cadherin (N-Cadherin) [Hatta et al., 1985; Hatta and Takeichi, 1986]. In contrast to epithelial cells and NBs, the apical domain of NSCs is restricted to a small membrane patch at the end of the apical process, which is attached to the ventricular lining [Aaku-Saraste et al., 1996] and represents only 1-2% of the cell's plasma membrane [Kosodo et al., 2004]. The basal domain includes the soma of the NSC and the basal process spanning the VZ and CP. This highly polarized morphology is the reason why the spindle orientation during cell division of mammalian NSCs was found to be not tilted as much as in *D. melanogaster* NBs. However, it is still organized by the mammalian orthologues of Insc and Pins (G-protein-signalling modulator 2, GPSM2) [Konno et al., 2008; Noctor et al., 2008; Peyre et al., 2011; Postiglione et al., 2011]. A slight shift in the plane of cell division is sufficient that one daughter cell inherits the majority of the apical-junctional complexes, already changing the fate of the daughter cells [Kosodo et al., 2004; Marthiens and ffrench-Constant, 2009; Kim et al., 2010] (Figure 5C). Especially during early neurogenesis, RGCs undergo direct neurogenesis, generating a neuron and a RGC through asymmetric cell division. Whereas apical RGCs later differentiate mostly via the generation of more restricted progenitor cells, like intermediate progenitor cells or outer RGCs (Figure 5D). These two cell types built up the subventricular zone (SVZ) and the intermediate zone (IZ) and exhibit a certain self-renewal capacity before undergoing neurogenic divisions [Haubensak et al., 2004; Noctor et al., 2004; Hansen et al., 2010; Betizeau et al., 2013; Pilz et al., 2013]. The plane of cell division becomes more important

during this time of development, as demonstrated by an increase in oblique and even vertical divisions [Haydar et al., 2003; Konno et al., 2008; Fietz et al., 2010; Hansen et al., 2010; Shitamukai et al., 2011; LaMonica et al., 2013]. Also, the inheritance of the basal process becomes an additional important factor for cell fate determination at this stage [Konno et al., 2008; Shitamukai et al., 2011; LaMonica et al., 2013], which is not observed during asymmetric cell division of early RGCs [Kosodo et al., 2008].

Whereas the connection between cellular polarization, spindle orientation and cell fate is fairly well understood, the intermediate cell fate determinants and their distribution during cell division remains a topic of intensive research. The asymmetric segregation of one cell fate determinant described in *D. melanogaster*, the RNA-binding protein Stau and its target mRNA prospero homeobox 1 (Prox1; the mammalian orthologue to Pros), was confirmed to be also involved in asymmetric cell division of mammalian NSCs [Vessey et al., 2012]. However, the distribution and function of Numb is still controversially discussed in literature. Initial studies in mammalian model systems, suggest an apical localization of Numb and basal localization of Notch1 in dividing RGC [Chenn and McConnell, 1995; Zhong et al., 1996; Zhong et al., 1997], which contradicts the critical role of Notch signalling during the maintenance of NSCs [Imayoshi et al., 2010]. Whereas the localization of Numb to the apical domain was reproduced in several studies since then, the functional role is still ambiguous: on the one hand, studies support the findings from *D. melanogaster*, linking mammalian Numb and Numblike (Nbl) to cell cycle exit and differentiation [Li et al., 2003; Klezovitch et al., 2004], on the other hand, Numb/Nbl seems to be important for RGC maintenance [Petersen et al., 2002; Petersen et al., 2004; Rasin et al., 2007]. In line with the latter, Numb/Nbl were also found to link apical PARD3 localization, Notch activation and RGC cell fate during asymmetric cell division in mouse [Bultje et al., 2009]. As Notch regulation by Numb seems to be more complicated in mammals than in *D. melanogaster*, the characterization of additional regulatory mechanisms for Notch signalling in mammalian asymmetric cell division is a pressing field of research.

3.3.4 Vesicles as asymmetry factors

Beside the so far discussed asymmetry of individual proteins or protein complexes during cell division, vesicles are meanwhile well-established as another group of asymmetry factors in several model systems, from *Caenorhabditis elegans* and *D. melanogaster* to zebrafish and mammals.

The evolutionary and developmentally earliest vesicle asymmetry was found in the *Caenorhabditis elegans* zygote. During its first division the endosome marker early endosome

antigene 1 (EEA1) accumulate at the anterior pole due to the activity of Par proteins [Andrews and Ahringer, 2007].

As mentioned in chapter 3.3.2 asymmetric cell division in *D. melanogaster* SOP cells also involves asymmetric segregation of vesicles. Two subpopulations of endosomes have been associated with cell fate decision of pII cells, $Rab11^+$ recycling endosomes and a subpopulation of $Rab5^+$ endosomes, marked by Smad anchor for receptor activation (Sara). For the recycling endosomes, the overall amount of $Rab11^+$ vesicles is indifferent between the daughter cells. In pIIb cells, however, the vesicles accumulate at the centrosomal region and this clustering promotes recycling of the vesicles to the cell surface [Emery et al., 2005]. Thereby the Notch ligand Delta is returned to the cell surface and triggers Notch signalling in the adjacent pIIa cell. For the $Sara^+$ endosomes, it was shown that both Notch receptors and ligands are present inside these vesicles and that they are asymmetrically segregated towards the pIIa cell [Coumailleau et al., 2009; Loubéry et al., 2014; Derivery et al., 2015; Loubéry et al., 2017]. Whereas the vesicle asymmetry is associated with a Notch signalling bias towards the receiving cell, the exact mechanism how $Sara^+$ vesicles activate the Notch pathway remains vague. Interestingly, the asymmetry of endosomes marked by Sara seems to be conserved in other model systems, like zebrafish spinal cord NSCs [Kressmann et al., 2015] and in *D. melanogaster* NBs [Coumailleau et al., 2009] and intestinal stem cells [Montagne and Gonzalez-Gaitan, 2014].

A study in primary human hematopoietic stem cells also identified several components of the endosomal pathway to be asymmetrically segregated during cell division [Beckmann et al., 2007]. However, a functional connection of vesicle asymmetries with cell fate decision is completely missing in this stem cell population. Recently, another vesicular compartment, namely lysosomes, was linked to asymmetric cell division in murine hematopoietic stem cells, where these vesicles influence the cell fate decision via a shift in the metabolic state of the daughter cells [Loeffler et al., 2019].

3.4 The endosomal-lysosomal pathway

As indicated in the last chapter, trafficking of vesicles within a cell can influence major cell fate decisions. Vesicle trafficking, in general, can be divided in two major directions either from the ER-Golgi network towards the plasma membrane or from the plasma membrane into the cell. Even so the first process plays important roles in Notch receptor and ligand availability (chapters 3.2.1 and 3.2.4), establishment of cellular polarity (chapter 3.3.1) and many other processes, in this study the focus was on processes involved in the trafficking from the plasma membrane and along the endolysosomal pathway.

3.4.1 Endocytosis

Endocytosis is the process of internalization of extracellular components, membrane-bound substances and transmembrane proteins into the cell. The process is initiated by the generation of membrane pits and the abscission of these invaginations from the plasma membrane to form intracellular endosomes. For the two best-understood endocytosis pathways, Clathrin-mediated endocytosis (CME) and caveolar-type endocytosis, the abscission from the plasma membrane is mediated by the large GTPase Dynamin [Kosaka and Ikeda, 1983; Henley et al., 1998; Sever et al., 2000]. Dynamin forms a helical polymer around the neck of invaginations [Merrifield et al., 2002; Roux et al., 2010] and the internal GTPase activity together with the actin cytoskeleton induces the vesicle formation [Henley et al., 1998; Stowell et al., 1999; Marks et al., 2001; Roux et al., 2006; Mooren et al., 2009]. The prior step of membrane invagination is induced by the eponymous Clathrin and Caveolin in CME and caveolar-type endocytosis, respectively. Whereas Clathrin is recruited to the membrane by adapter proteins, mainly adaptor protein 2 (AP2) [Höning et al., 2005; Schmid and McMahon, 2007], Caveolin accumulates at lipid-rafts within the plasma membrane [Fra et al., 1995; Deckert et al., 1996].

After internalization, vesicles and their cargoes can be targeted along different intracellular routes, either retrograde towards the Golgi apparatus, back to the plasma membrane for recycling or secretion, or through the endolysosomal pathway towards degradation of the cargo substances.

3.4.2 Endosomes

The direction of vesicles along these different routes is decided on the level of endosomes. The respective maturation processes are regulated by vesicle associated proteins, which are also commonly used as marker proteins to distinguish vesicle subtypes. One major group of these proteins is the Ras-related in brain (Rab) superfamily of small GTPases [Pereira-Leal and Seabra, 2001] which integrate in the vesicle membrane via lipid anchors [Alexandrov et al., 1994; Desnoyers et al., 1996]. Rab proteins can influence the membrane compositions, especially the content of phosphatidylinositol phosphates (PIPs) [Christoforidis et al., 1999; Shin et al., 2005], and, thereby trigger maturation [Renzis et al., 2002; Rink et al., 2005] and subcellular trafficking of the vesicles [Jordens et al., 2001; Hales et al., 2002; Johansson et al., 2007].

Directly after abscission, early endosomes are covered with Rab5, which, amongst other functions, triggers the generation of PI(3)P [Schu et al., 1993]. This, in turn, can recruit EEA1 which binds PI(3)P via its Fab1-YOTB-Vac1-EEA1 (FYVE) domain [Stenmark et al., 1996; Dumas et al., 2001; Stenmark et al., 2002] and induces early endosome fusion [Simonsen et al., 1998; Dumas et al., 2001].

Cargos within these early endosomes can have opposing destinies: recycling or degradation. The former is either accomplished by recycling to the plasma membrane in $Rab11^+$ recycling endosomes [Ullrich et al., 1996] or by retrograde transport to the Golgi apparatus catalysed by the retromer complex [Seaman, 2004]. The degradation route is initiated by the maturation of early endosomal vesicles to late endosomes, which is accompanied by a shift from Rab5 to Rab7 [Rink et al., 2005]. These $Rab7^+$ vesicles display an increase in intraluminal vesicles (ILVs) transforming them into multivesicular bodies (MVBs). The ILVs are generated with the help of the endosomal sorting complexes required for transport (ESCRT) machinery [Katzmann et al., 2001; Teis et al., 2008] or ESCRT-independent pathway, e.g. involving the sphingolipid ceramide or the tetraspanin cluster of differentiation 63 (CD63) [Trajkovic et al., 2008; van Niel et al., 2011; Edgar et al., 2014]. ILVs contain not only membrane proteins from the vesicle's limiting membrane, but also cytosolic components engulfed during ILV generation [Gibbings and Voinnet, 2010; Sahu et al., 2011]. Besides the classical view that ILVs are targeted for degradation, MVBs were also found to fuse with the plasma membrane releasing the ILVs as so-called exosomes [Raposo et al., 1996; Escola et al., 1998; Kobayashi et al., 2000] and therefore, functioning in intercellular communication [Korkut et al., 2009; Sheldon et al., 2010].

The maturation of endosomes is also accompanied by a drop in pH to 6.0-4.8 [Maxfield and Yamashiro, 1987], which is mainly achieved by an accumulation of vacuolar ATPases (v-ATPases) in late endosomes [Trombetta et al., 2003; Lafourcade et al., 2008]. To protect the limiting membrane from the increasingly acidic lumen the incorporation of glycoproteins, like lysosomal-associated membrane protein 1 LAMP1, is initiated at this stage [Szymanski et al., 2011].

3.4.3 Lysosomes and endolysosomes

The only subcellular compartment with an even lower pH than late endosomes are lysosomes, with a luminal pH of about 4.5 [Maxfield and Yamashiro, 1987]. To maintain the integrity of their limiting membrane, up to 50% of the membrane protein content is represented by the highly glycosylated LAMP1 and LAMP2 [Hunziker et al., 1996]. Primary lysosomes, also called dense-core lysosomes due to their appearance in electron microscopy [Bright et al., 1997], contain more than 60 different acidic hydrolases (proteases, lipases and glycosidases) [Schröder et al., 2010]. They represent a hub for several cellular degradation pathways, including phagocytosis, autophagy as well as endocytosis [Inpanathan and Botelho, 2019]. Fusion of the respective vesicles with lysosomes generates hybrid organelles, termed phagolysosomes, autolysosomes and endolysosomes, respectively, and brings the lysosomal proteases together with the cargos targeted for degradation. The degradation products, amino acids, sugars and lipids, are recycled

back to the cytoplasm [Sagné and Gasnier, 2008] or transported back to the Golgi apparatus [Saftig and Klumperman, 2009] to fuel new anabolic processes.

Beside this well-established function of lysosomes, there is more and more evidence that these vesicles have other functions, e.g. nutrient sensing [Sancak et al., 2010; Zoncu et al., 2011], secretion of proteins to the extracellular space [Rodríguez et al., 1997; Jaiswal et al., 2002; Rao et al., 2004] and as asymmetry factors during cell division as mentioned in chapter 3.3.4.

3.5 Aim of the study

Previous, unpublished data from the Koch lab on human ESC-derived long term (lt)-NES cells [Koch et al., 2009] gave first hints that vesicles might act as asymmetry factors during human NSC division. Taken together with studies from the *D. melanogaster* and zebrafish nervous system and recently in mammalian hematopoietic stem cells, segregation of vesicles might represent an asymmetry mechanism conserved across species and stem cell populations.

Therefore, the first aim of this thesis was to confirm vesicle asymmetries in iPSC-derived NSCs, to identify the exact vesicular compartment in an unbiased screening and to link asymmetries during mitosis to neuronal differentiation.

In the second part of the study, Notch as a cell fate determinant crucially involved in neurodevelopment was the focus of attention. The role of known Notch regulators, like Numb, during asymmetric cell division of mammalian NSCs is still inconclusive. Therefore, an additional regulatory mechanism of the Notch signalling pathway via the internalization of the receptors was suggested and evaluated in the human NSC model system.

To finally establish a functional connection of vesicle asymmetries and Notch signalling during cell division, two state-of-the-art technologies shall be utilized: the CRISPR/Cas9 technology and the organoid model system. The former should be used to establish a new HES1-reporter cell line and explore Notch signalling activity in living, actively dividing cells. The latter was employed to replicate essential findings in a 3D setting more closely resembling *in vivo* neurogenesis.

4 Material

4.1 Cell lines

Table 1: Cell lines

Cell line	Source	Donor/genetic background	Cell type	Reprogramming method
Ctrl#1 iPSC	Bonn, Germany	healthy, male age 33	dermal fibroblasts	Sendai virus
Ctrl#2 iPSC	Mannheim, Germany	healthy, female age 44	dermal fibroblasts	Sendai virus
HES1-reporter	This thesis	Ctrl#2 iPSC	N/A	N/A

4.2 Cell culture reagents

All cell culture reagents were prepared under sterile conditions or sterile-filtered after preparation.

Table 2: Cell culture media and solutions

Wash medium			
Concentration	Substance	Distributor (headquarter)	Cat. #
	DMEM/F12	Invitrogen (Carlsbad, USA)	11320074
1% (v/v)	Penicillin/Streptomycin	Invitrogen (Carlsbad, USA)	15140122
Essential 8 (E8) medium			
Concentration	Substance	Distributor (headquarter)	Cat. #
	DMEM/F12 with HEPES	Invitrogen (Carlsbad, USA)	11330057
1% (v/v)	Penicillin/Streptomycin	Invitrogen (Carlsbad, USA)	15140122
14 ng/ml	sodium selenite	Sigma-Aldrich (St. Louis, USA)	S5261
64 µg/ml	L-ascorbic acid phosphate	Sigma-Aldrich (St. Louis, USA)	A8960
20 µg/ml	Insulin	Sigma-Aldrich (St. Louis, USA)	91077C
11 µg/ml	Transferrin	Sigma-Aldrich (St. Louis, USA)	T3705
100 ng/ml	FGF2-154	Cell Guidance Systems (Cambridge, UK)	GFH146
1 ng/ml	TGF beta	Cell Guidance Systems (Cambridge, UK)	GFH39
E8 freezing medium			
Concentration	Substance	Distributor (headquarter)	Cat. #
	E8 medium	N/A	N/A
10% (v/v)	DMSO	Sigma-Aldrich (St. Louis, USA)	D5879
10 µM	Y-27632	Cell Guidance Systems (Cambridge, UK)	SM02

Table to be continued on next page

Table continued from previous page

N2 supplement			
Concentration	Substance	Distributor (headquarter)	Cat. #
	DMEM/F12	Invitrogen (Carlsbad, USA)	11320074
1% (v/v)	Penicillin/Streptomycin	Invitrogen (Carlsbad, USA)	15140122
500 µg/ml	Insulin	Sigma-Aldrich (St. Louis, USA)	91077C
10 mg/ml	Transferrin	Sigma-Aldrich (St. Louis, USA)	T3705
520 ng/ml	Sodium selenite	Sigma-Aldrich (St. Louis, USA)	S5261
1.611 mg/ml	Putrescine	Sigma-Aldrich (St. Louis, USA)	51799
630 ng/ml	Progesterone	Sigma-Aldrich (St. Louis, USA)	P8783
Neural induction medium			
Concentration	Substance	Distributor (headquarter)	Cat. #
	DMEM/F12	Invitrogen (Carlsbad, USA)	11320074
1% (v/v)	Penicillin/Streptomycin	Invitrogen (Carlsbad, USA)	15140122
0.5% (v/v)	N2 supplement	N/A	N/A
1% (v/v)	B27 supplement	Invitrogen (Carlsbad, USA)	17504044
1% (v/v)	GlutaMAX	Invitrogen (Carlsbad, USA)	35050038
1% (v/v)	Non-essential amino acids	Invitrogen (Carlsbad, USA)	11140035
4.44 mM	Glucose	Carl Roth (Karlsruhe, Germany)	HN06.2
200 nM	LDN193189	Stemcell Technologies (Vancouver, Canada)	72148
500 nM	A83-01	Tocris Bioscience (Bristol, UK)	2939
2 µM	XAV939	Cell Guidance Systems (Cambridge, UK)	SM38
SM-NSC medium			
Concentration	Substance	Distributor (headquarter)	Cat. #
	DMEM/F12	Invitrogen (Carlsbad, USA)	11320074
1% (v/v)	Penicillin/Streptomycin	Invitrogen (Carlsbad, USA)	15140122
0.5% (v/v)	N2 supplement	N/A	N/A
1% (v/v)	B27 supplement	Invitrogen (Carlsbad, USA)	17504044
1% (v/v)	Glutamine	Invitrogen (Carlsbad, USA)	35050038
4.44 mM	Glucose	Carl Roth (Karlsruhe, Germany)	HN06.2
3 µM	CHIR99021	Cell Guidance Systems (Cambridge, UK)	SM13
500 nM	Purmorphamine	Cell Guidance Systems (Cambridge, UK)	SM30
Rosette-type NSC medium			
Concentration	Substance	Distributor (headquarter)	Cat. #
	DMEM/F12	Invitrogen (Carlsbad, USA)	11320074
1% (v/v)	Penicillin/Streptomycin	Invitrogen (Carlsbad, USA)	15140122
0.5% (v/v)	N2 supplement	N/A	N/A
1% (v/v)	B27 supplement	Invitrogen (Carlsbad, USA)	17504044
8.88 mM	Glucose	Carl Roth (Karlsruhe, Germany)	HN06.2
10 ng/µl	EGF	Cell Guidance Systems (Cambridge, UK)	GFH26
10 ng/µl	FGF2-147	Cell Guidance Systems (Cambridge, UK)	GFH28

Table to be continued on next page

Table continued from previous page

Neuronal differentiation medium			
Concentration	Substance	Distributor (headquarter)	Cat. #
	DMEM/F12	Invitrogen (Carlsbad, USA)	11320074
1% (v/v)	Penicillin/Streptomycin	Invitrogen (Carlsbad, USA)	15140122
0.5% (v/v)	N2 supplement	N/A	N/A
1% (v/v)	B27 supplement	Invitrogen (Carlsbad, USA)	17504044
1% (v/v)	GlutaMAX	Invitrogen (Carlsbad, USA)	35050038
1% (v/v)	Non-essential amino acids	Invitrogen (Carlsbad, USA)	11140035
4.44 mM	Glucose	Carl Roth (Karlsruhe, Germany)	HN06.2
Cytobuffer			
Concentration	Substance	Distributor (headquarter)	Cat. #
240 mM	Myo-Inositol	Sigma-Aldrich (St. Louis, USA)	I5125
5 mg/ml (w/v)	Polyvinylalcohol	Sigma-Aldrich (St. Louis, USA)	P8136
0.2X	PBS	Sigma-Aldrich (St. Louis, USA)	D8537
NSC freezing medium			
Concentration	Substance	Distributor (headquarter)	Cat. #
70% (v/v)	KnockOut™ Serum Replacement	Invitrogen (Carlsbad, USA)	10828028
20% (v/v)	Cytobuffer	N/A	N/A
10% (v/v)	DMSO	Sigma-Aldrich (St. Louis, USA)	D5879
live cell imaging solution			
Concentration	Substance	Distributor (headquarter)	Cat. #
20 mM	HEPES pH 7.4	Carl Roth (Karlsruhe, Germany)	9105
140 mM	NaCl	Sigma-Aldrich (St. Louis, USA)	31434
2.5 mM	KCl	AppliChem (Darmstadt, Germany)	A3582
1.8 mM	$CaCl_2$	Sigma-Aldrich (St. Louis, USA)	31307
1 mM	$MgCl_2$	Merck (Darmstadt, Germany)	105833
10 mM	Glucose	Carl Roth (Karlsruhe, Germany)	HN06.2

Table 3: Chemicals used in cell culture and their respective diluents

Chemicals	Diluent	Distributor (headquarter)	Cat. #
A83-01	DMSO	Tocris Bioscience (Bristol, UK)	2939
BafilomycinA	Ethanol	VWR (Radnor, USA)	J61835.MX
CHIR99021	DMSO	Cell Guidance Systems (Cambridge, UK)	SM13
Cycloheximide	H_2O	Sigma-Aldrich (St. Louis, USA)	C1988
DAPT	DMSO	Cell Guidance Systems (Cambridge, UK)	SM15
DLL1-6xHis	PBS	Sino Biological (Beijing, China)	11635-H08H
DLL1-6xHis	H_2O	R&D Systems (Minneapolis, USA)	1818-DL-050
DMSO	N/A	Sigma-Aldrich (St. Louis, USA)	D5879
Dynasore	DMSO	Cayman Chemical (Ann Arbor, USA)	14062
EGF	H_2O	Cell Guidance Systems (Cambridge, UK)	GFH26
Ethanol	N/A	Sigma-Aldrich (St. Louis, USA)	32205
FGF2-147	H_2O	Cell Guidance Systems (Cambridge, UK)	GFH28
FGF2-154	0.1% BSA in H_2O	Cell Guidance Systems (Cambridge, UK)	GFH146
Insulin	10 mM NaOH	Sigma-Aldrich (St. Louis, USA)	91077C
L-ascorbic acid	H_2O	Sigma-Aldrich (St. Louis, USA)	A4544

Table to be continued on next page

Table continued from previous page

L-ascorbic acid phosphate	H_2O	Sigma-Aldrich (St. Louis, USA)	A8960
Laminin	N/A	Invitrogen (Carlsbad, USA)	23017015
LDN193189	DMSO	Stemcell Technologies (Vancouver, Canada)	72148
Leupeptin	H_2O	SERVA Electrophoresis (Heidelberg, Germany)	51867.02
Nocodazole	DMSO	Sigma-Aldrich (St. Louis, USA)	M1404
Poly-L-Lysine hydrobromide	H_2O	Sigma-Aldrich (St. Louis, USA)	P2636
Progesteron	Ethanol	Sigma-Aldrich (St. Louis, USA)	P8783
Puromycin	H_2O	EMD Millipore (Burlington, USA)	540222
Purmorphamine	DMSO	Cell Guidance Systems (Cambridge, UK)	SM30
Putrescine	H_2O	Sigma-Aldrich (St. Louis, USA)	51799
Sodium selenite	H_2O	Sigma-Aldrich (St. Louis, USA)	A8960
TGFβ	H_2O	Cell Guidance Systems (Cambridge, UK)	GFH39
Transferrin	H_2O	Sigma-Aldrich (St. Louis, USA)	T3705
Trypsin inhibitor	PBS	Invitrogen (Carlsbad, USA)	17075029
XAV939	DMSO	Cayman Chemical (Ann Arbor, USA)	13596
Y-27632	H_2O	Cell Guidance Systems (Cambridge, UK)	SM02

Table 4: Ready-to-use solutions for cell culture

Solution	Distributor (headquarter)	Cat. #
BSA solution (7.5%)	Invitrogen (Carlsbad, USA)	15260037
DPBS	Sigma-Aldrich (St. Louis, USA)	D8537
Geltrex	Invitrogen (Carlsbad, USA)	A1413302
Laminin	Invitrogen (Carlsbad, USA)	23017015
TrypLE Express	Invitrogen (Carlsbad, USA)	12605028
Trypsin-EDTA (10x)	Invitrogen (Carlsbad, USA)	15400054

4.3 Bacteria and respective solutions

Amplification of plasmid DNA was performed in *Escherichia coli* DH5a (New England Biolabs, Cat. #C2987H).

Table 5: Bacterial culture media

SOC medium			
Concentration	Substance	Distributor (headquarter)	Cat. #
2% (w/v)	Bacto-Tryptone	BD Biosciences (Franklin Lakes, USA)	211705
0.5% (w/v)	Yeast Extract	BD Biosciences (Franklin Lakes, USA)	212750
10 mM	NaCl	Sigma-Aldrich (St. Louis, USA)	31434
2.5 mM	KCl	AppliChem (Darmstadt, Germany)	A3582
10 mM	$MgCl_2$	Merck (Darmstadt, Germany)	105833
10 mM	$MgSO_4$	Merck (Darmstadt, Germany)	105886
200 mM	Glucose	Carl Roth (Karlsruhe, Germany)	HN06.2

Table to be continued on next page

Table continued from previous page

LB medium			
Concentration	Substance	Distributor (headquarter)	Cat. #
20% (w/v)	LB medium powder	Carl Roth (Karlsruhe, Germany)	X968.4
100 µg/ml	Ampicillin	Sigma-Aldrich (St. Louis, USA)	A9518
LB agar			
Concentration	Substance	Distributor (headquarter)	Cat. #
20% (w/v)	LB medium powder	Carl Roth (Karlsruhe, Germany)	X968.4
15% (w/v)	Bacto-Agar	BD Biosciences (Franklin Lakes, USA)	214010
100 µg/ml	Ampicillin	Sigma-Aldrich (St. Louis, USA)	A9518

4.4 Plasmids

Table 6: Plasmids used for cloning and nucleofection

Name	backbone	Insert (*promoter*-transgene)	Application	Source	Cat. #
pMK243	pBluescript	AAVS1-*TetOn*-OsTIR1 *PGK*-TetR *PGK*-Puromycin-AAVS1	cloning	Addgene (Watertown, USA)	72835
pSpCas9(BB)-2A-Puro	px459	*U6*-empty *CMV*-Cas9-T2A-Puromycin	cloning	Addgene (Watertown, USA)	62988
Cytbow	pBluescript	PB5'-*CAG*-H2B-EBFP2-tdTomato-mTurquoise2-mEYFP-PB3'	cloning	Loulier et al., 2014	N/A
HES5 reporter	pBluescript	*Hes5-1*-Venus-NLS-PEST-3'UTR$_{Hes5-1}$	cloning	Vilas-Boas et al., 2011	N/A
HES1 gRNA-plasmid	px459	*U6*-HES1 gRNA *CMV*-Cas9-T2A-Puromycin	nucleofection	this thesis	N/A
HES1 HDR-template	pBluescript	HES1 5'HDR-T2A-tdTomato-NLS-PEST-HES1 3'HDR	nucleofection	this thesis	N/A

4.5 PCR and cloning components

All oligonucleotides and primers were purchased from Integrated DNA Technologies, Inc. (Coralville, USA).

Table 7: Primers used for PCRs

Gene/cDNA	forward/ reverse	Sequence (5' -> 3')	Application
18S	forward	AAACGGCTACCACATCCAAG	RT-PCR
	reverse	CCTCCAATGGATCCTCGTTA	
FOXA2	forward	CCACCACCAACCCCACAAAATG	RT-PCR
	reverse	TGCAACACCGTCTCCCCAAAGT	

Table to be continued on next page

Table continued from previous page

FOXG1	forward	CCCTCCCATTTCTGTACGTTT	RT-PCR
	reverse	CTGGCGGCTCTTAGAGAT	
HOXB2	forward	TTTAGCCGTTCGCTTAGAGG	RT-PCR
	reverse	CGGATAGCTGGAGACAGGAG	
HOXB4	forward	ACACCCGCTAACAAATGAGG	RT-PCR
	reverse	GCACGAAAGATGAGGGAGAG	
NES	forward	GGCGCACCTCAAGATGTCC	RT-PCR
	reverse	CTTGGGGTCCTGAAAGCTG	
PAX5	forward	AGGATGCCGCTGATGGAGTAC	RT-PCR
	reverse	TGGAGGAGTGAATCAGCTTGG	
PAX6	forward	CCCCACATATGCAGACACACA	RT-PCR
	reverse	GAACTGACACACCAGGGGAAA	
GAPDH	forward	TCGGAGTCAACGGATTTGGT	qPCR
	reverse	TGAAGGGGTCATTGATGGCA	
HES1	forward	AAAAATTCCTCGTCCCCGGT	qPCR
	reverse	GGCTTTGATGACTTTCTGTGCT	
HES5	forward	TGAAGCACAGCAAAGCCTTC	qPCR
	reverse	GCAGGCACCACGAGTAGC	
HEY1	forward	TAATTGAGAAGCGCCGACGA	qPCR
	reverse	GCTTAGCAGATCCCTGCTTCT	
HES1	forward	CTCGCTGGTACTGCGTTCTC	genotyping
HES1	reverse	TGGGGAGTTTAGGAGGAGGG	genotyping
HES1-T2A	reverse	GGGATTCTCCTCCACGTCACC	genotyping
U6-gRNA	forward	GGGCCTATTTCCCATGATTCCTTCA	genotyping
	reverse	GACTCGGTGCCACTTTTTCAAGTT	
Cas9-Puro	forward	ACAAAGTGCTGTCCGCCTAC	genotyping
	reverse	TCCGGGGAGCACGACG	
Myco	forward	GGGAGCAAACAGGATTAGATACCCT	Mycoplasma PCR
	reverse	TGCACCATCTGTCACTCTGTTAACCTC	

Table 8: Primers and Oligonucleotides used for molecular cloning

Construct	forward/ reverse	Sequence (5' -> 3') with restriction sites/*overhangs associated with restriction sites*
gRNA for HES1 locus	sense	*CACC*GGGAGGCCGTGGCGGAACTGA
	antisense	*AAAC*TCAGTTCCGCCACGGCCTCCC
HES1 5'-homology arm	forward	CGTGAATTCCTGGGGGTCACTGGTTTAG
	reverse	GTTGCGGCCGCACTGTCGACGTTCCGCCACGGCCTC
HES1 3'-homology arm	forward	GAGTCGACAGTACCGGTCGGGAGCTCCACCTCTCTTCCCTCCGG
	reverse	GCAGCGGCCGCTTGCTTTAAGAGGGTGCG
T2A	sense	*TCGA*CGAGGGCAGAGGAAGTCTTCTAACATGCGGTGACGTGGA GGAGAATCCCGGCCCTA
	antisense	*CCGG*TAGGGCCGGGATTCTCCTCCACGTCACCGCATGTTAGAAG ACTTCCTCTGCCCTCG
tdTomato	forward	TGCACCGGTATGGTGAGCAAGGGCGAG
	reverse	ACGGAGCTCGTAACGCGTCTTGTACAGCTCGTCCATG
NLS-PEST	forward	TGCACGCGTCCTCCAAAAAAGAAGAGAAAG
	reverse	TCGGAGCTCCTACACATTGATCCTAGCAG

Table 9: PCR and qPCR reaction mixture

PCR reaction			
Concentration	Substance	Distributor (headquarter)	Cat. #
1X	reaction buffer	Biozym (Hessisch Oldendorf, Germany)	331610
each 500 µM	dNTPs	Steinbrenner Laborsysteme (Wiesenbach, Germany)	SL-Set-S-dNTPs
each 200 nM	Primer	Integrated DNA Technologies (Coralville, USA)	N/A
0.625 U	Taq DNA Polymerase	Biozym (Hessisch Oldendorf, Germany)	331610
200 ng/10 ng	genomic DNA/cDNA	N/A	N/A
1% (v/v)	DMSO (for genomic DNA only)	Sigma-Aldrich (St. Louis, USA)	D5879
qPCR reaction			
Concentration	Substance	Distributor (headquarter)	Cat. #
1X	reaction buffer	Promega (Madison, USA)	M890A
2.5 mM	$MgCl_2$	Promega (Madison, USA)	A351B
each 200 µM	dNTPs	Steinbrenner Laborsysteme (Wiesenbach, Germany)	SL-Set-S-dNTPs
each 100 nM	Primer	Integrated DNA Technologies (Coralville, USA)	N/A
4% (v/v)	DMSO	Sigma-Aldrich (St. Louis, USA)	D5879
1X	Syber® Green I	Sigma-Aldrich (St. Louis, USA)	S9430
25 nM	ROX	GENAXXON (Ulm, Germany)	A351513
0.75 U	GoTaq® DNA Polymerase	Promega (Madison, USA)	M780B
10 ng	cDNA	N/A	N/A

Table 10: PCR and qPCR program

PCR program		
Temperature	Time	Cycles
95°C	5 min	
95°C	20 sec	
60°C	20 sec	35
72°C	1 min/500 bp	
72°C	10 min	
4°C	∞	

qPCR program		
Temperature	Time	Cycles
50°C	2 min	
95°C	10 min	
95°C	20 sec	
60°C	20 sec	40
72°C	20 sec	
95°C	15 sec	
60°C	1 min	
95°C	0.05°C/sec	

4.6 Antibodies

Table 11: Primary antibodies for Western Blot and immunofluorescence (IF) staining with respective permeabilization method

Antigen	Host	Dilution		Distributor (headquarter)	Cat.#
		IF (permeab.)	Western Blot		
Actin	mouse		1:10,000	Cell Signaling Technology (Danvers, USA)	3700
Clathrin	rabbit	1:50 (Saponin)		Cell Signaling Technology (Danvers, USA)	4796
GAD65	mouse	1:250 (Saponin)		Biolegend (San Diego, USA)	844502
GFAP	mouse	1:500 (Triton)		Synaptic Systems (Göttingen, Germany)	173011
EEA1	rabbit		1:1,000	Cell Signaling Technology (Danvers, USA)	3288
EEA1	mouse	1:100 (Saponin)		Cell Signaling Technology (Danvers, USA)	48453S
6xHis-tag	chicken	1:500 (Saponin)		Biotrend (Cologne, Germany)	CHIS-45A-Z
HuC/D	mouse	1:500 (Triton)		Thermo Fisher Scientific (Waltham, USA)	A-21271
LAMP1	mouse	1:400 (Saponin)		Developmental Studies Hybridoma Bank (Iowa City, USA)	H4A3
LAMP1	rabbit	1:200 (Saponin)	1:1,000	Cell Signaling Technology (Danvers, USA)	9091
CD63	mouse	1:400 (Saponin)		ExBio Praha (Vestec, Czech Republic)	11-343-C100
LC3A/B	rabbit	1:100 (Saponin)		Cell Signaling Technology (Danvers, USA)	12741S
MAP2	chicken	1:6000 (Triton)		Biolegend (San Diego, USA)	822501
Nestin	mouse	1:600 (Triton)		R&D Systems (Minneapolis, USA)	MAB-1259
NeuN	rabbit	(1:100) Triton		Cell Signaling Technology (Danvers, USA)	24307
Notch1	rabbit	1:200 (Saponin)	1:1,000	Cell Signaling Technology (Danvers, USA)	4380
Notch1 ICD	rabbit		1:1,000	Cell Signaling Technology (Danvers, USA)	4147
Notch1 ECD	mouse	1:50 (Saponin)		Biolegend (San Diego, USA)	819101
Notch2	rabbit	1:200 (Saponin)	1:500	Cell Signaling Technology (Danvers, USA)	4530
OKT3/4	mouse	1:500 (Triton)		Santa Cruz Biotechnology (Dallas, USA)	sc5279
PAX6	rabbit	1:500 (Triton)		Biolegend (San Diego, USA)	901301
PKCλ	mouse	1:100 (Triton)		BD Bioscience (Franklin Lakes, USA)	610208
Pre-senilin1	mouse		1:1,000	Biolegend (San Diego, USA)	823404

Table to be continued on next page

Table continued from previous page

Rab5	mouse	1:100 (Saponin)		Cell Signaling Technology (Danvers, USA)	46449S
Rab7	rabbit	1:100 (Saponin)		Cell Signaling Technology (Danvers, USA)	9367T
Rab11	rabbit	1:100 (Saponin)		Cell Signaling Technology (Danvers, USA)	5589T
Sara/ ZFYVE9	rabbit	1:100 (Saponin)	1:1,000	Sigma-Aldrich (St. Louis, USA)	HPA065852
SOX2	rabbit	1:500 (Triton)		Cell Signaling Technology (Danvers, USA)	3579
SSEA4	mouse	1:100 (Triton)		Developmental Studies Hybridoma Bank (Iowa City, USA)	MC-813-70
TAU	guinea pig	1:300		Synaptic Systems (Göttingen, Germany)	314004
TUBB3	guinea pig	1:1,000 (Triton)		Synaptic Systems (Göttingen, Germany)	302 304
VGLUT1	guinea pig	1:200 (Saponin)		Synaptic Systems (Göttingen, Germany)	135304
ZO-1	rat	1:50 (Triton)		Developmental Studies Hybridoma Bank (Iowa City, USA)	R26.4C

Table 12: Secondary antibodies for IF staining and Western Blot

Antigene	Conjugate	Dilution	Distributor (headquarter)	Cat. #
mouse IgG	DyeLight680	1:15,000	Cell Signaling Technology (Danvers, USA)	5470
mouse IgG	DyeLight800	1:15,000	Cell Signaling Technology (Danvers, USA)	5257
rabbit IgG	DyeLight800	1:15,000	Cell Signaling Technology (Danvers, USA)	5151
chicken	AF633	1:1,000	Invitrogen (Carlsbad, USA)	A21103
guinea pig	AF555	1:1,000	Invitrogen (Carlsbad, USA)	A21435
mouse	AF568	1:1,000	Invitrogen (Carlsbad, USA)	A11004
mouse	AF647	1:1,000	Invitrogen (Carlsbad, USA)	A21236
rabbit	AF488	1:1,000	Invitrogen (Carlsbad, USA)	A11008
rabbit	AF647	1:1,000	Invitrogen (Carlsbad, USA)	A21244
rat	AF555	1:1,000	Invitrogen (Carlsbad, USA)	A21434

Table 13: Fluorescent probes

Reagent	Conjugate	Dilution/ Concentration	Distributor (headquarter)	Cat. #
Choleratoxin subunit B	AF555	10 µg/ml	Molecular Probes (Eugene, USA)	C-34776
DAPI	N/A	300 nM	Biolegend (San Diego, USA)	422801
LysoTracker™ DeepRed	N/A	0.1 nM	Thermo Fisher Scientific (Waltham, USA)	L12492
Phalloidin	ATTO565	1:2000	ATTO-TEC (Siegen, Germany)	AD 565-81

4.7 Enzymes

Table 14: Enzymes used in molecular biology

Name	Distributor (headquarter)	Cat. #
DNase I, Amplification Grade	Sigma-Aldrich (St. Louis, USA)	AMPD1
GoTaq® G2 Flexi DNA Polymerase	Promega (Madison, USA)	M780B
Phusion® High-Fidelity DNA Polymerase	New England Biolabs (Ipswich, USA)	M0530S
T4 DNA Ligase	New England Biolabs (Ipswich, USA)	M0202L
T4 Polynucleotide kinase	New England Biolabs (Ipswich, USA)	M0201S
Taq DNA Polymerase	Biozym (Hessisch Oldendorf, Germany)	331610
AgeI-HF	New England Biolabs (Ipswich, USA)	R3552S
BbsI	New England Biolabs (Ipswich, USA)	R0539S
EcoRI-HF	New England Biolabs (Ipswich, USA)	R3101S
MluI-HF	New England Biolabs (Ipswich, USA)	R3198L
NotI-HF	New England Biolabs (Ipswich, USA)	R3189L
SacI-HF	New England Biolabs (Ipswich, USA)	R3156S
SalI-HF	New England Biolabs (Ipswich, USA)	R3138S

4.8 Kits

Table 15: Kits

Name	Distributor (headquarter)	Cat. #
ExtractMe Genomic DNA	blirt (Gdańsk, Poland)	EM13-050
Cell Line Nucleofector™ Kit V	Lonza (Basel, Swiss)	VCA-1003
iScript cDNA synthesis	Bio-Rad Laboratories (Hercules, USA)	1708891BUN
peqGOLD Gel extraction kit	VWR (Radnor, USA)	12-2501-02
peqGOLD Plasmid miniprep kit	VWR (Radnor, USA)	12-6942-02
peqGOLD TriFast	VWR (Radnor, USA)	30-2010
pHrodo iFL Green Microscale Protein Labeling Kit	Thermo Fisher Scientific (Waltham, USA)	P36015
PierceTM BCATM Protein-Assay	Thermo Fisher Scientific (Waltham, USA)	23227
PureLink™ HiPure Plasmid Filter Midiprep Kit	Thermo Fisher Scientific (Waltham, USA)	K210015

4.9 Chemicals, buffers and solutions

Table 16: Chemicals

Name	Distributor (headquarter)	Cat. #
30% Bis/Acrylamide	Carl Roth (Karlsruhe, Germany)	3029.1
Agarose	Sigma-Aldrich (St. Louis, USA)	A9539
Chloroform	Sigma-Aldrich (St. Louis, USA)	32211
DEPC	Carl Roth (Karlsruhe, Germany)	K028.1
DMSO	Sigma-Aldrich (St. Louis, USA)	D5879
Ethanol	Th. Geyer (Renningen, Germany)	2246.1000

Table to be continued on next page

Table continued from previous page

FBS	Invitrogen (Carlsbad, USA)	10270-106
37% HCl	Th. Geyer (Renningen, Germany)	836.1000
2-Propanol	Th. Geyer (Renningen, Germany)	1157
PeqGreen	VWR (Radnor, USA)	732-3196
PFA	Sigma-Aldrich (St. Louis, USA)	16005
Powdered milk	Carl Roth (Karlsruhe, Germany)	T145.3
10x Tris-Tricine-SDS buffer	Sigma-Aldrich (St. Louis, USA)	T1165

Table 17: Molecular ladders

Name	Distributor (headquarter)	Cat. #
Quick-Load® 100 bp DNA ladder	New England Biolabs (Ipswich, USA)	N0467L
Protein ladder PS10 Plus (11-180 kDa)	GeneOn (Ludwigshafen am Rhein, Germany)	310003

Table 18: Buffers and solutions for IF staining

1X PBS			
Concentration	Substance	Distributor (headquarter)	Cat. #
137 mM	NaCl	Th. Geyer (Renningen, Germany)	1367
2.7 mM	KCl	Th. Geyer (Renningen, Germany)	1632
10 mM	Na_2HPO_4	Th. Geyer (Renningen, Germany)	8622
1.8 mM	KH_2PO_4	Th. Geyer (Renningen, Germany)	1648
Acetic acid buffer			
Concentration	Substance	Distributor (headquarter)	Cat. #
200 mM	Acetic acid pH 2.0	Sigma-Aldrich (St. Louis, USA)	33209
500 mM	NaCl	Sigma-Aldrich (St. Louis, USA)	31434
Mounting solution			
Concentration	Substance	Distributor (headquarter)	Cat. #
100 mM	Tris-HCl pH 8.5	Carl Roth (Karlsruhe, Germany)	4855.5
25% (v/v)	Glycerol	Sigma-Aldrich (St. Louis, USA)	15523
10% (w/v)	Mowiol 4-88	Sigma-Aldrich (St. Louis, USA)	81381
0.6% (w/v)	DABCO	Carl Roth (Karlsruhe, Germany)	0718.2

Table 19: Buffers and solutions used for the work with DNA

Lysis buffer for DNA isolation			
Concentration	Substance	Distributor (headquarter)	Cat. #
100 mM	Tris-HCl pH 8.5	Carl Roth (Karlsruhe, Germany)	4855.5
200 mM	NaCl	Sigma-Aldrich (St. Louis, USA)	31434
5 mM	EDTA	Thermo Fisher Scientific (Waltham, USA)	147850010
0.2 % (w/v)	SDS	Carl Roth (Karlsruhe, Germany)	CN30.1
133 ng/µl	Proteinase K	GeneOn (Ludwigshafen am Rhein, Germany)	405-001
1X TAE			
Concentration	Substance	Distributor (headquarter)	Cat. #
40 mM	Tris	Carl Roth (Karlsruhe, Germany)	4855.5
20 mM	Acetic acid	Sigma-Aldrich (St. Louis, USA)	33209
1 mM	EDTA	Thermo Fisher Scientific (Waltham, USA)	147850010

Table to be continued on next page

Table continued from previous page

10X DNA loading buffer			
Concentration	Substance	Distributor (headquarter)	Cat. #
50 mM	Tris-HCl pH 7.6	Carl Roth (Karlsruhe, Germany)	4855.5
60% (v/v)	Glycerol	Sigma-Aldrich (St. Louis, USA)	15523
0.25% (w/v)	Bromophenol blue	Sigma-Aldrich (St. Louis, USA)	B-8026

Table 20: Buffers and solutions for sucrose gradient centrifugation

Sucrose solution			
Concentration	Substance	Distributor (headquarter)	Cat. #
10-50% (w/v)	Sucrose	Sigma-Aldrich (St. Louis, USA)	S9378
3 mM	Imidazole pH 7.4	Sigma-Aldrich (St. Louis, USA)	I5513
1 mM	EDTA	Thermo Fisher Scientific (Waltham, USA)	147850010
Homogenization buffer A			
Concentration	Substance	Distributor (headquarter)	Cat. #
3 mM	Imidazole pH 7.4	Sigma-Aldrich (St. Louis, USA)	I5513
1 mM	EDTA	Thermo Fisher Scientific (Waltham, USA)	147850010
Homogenization buffer B			
Concentration	Substance	Distributor (headquarter)	Cat. #
500 mM	Sucrose	Sigma-Aldrich (St. Louis, USA)	S9378
3 mM	Imidazole pH 7.4	Sigma-Aldrich (St. Louis, USA)	I5513
1 mM	EDTA	Thermo Fisher Scientific (Waltham, USA)	147850010
0.06 mM	Cycloheximide	Sigma-Aldrich (St. Louis, USA)	C1988
1X	Protease inhibitor	Thermo Fisher Scientific (Waltham, USA)	A32955

Table 21: Buffers and solutions for protein biochemistry

Lysis buffer for protein isolation			
Concentration	Substance	Distributor (headquarter)	Cat. #
50 mM	Tris-HCl pH 7.4	Carl Roth (Karlsruhe, Germany)	4855.5
150 mM	NaCl	Sigma-Aldrich (St. Louis, USA)	31434
0.2% (v/v)	Triton X-100	Merck (Darmstadt, Germany)	1.08603
25 mM	EDTA	Thermo Fisher Scientific (Waltham, USA)	147850010
0.2% (w/v)	SDS	Carl Roth (Karlsruhe, Germany)	CN30.1
1X	Protease inhibitor	Thermo Fisher Scientific (Waltham, USA)	A32955
6X Protein loading buffer			
Concentration	Substance	Distributor (headquarter)	Cat. #
93.75 mM	Tris-HCl pH 6.8	Carl Roth (Karlsruhe, Germany)	4855.5
6% (w/v)	SDS	Carl Roth (Karlsruhe, Germany)	CN30.1
6% (v/v)	Glycerol	Sigma-Aldrich (St. Louis, USA)	15523
9% (v/v)	beta-Mercaptoethanol	Merck (Darmstadt, Germany)	805740
0.25% (w/v)	Bromophenol blue	Sigma-Aldrich (St. Louis, USA)	B-8026

Table to be continued on next page

Table continued from previous page

SDS-PAGE gel buffer			
Concentration	Substance	Distributor (headquarter)	Cat. #
3 M	Tris-HCl pH 8.45	Carl Roth (Karlsruhe, Germany)	4855.5
0.3% (w/v)	SDS	Carl Roth (Karlsruhe, Germany)	CN30.1
SDS-Polyacrylamide separating gel			
Concentration	Substance	Distributor (headquarter)	Cat. #
33.3% (v/v)	SDS-PAGE gel buffer	N/A	N/A
10% (v/v)	Bis/Acrylamide	Carl Roth (Karlsruhe, Germany)	3029.1
10% (v/v)	Glycerol	Sigma-Aldrich (St. Louis, USA)	15523
0.028% (w/v)	Ammonium persulfate	Sigma-Aldrich (St. Louis, USA)	A3678
0.09% (v/v)	TEMED	Sigma-Aldrich (St. Louis, USA)	T9281
SDS-Polyacrylamide stacking gel			
Concentration	Substance	Distributor (headquarter)	Cat. #
24.8% (v/v)	SDS-PAGE gel buffer	N/A	N/A
3.84% (v/v)	Bis/Acrylamide	Carl Roth (Karlsruhe, Germany)	3029.1
0.0672% (w/v)	Ammonium persulfate	Sigma-Aldrich (St. Louis, USA)	A3678
0.224% (v/v)	TEMED	Sigma-Aldrich (St. Louis, USA)	T9281
SDS-PAGE anode buffer			
Concentration	Substance	Distributor (headquarter)	Cat. #
200 mM	Tris-HCl pH 8.8	Carl Roth (Karlsruhe, Germany)	4855.5
Western Blot transfer buffer			
Concentration	Substance	Distributor (headquarter)	Cat. #
25 mM	Tris	Carl Roth (Karlsruhe, Germany)	4855.5
192 mM	Glycine	Thermo Fisher Scientific (Waltham, USA)	G/0800/60
20% (v/v)	Methanol	VWR (Radnor, USA)	20847.307
0.08% (w/v)	SDS	Carl Roth (Karlsruhe, Germany)	CN30.1
1X TBS-T			
Concentration	Substance	Distributor (headquarter)	Cat. #
50 mM	Tris-HCl pH 7.4	Carl Roth (Karlsruhe, Germany)	4855.5
150 mM	NaCl	Sigma-Aldrich (St. Louis, USA)	31434
0.1% (v/v)	TWEEN®20	Sigma-Aldrich (St. Louis, USA)	P2287
Stripping buffer			
Concentration	Substance	Distributor (headquarter)	Cat. #
25 mM	Glycine pH 2.0	Thermo Fisher Scientific (Waltham, USA)	G/0800/60

4.10 Consumables

Table 22: Consumables

Consumables		Distributor (headquarter)	Cat. #
Cell culture dishes	3.5 cm	Sarstedt (Nümbrecht, Germany)	833900
	3.5 cm	ibidi (Gräfelfing, Germany)	81156
	3.5 cm + 4 well insert	ibidi (Gräfelfing, Germany)	80406
	6 cm	Sarstedt (Nümbrecht, Germany)	833901300

Table to be continued on next page

Table continued from previous page

Cell culture plates	6-well	Sarstedt (Nümbrecht, Germany)	833920005
	24-well	Sarstedt (Nümbrecht, Germany)	833922300
	48-well	Sarstedt (Nümbrecht, Germany)	833923300
	384-well	ibidi (Gräfelfing, Germany)	88411
Cell scraper		Santa Cruz Biotechnology (Dallas, USA)	sc-395251
Coverslips	12 mm	VWR (Radnor, USA)	631-1577
Cryovials	1 ml	Greiner (Kremsmünster, Austria)	123280
Blotting membrane	Nitrocellulose 0.2 µm	GE Healthcare (Chicago, USA)	10600001
Filter bottles	1 l; 0.2 µm	Sarstedt (Nümbrecht, Germany)	833942001
Filter paper		Kimberly-Clark Professional (Irving, USA)	6035080
Microscopy slides		Carl Roth (Karlsruhe, Germany)	H868.1
qPCR plate		Steinbrenner Laborstysteme (Wiesenbach, Germany)	4TI-0910/C
qPCR seal		Steinbrenner Laborstysteme (Wiesenbach, Germany)	4ti-0500
Pasteur pipette		Th. Geyer (Renningen, Germany)	7691061
PCR strips	8x 200 µl	Biozym (HESsisch Oldendorf, Germany)	710971
Petri dishes	10 cm	Corning (Corning, USA)	351029
Pipette tips	10 µl	Sarstedt (Nümbrecht, Germany)	701130
	200 µl	Sarstedt (Nümbrecht, Germany)	70760002
	1250 µl	Sarstedt (Nümbrecht, Germany)	701186
Serological pipettes	5 ml	Sarstedt (Nümbrecht, Germany)	861253001
	10 ml	Sarstedt (Nümbrecht, Germany)	861254001
	25 ml	Sarstedt (Nümbrecht, Germany)	861685001
Syringes	1 ml	B. Braun (Melsungen, Germany)	2023-02-01
	20 ml	BD Biosciences (Franklin Lakes, USA)	300296
	50 ml	Sarstedt (Nümbrecht, Germany)	946077137
Syringe filter	0.2 µm	Sarstedt (Nümbrecht, Germany)	831826001
Syringe needles	22G x 1 ¼”	BD Biosciences (Franklin Lakes, USA)	300900
Tubes	0.5 ml	Sarstedt (Nümbrecht, Germany)	72699
	1.5 ml	Sarstedt (Nümbrecht, Germany)	72690001
	2 ml	Th. Geyer (Renningen, Germany)	7695840
	15 ml	Sarstedt (Nümbrecht, Germany)	62554502
	50 ml	Sarstedt (Nümbrecht, Germany)	62547254
Ultracentrifuge tubes	14x95 mm	Beckman Coulter (Brea, USA)	344060

4.11 Technical equipment

Table 23: Technical equipment

Appliance	Name	Distributor (headquarter)
Agarose gel electrophoresis chamber	EasyPhor Midi	Biozym (Hessisch Oldendorf, Germany)
Agarose gel imaging system	GeneFlash	Syngene International (Bangalore, India)

Table to be continued on next page

Table continued from previous page

Autoclave	Laboklav	SHP Steriltechnik AG (Detzel Schloss, Germany)
Balance	BL610	Sartorius (Göttingen, Germany)
Balance	BP121S	Sartorius (Göttingen, Germany)
Block heater	Thermomixer comfort	Eppendorf (Hamburg, Germany)
Centrifuge	Labofuge 400R	Heraeus (Hanau, Germany)
Centrifuge	Z216MK	Hermle (Gosheim, Germany)
Centrifuge	5415D	Eppendorf (Hamburg, Germany)
Confocal microscope	TCS SP5 II	Leica (Wetzlar, Germany)
Counting chamber	Neubauer improved	Paul Marienfeld (Lauda-Königshofen, Germany)
Epifluorescence microscope	DM6 B	Leica (Wetzlar, Germany)
Freezer -80°C	Hera freeze	Thermo Fisher Scientific (Waltham, USA)
Freezer -150°C	VIP plus	Panasonic (Kadoma, Japan)
Freezing container	Mr. Frosty™	Thermo Fisher Scientific (Waltham, USA)
Incubator	C170 E3	Binder (Tuttlingen, Germany)
Inverse light microscope	DMIL LED	Leica (Wetzlar, Germany)
Liquid nitrogen store	Cryotech	Thermo King (Minneapolis, USA)
Live cell microscope	Celldiscoverer 7	Carl Zeiss (Oberkochen, Germany)
Micro-Spectrophotometer	NanoDrop®	Thermo Fisher Scientific (Waltham, USA)
Micropipettes	Transferpette®	Brand (Wertheim, Germany)
Nucleofector	Nucleofector II	Lonza (Basel, Swiss)
PAGE equipment	Mini-PROTEAN® Tetra System	Bio-Rad Laboratories (Hercules, USA)
Power supply for agarose gel electrophoresis	EPS301	Amersham plc (Little Chalfont, UK)
Power supply for SDS-PAGE	PowerPac Basic	Bio-Rad Laboratories (Hercules, USA)
PCR cycler	PTC-200	Bio-Rad Laboratories (Hercules, USA)
pH-meter	pH 597	WTW (Weilheim in Oberbayern, Germany)
Pipette-boy	Pipet Filler S1	Thermo Fisher Scientific (Waltham, USA)
Platereader	PowerWave XS	BIOTEK (Winooski, USA)
qPCR cycler	QuantStudio 7 Flex	Thermo Fisher Scientific (Waltham, USA)
Sonicator	Sonifier 250	Thermo Fisher Scientific (Waltham, USA)
Sterile laminar flow hood	Scanlaf Mars	Labogene (Lillerød, Denmark)
Table centrifuge	C1301-230V	Corning (Corning, USA)
Ultracentrifuge	L-70	Beckman Coulter (Brea, USA)
Vacuum pump	FTA-1	Thermo Fisher Scientific (Waltham, USA)
Vortexer	Bio Vortex V1	VWR (Radnor, USA)
Water conditioner	Milli-Q Q-POD	EMD Millipore (Burlington, USA)
Water bath		Thermo Fisher Scientific (Waltham, USA)
Western Blot equipment	Trans-Blot® Turbo™	Bio-Rad Laboratories (Hercules, USA)
Western blot imaging system	Odyssey	Li-Cor (Lincoln, USA)

4.12 Data processing and software

Table 24: Software for data processing

Software	Supplier (headquarter)
ApE – A plasmid editor	M. Wayne Davis
BioRender	BioRender (Toronto, Canada)
Excel 2019	Microsoft (Redmond, USA)
ImageJ	NIH (Rockville, USA)
Image Studio	Li-Cor (Lincoln, USA)
Leica Application Suite AF	Leica (Wetzlar, Germany)
Leica Application Suite X	Leica (Wetzlar, Germany)
Prism6	GraphPad (San Diego, USA)
QuantStudio Software	Thermo Fisher Scientific (Waltham, USA)
RStudio	RStudio (Boston, USA)
ZEN	Carl Zeiss (Oberkochen, Germany)

5 Methods

5.1 Cell culture

All cell types were handled under sterile conditions and maintained at 37°C and 5% CO_2 in 6-well plates unless otherwise stated. All medium and buffer compositions mentioned in this chapter can be found in Table 2. Media and solutions were stored at 4°C and prewarmed to room temperature (RT) before use.

5.1.1 Coating of cell culture plates, dishes and coverslips

For maintenance of all cell types, cell culture plates were coated with 1% (v/v) Geltrex (in Wash medium) overnight at 4°C or for 1 h at 37°C.

Coverslips for immunofluorescence (IF) staining were treated with 37% HCl for 1 h at RT. After 3 washing steps with dH_2O and an additional wash with 70% Ethanol, coverslips were autoclaved. These pre-treated coverslips as well as ibidi-plates and -dishes were coated with 100 µg/ml Poly-L-Lysin (in 25 mM boric acid, pH 8.4) overnight at 4°C. After 2 washing steps with ddH_2O, 2.5 µg/ml Laminin (in DPBS) was added and incubated overnight at 4°C or 2 h at 37°C.

5.1.2 Culturing and passaging of iPSCs

iPSCs were maintained in feeder-free conditions in E8 medium and medium was changed every day. Cultures were split once the colonies grow 70-90% confluent. Passaging was performed with 500 µM EDTA (in DPBS) by washing once and then incubating the cells at RT for 3-4 min in the solution. EDTA was removed and cells were washed from the plate using fresh E8 medium supplemented with 5 µM Y-27632. IPSC-colonies in suspension were transferred to a new, coated culture plate in a 1:6-1:10 ratio. Medium was changed after one day to E8 medium without Y-27632.

5.1.3 Cryopreservation of iPSCs

To cryopreserve iPSCs, an almost confluent well of a 6-well plate was treated with 500 µM EDTA (in DPBS) as described in chapter 5.1.2 and washed from the plate with Wash medium. Colonies were sedimented at 500 x g for 4 min and carefully resuspended in 1 ml of E8 freezing medium. Cyro vials were frozen in Isopropanol at -80°C and transferred to -150°C after 2-3 days.

Cryopreserved iPSC-colonies were quickly thawed at 37°C and carefully transferred to 14 ml of Wash medium. Colonies were sedimented at 500 x g for 4 min, resuspended in E8 medium supplemented with 10 µM Y-27632 and plated on one well of a 6-well plate. If necessary,

medium was changed after a few hours to remove dead cells and refresh the Y-27632. Next day, medium was changed to E8 medium without Y-27632.

5.1.4 Induction of SM-NSCs

Neural fate was induced by inhibiting Smad- and Wnt-signalling pathways in iPSCs (see also chapter 3.1.2). Therefore, a single cell suspension of iPSCs was prepared by treating the cells with TrypLE for 10 min at 37°C. TrypLE was diluted in Wash medium, cells were resuspended and the single cell suspension was centrifuged at 1200 x g for 4 min. Cell pellet was resuspended in E8 medium supplemented with 5 µM Y-27632 and plated in a 2:1 ratio on a coated well plate. Medium was changed to neural induction medium once the cells formed a confluent monolayer, usually on the day after the passaging. Afterwards, medium was changed every day for a total of 9-10 days, adapting the applied medium volume to the everyday consumptions. After this patterning phase, cells were split in a low density with TrypLE (as mentioned above) and the medium was changed to SM-NSC medium. Neural progenitor cells were kept at very low densities until the typical colony morphology can be observed and no spontaneous differentiation was visible anymore.

5.1.5 Culturing and passaging of SM-NSCs

Medium of SM-NSCs was changed every day and every other day on weekends. Cells were passaged by treatment with 1X Trypsin/EDTA (in DPBS) for 5 min at 37°C. Trypsin reaction was stopped by adding an equal volume of 0.5 mg/ml Trypsin inhibitor (in DPBS). Cells were resuspended and centrifuged at 1200 x g for 4 min. Pellet was resuspended in SM-NSC medium and transferred to a new, coated plate in a 1:4-1:10 ratio.

5.1.6 Cryopreservation of SM-NSCs

Single cell suspension of SM-NSCs was prepared as described in chapter 5.1.5. After centrifugation at 1200 x g for 4 min, cell pellet was carefully resuspended in 0.5 ml SM-NSC freezing medium per well. Cells were frozen in isopropanol at -80°C and transferred to -150°C after 2-3 days.

Thawing of cryopreserved SM-NSCs was performed at 37°C and cell suspension was transferred to 14 ml of Wash medium. Cells were sedimented at 1200 x g for 4 min, resuspended in SM-NSC medium and transferred to 1-2 wells of a 6-well plate, dependent on the pellet size.

5.1.7 Induction of rosette-type NSC and neuronal differentiation

SM-NSCs can be shifted to rosette-type NSCs by changing the medium to rosette-type NSC medium containing FGF2 and EGF as growth factors. In this condition, NSCs still proliferate, but in comparison to SM-NSCs show a certain amount of spontaneous differentiation. All experiments within the scope of this thesis were performed on rosette-type NSCs, whereas SM-NSCs were only used as a highly proliferative pre-amplifier cell type. NSCs were kept as rosette-type NSCs until the first spontaneous neuronal differentiation was visible, but for at least 3 days, before starting any experiment.

Maintenance and passaging of rosette-type NSCs are identical with the procedures for SM-NSCs descripted in chapter 5.1.5. For differentiation of rosette-type NSCs, medium was changed to neuronal differentiation medium for 4 weeks with 2 media changes per week.

5.1.8 DNA isolation and Mycoplasma polymerase chain reaction (PCR)

To exclude Mycoplasma contamination, all cells were regularly screened by PCR. Therefore, cells were washed twice with PBS and remove from the plate using a cell scraper. 150 µl lysis buffer was added and cells were lysed for 1 h at 37°C and 400 rpm. Proteinase K was inactivated afterwards by 10 min incubation at 95°C. DNA was precipitated by addition of 105 µl 2-propanol and incubation for 30 min at RT. After centrifugation for 10 min at 12,000 x g, the DNA pellet was washed twice with 75% (v/v) ethanol (in ddH_2O). The DNA pellet was air-dried, resuspended in 100 µl ddH_2O and DNA concentration was determined spectrophotometrically. DNA samples can be stored at -20°C until further analysis.

PCR reaction mixture, PCR program and the used primers to detect Mycoplasma DNA can be found in Tables Table 9, Table 10 and Table 7, respectively.

PCR products were analysed by agarose gel electrophoresis using 1% (w/v) Agarose (in 1X TAE) supplemented with 0.007% PeqGreen. After completion of the PCR reaction, the mix was diluted with DNA loading dye (final 1X) and subjected to electrophoresis with 100 V for 45 min.

DNA isolation and Mycoplasma PCR were kindly performed by Helene Schamber.

5.2 Generation of HES1-tdTomato reporter line

For targeted editing of the endogenous *HES1* locus, the Clustered regulatory interspaced palindromic repeats/CRISPR-associated protein 9 (CRISPR/Cas9) technology was utilized. This system was originally described as an adaptive defence mechanism in bacteria [Ishino et al., 1987; Mojica et al., 2000; Bolotin et al., 2005; Mojica et al., 2005; Pourcel et al., 2005] and is based on the nuclease activity of Cas9 [Makarova et al., 2006], which is directed to specific loci

via a guide RNA (gRNA). After the adoption of the system for usage in mammalian cells [Jinek et al., 2012], a variety of gene editing technologies arose, which highjack the cell-intrinsic DNA damage repair pathways activated by the Cas9-induced DNA double strand break. Here, the homology-directed repair (HDR) pathway [Kakarougkas and Jeggo, 2014] was used to insert an exogenous cassette encoding for a fluorescent reporter protein into the endogenous *HES1* locus.

5.2.1 Molecular cloning

To generate the HDR template, the two homology arms, corresponding to 889 bp upstream and 885 bp downstream of the gRNA binding site were amplified from genomic DNA isolated from Ctrl#2 iPSCs by PCR (for DNA isolation see chapter 5.1.8). Respective primer sequences can be found in Table 8 and PCR was performed as indicated in Table 9 and Table 10. PCR products were separated using Agarose gel electrophoresis as described above (chapter 5.1.8) and DNA fragments were isolated from the gel using the *peqGOLD Gel extraction kit* according to the manufacturer's protocol. DNA fragments and the backbone (pBluescript from pMK243) were incubated with the appropriate restriction enzymes in CutSmart buffer (final 1X; all from New England Biolabs) for 1 h at 37°C. Digested homology arms and the linearized backbone were purified again via Agarose gel electrophoresis and gel extraction. In the first step, the 5' homology arm (5'-HDR) was ligated to the backbone using T4 DNA Ligase with its respective buffer and an incubation for 1 h at RT. *Escherichia coli* DH5α were transformed by heat-shock at 42°C for 42 sec with the ligation mixture, plated on LB-Agar plates and clones were picked the next day. Overnight LB cultures of 5 ml were inoculated and used for plasmid isolation with the *peqGOLD Plasmid miniprep kit* according to the manufacturer's protocol. After screening of clones by restriction digestion, this plasmid was used as the backbone to insert the 3' homology arm (3'-HDR) in the same fashion. Between the two homology arms, the reporter was constructed starting with the T2A site. The respective oligonucleotides were annealed and phosphorylated by incubation with T4 Polynucleotide kinase for 30 min at 37°C, heating the mixture to 95°C for 5 min and slow cooling to 25°C at 0.1°C/sec. The backbone (containing the 5'- and 3'-HDR) was linearized using the appropriate restriction enzymes for 1 h at 37°C. Annealed oligonucleotides and the backbone were ligated and transformed as described above. In the final two steps, the tdTomato- and the NLS-PEST-sequences were amplified from the Cytbow-plasmid [Loulier et al., 2014] and the HES5 reporter-plasmid [Vilas-Boas et al., 2011], respectively. Restriction digestion, ligation and transformation was performed as described for the homology arms. The final HDR template was send for Sanger sequencing at Microsynth Seqlab GmbH (Göttingen, Germany) to exclude mutations.

The gRNA sequence targeting the last exon of the *HES1* locus was adapted from [Schmid-Burgk et al., 2016] and corresponds to bp 1834 to 1853 of the HES1 mRNA (Table 8). The oligonucleotides coding for the gRNA were annealed and phosphorylated as described for the T2A site. The target vector (pSpCas9(BB)-2A-Puro) was linearized with BbsI for 1 h at 37°C and purified using the *peqGOLD Gel extraction kit*. Ligation and transformation were performed as previously described. The correct insertion of the gRNA sequence was confirmed by Sanger sequencing performed by Microsynth Seqlab GmbH (Göttingen, Germany).

Both plasmids were further amplified using 200 ml-LB cultures of bacteria and the *PureLink™ HiPure Plasmid Filter Midiprep Kit* according to the manufacturer's protocol. The DNA concentration was measured spectrophotometrically and the plasmid preparations were used for nucleofection (chapter 5.2.2). Sequences for both plasmids can be found in the Appendix.

5.2.2 Nucleofection and clone selection

CRISPR/Cas9-mediated genome editing was performed on Ctrl#2-iPSCs using the Nucleofector II and the Cell Line Nucleofector™ Kit V (both Lonza). According to the manufacturer's protocol, provided buffers were equilibrated to RT before usage. The reaction mix was prepared by mixing 82 µl of Nucleofector™ Solution V with 18 µl of Supplement 1 and 1 µg of each plasmid, HES1 gRNA-plasmid and HES1 HDR-template.

IPSC colonies with a 60-70% confluency were treated with TrypLE for 10 min at 37°C. TrypLE was diluted with Wash medium to a total volume of 2 ml. Cells were resuspended and counted using a Neubauer counting-chamber. 1,000,000 cells were transferred to a 2 ml reaction tube and centrifuged at 500 x g for 5 min. Medium was removed completely and cell pellet was resuspended in 100 µl of reaction mix (see above). Cell suspension was transferred to the provided cuvette avoiding any air bubbles. Program B-027 of the Nucleofector II was applied and nucleofected cells were transferred to 900 µl of Penicillin/Streptomycin-free E8 medium with 5 µM Y-27632. After carefully resuspending, 400, 300, 200 and 100 µl were plated on one well of a 6-well plate each and medium was added up to 1.5 ml. As a control, non-nucleofected cells were seeded at the same densities.

Next day, medium was changed additionally adding 0.33 µg/ml Puromycin. On day 2 after nucleofection, Penicillin/Streptomycin was reintroduced to the medium. On day 3-4, Puromycin was withdrawn from the medium dependent on whether the non-nucleofected control cells of the respective cell density were completely dead. Hereafter, half of the medium was changed every day and Y-27632 was withdrawn once small colonies had formed.

Colonies were picked, as soon as, they reached an appropriate size or in case differentiation was visible in the centre of a colony. Therefore, cultures were pre-treated for 2 h with 5 µM Y-27632

(in E8 medium), colonies were picked manually and transferred to a 48-well plate with fresh E8 medium supplemented with 10 µM Y-27632. Half of the medium was changed every day. Clones were passaged with EDTA (see chapter 5.1.2) to two wells of a 12-well plate, of which one well was used for maintenance and the other for DNA isolation and subsequent genotyping and Mycoplasma PCR (see chapters 5.1.8 and 5.2.3).

Clones, which were identified by genotyping PCR to have integrated the reporter construct at the correct locus were expanded and cryopreserved back-ups were generated from several early passages (see chapter 5.1.3). Further, SNP analysis (chapter 5.2.4) was performed and SM-NSCs were induced (chapter 5.1.4) from promising clonal cell lines.

5.2.3 Genotyping PCR

DNA was isolated as described in chapter 5.1.8. PCR reaction was set up as described in Table 9 and Table 10 using the primers found in Table 7.

PCR products were analysed by agarose gel electrophoresis, as already described in chapter 5.1.8.

5.2.4 Single nucleotide polymorphism (SNP) analysis

Analysis of single nucleotide polymorphisms (SNPs) was performed to identify potential major karyotypic abnormalities in the edited cell line. Therefore, genomic DNA from one of the first passages after picking was isolated using the *ExtractMe Genomic DNA* kit according to the manufacturer's protocol.

900 ng of genomic DNA was sent to be analysed by Life&Brain Genomics (Bonn, Germany) using an Infinium® Global Screening Array-24 BeadChip (Illumina; San Diego, USA) and results were kindly processed by Josef Frank (Department of Genetic Epidemiology in Psychiatry – Central Institute for Mental Health, Mannheim).

5.3 RNA biology

5.3.1 RNA isolation

RNA was isolated to analyse gene expression in rosette-type NSCs. *PEQGOLD TriFast* was used for the isolation of RNA from 70-80% confluent wells of a 6-well plate according to the manufacturer's protocol. Cells were washed twice with ice-cold DPBS and resuspended by pipetting in 1 ml TriFast per well. After an incubation for 5 min at RT, lysate was transferred to a 1.5 ml reaction tube, 200 µl chloroform were added and mixed well by vortexing 15 sec. An incubation for 10 min at RT leads to separation of water and phenol phase, which were further

separated by centrifugation at 12,000 x g for 5 min. The upper, watery phase containing the RNA was transferred to a new 1.5 ml reaction tube and 500 µl of 2-propanol was added to precipitate the RNA. Mixture was incubated overnight at -20°C and then centrifuged 15 min at 12,000 x g and 4°C. RNA pellet was washed twice with 1 ml 75% ethanol (in DEPC-treated ddH_2O) and centrifuged for 10 min at 12,000 x g and 4°C. After the last centrifugation, pellet was air-dried and resuspended in 20 µl DEPC-treated ddH_2O by incubation for 30 min at 37°C and 400 rpm.
Potential contamination with genomic DNA was removed by the treatment of the RNA samples with DNase I (Sigma-Aldrich). To each sample 2.5 µl of DNase I and 2.5 µl of the respective reaction buffer was added and mixture was incubated for 15 min at RT. DNase I was inactivated by adding 2.5 µl of the provided stop solution and incubating 10 min at 70°C.
RNA concentration was determined spectrophotometrically and RNA samples were stored at -80°C.

5.3.2 Complementary DNA (cDNA) synthesis and reverse transcriptase-PCR (RT-PCR)

cDNA synthesis was performed with 0.5-1 µg of RNA using the *iScript cDNA synthesis* kit. Therefore, RNA was mixed with 4 µl of 5x iScript Reaction Mix and 1 µl of iScript Reverse Transcriptase and the reaction mix was added up to 20 µl with DEPC-treated ddH_2O. Mixture was incubated 5 min at 25°C, 20 min at 46°C and 1 min at 95°C. cDNA solution was then diluted to 10 ng/µl with ddH_2O and used for RT-PCR and qPCR (chapter 5.3.3), respectively.
For RT-PCR, primers, reaction mix and PCR program can be found in Table 7, Table 9 and Table 10, respectively.
PCR products were analysed by agarose gel electrophoresis using 1.5% (w/v) Agarose (in 1X TAE) supplemented with 0.007% PeqGreen. PCR reaction mix was diluted with DNA loading dye (final 1X) and subjected to electrophoresis with 100 V for 20 min.

5.3.3 Quantitative PCR (qPCR)

To analyse the activity of the Notch signalling pathway, the expression of downstream gene was quantified by qPCR. Therefore, rosette-type NSCs were treated with 20 µM DAPT, 100 nM Bafilomycin (BafA), 200 µM Leupeptin (Leu) or 0.1% (v/v) DMSO (all in rosette-type NSC medium) for 2 h before harvesting and RNA isolation (see chapter 5.3.1). After cDNA synthesis (see chapter 5.3.2), the qPCR reaction mix was prepared as indicated in Table 9 with the respective primers from Table 7. After running the qPCR program indicated in Table 10, threshold cycle (Ct) values and melting curves were calculated by the QuantStudio software. Relative fold changes were determined using the ΔΔCt method [Livak and Schmittgen, 2001] with GAPDH as a reference gene.

5.4 Protein biochemistry

5.4.1 Sucrose density gradient centrifugation

Sucrose gradients can be used to separate intracellular vesicles and other membranous structures, such as ER and mitochondria, according to their size and protein content. Thereby, the accumulation of proteins of interest can be analysed within subcellular compartments.

The sucrose density gradient centrifugation was performed as previously described with small adjustments [Araùjo et al., 2008] and the respective solutions can be found in Table 20. The sucrose gradient was prepared with Sucrose solutions ranging from 10-50% Sucrose with 5% increments. 1 ml of each solution was added to an ultracentrifuge tube (starting with 50% Sucrose) and frozen on dry-ice, before the next solution was added. The prepared gradients were stored at -80°C and slowly thawed at 4°C before use. The thawing process leads to slow mixture of the different phases and thereby, a continuous sucrose gradient was formed.

Rosette-type NSCs were cultured on 10 cm-dishes and two confluent dishes were used for one sucrose gradient. Cells were washed thrice with ice-cold DPBS, removed from the plate with a cell scraper and transferred to a 15 ml-falcon tube. Cells were sedimented for 5 min at 200 x g and 4°C. Supernatant was removed completely and pellet was washed once with 3 times the pellet volume of homogenization buffer A without resuspending the pellet. Cells were again centrifuged for 10 min at 200 x g and 4°C. The pellet was resuspended carefully in one time the pellet volume of homogenization buffer A until no big cell clumps were visible and incubated for 20 min on ice. An equal volume of homogenization buffer B was added. Cells were lysed by passaging them 10-times through a 22G syringe needle. Nuclei should stay intact by that procedure and were sedimented for 10 min at 2,000 x g and 4°C. The supernatant containing all cytosolic proteins and subcellular structures were carefully transferred on top of the Sucrose gradient and centrifugation was performed in an ultracentrifuge for 16 h at 210,000 x g and 4°C. After the separation, 500 µl fractions were collected and snap frozen in liquid nitrogen. Vesicular structures were disrupted by 3 freeze-thaw cycles using a water bath at 37°C and liquid nitrogen. Fractions were stored at -80°C until analysed by SDS-PAGE and Western Blot (chapters 5.4.3 and 5.4.4).

5.4.2 Preparation of protein extracts

Protein lysates from rosette-type NSCs were prepared from confluent wells of a 6-well plate. To analyse the activation of Notch signalling pathway, cells were treated before harvesting for 2 h with 20 µM DAPT, 100 nM BafA, 200 µM Leu or 0.1% (v/v) DMSO (all in rosette-type NSC medium). Cells were washed twice with ice-cold DPBS and removed from the plate with a cell

scraper. For cell lysis, 100 µl protein lysis buffer was added per well and mixed by pipetting. Suspension was incubated 10 min at RT and 50 min on ice vortexing once and a while. Genomic DNA was sheared by sonification using 20% duty cycles, 50% output and 7 pulses. Cell debris was removed by centrifugation for 15 min at 16.000 x g and 4°C. Supernatants were transferred to a new reaction tube and the protein concentration was determined using the *Pierce™ BCA protein assay* kit according to the manufacturer's protocol. Protein samples were stored at -20°C until analysed by SDS-PAGE and Western Blot (chapters 5.4.3 and 5.4.4).

5.4.3 Sodium dodecyl sulphate-polyacrylamide gel electrophoresis (SDS-PAGE)

For protein analysis via SDS-PAGE, 20 µg of protein extracts (chapter 5.4.2) or 40 µl of Sucrose gradient fractions (chapter 5.4.1) were diluted in protein loading dye (final 1X) and incubated at 95°C for 5 min. Samples were loaded on SDS-polyacrylamide gels and Tris-Tricine buffer and anode buffer was added to the cathode and anode compartment, respectively (see Table 21). Electrophoresis was started with a constant voltage of 30 V until the samples were concentrated at the stacking gel boarder, then voltage was increased to 110 V.

5.4.4 Western Blot

After SDS-PAGE, proteins were transferred from the gel onto a Nitrocellulose membrane, which were pre-soaked together with the filter paper in Western Blot transfer buffer (Table 21). Transfer was performed with the Trans-Blot® Turbo™ transfer system (Bio-Rad) and a constant current of 1 A for 45 min. Afterwards, membranes were blocked for 1 h in 5% (w/v) milk powder in TBS-T. Proteins of interest were stained with primary antibodies diluted in 5% (w/v) milk powder in TBS-T overnight at 4°C. Membranes were washed thrice with TBS-T for 10 min and secondary antibodies diluted in TBS-T were added for 1 h at RT in the dark. Membranes were washed again thrice with TBS-T for 10 min and imaged with the Odyssey imaging system (Li-Cor). To analyse cleaved Notch1 ICD and unprocessed Notch1 receptors on the same membrane, membranes stained for Notch1 ICD were stripped and reprobed with Notch1 antibody. Stripping was achieved by incubating the membrane once for 5 min and once for 40 min in stripping buffer (Table 21). Stripped membranes were washed thrice with TBS-T for 10 min and the staining procedure was repeated starting with membrane blocking.

5.5 Immunofluorescence (IF) staining and analysis

5.5.1 IF staining of 2D cultured cells

Rosette-type NSCs were passaged onto coated coverslips as described in chapter 5.1.5 in a density of 100,000 cells/coverslip and usually cultivated for 3 days after the split, unless otherwise stated. For the basic characterization of SM-NSCs and iPSCs, cells were passaged as described in chapters 5.1.2 and 5.1.5, respectively, with an appropriate ratio and cultured for at least 3 more days before fixation and staining.

Before staining, cells were washed once with PBS and fixed with 4% PFA (in PBS) for 10 min at RT. After one brief washing step with PBS, PFA-reaction was quenched by adding 25 mM Glycine (in PBS) for 10 min at RT. Cells were washed again briefly in PBS and then blocked for 1 h at RT. Blocking solution of 10% FBS (in PBS) was used and dependent on the primary antibody supplemented with either 0.1% Saponin or 0.3% Triton X-100 for permeabilization (see Table 11). Afterwards primary antibodies were diluted in the respective blocking solution and incubated with the cells overnight at 4°C. Cells were washed thrice with either Saponin-supplemented blocking solution or PBS for 10 min and incubated for 1 h at RT with secondary antibodies diluted in respective blocking solution. Where appropriate, secondary antibody solution was supplemented with 1:2000 Phalloidin-ATTO565. To remove excess antibodies, cells were washed twice with PBS and then DNA was counterstained with DAPI for 10 min at RT. One final washing step with PBS and one with ddH_2O were performed and coverslips were mounted on object slides with mounting solution.

To establish the dependency of Notch receptor colocalization with vesicles on Dynamin-mediated endocytosis, cells were treated with 50 µM Dynasore (in rosette-type NSC medium) for 1 h at 37°C before fixation and staining.

For labelling of lipid rafts with Choleratoxin subunit B (CTB), living cells were incubated with 10 µg/ml CTB (in rosette-type NSC medium) for 1 h at 4°C. Fixation was performed as described above and cells were blocked in 10% FBS (in PBS) for 1 h. Notch1 ECD on the cell surface was stained by overnight incubation with primary antibody diluted in blocking solution. After three washing steps with PBS for 10 min, cell were blocked again with 10% FBS (in PBS) supplemented with 0.1% Saponin. The second primary antibody against Clathrin was added and the IF staining was finished as described above.

For analysis of Notch ligand internalization, cells were incubated with 10 ng/ml of DLL1 or JAG1 (in rosette-type NSC medium) for up to 30 min at 37°C. To stop the internalization process the cells were placed on ice and washed with ice-cold PBS once. To remove non-internalized ligands from the cell surface, coverslips were washed in acetic acid buffer for 5 min on ice with slight

agitation. Before continuing with the staining protocol described above, cells were washed 4-5 times extensively with ice-cold PBS to restore pH.

5.5.2 IF staining of 3D organoid sections

Forebrain organoids for IF staining were generously generated by Ammar Jabali as described previously [Krefft et al., 2018] and PFA-fixed at day 20 after embryoid body formation. Cryo-sectioning was kindly performed by Helene Schamber.

The cryo-sections were thawed for 15 min at RT and rehydrated in PBS for 5 min. Then, sections were subjected to the same staining procedure as described for 2D cultures (chapter 5.5.1), starting with blocking and permeabilization with 0.3% Triton X-100 and 10% FCS (in PBS).

5.5.3 Image acquisition

2D cell cultures for basic characterization of cell types and for colocalization and asymmetry quantification were imaged using Leica DM6 B microscope. For higher magnification recordings of lipid rafts/Clathrin-pits and the Notch ligand internalization, the Leica confocal TCS SP5 II microscope was used. Overview images of the 3D organoid slices were taken at the Leica DM6 B microscope and sections were pre-screened for DAPI and Phalloidin staining to identify dividing cells. These mitotic events were then imaged at the Leica confocal TCS SP5 II microscope for further quantification.

5.5.4 Colocalization analysis

For colocalization analysis the small volume computational clearing (SVCC) algorithm from the Leica Application Suite X software was applied to reduce background fluorescence and the recorded z-stacks were collapsed using maximum intensity projection in ImageJ. Regions of interest (ROIs) for individual cells were set manually and $DAPI^+$ nuclear regions were excluded from the analysis. The ImageJ plugin *EzColocalization* was used to process a batch of images and calculate Spearman's and Manders' coefficients [Stauffer et al., 2018]. The threshold for the LAMP1 and Notch staining was set to 10% and 20%, respectively.

5.5.5 Asymmetry quantification in 2D

Asymmetric segregation of vesicle markers and Notch receptors was analysed in rosette-type NSCs, which were cultured in normal growth conditions (+FGF2) or in FGF2-withdrawal conditions (-FGF2) for 3 days.

Z-stacks recorded from individual mitotic events in late telophase were collapsed using sum intensity projection in ImageJ. ROIs for the two daughter cells were set manually based on

Phalloidin staining, the sum intensity density was calculated for each daughter cell and background was subtracted. For the analysis of vesicle asymmetries, the daughter cell with the higher sum intensity density was defined as *cell1* and the asymmetry index A was calculated as in (1).

$$(1) \qquad A = \frac{\text{intensity} \sum cell1 - \text{intensity} \sum cell2}{\text{intensity} \sum cell1 + \text{intensity} \sum cell2}$$

With that, A ranges from 0, indicating a completely symmetric distribution of the respective vesicle marker, to 1, indicating a perfect segregation to daughter *cell1*. An asymmetric cell division was defined as a mitotic event with A > 0.2.

For the correlation of LAMP1 and Notch1/2 signal, definition for *cell1* and *cell2* was maintained from the LAMP1 quantification and A(Notch) was calculated as in (1). Thereby, positive values for A indicate segregation of Notch receptors and LAMP1 to the same daughter cell, whereas negative A indicates a Notch receptor accumulation in the daughter cell with less LAMP1 signal. Besides, the DAPI signal and the area of the daughter cells were analysed in the same manner and daughter cell pairs with A(DAPI) or A(area) > 0.2 were excluded from further analysis.

5.5.6 Asymmetry quantification in 3D

For the asymmetry quantification in organoid sections, the mitotic events were first grouped into planar, intermediate and delaminating based on the Phalloidin staining and the relation to the apical membrane. Planar divisions had similar amount of contact area of both daughter cells with the apical membrane, delaminating divisions showed attachment of only one daughter and in intermediate divisions both daughter cells had contact with the apical membrane, but to a clearly divergent extent.

The ROIs for the daughter cells were set based on the Phalloidin staining in each of the individual z-planes. The respective intensity sums were quantified by ImageJ and summed for each daughter cell in Excel. Then the same formula as described for the analysis of 2D cultures was applied to calculate A(LAMP1) and A(Notch1) (see (1) in chapter 5.5.5). The definition of daughter *cell1* and *cell2* was performed as follows: for delaminating and intermediate divisions *cell1* is the daughter cell with more contact to the apical membrane and for planar divisions daughter cells were randomly assigned as *cell1* and *cell2*.

For each batch of organoids, sections from at least 2-3 organoids were analysed.

5.6 Live cell imaging

For most of the live cell imaging experiments the Celldiscoverer 7 (Zeiss) was used. For the generation of kymographs of the Notch ligand internalization additional time-lapse videos were recorded at the Leica TCS SP5 II confocal microscope. The microscope chamber was equilibrated to 37°C (and 5% CO_2 at the Celldiscoverer 7) before the start of an imaging session.

5.6.1 Labelling of recombinant DLL1-His with pHrodo and live cell imaging

To visualize the dynamics of Notch ligand internalization one of the recombinant ligands, namely DLL1, was labelled with the *pHrodo iFL Green Microscale Protein Labeling Kit* according to the manufacturers' protocol. In brief, recombinant DLL1-peptide was reconstituted at 500 µg/ml in ddH_2O and 10 µl of 1 M sodium bicarbonate was added to 100 µl of this peptide solution. pHrodoTM iFL STP ester was reconstituted in DMSO and 6.1 µl of the 2 mM pHrodo solution was added to the peptide solution. After a 15 min incubation at RT in the dark, the labelled peptide was purified using the provided spin columns and gel resin. DLL1-pHrodo solution was aliquoted and stored at -20°C.

For live cell imaging, rosette-type NSCs were plated in a 384-well ibidi plate in a density of 15,000 cells/well and cultivated for 3 more days. Before imaging, medium was replaced by imaging buffer (Table 2) and cells were loaded with 0.1 nM LysoTracker for 30 min at 37°C. 5 µl of DLL1-pHrodo solution were added to 25 µl of imaging buffer and the imaging was started 5 min afterwards. Z-stacks of 7 µm (step size 0.5 µm) were recorded at 3 different locations within one well. The time between frames was set to 200 sec and cells were observed up to 1 h after DLL1-pHrodo addition.

To analyse the dependency of DLL1 internalization on Dynamin-mediated endocytosis, cells were pre-treated while LysoTracker loading with 50 µM Dynasore for 30 min.

For kymograph analysis, rosette-type NSCs were seeded in a density of 10,000 cells/well on a 3.5 cm ibidi dish with a 4 well insert and cultured for 3 days. Medium was replaced by imaging buffer containing 100 nM LysoTracker and cells were incubated for 30 min. Directly before imaging, 2 µl of pHrodo-labelled DLL1 was added to 10 µl of buffer. A single z-plane was imaged over a period of 1 h with a frame time of 30 sec. Kymographs were generated using the ImageJ plugin *Multi Kymograph* with a linewidth of 9 pixels.

5.6.2 Imaging of HES1-tdTomato reporter NSCs

For time-lapse imaging of HES1-tdTomato reporter, the rosette-type NSCs of the HES1-reporter line and the respective wild-type line (Ctrl#2) were seeded on 24-well plates in a ratio of 1:10 at

a cell density of 100,000 cells/well and cultured for 3 days. Medium was changed 10 min before the start of the imaging and was supplemented with 100 µM Cycloheximide, 20 µM DAPT, 100 nM BafA, 200 µM Leu or 0.1% (v/v) DMSO. Cells were observed for 10-12 h with 10 min between frames. At least 3 tile regions per condition were imaged in each experiment and analysis of the fluorescence intensity densities was performed in ImageJ by manually tracking 2-4 nuclei per video.

5.6.3 LysoTracker imaging during cell division and tracking of daughter cells

To analyse the functional outcome of asymmetric segregation of acidic vesicles, live cell imaging of mitotic events was performed and daughter cells were tracked after cell division. Therefore, rosette-type NSCs of the HES1-reporter line were mixed in a 1:10 ratio with respective wild-type Ctrl#2 NSCs and 400,000 cells were seeded on a 3.5 cm ibidi dish. After 3 days, medium was changed to rosette-type NSC medium supplemented with 75 nM Nocodazole and cells were further cultivated for 4-5 h. Then, cells were washed twice extensively with Wash medium and fresh rosette-type NSC medium supplemented with 0.1 nM LysoTracker was added. Imaging was started 30 min after the first washing step. For the first 90 min, a z-stack of 7 µm (step size 0.5 µm) was acquired for up to 30 tile regions with a frame time of 200 sec to closely observe the mitotic event and the LysoTracker distribution in late telophase. To track the daughter cells over a longer period, single z-planes were recorded from each tile region every 10 min over a period of 2:10 – 10:00 h after removal of Nocodazole.

ImageJ was used for the analysis of LysoTracker asymmetry and for the tracking of the daughter cells. The former was performed equivalent to asymmetry quantification in IF staining (chapter 5.5.5). In brief, background was subtracted using the rolling ball algorithm (with a ball radius of 5 pixels) and z-stacks were collapsed using the sum intensity projection. ROIs for the two daughter cells were set manually based on the brightfield and tdTomato-signal in the time frame representing late telophase. The sum intensity density of LysoTracker was measured in this time frame and the asymmetry index A was calculated as described in formula (1) in chapter 5.5.5. Mitotic events with an A(LysoTracker) > 0.2 were considered asymmetric.

HES1-tdTomato signal of the two daughter cells was analysed starting 1:30 h up to 6:00 h after mitosis (28 time points). Daughter cells were tracked manually in ImageJ, the sum intensity density for tdTomato was measured and values were z-normalized within individual experiments. Time series of daughter cell pairs were then concatenated, in the way that the daughter cell with the higher LysoTracker signal was defined as *cell1* and assigned to time points 1 to 28 and corresponding daughter cell with lower LysoTracker signal (*cell2*) was set to time points 29 to 56. The individual concatenated time series were normalized to the first time point

of *cell2* and rescaled to an intensity range of 0 to 1. Intensity differences within each daughter cell pair were calculated for each time point and averaged for the group of LysoTracker-symmetric and -asymmetric mitotic events. Clustering of time series was performed in R Studio using the *time course inspector* package [Dobrzyński et al., 2020] based on the Euclidean distance of the complete, concatenated time series. Number of clusters was determined after visual inspection of the heatmaps and the mean HES1 expression progression in the daughter cells was calculated for each cluster. Based on this mean HES1 differences between daughter cells, clusters were assigned to four groups to represent symmetric, opposed asymmetric, slightly asymmetric and highly asymmetric HES1 expression.

5.7 Statistical analysis

Quantifications were performed on at least 3 technical replicates and, where applicable, on two independent cell lines. Results are shown as mean ± standard error of the mean (SEM).
Statistical analyses were performed with GraphPad Prism6. To examine whether the percentage of asymmetric vesicle distribution is significantly greater than zero, a one-sample t-test was performed. For comparisons with one variable one-way ANOVA (with Bonferroni post-hoc test) were used. For comparisons of data sets with more than one variable either two-way ANOVA (with Bonferroni post-hoc test) or Kruskal-Vallis test (with Dunn's post hoc test) were applied.
Following significance levels were defined: not significant (n.s.) > 0.05, * $p < 0.05$; ** $p < 0.01$; *** $p < 0.001$.

6 Results

Human iPSC technology offers the opportunity to study neurodevelopment in a human context. With the generation of stably proliferating NSCs it is possible to analyse aspects of stem cell proliferation and differentiation in a highly reproducible and standardized manner. Molecular mechanisms underlying the decision between proliferative or neurogenic cell division were so far mainly studied in non-human model systems, such as *D. melanogaster* and mouse. Human iPSC-derived NSCs can be used both to verify existing mechanistic ideas as well as to establish new human specific mechanistic pathways.

6.1 Human NSCs show high proliferative capacity and differentiate into neurons upon growth factor withdrawal

For this study, two independent iPSC-derived NSC lines were used. iPSCs were generated from dermal fibroblast of adult donors (male, age 33 years for Ctrl#1 and female, age 44 years for Ctrl#2) in the lab of Philipp Koch and neural fate was induced by dual-Smad- and Wnt-inhibition (Figure 6A). SM-NSCs were used as a highly proliferative cell population, growing in colonies and showing minimal amount of spontaneous neuronal differentiation, as visible in brightfield images (Figure 6B). By changing the culture conditions to medium containing FGF2 and EGF as growth factors, rosette-type NSCs were induced. These NSCs showed a typical rosette-

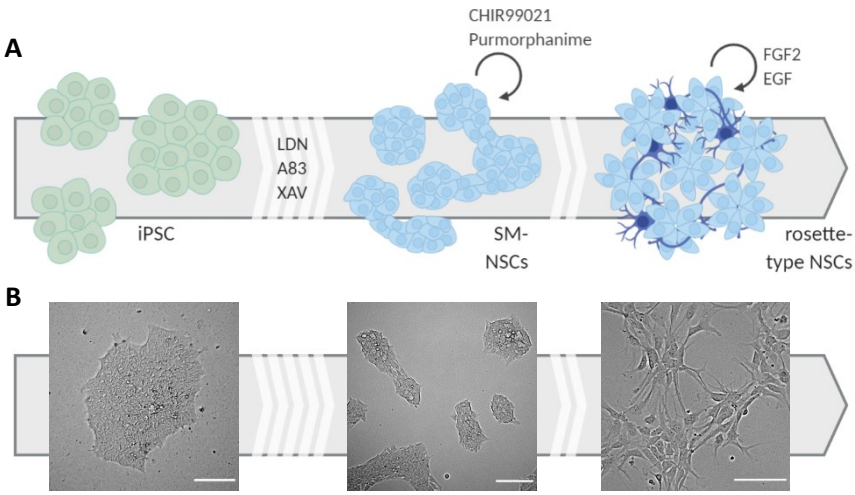

Figure 6: Neural induction of iPSCs and establishment of NSC lines.
(A) Human iPSCs were directed towards neuroectodermal fate by dual-Smad inhibition (LDN193189 and A83-01) and Wnt inhibition (XAV939) for 10 days and NSCs were further amplified as SM-NSCs with Wnt- and Shh-activation (CHIR99021 and Purmorphamine, respectively) forming homogenous colonies. Switch to FGF2-/EGF-containing medium induces a morphological change to rosette-type NSCs, which show a tendency to spontaneous differentiation. (B) Representative brightfield images of the different cell types are shown. Scale (B) 100 µm.

morphology, a continuous proliferative capacity and a small proportion of these cells routinely differentiated into neurons. All following experiments were performed on rosette-type NSC cultures once the first differentiating neurons appear in culture.

To further characterize this cell population, IF staining for typical NSC markers, Nestin and SOX2, and neuronal markers, TUBB3 and HuC/D, was performed. In both cell lines, the vast majority of cells expressed NSC markers and as expected from the cellular morphology, some neuronal differentiation was visible. (Figure 7A). NSCs showed a clear internal apical-basal polarisation within the neural rosettes, indicated by the apical accumulation of tight junction, marked by ZO-1, and the PAR complex component PKCλ (Figure 7B). Numb, however, which is known as an asymmetry factor in *D. melanogaster*, showed no clear intracellular polarization. The regional

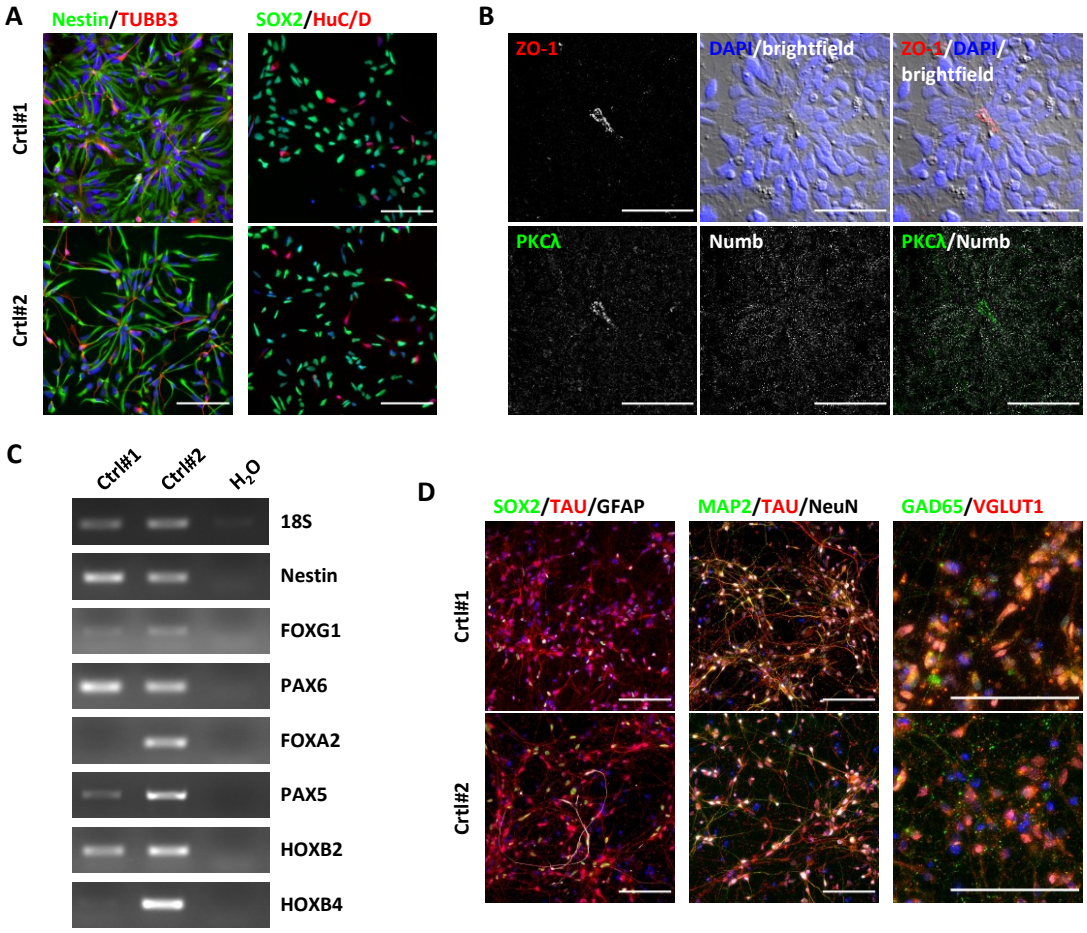

Figure 7: Rosette-type NSCs represent a heterogeneous, polarized NSC population from different brain regions with neurogenic potential.
(A) IF staining of two healthy control NSC lines (Ctrl#1/#2) for the NSC markers Nestin and SOX2 and the early neuronal markers TUBB3 and HuC/D showed rosette morphology and limited amount of spontaneous differentiation. (B) IF staining of Ctrl#1-NSCs for the tight junction component ZO-1 accumulating in the centre of neural rosettes, and the polarity factor PKCλ and asymmetry factor Numb. PKCλ localized apically within the rosette structure, whereas Numb showed no polarized localization. (C) RT-PCR confirmed a mixed regional identity ranging from forebrain (FOXG1, PAX6) to midbrain (FOXA2, PAX5) and hindbrain (HOXB2, HOXB4). (D) IF staining of NSC lines differentiated for 4 weeks for NSC marker (SOX2), mature neuron markers (TAU, MAP2 and NeuN), astrocyte marker (GFAP) and neuronal subtypes (VGLUT1 and GAD65). Scale (A,D) 100 µm, (B) 50 µm. DNA was counterstained with DAPI and depicted in blue pseudo-colour.

identity of the NSCs was analysed in more detail by RT-PCR revealing a heterogeneous expression pattern. In both cell lines, forebrain (FOXG1 and PAX6), midbrain (FOXA2 and PAX5) and hindbrain markers (HOXB2 and HOXB4) were expressed (Figure 7C). However, Ctrl#1-NSCs seemed to be more restricted to dorsal fore-/midbrain and rostral hindbrain areas, with no expression of the floorplate marker FOXA2 and caudal hindbrain marker HOXB4. Proliferation of rosette-type NSCs is dependent on the presence of the two growth factors and withdrawal induces differentiation. After 4 weeks of growth factor withdrawal, only a small percentage of cells still expressed SOX2 as a NSC marker (Figure 7D). The majority of cells differentiated and expressed mature neuronal markers, like TAU, MAP2 and NeuN. In differentiated cultures of the Ctrl#2 line, some cells showed expression of the astrocyte marker GFAP. Both NSC lines were able to produce glutamatergic as well as GABAergic neurons, marked by VGLUT1 and GAD65, respectively.

In case of a short-term FGF2 withdrawal, NSCs kept their self-renewal capacity and stem cell fate for the first days (Figure 8A). However, already at day 5 after withdrawal a reduction in proliferative capacity was detectable by a slight decrease in the overall number of cells compared to cultures treated with FGF2. This effect on proliferation became more evident after 7 days of FGF2 withdrawal. Beside the effect on proliferation, a relative increase in spontaneous neuronal differentiation was detectable (Figure 8B-C). The percentage of HuC/D$^+$ neurons in the -FGF2 condition was slightly increased after 3 days with 14.0%±1.2% compared to 9.3%±0.9% in the +FGF2 condition. The HuC/D$^+$ fraction after FGF2 withdrawal further increased to 18.1%±1.6% at day 5 and 26.2%±2.0% at day 7, which was significantly higher than the spontaneous differentiation observed with FGF2.

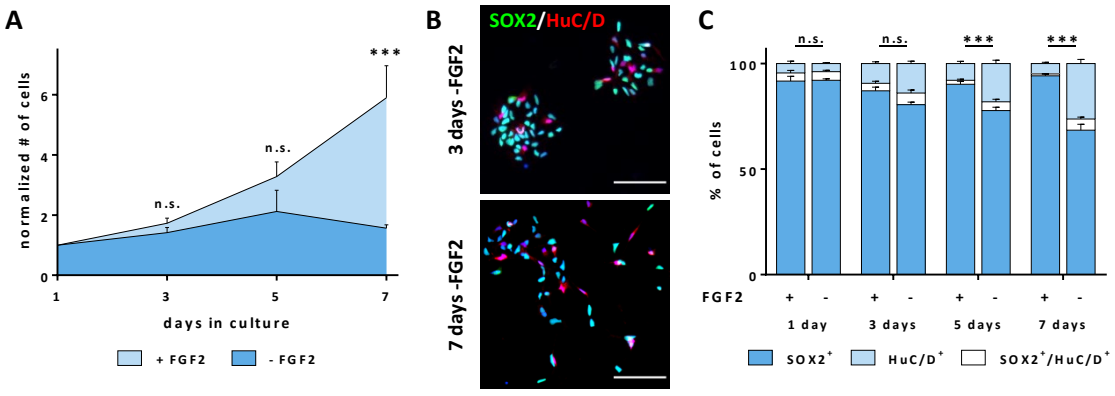

Figure 8: Withdrawal of FGF2 reduces self-renewal capacity and induces neuronal differentiation of NSCs.
(A) Total number of Ctrl#1-NSCs was quantified over the time course of 1 to 7 days after passaging in 10 random fields of view and normalized to day 1 (n = 3, two-way ANOVA with Bonferroni post-hoc test, mean ± SEM). (B-C) IF staining for SOX2 and HuC/D after withdrawal of FGF2 and respective quantification of SOX2$^+$, HuC/D$^+$ and SOX2$^+$/HuC/D$^+$ cells showing proportional increase in neurons over time (n = 3, two-way ANOVA with Bonferroni post-hoc test, mean ± SEM). Scale (B) 100 µm. DNA was counterstained with DAPI and depicted in blue pseudo-colour. *** $p < 0.001$, n.s. – not significant.

With their high proliferative capacity and the broad regional identity, rosette-type NSCs are a versatile tool to analyse global molecular features and pathways of NSC maintenance and differentiation and a good representation for human brain development. Withdrawal of one of the essential growth factors for NSC proliferation, can serve as a trigger for a timed spontaneous differentiation of NSCs to neurons. For the upcoming analysis of potential asymmetry factors in NSCs, 3 days of FGF2 withdrawal was chosen, since at this time point there is on the one hand still some remaining proliferation even without FGF2, on the other hand the switch towards neural differentiation has already started.

6.2 Neural differentiation is associated with an increase in asymmetric segregation of LAMP1$^+$ vesicles

One of the NSC lines (Ctrl#1) was used for an initial screening of different vesicle subtypes that potentially act as asymmetry factors during cell division. To determine the distribution of vesicles between the two daughter cells, an unbiased quantification method was established. The mitotic events in late telophase were identified by DAPI and Phalloidin staining (Figure 9A) and an asymmetry index A was calculated based on IF staining for the respective vesicle marker (for technical details see chapter 5.5.5). A mitotic event was considered asymmetric in case one daughter cell has a 50% higher sum intensity than the other daughter cell ($A > 0.2$).

This first screen was performed in proliferative conditions (+FGF2), as a certain amount of spontaneous differentiation was also found under these culturing conditions (Figure 7A). Neither various endosomal subtypes (marked by EEA1, Rab5, Rab7, Rab11) nor the human Sara orthologue ZFYVE9 or autophagosomes (marked by LC3) were found to be segregated asymmetrically in a significant percentage of mitotic events analysed (Figure 9B). CD63, LAMP1 and LAMP2, however, showed an asymmetric distribution in about 14-25% of cell divisions (Figure 9B-C). CD63 is considered a marker for MVBs and LAMP1/LAMP2 are typical lysosomal marker proteins. Due to the overlap in function and localization of LAMP proteins, all further analyses were concentrated on LAMP1 and CD63 and the asymmetry phenotype was reproduced using the second independent NSC line (Ctrl#2). Under proliferating conditions (+FGF2) similar results for the percentage of LAMP1 asymmetries were found, when comparing the two cell lines: 26.5%±2.8% for Ctrl#1 and 29.7%±2.9% for Ctrl#2 (Figure 9E). For CD63, the percentage of asymmetric cell division was found to be even higher in Ctrl#2-NSCs with 43.3%±2.2% compared to 38.0%±3.9% in Ctrl#1-NSCs (Figure 9D).

To connect these asymmetric cell divisions with neuronal differentiation, asymmetric segregation of CD63$^+$ and LAMP1$^+$ vesicles was quantified under culturing conditions inducing

differentiation (-FGF2). For CD63$^+$ vesicles a withdrawal of FGF2 for 3 days did not change the percentage of asymmetric cell divisions significantly, 20.71±1.63% for Ctrl#1 and 29.96±3.25% for Ctrl#2 (Figure 9D). Conversely, asymmetric distribution of LAMP1 during cell division was increased when FGF2 was removed from the medium. For Ctrl#1-NSCs percentage was increased from 26.53±2.84% to 38.05±3.92% and for Ctrl#2-NSCs from 30.21±2.62% to 40.21±2.83% (Figure 9E). The reproducibility in two independent cell lines suggests a conserved underlying mechanism for the targeted segregation of LAMP1$^+$ vesicles during mitosis of NSCs, whereas CD63 asymmetries cannot be associated with neuronal differentiation in this model system.

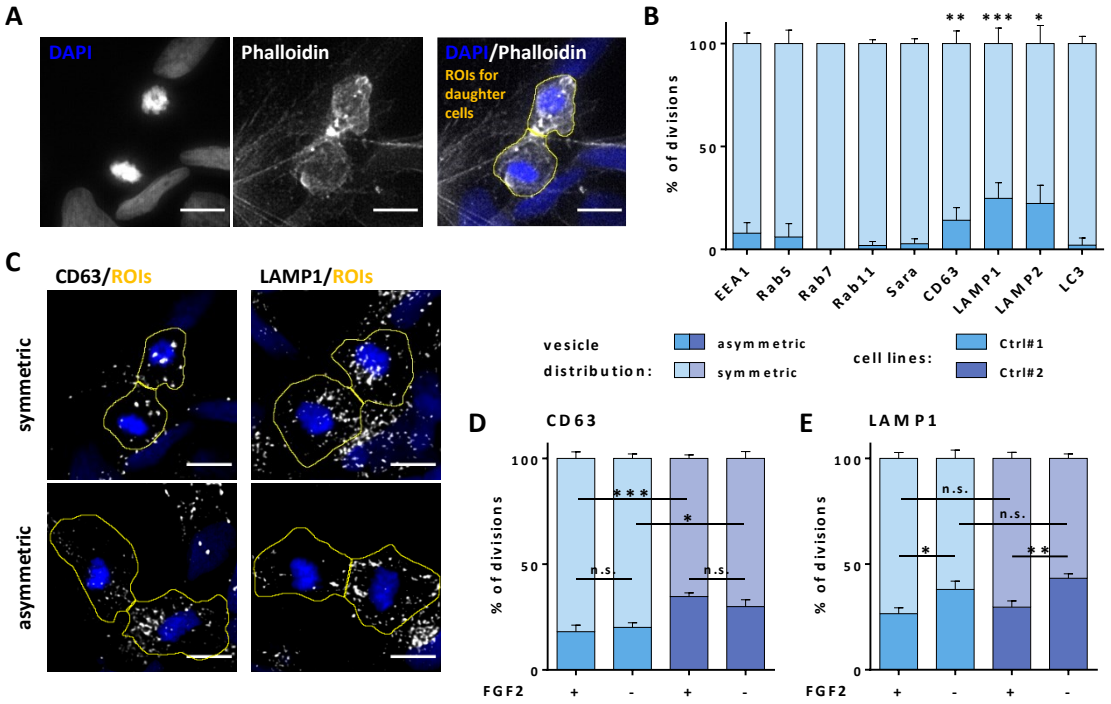

Figure 9: Asymmetric segregation of LAMP1$^+$ vesicles during cell division is increased upon FGF2 withdrawal. (A) Workflow to determine ROIs for daughter cells during telophase of mitosis based on DNA (DAPI) and F-actin (Phalloidin) staining. For technical details of the analysis see chapter 5.5.5. (B) Quantification of asymmetric segregation of different vesicle markers in Ctrl#1-NSCs in the presence of FGF2 (n = 3 coverslips, one-sample t-test, mean ± SEM). (C) Representative images of symmetrically and asymmetrically segregated CD63$^+$ and LAMP1$^+$ vesicles during cell division. ROIs for daughter cells (yellow line) were determined as depicted in (A). (D-E) Quantification of CD63- and LAMP1-asymmetry in two cell lines showed a consistent increase in LAMP1-asymmetries upon withdrawal of FGF2. Whereas, percentage of CD63-asymmetries were not changed significantly (N = 6 coverslips from 3 independent experiments, two-way ANOVA with Bonferroni post-hoc test, mean ± SEM). Scale (A,C) 10 µm. * $p < 0.05$, ** $p < 0.01$, *** $p < 0.001$, n.s. – not significant.

To establish how LAMP1$^+$ vesicles influence cell fate decisions during neuronal differentiation, the association of LAMP1 asymmetry with the distribution of Notch receptors was analysed. The Notch signalling pathway is a well-established cell fate determinant in NSCs maintaining their proliferative capacity and preventing their differentiation into neurons [Ishibashi et al., 1994; Ohtsuka et al., 2001]. Besides, it is known that Notch pathway components are segregated

within vesicles during SOP cell division in *D. melanogaster* [Coumailleau et al., 2009]. Taken these facts together, Notch receptors are promising candidates to be cargos of the asymmetrically distributed vesicles and thereby influencing the fate of the daughter cells. IF staining of Notch1 and Notch2 receptors with LAMP1 in dividing NSCs showed colocalization in some vesicle-like structures throughout mitotic phases (Figure 10A-B).

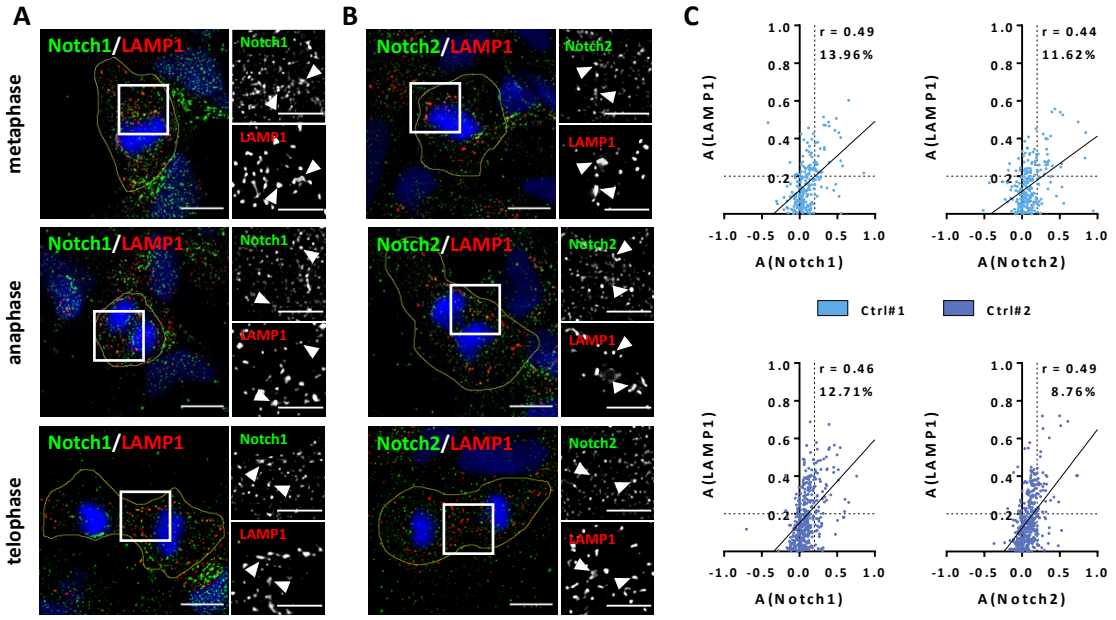

Figure 10: Distribution of Notch receptors correlate with LAMP1⁺ vesicle segregation during cell division. (A-B) IF staining of Ctrl#1-NSCs for Notch receptors and LAMP1 in different phases of cell division. Notch punctae partially colocalize with LAMP1⁺ vesicular structures throughout mitotic phases (white arrowheads in zoom images). (C) Quantification of Notch distribution in Ctrl#1- and Ctrl#2-NSCs during telophase and correlation of asymmetry factors A for LAMP1 and Notch1 and Notch2, respectively. Correlation factors r are indicated and the percentage of analysed cells with an asymmetric co-inheritance of LAMP1 and Notch receptors in the same daughter cell. Scale (A-B) 10 µm, zoom 5 µm. DNA was counterstained with DAPI and depicted in blue pseudo-colour.

To get an idea, whether LAMP1 asymmetry is predictive for Notch receptor distribution during late telophase, receptor signals were quantified analogous to the LAMP1 intensity described above. Asymmetry indices for Notch1 correlated well with LAMP1 distribution with correlation coefficients of 0.49 for Ctrl#1 and 0.46 for Ctrl#2 (Figure 10C). In 13.96% and 12.71% of the analysed cell divisions of Ctrl#1- and Ctrl#2-NSCs, respectively, LAMP1 and Notch1 were asymmetrically segregated into the same daughter cell. Similar results were obtained for the second Notch isoform, Notch2, with correlation coefficients of 0.44 and 0.49 and co-segregation in 11.62% and 8.76% of mitotic events analysed for Ctrl#1- and Ctrl#2-NSCs, respectively.

The very similar behaviour of the two analysed cell lines concerning both the increase in LAMP1 asymmetry upon FGF2 withdrawal and the correlation of LAMP1 and Notch receptor asymmetry, indicates that the processes might be a conserved mechanism of NSCs to switch from proliferative to neurogenic cell division. Therefore, all upcoming experiments were usually

performed on both cell lines and the representative results from one cell line are presented and discussed. The respective cell line is mentioned in each Figure legend.

6.3 Notch receptors are enriched in LAMP1$^+$ vesicles rather than in early endosomal vesicles

Punctured staining of Notch receptors in mitotic cells might hint at a regular endocytic internalization of the receptors. To narrow down the Notch-containing vesicular subpopulation and to verify the suggested presence of the receptors within endolysosomal vesicles, rosette-type NSCs in proliferative conditions (+FGF2) were analysed in more detail by colocalization analysis and sucrose density gradient centrifugation.

6.3.1 Notch receptors co-occur more with LAMP1$^+$ than with CD63$^+$ vesicles

IF staining in mitotic cells gave first evidence that LAMP1$^+$ vesicle colocalize with Notch receptor signals. To further verify that result, colocalization was quantified in non-mitotic cells assessing LAMP1$^+$ as well as CD63$^+$ vesicles (Figure 11A-B). The Spearman's rank correlation coefficients (SRCCs) [Spearman, 1904] revealed a slight correlation between Notch1 and Notch2 receptors

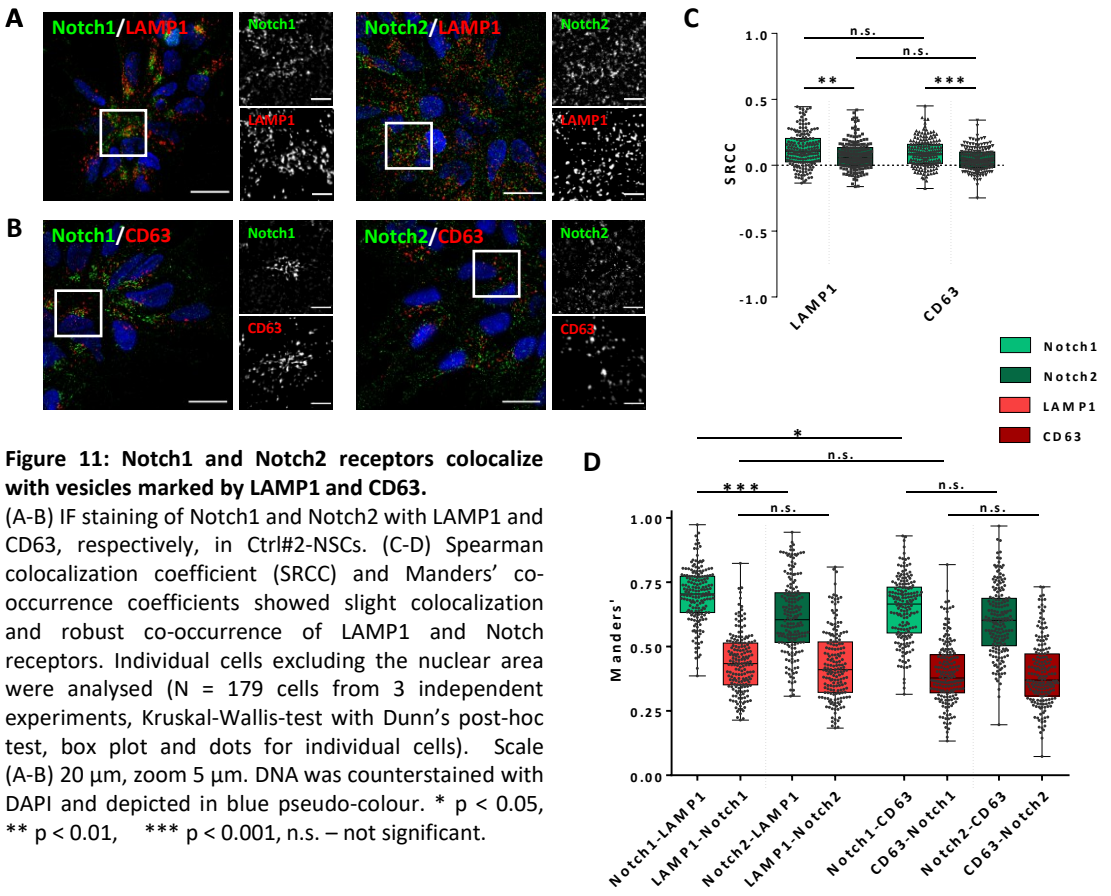

Figure 11: Notch1 and Notch2 receptors colocalize with vesicles marked by LAMP1 and CD63.
(A-B) IF staining of Notch1 and Notch2 with LAMP1 and CD63, respectively, in Ctrl#2-NSCs. (C-D) Spearman colocalization coefficient (SRCC) and Manders' co-occurrence coefficients showed slight colocalization and robust co-occurrence of LAMP1 and Notch receptors. Individual cells excluding the nuclear area were analysed (N = 179 cells from 3 independent experiments, Kruskal-Wallis-test with Dunn's post-hoc test, box plot and dots for individual cells). Scale (A-B) 20 µm, zoom 5 µm. DNA was counterstained with DAPI and depicted in blue pseudo-colour. * $p < 0.05$, ** $p < 0.01$, *** $p < 0.001$, n.s. – not significant.

and LAMP1 with SRCCs of 0.122±0.010 and 0.074±0.008, respectively (Figure 11C). The correlation with CD63 is slightly, but not significantly lower for both Notch1 (0.093±0.008) and Notch2 (0.045±0.006).

The analysis of co-occurrence according to Manders et al., 1993 revealed a co-occurrence of around 70.0±0.8% of Notch1$^+$ particles and 61.7±1.1% of Notch2$^+$ particles colocalizing with LAMP1$^+$ vesicles (Figure 11D). The reciprocal analysis of LAMP1 co-occurring with Notch receptors resulted in 43.6±0.8% and 42.9±1.0% of co-occurrence with Notch1 and Notch2, respectively. Similar to the SRCCs, the Manders' co-occurrence of Notch receptors with CD63 was slightly lower compared to LAMP1: Notch1-CD63 64.6±0.9%; Notch2-CD63 60.0±1.0%; CD63-Notch1 39.8±0.9%; CD63-Notch2 39.6±1.0%.

Taking co-occurrence and correlation analysis together, Notch receptors often co-occur with LAMP1$^+$ vesicles, but there are quite some LAMP1$^+$ vesicles, which do not contain any detectable Notch receptors. Colocalization of Notch2 receptors with the vesicle markers was in general lower compared to Notch1, and Notch1 was more often found in LAMP1$^+$ vesicles than in CD63$^+$ vesicles.

6.3.2 Notch receptors accumulate in the same sucrose fractions as LAMP1

Sucrose density gradient centrifugation was used as a second independent method to confirm results from IF staining. With increasing density along the sucrose gradient different subcellular compartments can be separated according to their protein content and size. Therefore, it is possible to analyse the vesicle subtypes containing a protein of interest, here Notch receptors. Endosomes are usually concentrated in "early" fractions, meaning fractions with a low sucrose concentration, whereas late endosomes and lysosomes should appear at higher sucrose concentrations [Araùjo et al., 2008].

The protein content of a total of 20 fractions along the Sucrose gradient was analysed by Western Blot (Figure 12A). The early endosome marker EEA1 was highly accumulated in the early fractions with its predominant peak in fractions 4-5 (Figure 12B). LAMP1 also showed a single peak with the highest protein level around fraction 11 of the sucrose gradient. CD63 as well as the human Sara orthologue ZFYVE9 exhibited two peaks along the gradient. For ZFYVE9, the first peak was shifted slightly in relation to EEA1 towards higher sucrose concentration, and the second peak coincided with the small EEA1-peak at fraction 12. CD63 accumulated in two major peaks around fractions 8 and 13, respectively.

The distribution of Notch1 and Notch 2 receptors was determined in relation to the vesicle markers (Figure 12C). Both receptor isoforms showed a single peak with the highest protein levels in fraction 10 and 11, respectively. Distribution of Notch2 receptors along the sucrose

gradient showed a small shoulder around fractions 6-9 and a steep incline towards fraction 10, which was not seen for Notch1 receptors. Comparing the Notch distribution to the vesicle markers the peaks of Notch receptors clearly coincided with the LAMP1 peak. However, Notch receptors showed a slightly higher presence in early fractions compared to LAMP1, starting from fractions 4-5.

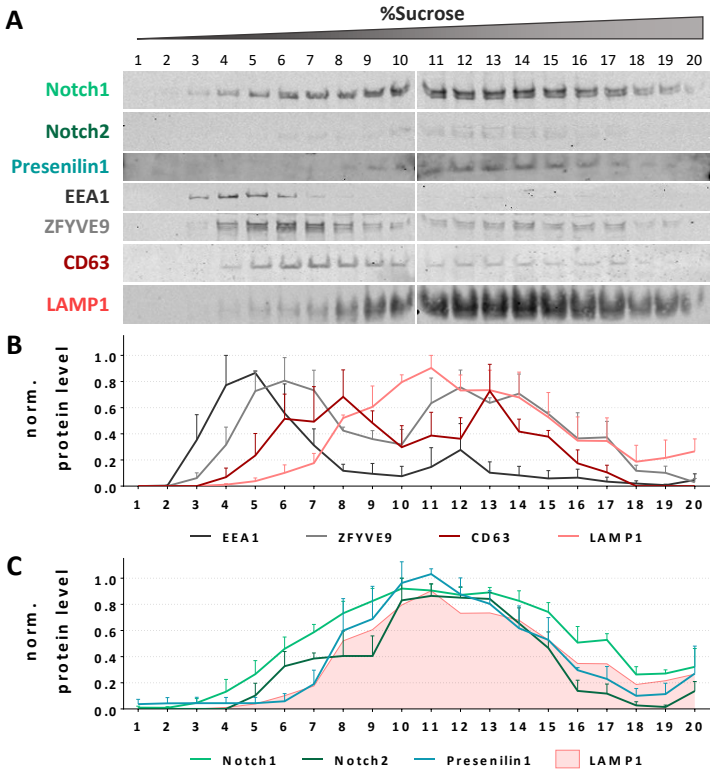

Figure 12: Notch receptor levels peak in the same fractions along the sucrose gradient as LAMP1. (A) Western Blot analysis of sucrose gradient fractions from Ctrl#1-NSCs for different vesicle markers (EEA1, ZFYVE9, LAMP1, CD63), Notch receptors and the γ-secretase subunit Presenilin 1. (B-C) Quantification of protein level across sucrose gradient fractions normalized to the fraction with the highest protein content for each protein. (B) EEA1$^+$ and LAMP1$^+$ vesicles accumulate in single peaks in fractions 4-5 and 11, respectively. The human Sara ortholog ZFYVE9 and CD63 show two peaks along the gradient. (C) Notch1, Notch2 as well as Presenilin1 showed a segregation along the sucrose gradient similar to LAMP1 (n = 3, mean + SEM, mean of LAMP1 is depicted in (C) as reference).

Together with the colocalization analyses performed, this suggests that Notch receptors are not exclusively present in LAMP1$^+$ vesicles, but certainly accumulate in the endolysosomal compartment. Interestingly, the γ-secretase subunit Presenilin1 showed a distribution along the sucrose gradient very similar to LAMP1 (Figure 12C). This already hints at a possible function of the transport of Notch receptors towards the endolysosomal compartment, as the last step of receptor activation, the cleavage by γ-secretase might take place within LAMP1$^+$ vesicles.

6.4 Notch1 receptors are internalized via the endocytic pathway in a Dynamin- and Clathrin-dependent process together with their ligands

To shed some light on the processes underlying the transport of Notch receptors from the plasma membrane towards LAMP1$^+$ vesicles, the internalization pathway was analysed. Further it was suggested in the last chapter that Notch receptors might be cleaved within the vesicles. Therefore, a ligand internalization assay was performed to establish whether ligand binding can trigger receptor endocytosis.

6.4.1 Notch1 receptors are internalized via CME

To pinpoint the exact mechanism of its endocytosis, the ECD of Notch1 (N1ECD) at the cell surface was stained together with Clathrin and a conjugated Choleratoxin subunit B (CTB). The latter can be used to stain lipid-rafts at the plasma membrane, which are locations of Caveolae-type endocytosis. Colocalization of N1ECD with Clathrin, rather than with CTB, suggests a Clathrin-mediated mechanism over a Caveolin-mediated process for the endocytosis of Notch1 receptors (Figure 13).

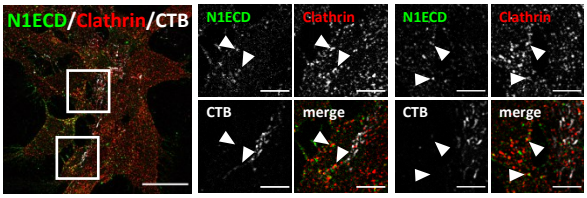

Figure 13: At the cell surface Notch1 receptors accumulate in Clathrin-coated membrane pits. IF staining for cell surface Notch1 ECD (N1ECD), Clathrin and lipid rafts via Choleratoxin subunit B (CTB) in Ctrl#2-NSCs. Colocalization of N1ECD and Clathrin is marked by arrowheads. Scale 20 µm, zoom 5 µm.

One step down the endocytic pathway, the Clathrin-coated membrane pits have to be abscised by Dynamin to form intracellular vesicles. Therefore, NSCs were treated with the Dynamin

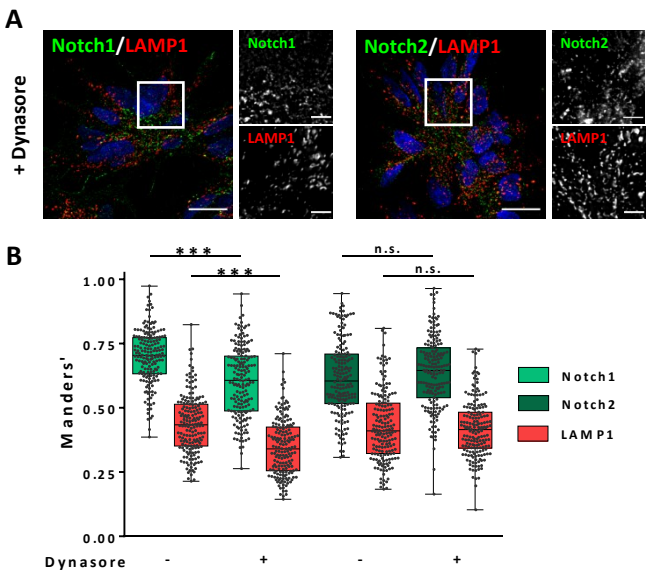

Figure 14: Notch1 is internalized via a Dynamin-mediated process. (A) IF for Notch1/2 and LAMP1 in Ctrl#2-NSCs, which were treated for 1 h with 50 µM Dynasore before fixation. (B) Manders' co-occurrence coefficients of LAMP1 and Notch receptors were determined with and without Dynasore treatment (see also Figure 11; N = 179 cells from 3 independent experiments, Kruskal-Wallis-test with Dunn's post-hoc test, box plot and dots for individual cells). Colocalization of Notch1 and LAMP1 is significantly decreased with the Dynasore treatment, whereas Notch2 colocalization with LAMP1 is unchanged. Scale (A) 20 µm, zoom 5 µm. DNA was counterstained with DAPI and depicted in blue pseudo-colour. *** $p < 0.001$, n.s. – not significant.

inhibitor Dynasore and the co-occurrence of Notch receptors and LAMP1$^+$ vesicles, as the proposed endpoint of the endocytic journey of the receptors, was quantified. (Figure 14A). The Manders' coefficients were significantly reduced from 70.0%±0.8% to 60.2%±1.0% for Notch1-LAMP1 and from 43.6%±0.8% to 34.7%±0.8% for LAMP1-Notch1 after 1 h of Dynasore treatment (Figure 14B). The co-occurence of Notch2, however, was not changed significantly with the Dynasore treatment.

Taken together, with the different distribution of Notch2 within the sucrose gradient (Figure 12) and the overall lower colocalization with LAMP1 (Figure 11), this might indicate a different regulation of Notch2 receptor internalization. Whereas the results are a good indication that internalization of Notch1 receptors is mediated by CME. Therefore, all further analysis were concentrated on Notch1 receptors.

6.4.2 Notch ligands are internalized into LAMP1$^+$ and LysoTracker$^+$ vesicles

So far, there are contradicting reports on whether proteolytic cleavage of Notch receptors take place at the plasma membrane or within subcellular vesicles. To get a first idea, whether cleaved or intact Notch receptor dimers are internalized in the NSC model presented here, the colocalization of the N1ECD with the ICD (recognized by Notch1 antibody) as well as with LAMP1$^+$ vesicles was assessed. The clear colocalization of N1ECD with Notch1 and LAMP1 indicated an internalization of the uncleaved Notch receptor heterodimer (Figure 15A-B). A colocalization of N1ECD and LC3$^+$ vesicles was not found, speaking against the intercellular degradation of Notch1 receptors by autophagy (Figure 15C).

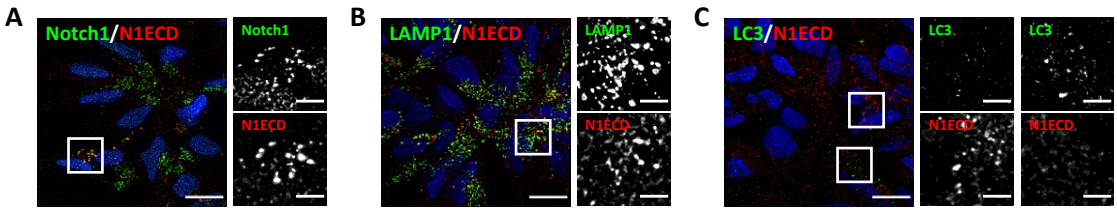

Figure 15: Notch1 receptor heterodimers are present within LAMP1$^+$ vesicles.
IF staining for the Notch1 ECD (N1ECD) with the Notch1 ICD (Notch1) (A), LAMP1 (B) and LC3 (C) in Ctrl#1-NSCs. The colocalization of ICD and ECD indicates internalization of receptor heterodimers and their transport to LAMP1$^+$ vesicles. Autophagy seems to be not involved in this process. Scale 20 µm, zoom 5 µm. DNA was counterstained with DAPI and depicted in blue pseudo-colour.

Therefore, it was hypothesized that Notch1 receptor endocytosis might be triggered by receptor-ligand interaction and the activating cleavage to take place intracellularly. This hypothesis was tested via a ligand internalization assay, where NSCs were treated with recombinant, soluble forms of the Notch receptor ligands DLL1 and JAG1 (both tagged with a 6xHistidine (His)-tag). IF staining for Notch receptors and the His-tagged DLL1 revealed that after

10 min the first internalized ligands were detectable and that DLL1-containing vesicular structures showed nearly complete colocalization with Notch1 receptors (Figure 16A). After 30 min a robust internalization of DLL1 together with Notch1 receptors was visible. At this time point, DLL1 was mainly found in LAMP1^{+} structures, but also some EEA1^{+}/DLL^{+} vesicles were detectable (Figure 16B). Further triple staining of DLL1 with Notch1 and LAMP1, showed partial colocalization of the three proteins within the same vesicular structure (Figure 16C). Similar behaviour was seen for JAG1 indicating that the internalization in this context is not dependent on the type of ligand bound by the receptor (Figure 16D).

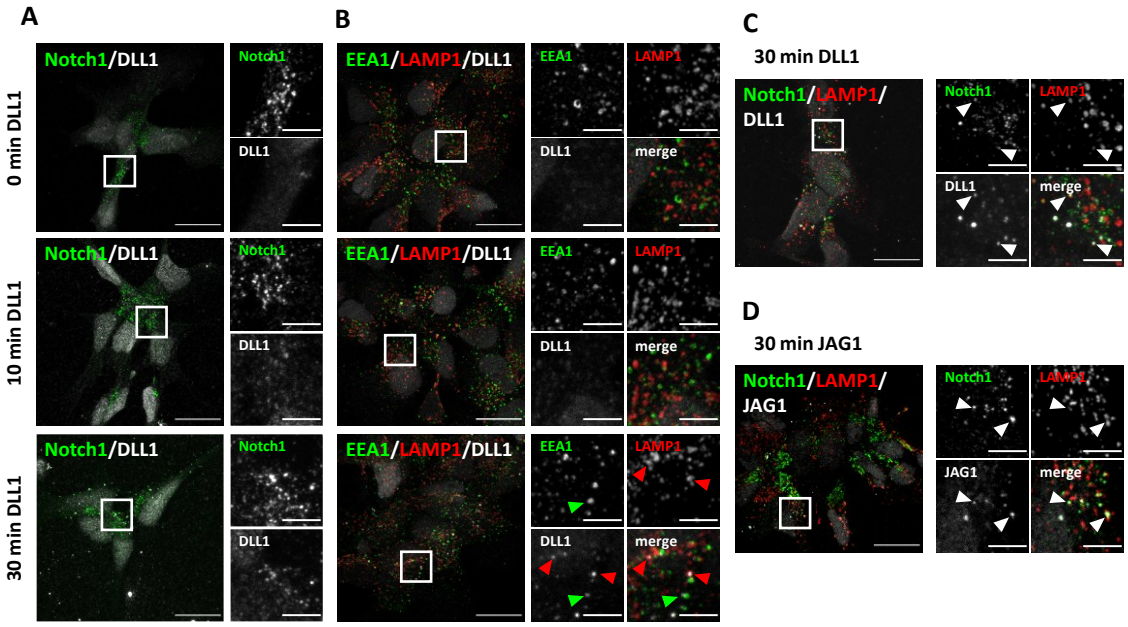

Figure 16: Notch ligands are internalized into LAMP1^{+} vesicles together with Notch1 receptors.
Ctrl#1/#2-NSCs were incubated with 10 µg/ml human recombinant DLL1-6xHis for 0, 10 and 30 min before fixation. (A-B) IF staining for Notch1 receptors and the vesicle markers EEA1 and LAMP1, respectively, showing first appearance of internalized His-tagged ligand after 10 min and robust internalization after 30 min with clear colocalization with Notch1 receptors. Partial overlap with EEA1 (green arrowheads) and LAMP1 (red arrowheads) is visible. (C-D) IF staining for ligands, Notch1 receptors and LAMP1 after 30 min of treatment with DLL1- and JAG1-6xHis, respectively, showing partially colocalization of internalized ligand-receptor complex with LAMP1 staining (arrowheads). Scale 20 µm, zoom 5 µm.

To get a deeper understanding of the dynamics of ligand internalization, the recombinant DLL1 peptide was tagged with pHrodo. This dye shows increased fluorescence with a decrease in pH and thereby can be used to track endocytosis in living cells. Already early endosomes have a slightly lower pH of around 6.5 than the extracellular space with a pH of 7.4 [Maxfield and Yamashiro, 1987]. The pH drops further along the endocytic pathway to reach 4.5 in endolysosomal vesicles. The latter can be labelled by the LysoTracker dye, which is cell permeable and becomes fluorescent in highly acidified environments, like late endosomes and lysosomes. LysoTracker functionality was confirmed by treatment with the v-ATPase inhibitor BafilomycinA (BafA), which diminished LysoTracker signal within 1 h (Figure 17A). Further, an IF

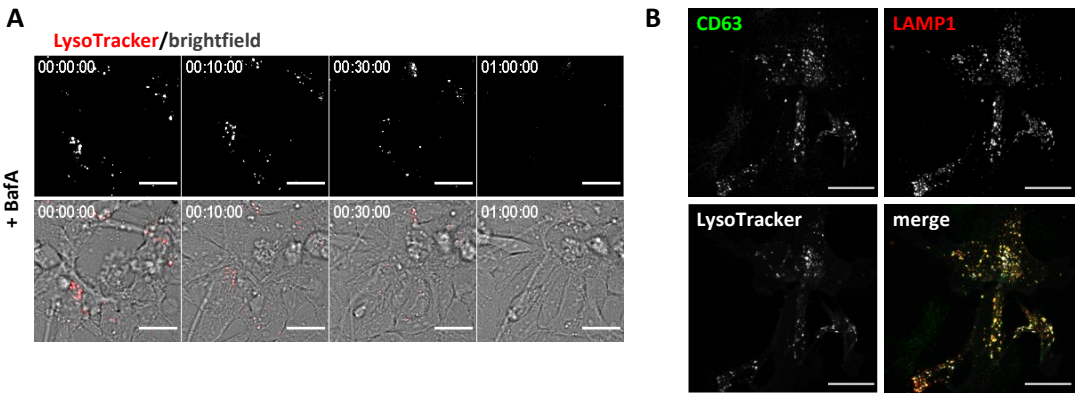

Figure 17: LysoTracker stains acidified, LAMP1⁺ vesicles.
(A) LysoTracker-stained Ctrl#2-NSCs were treated with v-ATPase inhibitor BafilomycinA (BafA) at 100 nM. Live cell imaging revealed dependency of LysoTracker fluorescence on vesicular acidification. (B) Ctrl#1-NSCs were stained for 30 min with LysoTracker and subsequently fixed and IF stained for LAMP1 and CD63 showing pronounced colocalization. Scale (A-B) 20 µm. Time scale (A) hh:minmin:secsec.

staining of LysoTracker-stained NSCs revealed almost complete colocalization of LysoTracker with LAMP1⁺ vesicular structures (Figure 17B).

Live cell imaging of DLL1-pHrodo internalization revealed the first intracellular pHrodo signals to appear after 20-30 min and a gradual colocalization with LysoTracker⁺ structures (Figure 18A). In line with the previous results, the internalization can be inhibited by treatment with the

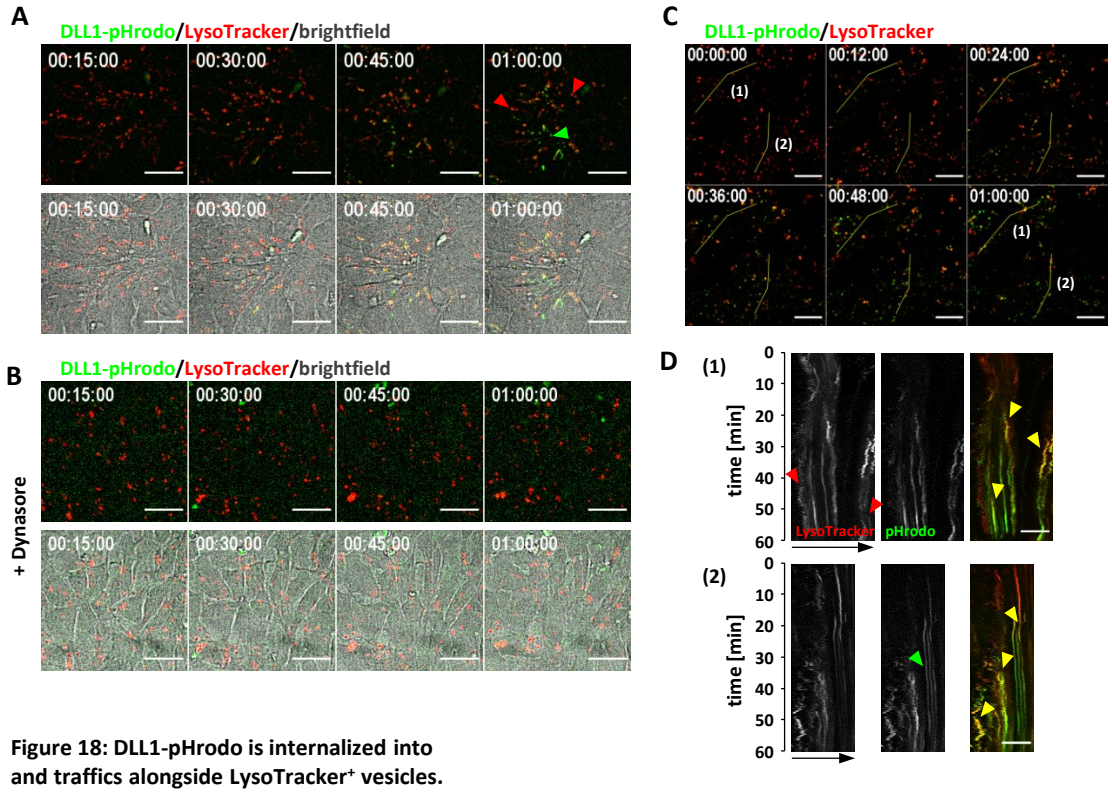

Figure 18: DLL1-pHrodo is internalized into and traffics alongside LysoTracker⁺ vesicles.
Soluble recombinant human Notch ligand DLL1 was labelled with pHrodo and internalization was imaged in living Ctrl#2-NSCs. (A-B) Internalization of DLL1-pHrodo is detectable after 30 min and can be blocked by pre-treatment for 30 min with 50 µM Dynasore. (C-D) Live cell confocal microscopy with a frame rate of 30 sec and two representative kymographs of LysoTracker and pHrodo dynamics along the lanes (1) and (2) indicated in (C). Scale (A-B) 20 µm, (C-D) 10 µm. Time scale (A-C) hh:minmin:secsec.

Dynamin-inhibitor Dynasore (Figure 18B). An additional confocal live cell imaging of the internalization brought the opportunity of a high frame rate and a simultaneous imaging of pHrodo and LysoTracker signal. Thereby, the high mobility of the vesicles within the cells was made visible. Kymographs show both the appearance and increase in the pHrodo signal as well as the trafficking of the pHrodo signal in parallel to the LysoTracker stained vesicles (Figure 18C-D). Some pHrodo^{+} structures remained or turned LysoTracker^{-}, which is probably due to the fact that LysoTracker only stains highly acidified vesicle, hence representing only a subfraction of all vesicles marked by LAMP1 (Figure 17B) and not staining endosomal vesicles.

Summing up, the internalization assay confirmed the Dynamin-mediated Notch receptor endocytosis, and suggests that the internalization is initiated before the S2 cleavage, which leads to the release of the ligand binding ECD of Notch receptors. This gives a good hint that the activating cleavages of Notch receptors occur after endocytosis.

6.5 Acidification of vesicles is necessary for activation of Notch signalling by receptor cleavage

The main open question, which is also highly controversially discussed in the literature, is whether internalization of Notch receptors and more specifically the pH drop within the vesicles is essential for the release of the NICD. A second conceivable outcome of trafficking Notch receptors towards lysosomes is the degradation of the receptors and thereby decreasing the Notch receptor availability at the cell surface. Both hypotheses were addressed by Western Blot

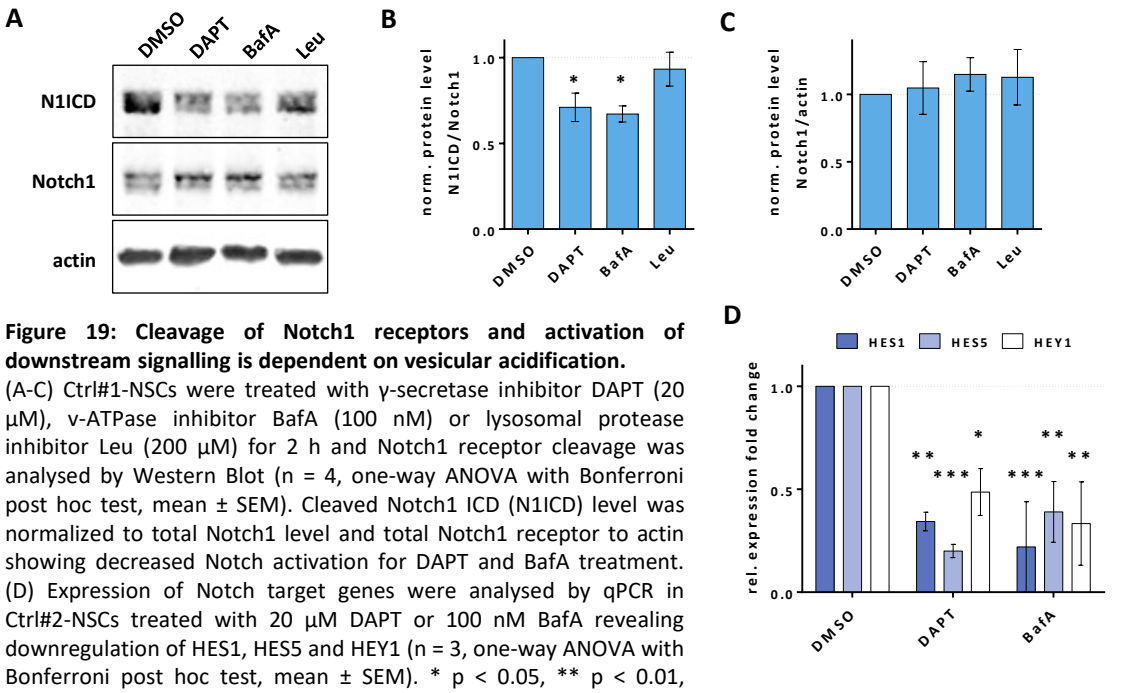

Figure 19: Cleavage of Notch1 receptors and activation of downstream signalling is dependent on vesicular acidification.
(A-C) Ctrl#1-NSCs were treated with γ-secretase inhibitor DAPT (20 µM), v-ATPase inhibitor BafA (100 nM) or lysosomal protease inhibitor Leu (200 µM) for 2 h and Notch1 receptor cleavage was analysed by Western Blot (n = 4, one-way ANOVA with Bonferroni post hoc test, mean ± SEM). Cleaved Notch1 ICD (N1ICD) level was normalized to total Notch1 level and total Notch1 receptor to actin showing decreased Notch activation for DAPT and BafA treatment. (D) Expression of Notch target genes were analysed by qPCR in Ctrl#2-NSCs treated with 20 µM DAPT or 100 nM BafA revealing downregulation of HES1, HES5 and HEY1 (n = 3, one-way ANOVA with Bonferroni post hoc test, mean ± SEM). * $p < 0.05$, ** $p < 0.01$, *** $p < 0.001$.

analysis of NSCs treated with γ-secretase inhibitor DAPT, the v-ATPase inhibitor BafA and the lysosomal protease inhibitor Leupeptin (Leu). The ratio between cleaved Notch1 ICD (N1ICD) and uncleaved Notch1 receptors was significantly decreased to 0.71±0.08 by DAPT treatment and to 0.67±0.05 by BafA treatment compared to the DMSO control (Figure 19A-B). Leu treatment, however, does not influence the N1ICD/Notch1 ratio. The amount of total Notch1 was also not changed significantly by any of the treatments (Figure 19C). These results indicate that the acidification of the endolysosomal vesicles is necessary for Notch receptor cleavage and hence Notch signalling activation. Further, the proteolytic function of lysosomes neither seems to have an impact on Notch receptor cleavage, nor on its degradation.

To verify that the reduced release of N1ICD by DAPT and BafA has an impact on signalling output, the expression of Notch downstream targets, HES1, HES5 and HEY1, was quantified by qPCR. In line with the Western Blot results, DAPT and BafA treatment significantly reduced the expression of all three analysed target genes to less than the half of the expression in the DMSO condition (Figure 19D).

Therefore, it can be stated that Notch signalling activation in human NSCs is dependent on Notch receptor internalization and cleavage of the receptors in the increasingly acidic environment of endolysosomes.

6.6 Expression of Notch downstream target HES1 can be visualized in HES1-tdTomato reporter cell line

In the further experiments, Notch pathway activity shall be analysed in living cells to establish whether asymmetric segregation of endolysosomes during mitosis induces a Notch signalling bias in the daughter cells. To this end, a reporter cell line was established using the CRISPR/Cas9-technology to edit the endogenous locus of one of the Notch downstream target genes, namely *HES1*. The construct, which was introduced, tagged the endogenous *HES1* with the sequence coding for the fluorescent protein tdTomato. The two proteins were linked via a T2A site leading to separation of tdTomato from the HES1 protein after translation facilitating normal HES1 function. For better visualization and quantification of tdTomato-fluorescence the protein was targeted to the nucleus by addition of a NLS. Further a PEST sequence was added to target tdTomato for fast proteasomal degradation and to be able to visualize dynamic changes in HES1 expression (Figure 20A-B).

6.6.1 Generation of HES1-tdTomato reporter cell line

The described reporter construct (tdTomato-NLS-PEST) was cloned into a vector holding two homology arms corresponding to the sequence around the stop codon in the last exon of the endogenous *HES1* locus. This HDR-template was introduced into Ctrl#2-iPSCs together with the respective HES1 gRNA-plasmid by nucleofection (Figure 20A). The latter, additionally, encodes for hSpCas9 and a Puromycin resistance for selection. After nucleofection, cells were seeded in clonal density and successfully nucleofected cells were selected by Puromycin treatment. Clones were picked and expanded as clonal cell lines for further validation. Screening of the different

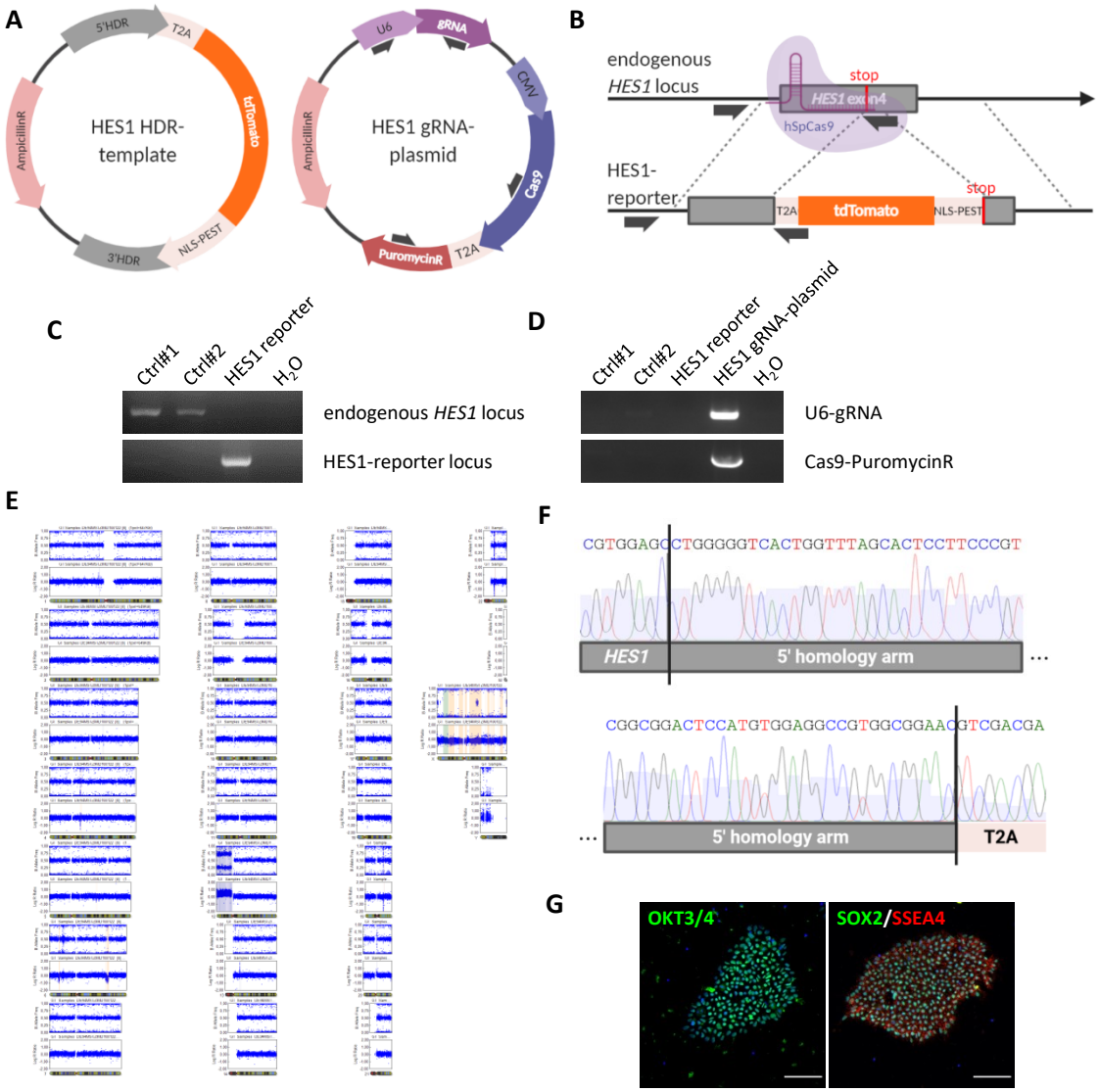

Figure 20: Generation of HES1-reporter cell line via CRISPR/Cas9-mediated tagging of the *HES1* locus.
(A-B) Plasmids cloned for CRISPR/Cas9-mediated gene editing and strategy for targeting of the endogenous *HES1* locus. Indicated by grey arrows are the primers used for genotyping PCR. (C-D) Genotyping PCR of the two wild-type cell lines and the HES1-reporter line indicating homozygous integration of the T2A-tdTomato-NLS-PEST construct (C) and no random integration of the HES1 gRNA-plasmid (D). (E) SNP analysis of HES1-reporter line. (F) Sequencing of the *HES1* locus after gene editing showing scarless integration of the reporter construct. (G) IF of HES1-reporter-iPSCs for pluripotency markers, OKT3/4, SSEA4 and SOX2. Scale (G) 100 µm. DNA was counterstained with DAPI and depicted in blue pseudo-colour.

clonal lines was performed by genotyping PCR, which amplifies either the wild type, unedited allele or the edited locus (Figure 20B-C). In a second PCR, the possibility of a random integration of the HES1 gRNA-plasmid was excluded (Figure 20D). One of the successfully edited clonal cell lines, from now on termed HES1-reporter, was further quality controlled by SNP analysis and sequencing of the edited locus. SNP analysis revealed a duplication of the p-arm of chromosome 12, which is a common cell culture artefact [Laurent et al., 2011] and is probably introduced during clonal expansion (Figure 20E). As no genes associated with the Notch signalling pathway are located on that chromosome arm, the cell line was considered suitable for the following analyses. Further, sequencing of the HES1 locus showed a scarless integration of the tdTomato construct and no point mutations within the 5' homology arm, encoding for the C-terminus of HES1 (Figure 20F). The pluripotency of the HES1-reporter line was confirmed by homogenous expression of typical pluripotency markers, OKT3/4, SSEA4 and SOX2 (Figure 20E).

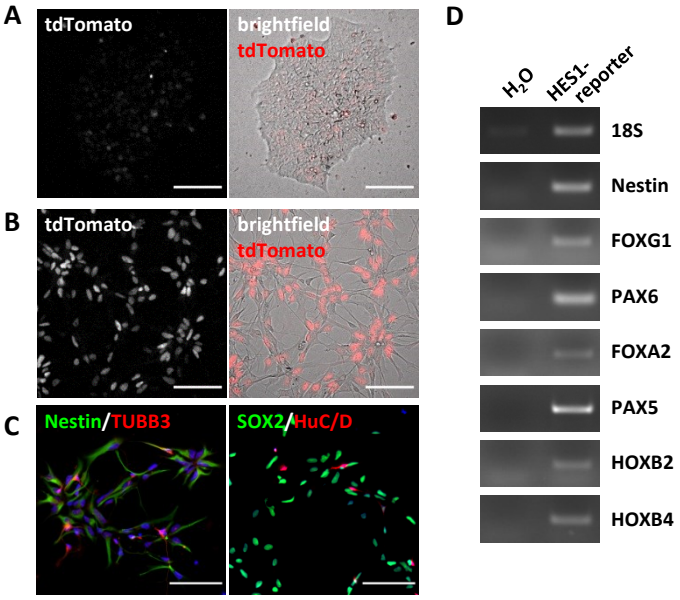

Figure 21: Characterization of rosette-type NSCs generated from HES1-reporter-iPSCs.
(A-B) Brightfield images and tdTomato-signal before and after neural induction. Notch signalling activity is mostly inactive in iPSCs (A), whereas, rosette-type NSCs are highly dependent on Notch signalling, which is reflected by HES1-reporter expression (B). (C) HES1-reporter-NSCs express typical NSC markers (Nestin and SOX2) and show some spontaneous, neuronal differentiation marked by TUBB3 and HuC/D. (D) Regional identity of HES1-reporter NSCs were analysed by RT-PCR and indicate a mixed regional identity of NSCs across fore-, mid- and hindbrain. Scale (A-C) 100 µm. DNA was counterstained with DAPI and depicted in blue pseudo-colour.

IPSC proliferation and the maintenance of their stem cell character is known to be mostly independent of Notch signalling [Yu et al., 2008], which was confirmed by the absence of tdTomato and hence HES1 expression in the HES1-reporter-iPSCs (Figure 21A). Induction of the neuroectodermal fate by dual-Smad- and Wnt-inhibition, however, induces a robust expression of tdTomato and fluorescence was, as expected, located in the nucleus of HES1-reporter-NSCs (Figure 21B). The HES1-reporter-NSCs expressed typical NSC markers, such as Nestin and SOX2, and showed similar spontaneous neuronal differentiation, marked by TUBB3 and HuC/D, as the respective wild-type Ctrl#2-NSCs (Figure 21C and Figure 7A-B). The expression of different brain

region markers was also comparable with the parental Ctrl#2-NSCs and indicated a mixed NSCs population from diverse brain regions (Figure 21D and Figure 7D).

6.6.2 Stability of tdTomato protein and sensitivity towards inhibition of Notch signalling

To establish the functionality of the HES1-reporter and the dependency of tdTomato expression on active Notch signalling, HES1-reporter-NSCs were treated with the γ-secretase inhibitor DAPT. Long term treatment of NSCs with DAPT is known to push neuronal differentiation of NSCs [Elkabetz et al., 2008]. This effect was confirmed in HES1-reporter-NSCs, where a decrease in tdTomato fluorescence upon DAPT treatment was associated with a shift towards neuronal morphology (Figure 22A). To determine the half-life of the tdTomato protein, protein translation was inhibited by Cycloheximide treatment. The decrease in tdTomato signal was quantified in individual cells and fitted to an exponential decay. The half-life was thereby estimated to be around 3.5 h (Figure 22B).

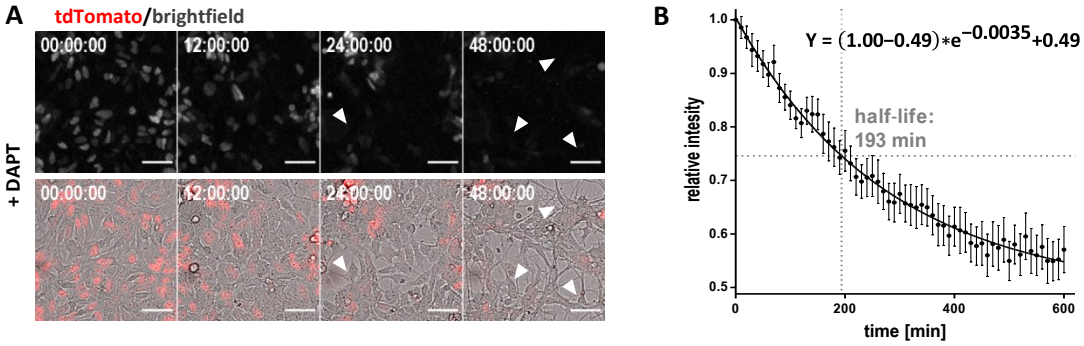

Figure 22: TdTomato expression is dependent on active Notch signalling and has a half-life of around 3.5 h. (A) HES1-reporter NSCs were treated with γ-secretase inhibitor DAPT (10 µM) for up to 48 h. Imaging of cellular morphology and the tdTomato signal over time showed appearance of cells with neuronal morphology (arrowheads) and simultaneous fading of the tdTomato fluorescence. (B) Cycloheximide (100 µM) chase was combined with live cell imaging and individual cells were tracked. The decay in the sum intensity density was analysed and fitted to an exponential decay revealing a half life of 193 min (N = 22 cells from 3 independent experiments). Scale (A) 50 µm. Time scale (A) hh:minmin:secsec.

Corresponding to the experiments presented in chapter 6.5, HES1-reporter-NSCs were treated with DAPT, BafA and Leu and HES1 expression was traced by tdTomato fluorescence. In line with the previous results, tdTomato signal is decreased over time by DAPT and BafA, but not by Leu treatment (Figure 23 and Figure 19). DAPT treatment showed a slightly stronger and faster reduction compared to BafA treatment. This indicates that the HES1-reporter is able to visualize Notch signalling dynamics as well as slight differences in Notch signalling activity, making it a versatile tool for the upcoming experiments.

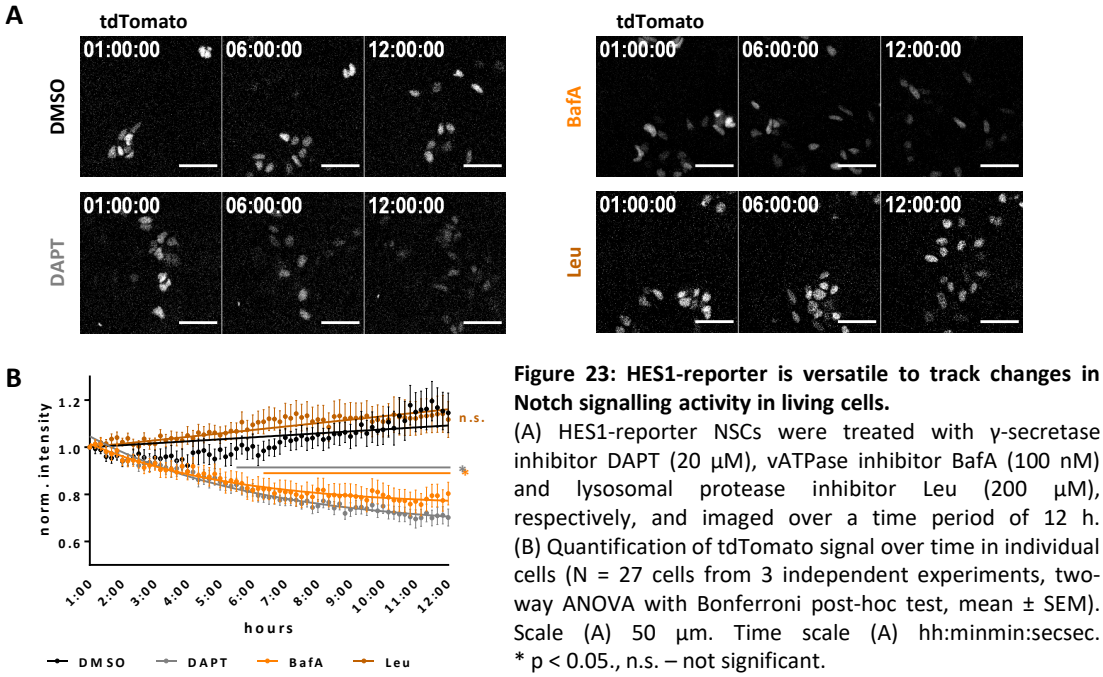

Figure 23: HES1-reporter is versatile to track changes in Notch signalling activity in living cells.
(A) HES1-reporter NSCs were treated with γ-secretase inhibitor DAPT (20 µM), vATPase inhibitor BafA (100 nM) and lysosomal protease inhibitor Leu (200 µM), respectively, and imaged over a time period of 12 h. (B) Quantification of tdTomato signal over time in individual cells (N = 27 cells from 3 independent experiments, two-way ANOVA with Bonferroni post-hoc test, mean ± SEM). Scale (A) 50 µm. Time scale (A) hh:minmin:secsec. * $p < 0.05$., n.s. – not significant.

6.7 Asymmetric segregation of acid vesicles during cell division leads to differences in Notch signalling activity in the daughter cells

So far, it was shown that Notch receptors are internalized into LAMP1^{+}/LysoTracker^{+} vesicles upon ligand binding to induce the release of the ICD and activation of downstream signalling. Besides, LAMP1^{+} vesicles were asymmetrically segregated during mitosis and this asymmetry was correlated with NSCs in neurogenic culturing conditions. To establish whether the asymmetric segregation of these vesicles can influence the cell fate of the daughter cells by biasing Notch signalling, live cell imaging with the HES1-reporter cell line was utilized (Figure 24A). NSCs were treated with Nocodazole to synchronize the cells at the beginning of mitosis and to ensure a timed entry into mitosis upon Nocodazole removal. Imaging of LysoTracker during mitosis was used to identify symmetric and asymmetric cell divisions (Figure 24B,D) analogous to the IF staining in fixed cells (Figure 9). A total of 124 symmetric and 31 asymmetric cell divisions were analysed (Figure 24D). In the second part of the imaging HES1 expression in the daughter cells was tracked by tdTomato fluorescence (Figure 24C). The signal intensity was quantified starting 1.5 h after telophase up to 6 h after mitosis and the differences of HES1 expression within daughter cell pairs was calculated for each time point (Figure 24E). Daughter cells arising from an asymmetric cell division showed a tendency towards a higher HES1 expression in the LysoTracker^{high} daughter cell (*daughter cell 1*). However, the variation between the mitotic events analysed was high and this trend was not significant at any time point.

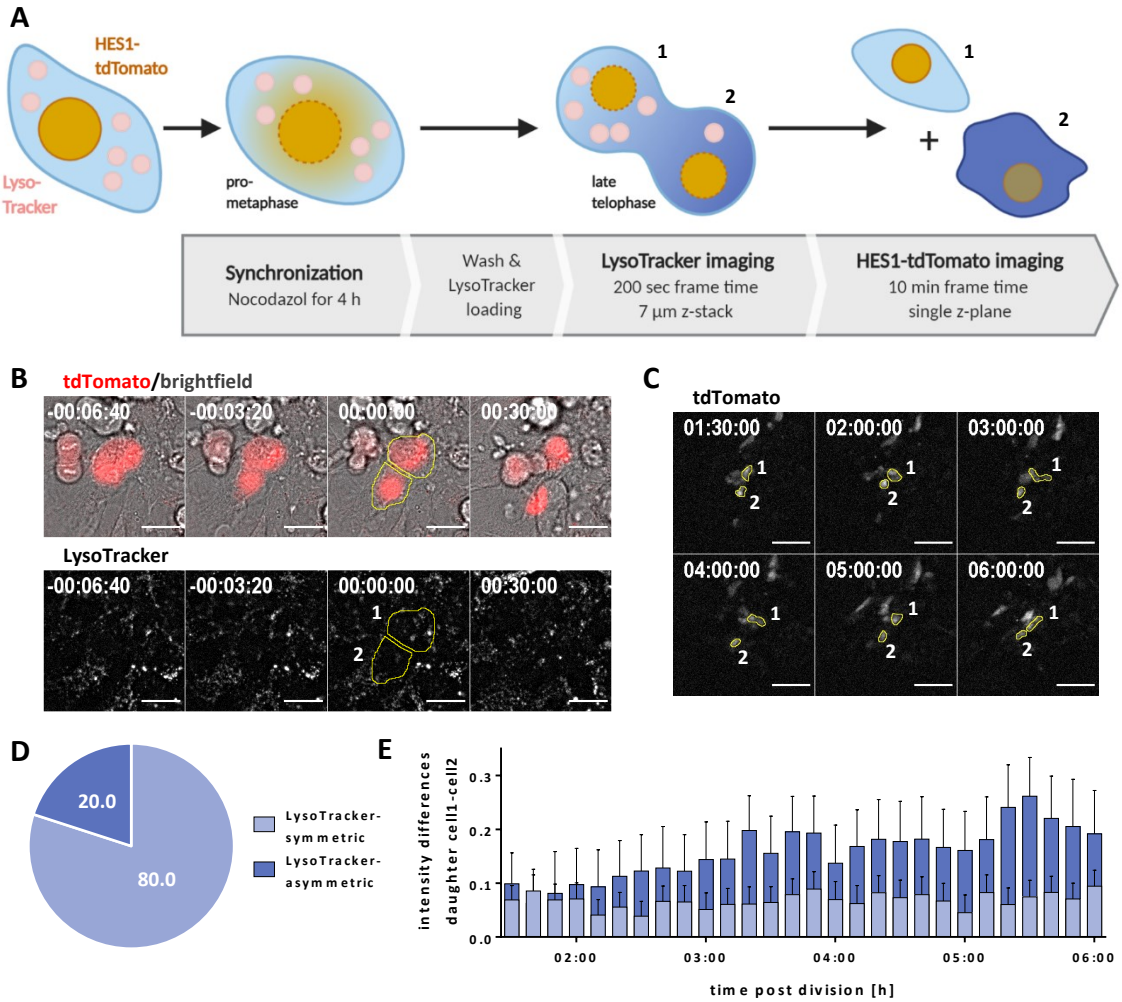

Figure 24: Asymmetric segregation of LysoTracker predicts a bias in HES1 expression after cell division.
(A) Schematic representation of the experimental work flow, with the synchronization of proliferating NSCs by treatment with 75 nM Nocodazol and a two-part live cell imaging to track LysoTracker signal during mitosis (B) and HES1-reporter expression in the respective daughter cells 1 and 2 (C). (D) Percentage of LysoTracker-symmetric and -asymmetric cell divisions analysed (N = 155 from 10 different experiments) (E) Quantification of the mean intensity differences between the two daughter cells starting 1:30 h to 6:00 h after division (N = 124/31 for symmetric/asymmetric divisions from 10 different experiments, mean + SEM). LysoTracker-asymmetric mitotic events showed increasingly biased HES1 expression in the daughter cells. Scale (B) 20 µm, (C) 50 µm. Time scale (B-C) hh:minmin:secsec.

Therefore, HES1 expression dynamics for individual daughter cell pairs were clustered by their Euclidean distance (Figure 25A, for technical details see chapter 5.6.3). Six clusters were identified and grouped into clusters with (1) symmetric HES1 expression (clusters 3 and 5), (2) asymmetric HES1 expression that opposes the LysoTracker distribution (clusters 4 and 6), (3) slightly asymmetric HES1 expression in line with LysoTracker segregation during mitosis (cluster 1) and (4) highly asymmetric HES1 expression (cluster 2) (Figure 25B-C). When analysing the distribution of these different clusters separately for LysoTracker-symmetric and -asymmetric mitotic events, an increase in the cluster frequency of highly asymmetric HES1 expression was detected from 12.1% to 25.8% (Figure 25D). This increase went along with a drop in the group

of symmetric and opposed asymmetric HES1 expression of 4.1 and 9.7 percentage points, respectively.

Taken together, an asymmetric segregation of LysoTracker^{+} vesicles shifts HES1 expression towards the LysoTracker^{high} daughter cell. This is in line with the assumption that acidic vesicles act as asymmetry factors during mitosis and as signalling hubs for Notch receptor activation. The directed shuttling of endolysosomes, therefore, represent one mechanism how Notch signalling can be biased and the cell fate of the daughter cells can be predestined during NSC division.

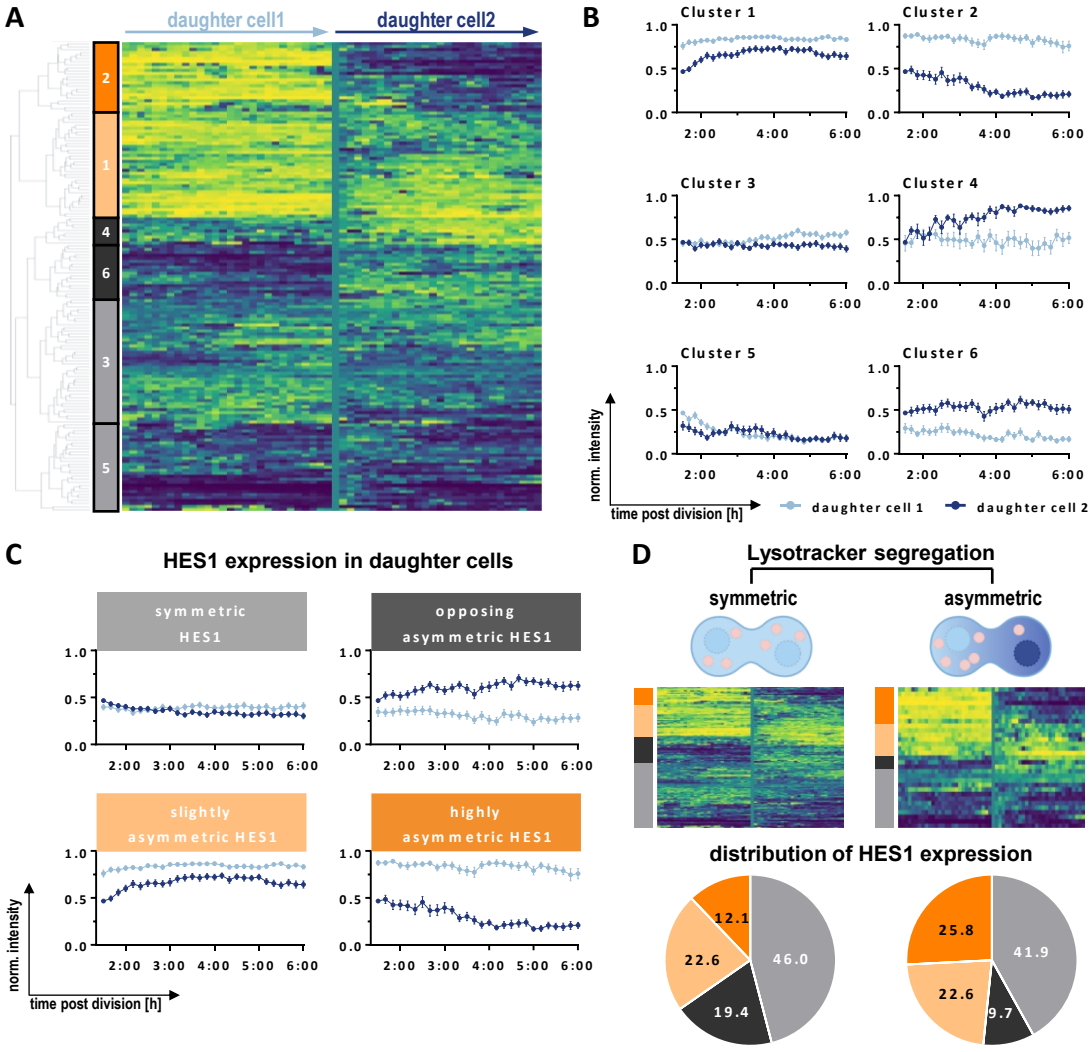

Figure 25: Clustering of HES1 dynamics reveals a shift towards highly asymmetric HES1 expression after asymmetric segregation of LysoTracker during mitosis.
(A) Heatmap of tdTomato intensities in daughter cell pairs after clustering with the R package *time course inspector*. The number of clusters were assigned after visual inspection. (B) The mean intensity dynamics for the two daughter cells in each cluster are depicted (N = 35/23/41/9/29/18 for clusters 1-6, mean ± SEM). (C) Clusters were assigned to 4 groups representing daughter cell pairs with symmetric, opposed asymmetric, slightly and highly asymmetric HES1 expression (mean ± SEM). (D) Heatmaps of tdTomato intensities and cluster distribution in daughter cell pairs originating from symmetric and asymmetric cell division based on LysoTracker segregation during mitosis (see Figure 24). A shift towards asymmetric HES1 expression is seen in LysoTracker-asymmetric mitotic events.

6.8 Asymmetric distribution of LAMP1 and Notch1 during cell division in 3D forebrain organoids

In the developing brain, NSCs are engrafted in a 3D environment, which cannot be modelled in the so far used 2D cell culture system. Therefore, the organoid system was employed to verify LAMP1^{+} vesicles as asymmetry factors in a 3D context, which resembles the *in vivo* situation more closely. To generate forebrain organoids, the neural fate was induced in iPSC-derived EBs and NSCs self-organize into cortical loop-like structures (Figure 26A-B). NSCs within the developing loops were identified by SOX2 expression and the onset of neurogenesis was visible

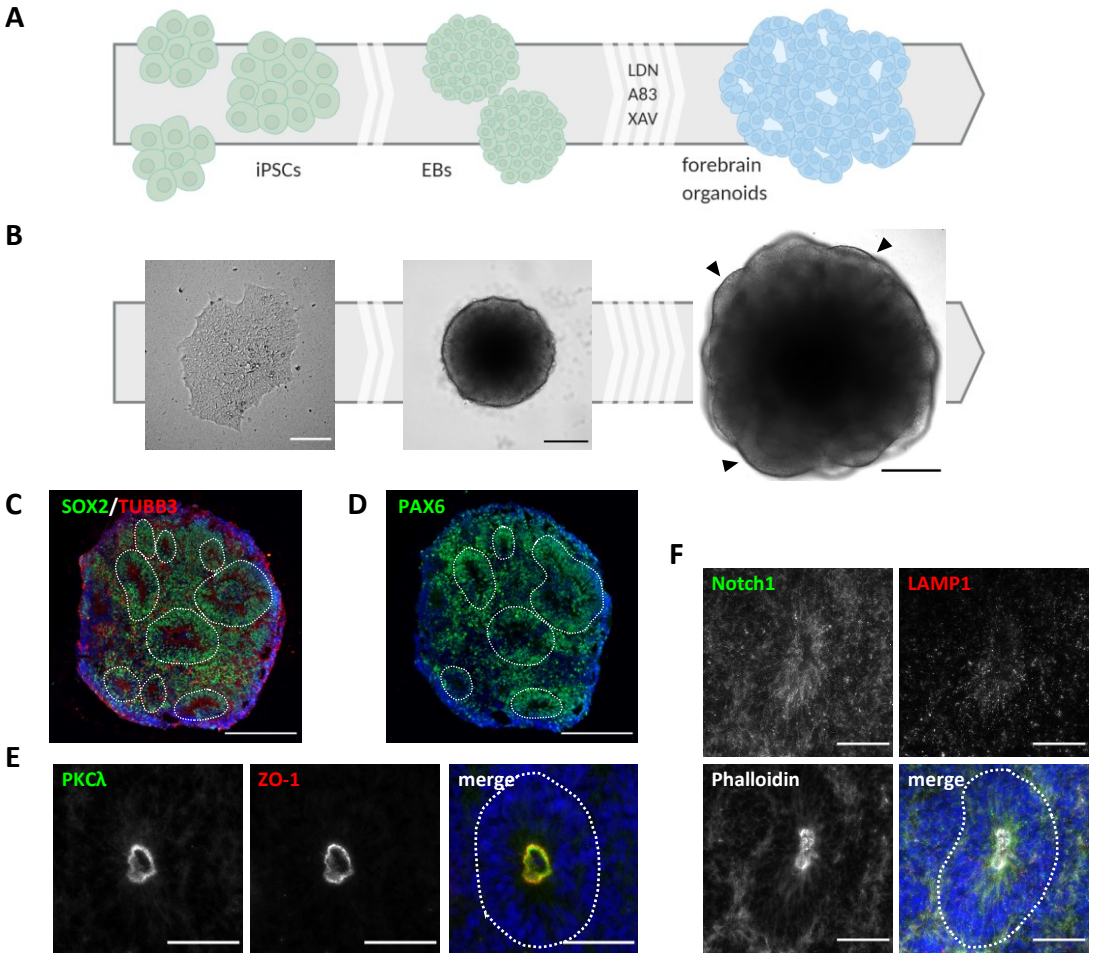

Figure 26: Neural induction protocol and basic characterization of 3D forebrain organoids.
(A) Human iPSCs were aggregated to form embryoid bodies (EBs), which were induced to neuroectodermal fate by dual-Smad- and Wnt-inhibition (LDN193189, A83-01 and XAV939) for 5 days. (B) Respective brightfield images show EB formation and developing loop structures (arrowheads) in 20 day-old organoids obtained from Ctrl#2-iPSCs. (C-F) IF staining in consecutive organoid slices from 20 day-old organoids, loops are marked by dotted lines. (C) NSC marker SOX2 is expressed homogenously within the cortical loops. Neuronal marker TUBB3 marks the first neurons of the developing CP around the loops. (D) Expression of PAX6 confirming forebrain identity of NSCs. (E) Polarity factor PKCλ and tight junctions marked by ZO-1 showing accumulation at the apical membrane of each loop. (F) IF staining for LAMP1 and Notch1 counterstained with Phalloidin marking cell structures and actin accumulation along the apical membrane. Scale (B) 100 µm (white), 300 µm (black), (C-D) 300 µm, (E-F) 50 µm. DNA was counterstained with DAPI and depicted in blue pseudo-colour.
Organoids were generously generated, fixed and sectioned by Ammar Jabali and Helene Schamber.

by the appearance of the first TUBB3^{+} neurons around the loop structures (Figure 26C). The forebrain identity was confirmed by the expression of the forebrain marker PAX6 throughout the organoid (Figure 26D). Internal polarization of NSCs within the loops was verified by the apical localization of polarity complexes and tight junctions, marked by PKCλ and ZO-1, respectively (Figure 26E). This apical membrane was further characterized by the accumulation of actin stained by Phalloidin (Figure 26F). In the following, mitotic NSCs at the apical lining were analysed for their intracellular distribution of LAMP1 and Notch1.

Dependent on the orientation and the attachment of the dividing cell to the apical membrane, the mitotic events were grouped into different division modes: planar, intermediate and delaminating cell divisions (Figure 27A). A division was considered planar, in case both daughter

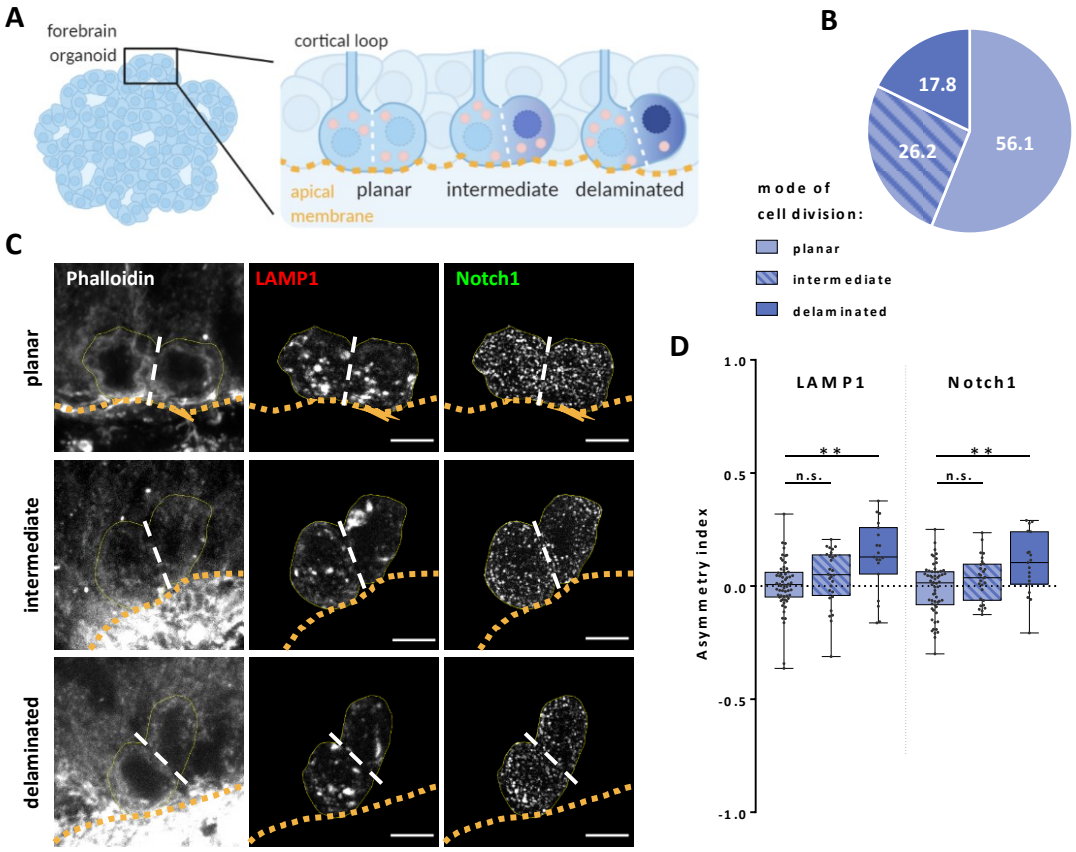

Figure 27: Delaminating cell divisions in forebrain organoids are associated with asymmetric distribution of LAMP1 and Notch1 between the daughter cells.
(A) Schematic representation of a cortical loop structure within forebrain organoids with planar/proliferative, delaminating/neurogenic and intermediate NSC divisions at the apical membrane. (B) Total number of planar, intermediate and delaminating cell divisions analysed (N = 107 from 3 independent batches of organoids). (C) IF staining for LAMP1 and Notch1 counterstained with Phalloidin. ROIs (yellow lines) for daughter cell pairs were determined based on the Phalloidin staining and the mode of cell division was determined in relation to the apical membrane (yellow dashed line). Shown is the LAMP1 and Notch1 staining within the ROIs. (D) Quantification of the asymmetry indices for LAMP1 and Notch1 showing an increasing asymmetric segregation to the apical daughter cell during intermediate and delaminating cell divisions (N = 60/28/19 for planar/intermediate/neurogenic division from 3 independent batches of organoids, Kruskal-Wallis-test with Dunn's post-hoc test, box plot and dots for individual mitotic event). Scale (C) 5 µm. ** $p < 0.01$, n.s. – not significant.

cells showed a similar level of contact to the apical membrane. A delaminating cell division was defined as a division where only one of the daughter cells is attached to the apical membrane, whereas the second daughter cell is completely delaminated. Finally, an intermediate cell division was presumed, if the contact surface area to the apical membrane is clearly unequally distributed between the daughter cells. Mitotic events were identified by DAPI staining and the described modes of cell division were distinguished by Phalloidin staining (Figure 27B-C). The asymmetry indices A for LAMP1 and Notch1 were calculated, similar to the 2D experiments (see Figure 9 and Figure 10). Planar cell divisions exhibited a mostly symmetric distribution of $LAMP1^{+}$ vesicles and Notch receptors with asymmetry indices of A(LAMP1) = 0.005±0.014 and A(Notch1) = -0.012±0.015 (Figure 27D). Already in intermediate cell divisions, a trend towards a more asymmetric segregation of both proteins was seen, with A(LAMP1) = 0.037±0.024 and A(Notch1) = 0.031±0.018. In delaminating divisions, both A(LAMP1) and A(Notch1) were significantly increased to 0.130±0.036 and 0.098±0.031, respectively. This shows a biased segregation of endolysosomes and Notch1 receptors towards the daughter cell located closer to the apical membrane. Together with the knowledge that these delaminating divisions probably represent neurogenic division [Kosodo et al., 2004], where the apical cell retains its NSC properties and the more basal cell matures into a neuron, this further supports the proposed mechanism:

$LAMP1^{+}$ vesicles act as asymmetry factors during the division of human NSCs and represent one pathway to establish a bias in Notch receptor signalling. The $LAMP1^{high}$- and $Notch1^{high}$-daughter cell remains a stem cell, whereas the $LAMP1^{low}$- and $Notch^{low}$-daughter cells is pushed towards neuronal differentiation.

7 Discussion

In the first part of this thesis LAMP1$^+$ vesicles were established as asymmetry factors in human iPSC-derived NSCs and the asymmetric segregation during mitosis was associated with neurogenesis. In a second step, the accumulation of Notch receptors in endolysosomes and the impact of lysosomal acidification on Notch receptor cleavage was revealed. At last, 2D live cell imaging and 3D forebrain organoids were employed to link vesicle asymmetries with a bias in Notch signalling activity and neurogenic cell divisions, respectively.

7.1 Human iPSC-derived NSCs as a model system for asymmetric cell division

Studying human embryonic brain development is a tough subject due to the lack in specimen material to study. Human iPSCs and their derivatives are a possible solution to this issue. In this thesis, iPSC-derived NSCs were assessed as a potential model system for human neurodevelopment, more specifically to study asymmetric cell division.

In other model systems, e.g. in *D. melanogaster*, the process of asymmetric cell division is highly dependent on cellular polarization [Kuchinke et al., 1998; Wodarz et al., 2000]. Also, in mammalian RGCs apical-basal polarity is established and influences the switch from symmetric to asymmetric cell division [Konno et al., 2008; Postiglione et al., 2011]. Therefore, the basis for all further analyses in this thesis was to confirm cellular polarization of the NSC cultures used. Previously, polarization of rosette-type NSCs, but not of SM-NSCs [Reinhardt et al., 2013], was observed, with an accumulation of apico-junctional complexes at the centre of each neural rosette [Koch et al., 2009]. This was replicated by IF staining for the PAR complex component PKCλ and tight junctions, which were similarly located apically within the analysed NSCs (Figure 7).

Advantages of *in vitro* culturing of NSCs are on the one hand the scalable expansion of the cells in the presence of growth factors, and on the other hand the timed induction of neurogenesis, which is especially important for the scope of this thesis. Withdrawal of growth factors is usually used to generate mature neuronal cells within several weeks (Figure 7). In the first days of withdrawal, however, NSCs are characterized by their remaining proliferative capacity, which is gradually overturned by neuronal differentiation (Figure 8). This time window was exploited here to investigate asymmetric cell division and identify potential asymmetry factors.

As a second model system, forebrain organoids were used to verify asymmetry factors identified in 2D cultured NSCs. The apical-basal polarity of the cortical loop structures as the basis for asymmetric cell division was confirmed in a number of publications [Kadoshima et al., 2013;

Lancaster et al., 2013], including the protocol that was applied to generate the organoids analysed in this thesis (Figure 26 and Iefremova et al., 2017; Krefft et al., 2018). Additionally, the 3D setting allows the identification of mitotic events with potentially different cell fates by spindle orientation and apical membrane attachment. The latter was here determined by Phalloidin staining (Figure 26), as actin is known to accumulate around adherens junctions representing the contact points to the apical membrane. Using high resolution microscopy, Marthiens and ffrench-Constant, 2009 found that actin accumulates between the apical PAR complex and the slightly more basal N-Cadherin-containing tight junctions, both of which are implicated in cell fate decisions [Kosodo et al., 2004; Marthiens and ffrench-Constant, 2009]. Therefore, the asymmetric distribution of actin between daughter cells during mitosis serves as a good proxy for the distribution of polarity as well as junctional complexes in the organoid system. The time point of the analysis (day 20 after EB formation) was chosen briefly after neurogenesis sets in and the first neurons appear within the developing CP (Figure 26). Therefore, a majority of cell divisions were still grouped as proliferative (56% planar), and a percentage of 44% were identified as being potentially neurogenic cell divisions (18% delaminating and 26% intermediate) (Figure 27). This makes it possible to analyse the different cell division modes and the distribution of potential asymmetry factors within the same organoid.

Combining these two cell culture systems, makes iPSC-derived NSCs a powerful tool to study human neurodevelopment, including asymmetric cell division. The scalable 2D system is especially useful for screening and molecular analyses as well as live cell imaging. Whereas the 3D organoid model can be used to tackle questions like spindle orientation and the influence of the tissue context on cell fate.

7.2 Vesicles as asymmetry factors in human NSCs

The role model of vesicles as asymmetry factors are Sara$^+$ endosomes, which are mainly studied during asymmetric cell division of *D. melanogaster* SOP cell. In this model system, Sara$^+$ vesicles are thought to represent a specified subpopulation of endosomes, which are asymmetrically segregated, whereas the overall population of Rab5$^+$ endosomes show no asymmetry during mitosis [Coumailleau et al., 2009]. A similar mechanism has been established in the spinal cord and recently also in the brain of zebrafish [Kressmann et al., 2015; Zhao et al., 2020]. As this suggests a conserved underlying mechanism in NSC division, different vesicle subtypes were analysed here as potential asymmetry factors in the human NSC model systems.

Based on published studies on asymmetric cell division [Kressmann et al., 2015; Loeffler et al., 2019; Zhao et al., 2020], equivalent standards were used to identify asymmetric segregation of proteins in this thesis. Mitotic events are considered asymmetric, in case one daughter cell inherits 1.5 times or 50% more vesicles than the other daughter cell. Applying this cut-off revealed, however, no asymmetries of classical endosomal markers in the performed screening, including the human Sara orthologue ZFYVE9. In contrast, the here presented data suggests different vesicular compartments to be asymmetrically distributed during human NSC division, namely CD63$^+$ and LAMP1/2$^+$ vesicles (Figure 9). These are considered typical markers for MVB and lysosomes, respectively [Hunziker et al., 1996; Escola et al., 1998]. Therefore, it seems that in the human context rather late stages within the endolysosomal pathway are segregated during cell division compared to early endosomal stages in *D. melanogaster* and zebrafish. Although this is the first evidence from NSCs, it is in line with findings from mammalian hematopoietic stem/progenitor cells, where CD63 and lysosomes were described as asymmetry factors [Beckmann et al., 2007; Loeffler et al., 2019]. Interestingly, also in the hematopoietic system no direct link between asymmetric distribution of CD63 and any cell fate decision has been described, similar to the missing link of CD63 asymmetry and neuronal differentiation found in this thesis (Figure 9). Lysosomes, on the contrary, influence the metabolic state of hematopoietic stem cells and thereby their cell fate [Loeffler et al., 2019].

In general, the work with marker proteins to identify vesicular subpopulations should be taken with caution, as there are no sharp borders but rather a gradient of these proteins along the endocytic pathway [Rink et al., 2005]. Several studies show overlap of different endosomal marker proteins at subcellular structures, e.g. presence of LAMP1 on endosomal vesicles [Akasaki et al., 1996; Peden et al., 2004; Ebrahim and Thilo, 2011; Humphries et al., 2011; Cheng et al., 2018; Shearer and Petersen, 2019]. Co-staining of LAMP1 and CD63 also showed a considerable co-localization in NSCs (Figure 17) as well as in other mammalian cell lines [Rous et al., 2002; Shapiro et al., 2007; Baba et al., 2020]. Recent studies underline a highly dynamic equilibrium especially between late endosomes and endolysosomes [Bright et al., 2016; Bissig et al., 2017]. Also, the localization of Sara to Rab5$^+$ early endosomes [Di Guglielmo et al., 2003; Coumailleau et al., 2009] can be discussed, as Sara was also described to colocalize with hepatocyte growth factor-regulated tyrosine kinase substrate (Hrs) [Bökel et al., 2006] which is associated with MVB formation [Kobayashi et al., 2000; Bache et al., 2003]. The results from the here presented sucrose density gradient centrifugation hint in a similar direction (Figure 12). Here, the human Sara orthologue ZFYVE9 and CD63 showed a similar distribution with two peaks, so ZFYVE9 in human NSCs also seems to be associated with rather late endosomes and MVBs. This might indicate that asymmetry in *D. melanogaster* is indeed also mediated by a

vesicular compartment further down the endolysosomal pathway, closer to LAMP1$^+$ vesicles identified in the human context.

The study design here had the advantage that it not only focussed on fixed and stained cells, where the separation of vesicle markers might be unclear, but the results were additionally confirmed in living cells by LysoTracker imaging (Figure 24). Its fluorescence is solely dependent on the pH, therefore underlines that late, highly acidic stages of endolysosomal vesicles act as asymmetry factors in human NSCs in about 20% of mitotic event in proliferative conditions (Figure 24). Besides, the use of IF staining together with LysoTracker imaging circumvents the necessity to use fluorescently tagged proteins, which are commonly utilized in studies of asymmetric cell division [Coumailleau et al., 2009; Loeffler et al., 2019]. It is sufficiently well-known that fluorescent fusion-proteins for the visualization of protein dynamics have to be carefully designed not to affect protein function and localization [Snapp, 2005]. Indeed, this issue was also addressed in the most recent study on asymmetry in hematopoietic stem cells, where mCherry-Numb fusion protein showed clear asymmetry, whereas Numb-Venus did not [Loeffler et al., 2019].

To conclude, endolysosomal vesicles were identified as asymmetry factors in human NSCs by two independent techniques based on the localization of endogenous vesicle markers and the intrinsic acidification of endolysosomal vesicles.

7.3 Acidified vesicles as signalling hubs for Notch receptors

Independent of the vesicular compartment and the cell type involved, vesicles identified as asymmetry factors were regularly found to be biased towards the daughter cell with high Notch signalling activity [Coumailleau et al., 2009; Kressmann et al., 2015; Loeffler et al., 2019; Zhao et al., 2020]. Even if the type of vesicles facilitating the asymmetry might not be identical, the downstream mechanism deciding over the cell fate of the daughter cells is potentially conserved across species and stem cell populations.

The importance of Notch signalling for mammalian NSC maintenance not only *in vivo*, but also *in vitro* is well-established. Blocking Notch cleavage by the γ-secretase inhibitor DAPT is commonly used to induce rapid neuronal differentiation of NSCs *in vitro* [Crawford and Roelink, 2007; Elkabetz et al., 2008; Woo et al., 2009; Borghese et al., 2010]. This was confirmed for the NSCs used in this thesis, as DAPT treatment for two days diminished Notch signalling and pushed a majority of cells to adopt a neuronal morphology (Figure 22). This intrinsic dependency on Notch signalling is on the one hand a great advantage over other human cell lines often used to study molecular aspects of Notch signalling. In NSCs no exogenous expression of Notch pathway

components is necessary, therefore, it is possible to study the pathway without potential disturbances by overexpression artefacts. Especially in this tightly controlled pathway, which also exhibit elaborate cell-type specific regulatory mechanisms, it is important to study the signalling in the endogenous setting. On the other hand, any disruption or manipulation of Notch signalling activity can trigger differentiation and the loss of the stem cell population. This makes it hard to perform loss-of-function analysis in this system and is a potential drawback.

In the steady-state, endogenous Notch receptors were found predominantly in LAMP1^{+} vesicles in human NSCs, which was verified not only by IF staining but also by sucrose density gradient centrifugation (Figure 11 and Figure 12). Therefore, the endocytic route of Notch receptors was analysed in more detail. On the one hand, to provide a potential functional link between Notch signalling and LAMP1 asymmetries during NSC division. On the other hand, to shed some light on still controversially discussed questions about the importance of endocytosis for Notch pathway activity: (1) is the endocytosis of Notch ligands necessary for inducing receptor cleavage (2) is the endocytosis of the Notch receptors necessary for the activation (3) is Notch receptor cleavage in intracellular vesicles mediated by ligand binding?

First, the endocytosis of Notch ligands is thought to apply a pulling force on the Notch receptor heterodimers leading to its disassembly and S2/S3 cleavages [Parks et al., 2000; Gordon et al., 2015; Lovendahl et al., 2018]. However, there is also evidence that the signal-receiving cell might provide this pulling force by transendocytosis of the ligand [Klueg and Muskavitch, 1999; Varnum-Finney et al., 2000; Chapman et al., 2016]. Additionally, soluble variants of Notch ligands were found to activate the signalling pathway in non-vertebrates as well as human keratinocytes [Qi et al., 1999; Aho, 2004; Chen and Greenwald, 2004], which suggests Notch signalling to be at least in part independent of a mechanical force separating the receptor heterodimer. The latter view, can be supported by a series of data presented in this thesis. Co-staining of Notch1ECD with the Notch1 antibody, targeting the ICD, suggests the presence of intact heterodimers within the same vesicular structures (Figure 15). Also, the internalization of the Notch ligands DLL1 and JAG1 in complex with the receptor (Figure 16), hints into the direction that Notch receptors are internalized before S2 cleavage occurs and the ECD bound by the ligand dissociates from the receptor.

Concerning the second point, the internalization of Notch receptors itself was already described almost 25 years ago [Seugnet et al., 1997]. The functional outcome of this process, however, is still controversially discussed with evidence suggesting receptor degradation or receptor activation, respectively. The former is supported by several studies that show Notch receptor targeting for lysosomal degradation by ubiquitination or association with β-arrestin [McGill and McGlade, 2003; Mukherjee et al., 2005; McGill et al., 2009; Puca et al., 2013]. Also, disruption

of lysosomal biogenesis was recently found to enhance Notch signalling due to lower degradation rates [Gomez-Lamarca et al., 2015; Zhou et al., 2016]. Notch receptor degradation via the autophagic pathway was further reported to play a role in starved cells [Wu et al., 2016; Tao et al., 2018]. In these studies, Notch receptors were both recycled from the plasma membrane and redirected already on their way to the cell surface in form of the uncleaved full-length protein [Wu et al., 2016]. However, taking all results presented here together, they point into another direction. Treatment with lysosomal protease inhibitor does neither alter Notch1 protein level, nor Notch1 receptor cleavage (Figure 19). Autophagy also seems to be not involved in the shuttling of Notch1 receptors towards lysosomal vesicles in human NSCs, as no colocalization between Notch1ECD and $LC3^+$ autophagosomes was observed (Figure 15). Redirection of the full-length receptor pro-form for degradation within $LAMP1^+$ vesicles can also be excluded, as Western Blot analysis of sucrose fractions clearly showed accumulation of S1 cleaved Notch1 in $LAMP1^+$ fractions (Figure 12).

On the contrary, results from this study are more in line with the idea that Notch receptor activation occurs within the increasingly acidic endolysosomal vesicles [Gupta-Rossi et al., 2004; Vaccari et al., 2008; Yan et al., 2009; Windler and Bilder, 2010] upon CME [Windler and Bilder, 2010; Chapman et al., 2016]. Consistently, Notch1 receptor were found to accumulate in Clathrin-coated membrane pits on the cell surface (Figure 13) and their internalization dependent on Dynamin (Figure 14 and Figure 18). Notch2 receptor localization to $LAMP1^+$ vesicles, however, seemed to be independent of Dynamin. Although the transcriptional activity of Notch1 and Notch2 ICDs was found to be equivalent [Liu et al., 2015], a newly described Notch regulator in human NSCs, namely the Notch2 paralog Notch2NL [Fiddes et al., 2018; Suzuki et al., 2018], might be an explanation for a divergent regulation of Notch2 in this cell type. Further, the sucrose density gradient centrifugation showed a clear accumulation of Presenilin 1 along with Notch receptors in $LAMP1^+$ fractions (Figure 12). This is in line with findings that components of the γ-secretase complex are located at lysosomal membranes [Bagshaw et al., 2003; Pasternak et al., 2003]. Additionally, the sole possibility to stain for Notch receptors colocalizing with $LAMP1^+$ vesicles (Figure 11) indicates that the transport of receptors to these vesicles has to take place before S3 cleavage. Release of the ICD from the membrane would lead to the loss of the antigen recognized by the Notch1 and Notch2 antibodies from the surface of the $LAMP1^+$ structures. This can also explain the high variance in colocalization found between individual cells (Figure 11), as dependent on the stage of a cell within the signalling pathway the ICD might already be released into the cytosol and translocated to the nucleus. Supporting this mechanism, the cleavage properties of the involved proteases have to be mentioned. ADAM family proteases as well as the γ-secretase complex were found to have higher affinities to target

proteins and more efficient protease activity in acidic environment compared to the neutral pH of the extracellular or cytosolic space [McLendon et al., 2000; Carey et al., 2005; Carey et al., 2011]. This was confirmed here by inhibition of v-ATPase, which is necessary for the acidification of endolysosomal vesicles [Trombetta et al., 2003; Lafourcade et al., 2008] and was already found to be important for Notch signal activation [Yan et al., 2009; Valapala et al., 2013; Tognon et al., 2016]. Treatment with the v-ATPase inhibitor BafA reduced Notch1 receptor cleavage and repressed transcription of downstream targets (Figure 19). Interestingly, a study by Tagami et al., 2008 showed that cleavage of Notch receptors can indeed occur both at the plasma membrane and in endocytic vesicles, generating two distinct ICD variants. Whereas cleavage of Notch receptors at the plasma membrane generates a longer, more stable ICD, the ICD produced after Notch receptor internalization is three amino acids shorter and also showed an increased turnover. Taken into account that the oscillation of Notch signalling was found to be essential for the proliferation and maintenance of NSCs [Shimojo et al., 2008], endocytosis prior to receptor cleavage and hence the release of an unstable ICD variant might facilitate a faster shutdown of Notch signalling in this context.

The last controversial point is whether Notch receptor activation after endocytosis is triggered by ligand interaction. The internalization of recombinant Notch ligands shown in this thesis demonstrates that soluble ligands bound on the cell surface can be internalized together with the receptor (Figure 16 and Figure 18). Whether such ligand variants can trigger Notch receptor cleavage is, however, unclear with several studies supporting [Qi et al., 1999; Aho, 2004; Chen and Greenwald, 2004] and contradicting Notch activation by soluble ligands [Sun and Artavanis-Tsakonas, 1997; Masuya et al., 2002; Urs et al., 2008; Klose et al., 2015]. However, also membrane bound Notch ligands can undergo endocytosis into the signal-receiving cell. One model suggests that ligands from the neighbouring signal-sending cell can undergo transendocytosis, but the molecular mechanism behind these observations remains elusive [Seugnet et al., 1997; Klueg and Muskavitch, 1999; Chapman et al., 2016]. A second potential mechanism is the internalization of receptors and ligands from the plasma membrane of the same cell. Usually, this cis-interactions of receptors and ligands located at the same membrane leads to a parallel binding and hence inactivation of the Notch pathway [Fiuza et al., 2010; Sprinzak et al., 2010]. However, after endocytosis and the maturation of endosomes to MVBs it is thought that an antiparallel trans-interaction is facilitated by the localization of ligands and receptors to ILVs and the limiting vesicle membrane, respectively [Coumailleau et al., 2009; Kressmann et al., 2015]. This might be supported by the partial colocalization of Notch receptors and CD63, as a MVB marker (Figure 11). Further support for intravesicular interaction can be seen in the affinity increase between Notch and Delta in an acidic environment [Pei and Baker,

2008], e.g. found along the endocytic pathway. Another completely different model is supported by several studies in *D. melanogaster* and suggests that Notch receptor activation can be facilitated by endocytosis and shuttling to endolysosomal vesicles alone [Wilkin et al., 2008; Yamada et al., 2011; Schneider et al., 2013]. Here, the activation is independent of ligand-receptor interaction and seems to be dependent on a specialized ADAM protease, namely ADAM17 [Bozkulak and Weinmaster, 2009].

Summing up, it was verified that endogenous Notch1 receptor heterodimers are endocytosed in human NSCs. This process is mediated by CME and rather triggers receptor activation due to the drop in pH, than receptor degradation and shutdown of Notch signalling. It remains to be determined whether receptor cleavage is independent of ligand binding, induced by ligand binding on the cell surface and transendocytosis or receptor-ligand-interaction within subcellular vesicles. During asymmetric cell division Notch receptor transport in endolysosomal vesicles is supposed to generate a bias in Notch signalling activity by the spatially restricted release of the ICD in one of the daughter cells.

7.4 Asymmetry of vesicles predicts cell fate decision

This proposed bias in Notch signalling activity and the downstream cell fate decision was therefore analysed in the concluding experiments of this thesis.

Active Notch signalling results, amongst others, in expression of HES1 which is crucial for the maintenance of NSC fate by repressing neuronal differentiation [Ishibashi et al., 1994; Ohtsuka et al., 2001]. Therefore, HES1 expression was used as a marker for Notch signalling activity and a predictor of cell fate after a mitotic event. The reporter line generated and characterized in this thesis is based on the expression of a fluorescent protein from the endogenous locus of the *HES1* gene. Commonly used reporters for Notch signalling activity are often based on the exogenous delivery of synthetic plasmid reporters by transfection or transduction. Similar to the overexpression of Notch pathway components these reporters might disrupt the signalling activity by sequestering Notch ICD at the exogenous CSL motifs influencing the expression of endogenous Notch target genes. As the signalling pathway is not further amplified within the cell this could significantly alter downstream gene expression, including e.g. feedback loops important for Notch signal oscillation in NSCs [Takebayashi et al., 1994; Hirata et al., 2002; Shimojo et al., 2008].

The HES1-reporter line presented is the first human reporter cell line described that is based on the expression of a fluorescent protein from the endogenous *HES1* locus (Figure 20 and Figure 21). With this strategy, a maximum of two copies of the reporter construct can be inserted

within the genome, making it necessary to use a bright fluorophore to detect expression. The tdTomato protein was therefore chosen due to its brightness and relatively low maturation time of about 60 min [Shaner et al., 2004]. With its excitation and emission wavelength within the red spectrum, 554 nm and 581 nm, respectively, autofluorescent background in the green spectrum is avoided, which makes it useful for live cell and even *in vivo* imaging [Winnard et al., 2006; Wu et al., 2017; Syverud et al., 2018]. However, as the name indicates tdTomato is a dimeric and hence relatively big protein (54.2 kDa). Therefore, the fluorophore was uncoupled from the HES1 protein by a self-cleaving T2A site [Donnelly et al., 2001; Szymczak and Vignali, 2005] to avoid functional impairments. The nuclear localization of tdTomato was facilitated by the fusion to a NLS sequence, which made it easier to quantify the total tdTomato signal within individual cells. The efficient transport of the fluorescent protein into the nucleus can be observed after mitosis. Whereas the protein was detectable throughout the cytoplasm during mitosis, the fluorescence signal was restricted to the nucleus within a few minutes after cell division, when the nuclear envelop was re-established (Figure 24). To capture dynamic changes in HES1 expression, the half-life of tdTomato, which is estimated to be longer than 24 h [Verkhusha et al., 2003], needed to be reduced. This was achieved by an additional PEST sequence, which is known to increase fluorophore turnover in reporter constructs [Li et al., 1998; Corish and Tyler-Smith, 1999], including a Notch signalling reporter used in chicken embryos [Vilas-Boas et al., 2011]. The fusion of PEST sequences to fluorescent proteins can reduce their half-life down to 2 h [Li et al., 1998]. Such a reduction was not observed in the present HES1-tdTomato reporter, however, the half-life of around 3.5 h (Figure 22) was sufficient to track changes in HES1 expression within a time frame of several hours after mitosis. With this half-life even slight oscillations of HES1 expression known to be important for NSC maintenance [Shimojo et al., 2008] were observed in individual cells (data not shown). However, quantification of Notch signalling activity was performed on randomly selected cells located throughout the cell culture vessel. Therefore, a synchronization, which was described in neighbouring cells [Delaune et al., 2012], was not to be expected in this subset of analysed cells and the oscillation effects cannot be seen after averaging the intensity values. Besides, the effects of disrupting the Notch pathway by DAPT and BafA, which were seen in Western Blot and qPCR (Figure 19), were reproduced in live cell imaging (Figure 23).

Taking the maturation time and half-life of tdTomato into account, the quantification of HES1 dynamics after cell division was started around 1.5 h after the final stages of mitosis. This should enforce that HES1 expression directly after mitosis is analysed. The restriction of the imaging window to 6 h after mitosis should prevent that later signalling events, e.g. induced by differences in cell density and lateral inhibition, have an impact on the results. It has to be

mentioned that HES1 expression is not solely dependent on Notch signalling. There are reports that HES1 expression in mammalian NSCs is e.g. also dependent on FGF2 signalling [Sanalkumar et al., 2010; Sato et al., 2010; Lahti et al., 2011]. As FGF2 is used as a growth factor for the maintenance of rosette-type NSCs, there is the possibility that the expression of tdTomato is in part influenced by FGF2. This was ruled out by the decrease of reporter expression by DAPT treatment, that diminishes tdTomato fluorescence even in the presence of FGF2 in the medium (Figure 23). Further, the changes between daughter cells after mitosis are unlikely caused by FGF2 signalling as the medium conditions provide a global abundance of the growth factor to all cells in culture.

With the combined live cell imaging of HES1-reporter NSCs and LysoTracker it was possible to support the working hypothesis: an asymmetric segregation of acidic vesicles during mitosis leads to a HES1 expression bias in the daughter cells and clustering of HES1 expression pattern made the picture even more clear. Similar to the study in hematopoietic stem cells which applied a comparable clustering approach [Loeffler et al., 2019], certain amount of HES1 asymmetries after LysoTracker-symmetric divisions and vice versa were reported. Beside the fact, that vesicle segregation is very likely not the only process involved in Notch signal regulation and hence HES1 expression, some experimental issues may also add to these variations. LysoTracker only stains a subset of $LAMP1^{+}$ vesicles (Figure 17) [Johnson et al., 2016], which might create a technical limitation for the precision of live cell imaging compared to IF staining. However, a comparable percentage of LysoTracker and LAMP1 asymmetries in mitotic NSCs (20% and 26-30%, respectively; Figure 24 and Figure 8) showed that this effect is probably negligible in this setting. The sharp, arbitrary threshold set to differentiate between LysoTracker-symmetric and -asymmetric cell divisions might also add some inaccuracy to the system. As mentioned in chapter 7.2, the threshold is set based on several publications on asymmetric cell division [Kressmann et al., 2015; Loeffler et al., 2019; Zhao et al., 2020]. However, it is possible that especially with the linear Notch signalling pathway, where the signal is not further amplified, gradual effects may have a greater influence in the current paradigm. And still, a clear shift of HES1 expression patterns from symmetric and opposing asymmetric to highly asymmetric was observed upon LysoTracker asymmetry supporting the working hypothesis (Figure 25).

Thus, the segregation of acidic vesicles can be considered at least one part of the explanation for a Notch signalling bias between daughter cells after asymmetric cell division. Especially in a mammalian context this is one of the few pathways so far described to generate this kind of Notch signalling bias, whereas e.g. the role of the most important Notch regulator in *D. melanogaster*, namely Numb, remains highly controversial [Petersen et al., 2002; Li et al., 2003; Klezovitch et al., 2004; Petersen et al., 2004; Rasin et al., 2007]. In line, Numb distribution with

2D NSCs showed no clear polarization within the neural rosettes (Figure 7 and data not shown). A study by Chapman et al., 2006 gives a potential explanation, as mammalian Numb and Nbl are degraded in the presence of high levels of cleaved Notch ICD. The highly active Notch signalling in mammalian NSC might therefore reduce Numb and Nbl protein level so that they cannot pursue their function as asymmetry factors during asymmetric cell division.

Therefore, a connection between the upstream processes, like mitotic spindle orientation and differential inheritance of polarity factors which are also fairly well-understood in mammals [Kosodo et al., 2004; Konno et al., 2008; Marthiens and ffrench-Constant, 2009; Postiglione et al., 2011], and the downstream cell fate decision by Notch signalling remains vague. The asymmetric segregation of Notch1 receptors as a cargo of $LAMP1^{+}$ vesicles described here might be one of the missing links. Confirming the results obtained from 2D cultures of NSCs in human forebrain organoids further hints in that direction (Figure 27). Asymmetry of both proteins seems to be dependent on the attachment of the daughter cells to the apical membrane and is increasing from planar to intermediate and delaminating cell divisions. This gradual increase is in line with findings that polarity as well as junctional complexes can influence cell fate [Kosodo et al., 2004]. However, the asymmetric distribution of polarity complexes was also found to be sufficient to induce differences in cell fate, and both daughter cells retain their contact to the apical membrane [Marthiens and ffrench-Constant, 2009]. Therefore, a closer look on the distribution of polarity factors might give some further insides into the pathway upstream of vesicle segregation.

Reproducing LAMP1 and Notch1 asymmetry in this 3D context adds the last step to the proposed mechanism, as the asymmetric distribution can thereby not only be linked to an immediate change in Notch activity after division, but also to a downstream commitment to a neuronal cell fate.

8 Conclusion and Outlook

Taken together, iPSC-derived NSCs were established as a versatile tool to study asymmetric cell division and cell fate decision in a highly controlled cell population *in vitro*. Together with the fast evolving field of human brain organoids, this opens up the possibility for the first time to study human-specific aspects of early neurodevelopment on a detailed molecular level.

The main findings presented in this thesis can be summarized as follows (Figure 28):

1) Acidic, LAMP1$^+$ vesicles are asymmetry factors linked to neuronal differentiation
2) Notch receptors are internalized as heterodimers by CME
3) Accumulation of Notch receptors in acidic vesicles triggers their cleavage
4) Asymmetry of endolysosomal vesicles predict a bias in Notch signalling activity and is associated with neurogenic cell divisions

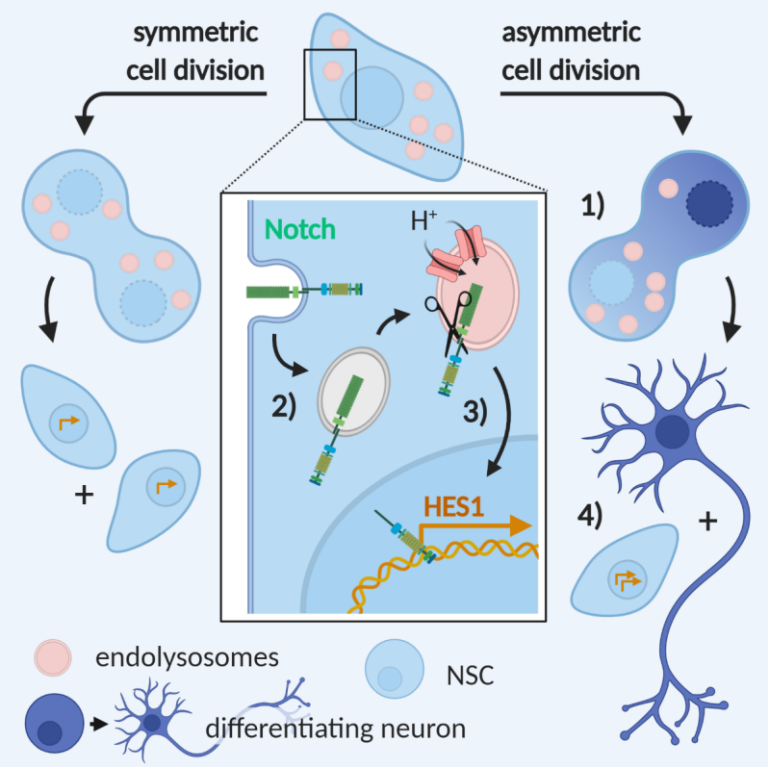

Figure 28: Proposed role of endolysosomes as signalling hubs for Notch receptor signalling and cell fate decision.

This elevates endolysosomes to new signalling hubs for the Notch pathway and their asymmetric segregation to one of the evolutionary best conserved asymmetry mechanism to bias the activity of Notch signalling.

One of the open question concerning Notch activation in acidic vesicles remains whether this signalling might be independent of ligand interaction with the receptor or how the ligand binding is achieved within the vesicular compartment.

Also, the mechanistic details regulating the suggested pathway upstream of the asymmetric vesicle segregation have to be elucidated further. It is tempting to speculate that the classical polarity factors mediating apical-basal polarity are involved. Some published findings give first indications in this direction: aPKC can recruit ADAM10 protease necessary for S2 cleavage [Britton et al., 2017] and triggers transport of Notch receptors towards lysosomes [Sjöqvist et al., 2014]. The CRB complex is also found to be involved in Notch receptor endocytosis and activation [Ohata et al., 2011; Nemetschke and Knust, 2016]. The asymmetry of $Sara^+$ vesicles in *D. melanogaster* of course provides substantial indications that cellular polarity triggers vesicle segregation, either directly [Loubéry et al., 2014] or indirectly via the asymmetric assembly of the mitotic spindle which $Sara^+$ vesicles use for trafficking [Derivery et al., 2015]. In zebrafish, however, Sara distribution was found to be independent of Par3 [Kressmann et al., 2015] and recent findings suggest a bias of $Sara^+$ vesicles in an anterior-posterior manner [Zhao et al., 2020]. This might indicate that similar to *D. melanogaster* SOP cells, not only apical-basal polarity, but also PCP can influence vesicle asymmetry in vertebrates. In contrast to the findings in mammals [Kosodo et al., 2004; Marthiens and ffrench-Constant, 2009] and the evidence provided in this thesis, components of the Par complex in the developing zebrafish brain accumulate in the differentiating daughter cell [Dong et al., 2012].

Therefore, further research is necessary to reveal the connections between asymmetric inheritance of polarity factors, vesicles as asymmetry factors and cell fate decision, which probably vary in their molecular details between species. The human-specific aspect can now be unravelled using iPSC-derived NSC model systems, with a starting point set by this thesis.

References

Aaku-Saraste, E., Hellwig, A., and Huttner, W.B. (1996). Loss of occludin and functional tight junctions, but not ZO-1, during neural tube closure--remodeling of the neuroepithelium prior to neurogenesis. Developmental biology *180*, 664-679.

Acar, M., Jafar-Nejad, H., Takeuchi, H., Rajan, A., Ibrani, D., Rana, N.A., Pan, H., Haltiwanger, R.S., and Bellen, H.J. (2008). Rumi is a CAP10 domain glycosyltransferase that modifies Notch and is required for Notch signaling. Cell *132*, 247-258.

Aho, S. (2004). Soluble form of Jagged1: unique product of epithelial keratinocytes and a regulator of keratinocyte differentiation. Journal of cellular biochemistry *92*, 1271-1281.

Akasaki, K., Michihara, A., Fujiwara, Y., Mibuka, K., and Tsuji, H. (1996). Biosynthetic transport of a major lysosome-associated membrane glycoprotein 2, lamp-2: a significant fraction of newly synthesized lamp-2 is delivered to lysosomes by way of early endosomes. Journal of biochemistry *120*, 1088-1094.

Alexandrov, K., Horiuchi, H., Steele-Mortimer, O., Seabra, M.C., and Zerial, M. (1994). Rab escort protein-1 is a multifunctional protein that accompanies newly prenylated rab proteins to their target membranes. The EMBO journal *13*, 5262-5273.

Ali, F., Hindley, C., McDowell, G., Deibler, R., Jones, A., Kirschner, M., Guillemot, F., and Philpott, A. (2011). Cell cycle-regulated multi-site phosphorylation of Neurogenin 2 coordinates cell cycling with differentiation during neurogenesis. Development (Cambridge, England), 4267-4277.

Allache, R., Marco, P. de, Merello, E., Capra, V., and Kibar, Z. (2012). Role of the planar cell polarity gene CELSR1 in neural tube defects and caudal agenesis. Birth defects research. Part A, Clinical and molecular teratology, 176-181.

Amit, M., Carpenter, M.K., Inokuma, M.S., Chiu, C.P., Harris, C.P., Waknitz, M.A., Itskovitz-Eldor, J., and Thomson, J.A. (2000). Clonally derived human embryonic stem cell lines maintain pluripotency and proliferative potential for prolonged periods of culture. Developmental biology *227*, 271-278.

Andrawes, M.B., Xu, X., Liu, H., Ficarro, S.B., Marto, J.A., Aster, J.C., and Blacklow, S.C. (2013). Intrinsic selectivity of Notch 1 for Delta-like 4 over Delta-like 1. The Journal of biological chemistry *288*, 25477-25489.

Andrews, R., and Ahringer, J. (2007). Asymmetry of early endosome distribution in C. elegans embryos. PloS one, e493.

Apelqvist, A., Li, H., Sommer, L., Beatus, P., Anderson, D.J., Honjo, T., Hrabe de Angelis, M., Lendahl, U., and Edlund, H. (1999). Notch signalling controls pancreatic cell differentiation. Nature *400*, 877-881.

Araùjo, M.E.G. de, Huber, L.A., and Stasyk, T. (2008). Isolation of endocitic organelles by density gradient centrifugation. Methods in molecular biology (Clifton, N.J.) *424*, 317-331.

Atwood, S.X., Chabu, C., Penkert, R.R., Doe, C.Q., and Prehoda, K.E. (2007). Cdc42 acts downstream of Bazooka to regulate neuroblast polarity through Par-6 aPKC. Journal of cell science *120*, 3200-3206.

Atwood, S.X., and Prehoda, K.E. (2009). aPKC phosphorylates Miranda to polarize fate determinants during neuroblast asymmetric cell division. Current biology : CB *19*, 723-729.

Baba, K., Kuwada, S., Nakao, A., Li, X., Okuda, N., Nishida, A., Mitsuda, S., Fukuoka, N., Kakeya, H., and Kataoka, T. (2020). Different localization of lysosomal-associated membrane protein 1 (LAMP1) in mammalian cultured cell lines. Histochemistry and cell biology, 199-213.

Bache, K.G., Brech, A., Mehlum, A., and Stenmark, H. (2003). Hrs regulates multivesicular body formation via ESCRT recruitment to endosomes. The Journal of cell biology *162*, 435-442.

Bachiller, D., Klingensmith, J., Kemp, C., Belo, J.A., Anderson, R.M., May, S.R., McMahon, J.A., McMahon, A.P., Harland, R.M., and Rossant, J., et al. (2000). The organizer factors Chordin and Noggin are required for mouse forebrain development. Nature *403*, 658-661.

Baek, J.H., Hatakeyama, J., Sakamoto, S., Ohtsuka, T., and Kageyama, R. (2006). Persistent and high levels of Hes1 expression regulate boundary formation in the developing central nervous system. Development (Cambridge, England) *133*, 2467-2476.

Bagshaw, R.D., Pasternak, S.H., Mahuran, D.J., and Callahan, J.W. (2003). Nicastrin is a resident lysosomal membrane protein. Biochemical and biophysical research communications *300*, 615-618.

Bain, J., Plater, L., Elliott, M., Shpiro, N., Hastie, C.J., McLauchlan, H., Klevernic, I., Arthur, J.S.C., Alessi, D.R., and Cohen, P. (2007). The selectivity of protein kinase inhibitors: a further update. The Biochemical journal *408*, 297-315.

Beatus, P., Lundkvist, J., Öberg, C., Pedersen, K., and Lendahl, U. (2001). The origin of the ankyrin repeat region in Notch intracellular domains is critical for regulation of HES promoter activity. Mechanisms of Development *104*, 3-20.

Beckmann, J., Scheitza, S., Wernet, P., Fischer, J.C., and Giebel, B. (2007). Asymmetric cell division within the human hematopoietic stem and progenitor cell compartment: identification of asymmetrically segregating proteins. Blood *109*, 5494-5501.

Bellaïche, Y., Beaudoin-Massiani, O., Stuttem, I., and Schweisguth, F. (2004). The planar cell polarity protein Strabismus promotes Pins anterior localization during asymmetric division of sensory organ precursor cells in Drosophila. Development (Cambridge, England) *131*, 469-478.

Bellaïche, Y., Radovic, A., Woods, D.F., Hough, C.D., Parmentier, M.-L., O'Kane, C.J., Bryant, P.J., and Schweisguth, F. (2001). The Partner of Inscuteable/Discs-Large Complex Is Required to Establish Planar Polarity during Asymmetric Cell Division in Drosophila. Cell *106*, 355-366.

Benedito, R., Roca, C., Sörensen, I., Adams, S., Gossler, A., Fruttiger, M., and Adams, R.H. (2009). The notch ligands Dll4 and Jagged1 have opposing effects on angiogenesis. Cell *137*, 1124-1135.

Benton, R., and Johnston, D.S. (2003). Drosophila PAR-1 and 14-3-3 Inhibit Bazooka/PAR-3 to Establish Complementary Cortical Domains in Polarized Cells. Cell *115*, 691-704.

Berdnik, D., Török, T., González-Gaitán, M., and Knoblich, J.A. (2002). The Endocytic Protein α-Adaptin Is Required for Numb-Mediated Asymmetric Cell Division in Drosophila. Developmental Cell *3*, 221-231.

Betizeau, M., Cortay, V., Patti, D., Pfister, S., Gautier, E., Bellemin-Ménard, A., Afanassieff, M., Huissoud, C., Douglas, R.J., and Kennedy, H., et al. (2013). Precursor diversity and complexity of lineage relationships in the outer subventricular zone of the primate. Neuron *80*, 442-457.

Betschinger, J., Mechtler, K., and Knoblich, J.A. (2006). Asymmetric segregation of the tumor suppressor brat regulates self-renewal in Drosophila neural stem cells. Cell *124*, 1241-1253.

Bilder, D., Li, M., and Perrimon, N. (2000). Cooperative regulation of cell polarity and growth by Drosophila tumor suppressors. Science (New York, N.Y.) *289*, 113-116.

Bilder, D., Schober, M., and Perrimon, N. (2003). Integrated activity of PDZ protein complexes regulates epithelial polarity. Nature cell biology *5*, 53-58.

Bissig, C., Hurbain, I., Raposo, G., and van Niel, G. (2017). PIKfyve activity regulates reformation of terminal storage lysosomes from endolysosomes. Traffic (Copenhagen, Denmark) *18*, 747-757.

Bökel, C., Schwabedissen, A., Entchev, E., Renaud, O., and González-Gaitán, M. (2006). Sara endosomes and the maintenance of Dpp signaling levels across mitosis. Science (New York, N.Y.) *314*, 1135-1139.

Bolotin, A., Quinquis, B., Sorokin, A., and Ehrlich, S.D. (2005). Clustered regularly interspaced short palindrome repeats (CRISPRs) have spacers of extrachromosomal origin. Microbiology (Reading, England) *151*, 2551-2561.

Boone, J.Q., and Doe, C.Q. (2008). Identification of Drosophila type II neuroblast lineages containing transit amplifying ganglion mother cells. Developmental neurobiology *68*, 1185-1195.

Borghese, L., Dolezalova, D., Opitz, T., Haupt, S., Leinhaas, A., Steinfarz, B., Koch, P., Edenhofer, F., Hampl, A., and Brüstle, O. (2010). Inhibition of notch signaling in human embryonic stem cell-derived neural stem cells delays G1/S phase transition and accelerates neuronal differentiation in vitro and in vivo. Stem cells (Dayton, Ohio) *28*, 955-964.

Bowman, S.K., Neumüller, R.A., Novatchkova, M., Du, Q., and Knoblich, J.A. (2006). The Drosophila NuMA Homolog Mud regulates spindle orientation in asymmetric cell division. Developmental Cell *10*, 731-742.

Bowman, S.K., Rolland, V., Betschinger, J., Kinsey, K.A., Emery, G., and Knoblich, J.A. (2008). The tumor suppressors Brat and Numb regulate transit-amplifying neuroblast lineages in Drosophila. Developmental Cell, 535-546.

Bozkulak, E.C., and Weinmaster, G. (2009). Selective use of ADAM10 and ADAM17 in activation of Notch1 signaling. Molecular and cellular biology *29*, 5679-5695.

Bright, N.A., Davis, L.J., and Luzio, J.P. (2016). Endolysosomes Are the Principal Intracellular Sites of Acid Hydrolase Activity. Current biology : CB *26*, 2233-2245.

Bright, N.A., Reaves, B.J., Mullock, B.M., and Luzio, J.P. (1997). Dense core lysosomes can fuse with late endosomes and are re-formed from the resultant hybrid organelles. Journal of cell science *110 (Pt 17)*, 2027-2040.

Britton, G.J., Ambler, R., Clark, D.J., Hill, E.V., Tunbridge, H.M., McNally, K.E., Burton, B.R., Butterweck, P., Sabatos-Peyton, C., and Hampton-O'Neil, L.A., et al. (2017). PKCθ links proximal T cell and Notch signaling through localized regulation of the actin cytoskeleton. eLife *6*.

Brou, C., Logeat, F., Gupta, N., Bessia, C., LeBail, O., Doedens, J.R., Cumano, A., Roux, P., Black, R.A., and Israël, A. (2000). A Novel Proteolytic Cleavage Involved in Notch Signaling. Molecular Cell *5*, 207-216.

Brückner, K., Perez, L., Clausen, H., and Cohen, S. (2000). Glycosyltransferase activity of Fringe modulates Notch-Delta interactions. Nature *406*, 411-415.

Bultje, R.S., Castaneda-Castellanos, D.R., Jan, L.Y., Jan, Y.-N., Kriegstein, A.R., and Shi, S.-H. (2009). Mammalian Par3 regulates progenitor cell asymmetric division via notch signaling in the developing neocortex. Neuron *63*, 189-202.

Cappello, S., Attardo, A., Wu, X., Iwasato, T., Itohara, S., Wilsch-Bräuninger, M., Eilken, H.M., Rieger, M.A., Schroeder, T.T., and Huttner, W.B., et al. (2006). The Rho-GTPase cdc42 regulates neural progenitor fate at the apical surface. Nature neuroscience *9*, 1099-1107.

Carey, R.M., Balcz, B.A., Lopez-Coviella, I., and Slack, B.E. (2005). Inhibition of dynamin-dependent endocytosis increases shedding of the amyloid precursor protein ectodomain and reduces generation of amyloid beta protein. BMC cell biology *6*, 30.

Carey, R.M., Blusztajn, J.K., and Slack, B.E. (2011). Surface expression and limited proteolysis of ADAM10 are increased by a dominant negative inhibitor of dynamin. BMC cell biology *12*, 20.

Castro, D.S., Martynoga, B., Parras, C., Ramesh, V., Pacary, E., Johnston, C., Drechsel, D., Lebel-Potter, M., Garcia, L.G., and Hunt, C., et al. (2011). A novel function of the proneural factor Ascl1 in progenitor proliferation identified by genome-wide characterization of its targets. Genes & development *25*, 930-945.

Castro, D.S., Skowronska-Krawczyk, D., Armant, O., Donaldson, I.J., Parras, C., Hunt, C., Critchley, J.A., Nguyen, L., Gossler, A., and Göttgens, B., et al. (2006). Proneural bHLH and Brn proteins coregulate a neurogenic program through cooperative binding to a conserved DNA motif. Developmental Cell *11*, 831-844.

Cau, E., Gradwohl, G., Casarosa, S., Kageyama, R., and Guillemot, F. (2000). Hes genes regulate sequential stages of neurogenesis in the olfactory epithelium. Development (Cambridge, England) *127*, 2323-2332.

Chambers, S.M., Fasano, C.A., Papapetrou, E.P., Tomishima, M., Sadelain, M., and Studer, L. (2009). Highly efficient neural conversion of human ES and iPS cells by dual inhibition of SMAD signaling. Nature biotechnology *27*, 275-280.

Chapman, G., Liu, L., Sahlgren, C., Dahlqvist, C., and Lendahl, U. (2006). High levels of Notch signaling down-regulate Numb and Numblike. The Journal of cell biology *175*, 535-540.

Chapman, G., Major, J.A., Iyer, K., James, A.C., Pursglove, S.E., Moreau, J.L.M., and Dunwoodie, S.L. (2016). Notch1 endocytosis is induced by ligand and is required for signal transduction. Biochimica et biophysica acta *1863*, 166-177.

Chartier, F.J.-M., Hardy, É.J.-L., and Laprise, P. (2011). Crumbs controls epithelial integrity by inhibiting Rac1 and PI3K. Journal of cell science *124*, 3393-3398.

Chastagner, P., Rubinstein, E., and Brou, C. (2017). Ligand-activated Notch undergoes DTX4-mediated ubiquitylation and bilateral endocytosis before ADAM10 processing. Science signaling *10*.

Chen, H., Thiagalingam, A., Chopra, H., Borges, M.W., Feder, J.N., Nelkin, B.D., Baylin, S.B., and Ball, D.W. (1997). Conservation of the Drosophila lateral inhibition pathway in human lung cancer: a hairy-related protein (HES-1) directly represses achaete-scute homolog-1 expression. Proceedings of the National Academy of Sciences of the United States of America *94*, 5355-5360.

Chen, N., and Greenwald, I. (2004). The lateral signal for LIN-12/Notch in C. elegans vulval development comprises redundant secreted and transmembrane DSL proteins. Developmental Cell *6*, 183-192.

Chen, S., Chen, J., Shi, H., Wei, M., Castaneda-Castellanos, D.R., Bultje, R.S., Pei, X., Kriegstein, A.R., Zhang, M., and Shi, S.-H. (2013). Regulation of microtubule stability and organization by mammalian Par3 in specifying neuronal polarity. Developmental Cell, 26-40.

Chen, X., and Macara, I.G. (2005). Par-3 controls tight junction assembly through the Rac exchange factor Tiam1. Nature cell biology *7*, 262-269.

Cheng, X.-T., Xie, Y.-X., Zhou, B., Huang, N., Farfel-Becker, T., and Sheng, Z.-H. (2018). Characterization of LAMP1-labeled nondegradative lysosomal and endocytic compartments in neurons. The Journal of cell biology, 3127-3139.

Chenn, A., and McConnell, S.K. (1995). Cleavage orientation and the asymmetric inheritance of notchl immunoreactivity in mammalian neurogenesis. Cell *82*, 631-641.

Choi, B.H. (1981). Radial glia of developing human fetal spinal cord: Golgi, immunohistochemical and electron microscopic study. Developmental Brain Research *1*, 249-267.

Choi, B.H., and Lapham, L.W. (1978). Radial glia in the human fetal cerebrum: a combined Golgi, immunofluorescent and electron microscopic study. Brain research *148*, 295-311.

Christoforidis, S., Miaczynska, M., Ashman, K., Wilm, M., Zhao, L., Yip, S.C., Waterfield, M.D., Backer, J.M., and Zerial, M. (1999). Phosphatidylinositol-3-OH kinases are Rab5 effectors. Nature cell biology *1*, 249-252.

Cordle, J., Redfieldz, C., Stacey, M., van der Merwe, P.A., Willis, A.C., Champion, B.R., Hambleton, S., and Handford, P.A. (2008). Localization of the delta-like-1-binding site in human Notch-1 and its modulation by calcium affinity. The Journal of biological chemistry *283*, 11785-11793.

Corish, P., and Tyler-Smith, C. (1999). Attenuation of green fluorescent protein half-life in mammalian cells. Protein engineering *12*, 1035-1040.

Coumailleau, F., Fürthauer, M., Knoblich, J.A., and González-Gaitán, M. (2009). Directional Delta and Notch trafficking in Sara endosomes during asymmetric cell division. Nature *458*, 1051-1055.

Couturier, L., Mazouni, K., and Schweisguth, F. (2013). Numb localizes at endosomes and controls the endosomal sorting of notch after asymmetric division in Drosophila. Current biology : CB *23*, 588-593.

Crawford, T.Q., and Roelink, H. (2007). The notch response inhibitor DAPT enhances neuronal differentiation in embryonic stem cell-derived embryoid bodies independently of sonic hedgehog signaling. Developmental dynamics : an official publication of the American Association of Anatomists *236*, 886-892.

Crossley, P.H., Martinez, S., and Martin, G.R. (1996). Midbrain development induced by FGF8 in the chick embryo. Nature *380*, 66-68.

Cuny, G.D., Yu, P.B., Laha, J.K., Xing, X., Liu, J.-F., Lai, C.S., Deng, D.Y., Sachidanandan, C., Bloch, K.D., and Peterson, R.T. (2008). Structure-activity relationship study of bone morphogenetic protein (BMP) signaling inhibitors. Bioorganic & medicinal chemistry letters, 4388-4392.

Deblandre, G.A., Lai, E.C., and Kintner, C. (2001). Xenopus Neuralized Is a Ubiquitin Ligase that Interacts with XDelta1 and Regulates Notch Signaling. Developmental Cell *1*, 795-806.

Deckert, M., Ticchioni, M., and Bernard, A. (1996). Endocytosis of GPI-anchored proteins in human lymphocytes: role of glycolipid-based domains, actin cytoskeleton, and protein kinases. The Journal of cell biology *133*, 791-799.

Del Bianco, C., Vedenko, A., Choi, S.H., Berger, M.F., Shokri, L., Bulyk, M.L., and Blacklow, S.C. (2010). Notch and MAML-1 complexation do not detectably alter the DNA binding specificity of the transcription factor CSL. PloS one *5*, e15034.

Delaune, E.A., François, P., Shih, N.P., and Amacher, S.L. (2012). Single-cell-resolution imaging of the impact of Notch signaling and mitosis on segmentation clock dynamics. Developmental Cell *23*, 995-1005.

Derivery, E., Seum, C., Daeden, A., Loubéry, S., Holtzer, L., Jülicher, F., and Gonzalez-Gaitan, M. (2015). Polarized endosome dynamics by spindle asymmetry during asymmetric cell division. Nature *528*, 280-285.

Desnoyers, L., Anant, J.S., and Seabra, M.C. (1996). Geranylgeranylation of Rab proteins. Biochemical Society transactions *24*, 699-703.

Dexter, J.S. (1914). The Analysis of a Case of Continuous Variation in Drosophila by a Study of Its Linkage Relations. The American Naturalist *48*, 712-758.

Di Guglielmo, G.M., Le Roy, C., Goodfellow, A.F., and Wrana, J.L. (2003). Distinct endocytic pathways regulate TGF-beta receptor signalling and turnover. Nature cell biology *5*, 410-421.

Diez del Corral, R., and Storey, K.G. (2004). Opposing FGF and retinoid pathways: a signalling switch that controls differentiation and patterning onset in the extending vertebrate body axis. BioEssays : news and reviews in molecular, cellular and developmental biology *26*, 857-869.

Dobrzyński, M., Jacques, M.-A., and Pertz, O. (2020). Mining single-cell time-series datasets with Time Course Inspector. Bioinformatics *36*, 1968-1969.

Dong, Z., Yang, N., Yeo, S.-Y., Chitnis, A., and Guo, S. (2012). Intralineage directional Notch signaling regulates self-renewal and differentiation of asymmetrically dividing radial glia. Neuron *74*, 65-78.

Donnelly, M.L.L., Luke, G., Mehrotra, A., Li, X., Hughes, L.E., Gani, D., and Ryan, M.D. (2001). Analysis of the aphthovirus 2A/2B polyprotein 'cleavage' mechanism indicates not a proteolytic reaction, but a novel translational effect: a putative ribosomal 'skip'. The Journal of general virology *82*, 1013-1025.

Dou, S., Zeng, X., Cortes, P., Erdjument-Bromage, H., Tempst, P., Honjo, T., and Vales, L.D. (1994). The recombination signal sequence-binding protein RBP-2N functions as a transcriptional repressor. Molecular and cellular biology *14*, 3310-3319.

Duman, J.G., Tzeng, C.P., Tu, Y.-K., Munjal, T., Schwechter, B., Ho, T.S.-Y., and Tolias, K.F. (2013). The adhesion-GPCR BAI1 regulates synaptogenesis by controlling the recruitment of the Par3/Tiam1 polarity

complex to synaptic sites. The Journal of neuroscience : the official journal of the Society for Neuroscience *33*, 6964-6978.

Dumas, J.J., Merithew, E., Sudharshan, E., Rajamani, D., Hayes, S., Lawe, D., Corvera, S., and Lambright, D.G. (2001). Multivalent Endosome Targeting by Homodimeric EEA1. Molecular Cell *8*, 947-958.

Ebrahim, R., and Thilo, L. (2011). Kinetic evidence that newly-synthesized endogenous lysosome-associated membrane protein-1 (LAMP-1) first transits early endosomes before it is delivered to lysosomes. Molecular membrane biology *28*, 227-242.

Edgar, J.R., Eden, E.R., and Futter, C.E. (2014). Hrs- and CD63-dependent competing mechanisms make different sized endosomal intraluminal vesicles. Traffic (Copenhagen, Denmark) *15*, 197-211.

Eiraku, M., Watanabe, K., Matsuo-Takasaki, M., Kawada, M., Yonemura, S., Matsumura, M., Wataya, T., Nishiyama, A., Muguruma, K., and Sasai, Y. (2008). Self-organized formation of polarized cortical tissues from ESCs and its active manipulation by extrinsic signals. Cell stem cell *3*, 519-532.

Elkabetz, Y., Panagiotakos, G., Al Shamy, G., Socci, N.D., Tabar, V., and Studer, L. (2008). Human ES cell-derived neural rosettes reveal a functionally distinct early neural stem cell stage. Genes & development *22*, 152-165.

Emery, G., Hutterer, A., Berdnik, D., Mayer, B., Wirtz-Peitz, F., Gaitan, M.G., and Knoblich, J.A. (2005). Asymmetric Rab 11 endosomes regulate delta recycling and specify cell fate in the Drosophila nervous system. Cell *122*, 763-773.

Escola, J.M., Kleijmeer, M.J., Stoorvogel, W., Griffith, J.M., Yoshie, O., and Geuze, H.J. (1998). Selective enrichment of tetraspan proteins on the internal vesicles of multivesicular endosomes and on exosomes secreted by human B-lymphocytes. The Journal of biological chemistry *273*, 20121-20127.

Estrach, S., Cordes, R., Hozumi, K., Gossler, A., and Watt, F.M. (2008). Role of the Notch ligand Delta1 in embryonic and adult mouse epidermis. The Journal of investigative dermatology *128*, 825-832.

Falk, A., Koch, P., Kesavan, J., Takashima, Y., Ladewig, J., Alexander, M., Wiskow, O., Tailor, J., Trotter, M., and Pollard, S., et al. (2012). Capture of neuroepithelial-like stem cells from pluripotent stem cells provides a versatile system for in vitro production of human neurons. PloS one *7*, e29597.

Fehon, R.G., Kooh, P.J., Rebay, I., Regan, C.L., Xu, T., Muskavitch, M.A.T., and Artavanis-Tsakonas, S. (1990). Molecular interactions between the protein products of the neurogenic loci Notch and Delta, two EGF-homologous genes in Drosophila. Cell *61*, 523-534.

Feng, L., Hatten, M.E., and Heintz, N. (1994). Brain lipid-binding protein (BLBP): a novel signaling system in the developing mammalian CNS. Neuron *12*, 895-908.

Fiddes, I.T., Lodewijk, G.A., Mooring, M., Bosworth, C.M., Ewing, A.D., Mantalas, G.L., Novak, A.M., van den Bout, A., Bishara, A., and Rosenkrantz, J.L., et al. (2018). Human-Specific NOTCH2NL Genes Affect Notch Signaling and Cortical Neurogenesis. Cell *173*, 1356-1369.e22.

Fietz, S.A., Kelava, I., Vogt, J., Wilsch-Bräuninger, M., Stenzel, D., Fish, J.L., Corbeil, D., Riehn, A., Distler, W., and Nitsch, R., et al. (2010). OSVZ progenitors of human and ferret neocortex are epithelial-like and expand by integrin signaling. Nature neuroscience *13*, 690-699.

Fiuza, U.-M., Klein, T., Martinez Arias, A., and Hayward, P. (2010). Mechanisms of ligand-mediated inhibition in Notch signaling activity in Drosophila. Developmental dynamics : an official publication of the American Association of Anatomists *239*, 798-805.

Fogg, V.C., Liu, C.-J., and Margolis, B. (2005). Multiple regions of Crumbs3 are required for tight junction formation in MCF10A cells. Journal of cell science *118*, 2859-2869.

Formosa-Jordan, P., and Ibañes, M. (2014). Competition in notch signaling with cis enriches cell fate decisions. PloS one *9*, e95744.

Fra, A.M., Williamson, E., Simons, K., and Parton, R.G. (1995). De novo formation of caveolae in lymphocytes by expression of VIP21-caveolin. Proceedings of the National Academy of Sciences of the United States of America *92*, 8655-8659.

Friedmann, D.R., and Kovall, R.A. (2010). Thermodynamic and structural insights into CSL-DNA complexes. Protein science : a publication of the Protein Society *19*, 34-46.

Fryer, C.J., White, J.B., and Jones, K.A. (2004). Mastermind recruits CycC:CDK8 to phosphorylate the Notch ICD and coordinate activation with turnover. Molecular Cell *16*, 509-520.

Fukuchi-Shimogori, T., and Grove, E.A. (2001). Neocortex patterning by the secreted signaling molecule FGF8. Science (New York, N.Y.) *294*, 1071-1074.

Gaiano, N., Nye, J.S., and Fishell, G. (2000). Radial Glial Identity Is Promoted by Notch1 Signaling in the Murine Forebrain. Neuron *26*, 395-404.

Gerrard, L., Rodgers, L., and Cui, W. (2005). Differentiation of human embryonic stem cells to neural lineages in adherent culture by blocking bone morphogenetic protein signaling. Stem cells (Dayton, Ohio), 1234-1241.

Giagtzoglou, N., Alifragis, P., Koumbanakis, K.A., and Delidakis, C. (2003). Two modes of recruitment of E(spl) repressors onto target genes. Development (Cambridge, England) *130*, 259-270.

Gibbings, D., and Voinnet, O. (2010). Control of RNA silencing and localization by endolysosomes. Trends in cell biology *20*, 491-501.

Gomez-Lamarca, M.J., Snowdon, L.A., Seib, E., Klein, T., and Bray, S.J. (2015). Rme-8 depletion perturbs Notch recycling and predisposes to pathogenic signaling. The Journal of cell biology *210*, 303-318.

Gordon, W.R., Vardar-Ulu, D., Histen, G., Sanchez-Irizarry, C., Aster, J.C., and Blacklow, S.C. (2007). Structural basis for autoinhibition of Notch. Nature structural & molecular biology *14*, 295-300.

Gordon, W.R., Zimmerman, B., He, L., Miles, L.J., Huang, J., Tiyanont, K., McArthur, D.G., Aster, J.C., Perrimon, N., and Loparo, J.J., et al. (2015). Mechanical Allostery: Evidence for a Force Requirement in the Proteolytic Activation of Notch. Developmental Cell *33*, 729-736.

Grandbarbe, L., Bouissac, J., Rand, M., Hrabé de Angelis, M., Artavanis-Tsakonas, S., and Mohier, E. (2003). Delta-Notch signaling controls the generation of neurons/glia from neural stem cells in a stepwise process. Development (Cambridge, England) *130*, 1391-1402.

Guarani, V., Deflorian, G., Franco, C.A., Krüger, M., Phng, L.-K., Bentley, K., Toussaint, L., Dequiedt, F., Mostoslavsky, R., and Schmidt, M.H.H., et al. (2011). Acetylation-dependent regulation of endothelial Notch signalling by the SIRT1 deacetylase. Nature *473*, 234-238.

Gupta-Rossi, N., Six, E., LeBail, O., Logeat, F., Chastagner, P., Olry, A., Israël, A., and Brou, C. (2004). Monoubiquitination and endocytosis direct gamma-secretase cleavage of activated Notch receptor. The Journal of cell biology *166*, 73-83.

Hakanen, J., Ruiz-Reig, N., and Tissir, F. (2019). Linking Cell Polarity to Cortical Development and Malformations. Frontiers in cellular neuroscience *13*, 244.

Hales, C.M., Vaerman, J.-P., and Goldenring, J.R. (2002). Rab11 family interacting protein 2 associates with Myosin Vb and regulates plasma membrane recycling. The Journal of biological chemistry *277*, 50415-50421.

Han, H., Tanigaki, K., Yamamoto, N., Kuroda, K., Yoshimoto, M., Nakahata, T., Ikuta, K., and Honjo, T. (2002). Inducible gene knockout of transcription factor recombination signal binding protein-J reveals its essential role in T versus B lineage decision. International immunology *14*, 637-645.

Hansen, D.V., Lui, J.H., Parker, P.R.L., and Kriegstein, A.R. (2010). Neurogenic radial glia in the outer subventricular zone of human neocortex. Nature *464*, 554-561.

Harris, T.J.C., and Peifer, M. (2005). The positioning and segregation of apical cues during epithelial polarity establishment in Drosophila. The Journal of cell biology *170*, 813-823.

Hartenstein, V., Rudloff, E., and Campos-Ortega, J.A. (1987). The pattern of proliferation of the neuroblasts in the wild-type embryo of Drosophila melanogaster. Roux's archives of developmental biology : the official organ of the EDBO *196*, 473-485.

Hartfuss, E., Galli, R., Heins, N., and Götz, M. (2001). Characterization of CNS precursor subtypes and radial glia. Developmental biology *229*, 15-30.

Hatakeyama, J., Bessho, Y., Katoh, K., Ookawara, S., Fujioka, M., Guillemot, F., and Kageyama, R. (2004). Hes genes regulate size, shape and histogenesis of the nervous system by control of the timing of neural stem cell differentiation. Development (Cambridge, England) *131*, 5539-5550.

Hatta, K., Okada, T.S., and Takeichi, M. (1985). A monoclonal antibody disrupting calcium-dependent cell-cell adhesion of brain tissues: possible role of its target antigen in animal pattern formation. Proceedings of the National Academy of Sciences of the United States of America *82*, 2789-2793.

Hatta, K., and Takeichi, M. (1986). Expression of N-cadherin adhesion molecules associated with early morphogenetic events in chick development. Nature *320*, 447-449.

Haubensak, W., Attardo, A., Denk, W., and Huttner, W.B. (2004). Neurons arise in the basal neuroepithelium of the early mammalian telencephalon: a major site of neurogenesis. Proceedings of the National Academy of Sciences of the United States of America *101*, 3196-3201.

Haydar, T.F., Ang, E., and Rakic, P. (2003). Mitotic spindle rotation and mode of cell division in the developing telencephalon. Proceedings of the National Academy of Sciences of the United States of America *100*, 2890-2895.

Henderson, S.T., Gao, D., Lambie, E.J., and Kimble, J. (1994). lag-2 may encode a signaling ligand for the GLP-1 and LIN-12 receptors of C. elegans. Development (Cambridge, England) *120*, 2913-2924.

Henley, J.R., Krueger, E.W., Oswald, B.J., and McNiven, M.A. (1998). Dynamin-mediated internalization of caveolae. The Journal of cell biology *141*, 85-99.

Hernandez, R.E., Putzke, A.P., Myers, J.P., Margaretha, L., and Moens, C.B. (2007). Cyp26 enzymes generate the retinoic acid response pattern necessary for hindbrain development. Development (Cambridge, England) *134*, 177-187.

Hicks, C., Johnston, S.H., diSibio, G., Collazo, A., Vogt, T.F., and Weinmaster, G. (2000). Fringe differentially modulates Jagged1 and Delta1 signalling through Notch1 and Notch2. Nature cell biology *2*, 515-520.

Hindley, C., Ali, F., McDowell, G., Cheng, K., Jones, A., Guillemot, F., and Philpott, A. (2012). Post-translational modification of Ngn2 differentially affects transcription of distinct targets to regulate the balance between progenitor maintenance and differentiation. Development (Cambridge, England) *139*, 1718-1723.

Hirata, H., Yoshiura, S., Ohtsuka, T., Bessho, Y., Harada, T., Yoshikawa, K., and Kageyama, R. (2002). Oscillatory expression of the bHLH factor Hes1 regulated by a negative feedback loop. Science (New York, N.Y.) *298*, 840-843.

Höning, S., Ricotta, D., Krauss, M., Späte, K., Spolaore, B., Motley, A., Robinson, M., Robinson, C., Haucke, V., and Owen, D.J. (2005). Phosphatidylinositol-(4,5)-bisphosphate regulates sorting signal recognition by the clathrin-associated adaptor complex AP2. Molecular Cell *18*, 519-531.

Houart, C., Caneparo, L., Heisenberg, C.-P., Barth, K.A., Take-Uchi, M., and Wilson, S.W. (2002). Establishment of the Telencephalon during Gastrulation by Local Antagonism of Wnt Signaling. Neuron *35*, 255-265.

Houart, C., Westerfield, M., and Wilson, S.W. (1998). A small population of anterior cells patterns the forebrain during zebrafish gastrulation. Nature *391*, 788-792.

Hozumi, K., Negishi, N., Suzuki, D., Abe, N., Sotomaru, Y., Tamaoki, N., Mailhos, C., Ish-Horowicz, D., Habu, S., and Owen, M.J. (2004). Delta-like 1 is necessary for the generation of marginal zone B cells but not T cells in vivo. Nature immunology *5*, 638-644.

Huenniger, K., Krämer, A., Soom, M., Chang, I., Köhler, M., Depping, R., Kehlenbach, R.H., and Kaether, C. (2010). Notch1 signaling is mediated by importins alpha 3, 4, and 7. Cellular and molecular life sciences : CMLS *67*, 3187-3196.

Humphries, W.H., Szymanski, C.J., and Payne, C.K. (2011). Endo-lysosomal vesicles positive for Rab7 and LAMP1 are terminal vesicles for the transport of dextran. PloS one, e26626.

Hunziker, W., Simmen, T., and Höning, S. (1996). Trafficking of lysosomal membrane proteins in polarized kidney cells. Nephrologie *17*, 347-350.

Hutterer, A., Betschinger, J., Petronczki, M., and Knoblich, J.A. (2004). Sequential roles of Cdc42, Par-6, aPKC, and Lgl in the establishment of epithelial polarity during Drosophila embryogenesis. Developmental Cell *6*, 845-854.

Hutterer, A., and Knoblich, J.A. (2005). Numb and alpha-Adaptin regulate Sanpodo endocytosis to specify cell fate in Drosophila external sensory organs. EMBO reports *6*, 836-842.

Iefremova, V., Manikakis, G., Krefft, O., Jabali, A., Weynans, K., Wilkens, R., Marsoner, F., Brändl, B., Müller, F.-J., and Koch, P., et al. (2017). An Organoid-Based Model of Cortical Development Identifies Non-Cell-Autonomous Defects in Wnt Signaling Contributing to Miller-Dieker Syndrome. Cell reports *19*, 50-59.

Ikeshima-Kataoka, H., Skeath, J.B., Nabeshima, Y., Doe, C.Q., and Matsuzaki, F. (1997). Miranda directs Prospero to a daughter cell during Drosophila asymmetric divisions. Nature *390*, 625-629.

Imayoshi, I., Isomura, A., Harima, Y., Kawaguchi, K., Kori, H., Miyachi, H., Fujiwara, T., Ishidate, F., and Kageyama, R. (2013). Oscillatory control of factors determining multipotency and fate in mouse neural progenitors. Science (New York, N.Y.), 1203-1208.

Imayoshi, I., Sakamoto, M., Yamaguchi, M., Mori, K., and Kageyama, R. (2010). Essential roles of Notch signaling in maintenance of neural stem cells in developing and adult brains. The Journal of neuroscience : the official journal of the Society for Neuroscience *30*, 3489-3498.

Imayoshi, I., Shimogori, T., Ohtsuka, T., and Kageyama, R. (2008). Hes genes and neurogenin regulate non-neural versus neural fate specification in the dorsal telencephalic midline. Development (Cambridge, England) *135*, 2531-2541.

Inpanathan, S., and Botelho, R.J. (2019). The Lysosome Signaling Platform: Adapting With the Times. Frontiers in cell and developmental biology *7*, 113.

Ishibashi, M., Moriyoshi, K., Sasai, Y., Shiota, K., Nakanishi, S., and Kageyama, R. (1994). Persistent expression of helix-loop-helix factor HES-1 prevents mammalian neural differentiation in the central nervous system. The EMBO journal *13*, 1799-1805.

Ishino, Y., Shinagawa, H., Makino, K., Amemura, M., and Nakata, A. (1987). Nucleotide sequence of the iap gene, responsible for alkaline phosphatase isozyme conversion in Escherichia coli, and identification of the gene product. Journal of bacteriology *169*, 5429-5433.

Iso, T., Sartorelli, V., Poizat, C., Iezzi, S., Wu, H.Y., Chung, G., Kedes, L., and Hamamori, Y. (2001). HERP, a novel heterodimer partner of HES/E(spl) in Notch signaling. Molecular and cellular biology *21*, 6080-6089.

Itoh, M., Kim, C.-H., Palardy, G., Oda, T., Jiang, Y.-J., Maust, D., Yeo, S.-Y., Lorick, K., Wright, G.J., and Ariza-McNaughton, L., et al. (2003). Mind Bomb Is a Ubiquitin Ligase that Is Essential for Efficient Activation of Notch Signaling by Delta. Developmental Cell *4*, 67-82.

Itoh, M., Sasaki, H., Furuse, M., Ozaki, H., Kita, T., and Tsukita, S. (2001). Junctional adhesion molecule (JAM) binds to PAR-3: a possible mechanism for the recruitment of PAR-3 to tight junctions. The Journal of cell biology *154*, 491-497.

Itskovitz-Eldor, J., Schuldiner, M., Karsenti, D., Eden, A., Yanuka, O., Amit, M., Soreq, H., and Benvenisty, N. (2000). Differentiation of human embryonic stem cells into embryoid bodies compromising the three embryonic germ layers. Molecular medicine (Cambridge, Mass.) *6*, 88-95.

Itsykson, P., Ilouz, N., Turetsky, T., Goldstein, R.S., Pera, M.F., Fishbein, I., Segal, M., and Reubinoff, B.E. (2005). Derivation of neural precursors from human embryonic stem cells in the presence of noggin. Molecular and cellular neurosciences *30*, 24-36.

Izumi, Y., Ohta, N., Hisata, K., Raabe, T., and Matsuzaki, F. (2006). Drosophila Pins-binding protein Mud regulates spindle-polarity coupling and centrosome organization. Nature cell biology *8*, 586-593.

Jaiswal, J.K., Andrews, N.W., and Simon, S.M. (2002). Membrane proximal lysosomes are the major vesicles responsible for calcium-dependent exocytosis in nonsecretory cells. The Journal of cell biology *159*, 625-635.

James, A.C., Szot, J.O., Iyer, K., Major, J.A., Pursglove, S.E., Chapman, G., and Dunwoodie, S.L. (2014). Notch4 reveals a novel mechanism regulating Notch signal transduction. Biochimica et biophysica acta *1843*, 1272-1284.

Jarriault, S., Brou, C., Logeat, F., Schroeter, E.H., Kopan, R., and Israel, A. (1995). Signalling downstream of activated mammalian Notch. Nature *377*, 355-358.

Jenny, A., Reynolds-Kenneally, J., Das, G., Burnett, M., and Mlodzik, M. (2005). Diego and Prickle regulate Frizzled planar cell polarity signalling by competing for Dishevelled binding. Nature cell biology *7*, 691-697.

Jinek, M., Chylinski, K., Fonfara, I., Hauer, M., Doudna, J.A., and Charpentier, E. (2012). A programmable dual-RNA-guided DNA endonuclease in adaptive bacterial immunity. Science (New York, N.Y.) *337*, 816-821.

Johansson, M., Rocha, N., Zwart, W., Jordens, I., Janssen, L., Kuijl, C., Olkkonen, V.M., and Neefjes, J. (2007). Activation of endosomal dynein motors by stepwise assembly of Rab7-RILP-p150Glued, ORP1L, and the receptor betalll spectrin. The Journal of cell biology *176*, 459-471.

Johnson, D.E., Ostrowski, P., Jaumouillé, V., and Grinstein, S. (2016). The position of lysosomes within the cell determines their luminal pH. The Journal of cell biology *212*, 677-692.

Jordens, I., Fernandez-Borja, M., Marsman, M., Dusseljee, S., Janssen, L., Calafat, J., Janssen, H., Wubbolts, R., and Neefjes, J. (2001). The Rab7 effector protein RILP controls lysosomal transport by inducing the recruitment of dynein-dynactin motors. Current biology : CB *11*, 1680-1685.

Joutel, A., Andreux, F., Gaulis, S., Domenga, V., Cecillon, M., Battail, N., Piga, N., Chapon, F., Godfrain, C., and Tournier-Lasserve, E. (2000). The ectodomain of the Notch3 receptor accumulates within the cerebrovasculature of CADASIL patients. The Journal of clinical investigation *105*, 597-605.

Kadoshima, T., Sakaguchi, H., Nakano, T., Soen, M., Ando, S., Eiraku, M., and Sasai, Y. (2013). Self-organization of axial polarity, inside-out layer pattern, and species-specific progenitor dynamics in human ES cell-derived neocortex. Proceedings of the National Academy of Sciences of the United States of America *110*, 20284-20289.

Kageyama, R., and Ohtsuka, T. (1999). The Notch-Hes pathway in mammalian neural development. Cell research *9*, 179-188.

Kageyama, R., Ohtsuka, T., Shimojo, H., and Imayoshi, I. (2008). Dynamic Notch signaling in neural progenitor cells and a revised view of lateral inhibition. Nature neuroscience *11*, 1247-1251.

Kageyama, R., Shimojo, H., and Imayoshi, I. (2015). Dynamic expression and roles of Hes factors in neural development. Cell and tissue research, 125-133.

Kakarougkas, A., and Jeggo, P.A. (2014). DNA DSB repair pathway choice: an orchestrated handover mechanism. The British journal of radiology *87*, 20130685.

Kakuda, S., and Haltiwanger, R.S. (2017). Deciphering the Fringe-Mediated Notch Code: Identification of Activating and Inhibiting Sites Allowing Discrimination between Ligands. Developmental Cell *40*, 193-201.

Kao, H.Y., Ordentlich, P., Koyano-Nakagawa, N., Tang, Z., Downes, M., Kintner, C.R., Evans, R.M., and Kadesch, T. (1998). A histone deacetylase corepressor complex regulates the Notch signal transduction pathway. Genes & development *12*, 2269-2277.

Karzbrun, E., Kshirsagar, A., Cohen, S.R., Hanna, J.H., and Reiner, O. (2018). Human Brain Organoids on a Chip Reveal the Physics of Folding. Nature physics, 515-522.

Katzmann, D.J., Babst, M., and Emr, S.D. (2001). Ubiquitin-Dependent Sorting into the Multivesicular Body Pathway Requires the Function of a Conserved Endosomal Protein Sorting Complex, ESCRT-I. Cell *106*, 145-155.

Kawaguchi, D., Furutachi, S., Kawai, H., Hozumi, K., and Gotoh, Y. (2013). Dll1 maintains quiescence of adult neural stem cells and segregates asymmetrically during mitosis. Nature communications *4*, 1880.

Kazanskaya, O., Glinka, A., and Niehrs, C. (2000). The role of Xenopus dickkopf1 in prechordal plate specification and neural patterning. Development (Cambridge, England) *127*, 4981-4992.

Kemphues, K.J., Priess, J.R., Morton, D.G., and Cheng, N. (1988). Identification of genes required for cytoplasmic localization in early C. elegans embryos. Cell *52*, 311-320.

Kidd, S., Kelley, M.R., and Young, M.W. (1986). Sequence of the notch locus of Drosophila melanogaster: relationship of the encoded protein to mammalian clotting and growth factors. Molecular and cellular biology *6*, 3094-3108.

Kiecker, C., and Lumsden, A. (2004). Hedgehog signaling from the ZLI regulates diencephalic regional identity. Nature neuroscience *7*, 1242-1249.

Kiecker, C., and Niehrs, C. (2001). A morphogen gradient of Wnt/beta-catenin signalling regulates anteroposterior neural patterning in Xenopus. Development (Cambridge, England) *128*, 4189-4201.

Kim, S., Lehtinen, M.K., Sessa, A., Zappaterra, M.W., Cho, S.-H., Gonzalez, D., Boggan, B., Austin, C.A., Wijnholds, J., and Gambello, M.J., et al. (2010). The apical complex couples cell fate and cell survival to cerebral cortical development. Neuron *66*, 69-84.

Kimelman, D., and Kirschner, M. (1987). Synergistic induction of mesoderm by FGF and TGF-β and the identification of an mRNA coding for FGF in the early xenopus embryo. Cell *51*, 869-877.

Klezovitch, O., Fernandez, T.E., Tapscott, S.J., and Vasioukhin, V. (2004). Loss of cell polarity causes severe brain dysplasia in Lgl1 knockout mice. Genes & development *18*, 559-571.

Klose, R., Berger, C., Moll, I., Adam, M.G., Schwarz, F., Mohr, K., Augustin, H.G., and Fischer, A. (2015). Soluble Notch ligand and receptor peptides act antagonistically during angiogenesis. Cardiovascular research *107*, 153-163.

Klueg, K.M., and Muskavitch, M.A. (1999). Ligand-receptor interactions and trans-endocytosis of Delta, Serrate and Notch: members of the Notch signalling pathway in Drosophila. Journal of cell science *112 (Pt 19)*, 3289-3297.

Kobayashi, T., Vischer, U.M., Rosnoblet, C., Lebrand, C., Lindsay, M., Parton, R.G., Kruithof, E.K., and Gruenberg, J. (2000). The tetraspanin CD63/lamp3 cycles between endocytic and secretory compartments in human endothelial cells. Molecular biology of the cell *11*, 1829-1843.

Koch, P., Opitz, T., Steinbeck, J.A., Ladewig, J., and Brüstle, O. (2009). A rosette-type, self-renewing human ES cell-derived neural stem cell with potential for in vitro instruction and synaptic integration. Proceedings of the National Academy of Sciences of the United States of America *106*, 3225-3230.

Konno, D., Shioi, G., Shitamukai, A., Mori, A., Kiyonari, H., Miyata, T., and Matsuzaki, F. (2008). Neuroepithelial progenitors undergo LGN-dependent planar divisions to maintain self-renewability during mammalian neurogenesis. Nature cell biology *10*, 93-101.

Kopan, R., Nye, J.S., and Weintraub, H. (1994). The intracellular domain of mouse Notch: a constitutively activated repressor of myogenesis directed at the basic helix-loop-helix region of MyoD. Development (Cambridge, England) *120*, 2385-2396.

Kopan, R., Schroeter, E.H., Weintraub, H., and Nye, J.S. (1996). Signal transduction by activated mNotch: importance of proteolytic processing and its regulation by the extracellular domain. Proceedings of the National Academy of Sciences of the United States of America *93*, 1683-1688.

Korinek, V., Barker, N., Moerer, P., van Donselaar, E., Huls, G., Peters, P.J., and Clevers, H. (1998). Depletion of epithelial stem-cell compartments in the small intestine of mice lacking Tcf-4. Nature genetics *19*, 379-383.

Korkut, C., Ataman, B., Ramachandran, P., Ashley, J., Barria, R., Gherbesi, N., and Budnik, V. (2009). Trans-synaptic transmission of vesicular Wnt signals through Evi/Wntless. Cell *139*, 393-404.

Kosaka, T., and Ikeda, K. (1983). Reversible blockage of membrane retrieval and endocytosis in the garland cell of the temperature-sensitive mutant of Drosophila melanogaster, shibirets1. The Journal of cell biology *97*, 499-507.

Kosodo, Y., Röper, K., Haubensak, W., Marzesco, A.-M., Corbeil, D., and Huttner, W.B. (2004). Asymmetric distribution of the apical plasma membrane during neurogenic divisions of mammalian neuroepithelial cells. The EMBO journal *23*, 2314-2324.

Kosodo, Y., Toida, K., Dubreuil, V., Alexandre, P., Schenk, J., Kiyokage, E., Attardo, A., Mora-Bermúdez, F., Arii, T., and Clarke, J.D.W., et al. (2008). Cytokinesis of neuroepithelial cells can divide their basal process before anaphase. The EMBO journal, 3151-3163.

Köster, M., Plessow, S., Clement, J.H., Lorenz, A., Tiedemann, H., and Knöchel, W. (1991). Bone morphogenetic protein 4 (BMP-4), a member of the TGF-β family, in early embryos of Xenopus laevis: analysis of mesoderm inducing activity. Mechanisms of Development *33*, 191-199.

Kovall, R.A., and Hendrickson, W.A. (2004). Crystal structure of the nuclear effector of Notch signaling, CSL, bound to DNA. The EMBO journal *23*, 3441-3451.

Krefft, O., Jabali, A., Iefremova, V., Koch, P., and Ladewig, J. (2018). Generation of Standardized and Reproducible Forebrain-type Cerebral Organoids from Human Induced Pluripotent Stem Cells. Journal of visualized experiments : JoVE.

Kressmann, S., Campos, C., Castanon, I., Fürthauer, M., and González-Gaitán, M. (2015). Directional Notch trafficking in Sara endosomes during asymmetric cell division in the spinal cord. Nature cell biology *17*, 333-339.

Kuchinke, U., Grawe, F., and Knust, E. (1998). Control of spindle orientation in Drosophila by the Par-3-related PDZ-domain protein Bazooka. Current Biology *8*, 1357-1365.

Kurooka, H., Kuroda, K., and Honjo, T. (1998). Roles of the ankyrin repeats and C-terminal region of the mouse notch1 intracellular region. Nucleic acids research *26*, 5448-5455.

Kurtz, A., Zimmer, A., Schnütgen, F., Brüning, G., Spener, F., and Müller, T. (1994). The expression pattern of a novel gene encoding brain-fatty acid binding protein correlates with neuronal and glial cell development. Development (Cambridge, England) *120*, 2637-2649.

Kusek, G., Campbell, M., Doyle, F., Tenenbaum, S.A., Kiebler, M., and Temple, S. (2012). Asymmetric Segregation of the Double-Stranded RNA Binding Protein Staufen2 during Mammalian Neural Stem Cell Divisions Promotes Lineage Progression. Cell stem cell *11*, 505-516.

Ladi, E., Nichols, J.T., Ge, W., Miyamoto, A., Yao, C., Yang, L.-T., Boulter, J., Sun, Y.E., Kintner, C., and Weinmaster, G. (2005). The divergent DSL ligand Dll3 does not activate Notch signaling but cell autonomously attenuates signaling induced by other DSL ligands. The Journal of cell biology *170*, 983-992.

Lafourcade, C., Sobo, K., Kieffer-Jaquinod, S., Garin, J., and van der Goot, F.G. (2008). Regulation of the V-ATPase along the endocytic pathway occurs through reversible subunit association and membrane localization. PloS one *3*, e2758.

Lahti, L., Saarimäki-Vire, J., Rita, H., and Partanen, J. (2011). FGF signaling gradient maintains symmetrical proliferative divisions of midbrain neuronal progenitors. Developmental biology, 270-282.

Lai, E.C., Deblandre, G.A., Kintner, C., and Rubin, G.M. (2001). Drosophila Neuralized Is a Ubiquitin Ligase that Promotes the Internalization and Degradation of Delta. Developmental Cell *1*, 783-794.

Lake, B.B., and Sokol, S.Y. (2009). Strabismus regulates asymmetric cell divisions and cell fate determination in the mouse brain. The Journal of cell biology, 59-66.

LaMonica, B.E., Lui, J.H., Hansen, D.V., and Kriegstein, A.R. (2013). Mitotic spindle orientation predicts outer radial glial cell generation in human neocortex. Nature communications *4*, 1665.

Lancaster, M.A., Renner, M., Martin, C.-A., Wenzel, D., Bicknell, L.S., Hurles, M.E., Homfray, T., Penninger, J.M., Jackson, A.P., and Knoblich, J.A. (2013). Cerebral organoids model human brain development and microcephaly. Nature, 373-379.

Laprise, P., Beronja, S., Silva-Gagliardi, N.F., Pellikka, M., Jensen, A.M., McGlade, C.J., and Tepass, U. (2006). The FERM protein Yurt is a negative regulatory component of the Crumbs complex that controls epithelial polarity and apical membrane size. Developmental Cell *11*, 363-374.

Lardelli, M., Dahlstrand, J., and Lendahl, U. (1994). The novel Notch homologue mouse Notch 3 lacks specific epidermal growth factor-repeats and is expressed in proliferating neuroepithelium. Mechanisms of Development *46*, 123-136.

Laurent, L.C., Ulitsky, I., Slavin, I., Tran, H., Schork, A., Morey, R., Lynch, C., Harness, J.V., Lee, S., and Barrero, M.J., et al. (2011). Dynamic changes in the copy number of pluripotency and cell proliferation genes in human ESCs and iPSCs during reprogramming and time in culture. Cell stem cell *8*, 106-118.

Le Borgne, R., and Schweisguth, F. (2003). Unequal Segregation of Neuralized Biases Notch Activation during Asymmetric Cell Division. Developmental Cell *5*, 139-148.

Lecourtois, M., and Schweisguth, F. (1998). Indirect evidence for Delta-dependent intracellular processing of Notch in Drosophila embryos. Current Biology *8*, 771-775.

Lee, C.-Y., Wilkinson, B.D., Siegrist, S.E., Wharton, R.P., and Doe, C.Q. (2006). Brat is a Miranda cargo protein that promotes neuronal differentiation and inhibits neuroblast self-renewal. Developmental Cell *10*, 441-449.

Levitt, P., and Rakic, P. (1980). Immunoperoxidase localization of glial fibrillary acidic protein in radial glial cells and astrocytes of the developing rhesus monkey brain. The Journal of comparative neurology *193*, 815-840.

Li, H.-S., Wang, D., Shen, Q., Schonemann, M.D., Gorski, J.A., Jones, K.R., Temple, S., Jan, L.Y., and Jan, Y.N. (2003). Inactivation of Numb and Numblike in Embryonic Dorsal Forebrain Impairs Neurogenesis and Disrupts Cortical Morphogenesis. Neuron *40*, 1105-1118.

Li, X., Zhao, X., Fang, Y., Jiang, X., Duong, T., Fan, C., Huang, C.C., and Kain, S.R. (1998). Generation of destabilized green fluorescent protein as a transcription reporter. The Journal of biological chemistry *273*, 34970-34975.

Li, Y., Chen, M., Hu, J., Sheng, R., Lin, Q., He, X., and Guo, M. (2021). Volumetric Compression Induces Intracellular Crowding to Control Intestinal Organoid Growth via Wnt/β-Catenin Signaling. Cell stem cell, 63-78.e7.

Li, Y., Muffat, J., Omer, A., Bosch, I., Lancaster, M.A., Sur, M., Gehrke, L., Knoblich, J.A., and Jaenisch, R. (2017). Induction of Expansion and Folding in Human Cerebral Organoids. Cell stem cell, 385-396.e3.

Li, Z., Wang, L., Hays, T.S., and Cai, Y. (2008). Dynein-mediated apical localization of crumbs transcripts is required for Crumbs activity in epithelial polarity. The Journal of cell biology *180*, 31-38.

Lissemore, J.L., and Starmer, W.T. (1999). Phylogenetic analysis of vertebrate and invertebrate Delta/Serrate/LAG-2 (DSL) proteins. Molecular phylogenetics and evolution *11*, 308-319.

Liu, Z., Brunskill, E., Varnum-Finney, B., Zhang, C., Zhang, A., Jay, P.Y., Bernstein, I., Morimoto, M., and Kopan, R. (2015). The intracellular domains of Notch1 and Notch2 are functionally equivalent during development and carcinogenesis. Development (Cambridge, England) *142*, 2452-2463.

Livak, K.J., and Schmittgen, T.D. (2001). Analysis of relative gene expression data using real-time quantitative PCR and the 2(-Delta Delta C(T)) Method. Methods (San Diego, Calif.) *25*, 402-408.

Lock, J.G., and Stow, J.L. (2005). Rab11 in recycling endosomes regulates the sorting and basolateral transport of E-cadherin. Molecular biology of the cell *16*, 1744-1755.

Loeffler, D., Wehling, A., Schneiter, F., Zhang, Y., Müller-Bötticher, N., Hoppe, P.S., Hilsenbeck, O., Kokkaliaris, K.D., Endele, M., and Schroeder, T. (2019). Asymmetric lysosome inheritance predicts activation of haematopoietic stem cells. Nature *573*, 426-429.

Logeat, F., Bessia, C., Brou, C., LeBail, O., Jarriault, S., Seidah, N.G., and Israël, A. (1998). The Notch1 receptor is cleaved constitutively by a furin-like convertase. Proceedings of the National Academy of Sciences of the United States of America *95*, 8108-8112.

Loubéry, S., Daeden, A., Seum, C., Holtzer, L., Moraleda, A., Damond, N., Derivery, E., Schmidt, T., and Gonzalez-Gaitan, M. (2017). Sara phosphorylation state controls the dispatch of endosomes from the central spindle during asymmetric division. Nature communications *8*, 15285.

Loubéry, S., Seum, C., Moraleda, A., Daeden, A., Fürthauer, M., and Gonzalez-Gaitan, M. (2014). Uninflatable and Notch control the targeting of Sara endosomes during asymmetric division. Current biology : CB *24*, 2142-2148.

Loulier, K., Barry, R., Mahou, P., Le Franc, Y., Supatto, W., Matho, K.S., Ieng, S., Fouquet, S., Dupin, E., and Benosman, R., et al. (2014). Multiplex cell and lineage tracking with combinatorial labels. Neuron *81*, 505-520.

Lovendahl, K.N., Blacklow, S.C., and Gordon, W.R. (2018). The Molecular Mechanism of Notch Activation. Advances in experimental medicine and biology *1066*, 47-58.

Lowe, L.A., Yamada, S., and Kuehn, M.R. (2001). Genetic dissection of nodal function in patterning the mouse embryo. Development (Cambridge, England) *128*, 1831-1843.

Lowell, S., Jones, P., Le Roux, I., Dunne, J., and Watt, F.M. (2000). Stimulation of human epidermal differentiation by Delta–Notch signalling at the boundaries of stem-cell clusters. Current Biology *10*, 491-500.

Lu, B., Rothenberg, M., Jan, L.Y., and Jan, Y.N. (1998). Partner of Numb Colocalizes with Numb during Mitosis and Directs Numb Asymmetric Localization in Drosophila Neural and Muscle Progenitors. Cell *95*, 225-235.

Lu, B., Usui, T., Uemura, T., Jan, L., and Jan, Y.-N. (1999). Flamingo controls the planar polarity of sensory bristles and asymmetric division of sensory organ precursors in Drosophila. Current Biology *9*, 1247-S1.

Luca, V.C., Kim, B.C., Ge, C., Kakuda, S., Di Wu, Roein-Peikar, M., Haltiwanger, R.S., Zhu, C., Ha, T., and Garcia, K.C. (2017). Notch-Jagged complex structure implicates a catch bond in tuning ligand sensitivity. Science (New York, N.Y.) *355*, 1320-1324.

Maier, M.M., and Gessler, M. (2000). Comparative analysis of the human and mouse Hey1 promoter: Hey genes are new Notch target genes. Biochemical and biophysical research communications *275*, 652-660.

Maine, E.M., Lissemore, J.L., and Starmer, W.T. (1995). A phylogenetic analysis of vertebrate and invertebrate Notch-related genes. Molecular phylogenetics and evolution *4*, 139-149.

Makarova, K.S., Grishin, N.V., Shabalina, S.A., Wolf, Y.I., and Koonin, E.V. (2006). A putative RNA-interference-based immune system in prokaryotes: computational analysis of the predicted enzymatic machinery, functional analogies with eukaryotic RNAi, and hypothetical mechanisms of action. Biology Direct *1*, 7.

Manabe, N., Hirai, S.-I., Imai, F., Nakanishi, H., Takai, Y., and Ohno, S. (2002). Association of ASIP/mPAR-3 with adherens junctions of mouse neuroepithelial cells. Developmental dynamics : an official publication of the American Association of Anatomists *225*, 61-69.

Manders, E.M.M., Verbeek, F.J., and Aten, J.A. (1993). Measurement of co-localization of objects in dual-colour confocal images. Journal of Microscopy *169*, 375-382.

Marks, B., Stowell, M.H., Vallis, Y., Mills, I.G., Gibson, A., Hopkins, C.R., and McMahon, H.T. (2001). GTPase activity of dynamin and resulting conformation change are essential for endocytosis. Nature *410*, 231-235.

Marthiens, V., and ffrench-Constant, C. (2009). Adherens junction domains are split by asymmetric division of embryonic neural stem cells. EMBO reports *10*, 515-520.

Martin-Belmonte, F., Gassama, A., Datta, A., Yu, W., Rescher, U., Gerke, V., and Mostov, K. (2007). PTEN-mediated apical segregation of phosphoinositides controls epithelial morphogenesis through Cdc42. Cell *128*, 383-397.

Masuya, M., Katayama, N., Hoshino, N., Nishikawa, H., Sakano, S., Araki, H., Mitani, H., Suzuki, H., Miyashita, H., and Kobayashi, K., et al. (2002). The soluble Notch ligand, Jagged-1, inhibits proliferation of CD34+ macrophage progenitors. International journal of hematology *75*, 269-276.

Matsuzaki, F., Ohshiro, T., Ikeshima-Kataoka, H., and Izumi, H. (1998). miranda localizes staufen and prospero asymmetrically in mitotic neuroblasts and epithelial cells in early Drosophila embryogenesis. Development (Cambridge, England) *125*, 4089-4098.

Maxfield, F.R., and Yamashiro, D.J. (1987). Endosome acidification and the pathways of receptor-mediated endocytosis. Advances in experimental medicine and biology *225*, 189-198.

Mayeuf-Louchart, A., Lagha, M., Danckaert, A., Rocancourt, D., Relaix, F., Vincent, S.D., and Buckingham, M. (2014). Notch regulation of myogenic versus endothelial fates of cells that migrate from the somite to the limb. Proceedings of the National Academy of Sciences of the United States of America *111*, 8844-8849.

McGill, M.A., Dho, S.E., Weinmaster, G., and McGlade, C.J. (2009). Numb regulates post-endocytic trafficking and degradation of Notch1. The Journal of biological chemistry *284*, 26427-26438.

McGill, M.A., and McGlade, C.J. (2003). Mammalian numb proteins promote Notch1 receptor ubiquitination and degradation of the Notch1 intracellular domain. The Journal of biological chemistry *278*, 23196-23203.

McGrew, L.L., Hoppler, S., and Moon, R.T. (1997). Wnt and FGF pathways cooperatively pattern anteroposterior neural ectoderm in Xenopus. Mechanisms of Development *69*, 105-114.

McGrew, L.L., Lai, C.J., and Moon, R.T. (1995). Specification of the anteroposterior neural axis through synergistic interaction of the Wnt signaling cascade with noggin and follistatin. Developmental biology *172*, 337-342.

McLendon, C., Xin, T., Ziani-Cherif, C., Murphy, M.P., Findlay, K.A., Lewis, P.A., Pinnix, I., Sambamurti, K., Wang, R., and Fauq, A., et al. (2000). Cell-free assays for gamma-secretase activity. FASEB journal : official publication of the Federation of American Societies for Experimental Biology *14*, 2383-2386.

Mello, C.C., Draper, B.W., and Prless, J.R. (1994). The maternal genes apx-1 and glp-1 and establishment of dorsal-ventral polarity in the early C. elegans embryo. Cell *77*, 95-106.

Meloty-Kapella, L., Shergill, B., Kuon, J., Botvinick, E., and Weinmaster, G. (2012). Notch ligand endocytosis generates mechanical pulling force dependent on dynamin, epsins, and actin. Developmental Cell *22*, 1299-1312.

Merrifield, C.J., Feldman, M.E., Wan, L., and Almers, W. (2002). Imaging actin and dynamin recruitment during invagination of single clathrin-coated pits. Nature cell biology *4*, 691-698.

Metz, C.W., and Bridges, C.B. (1917). Incompatibility of Mutant Races in Drosophila. Proceedings of the National Academy of Sciences of the United States of America *3*, 673-678.

Mojica, F.J., Díez-Villaseñor, C., Soria, E., and Juez, G. (2000). Biological significance of a family of regularly spaced repeats in the genomes of Archaea, Bacteria and mitochondria. Molecular microbiology *36*, 244-246.

Mojica, F.J.M., Díez-Villaseñor, C., García-Martínez, J., and Soria, E. (2005). Intervening sequences of regularly spaced prokaryotic repeats derive from foreign genetic elements. Journal of molecular evolution *60*, 174-182.

Moloney, D.J., Panin, V.M., Johnston, S.H., Chen, J., Shao, L., Wilson, R., Wang, Y., Stanley, P., Irvine, K.D., and Haltiwanger, R.S., et al. (2000). Fringe is a glycosyltransferase that modifies Notch. Nature *406*, 369-375.

Montagne, C., and Gonzalez-Gaitan, M. (2014). Sara endosomes and the asymmetric division of intestinal stem cells. Development (Cambridge, England) *141*, 2014-2023.

Mooren, O.L., Kotova, T.I., Moore, A.J., and Schafer, D.A. (2009). Dynamin2 GTPase and cortactin remodel actin filaments. The Journal of biological chemistry *284*, 23995-24005.

Morais-de-Sá, E., Mirouse, V., and St Johnston, D. (2010). aPKC phosphorylation of Bazooka defines the apical/lateral border in Drosophila epithelial cells. Cell *141*, 509-523.

Morgan, T.H. (1917). The Theory of the Gene. The American Naturalist *51*, 513-544.

Mukherjee, A., Veraksa, A., Bauer, A., Rosse, C., Camonis, J., and Artavanis-Tsakonas, S. (2005). Regulation of Notch signalling by non-visual beta-arrestin. Nature cell biology *7*, 1191-1201.

Mumm, J.S., Schroeter, E.H., Saxena, M.T., Griesemer, A., Tian, X., Pan, D.J., Ray, W.J., and Kopan, R. (2000). A Ligand-Induced Extracellular Cleavage Regulates γ-Secretase-like Proteolytic Activation of Notch1. Molecular Cell *5*, 197-206.

Murke, F., Castro, S., Giebel, B., and Görgens, A. (2015). Concise Review: Asymmetric Cell Divisions in Stem Cell Biology. Symmetry *7*, 2025-2037.

Nakashima, K., Takizawa, T., Ochiai, W., Yanagisawa, M., Hisatsune, T., Nakafuku, M., Miyazono, K., Kishimoto, T., Kageyama, R., and Taga, T. (2001). BMP2-mediated alteration in the developmental pathway of fetal mouse brain cells from neurogenesis to astrocytogenesis. Proceedings of the National Academy of Sciences of the United States of America *98*, 5868-5873.

Nam, Y., Sliz, P., Song, L., Aster, J.C., and Blacklow, S.C. (2006). Structural basis for cooperativity in recruitment of MAML coactivators to Notch transcription complexes. Cell *124*, 973-983.

Nam, Y., Weng, A.P., Aster, J.C., and Blacklow, S.C. (2003). Structural requirements for assembly of the CSL.intracellular Notch1.Mastermind-like 1 transcriptional activation complex. The Journal of biological chemistry *278*, 21232-21239.

Nandagopal, N., Santat, L.A., and Elowitz, M.B. (2019). Cis-activation in the Notch signaling pathway. eLife *8*.

Nemetschke, L., and Knust, E. (2016). Drosophila Crumbs prevents ectopic Notch activation in developing wings by inhibiting ligand-independent endocytosis. Development (Cambridge, England) *143*, 4543-4553.

Nichols, J.T., Miyamoto, A., Olsen, S.L., D'Souza, B., Yao, C., and Weinmaster, G. (2007). DSL ligand endocytosis physically dissociates Notch1 heterodimers before activating proteolysis can occur. The Journal of cell biology *176*, 445-458.

Nishimura, T., Kato, K., Yamaguchi, T., Fukata, Y., Ohno, S., and Kaibuchi, K. (2004). Role of the PAR-3-KIF3 complex in the establishment of neuronal polarity. Nature cell biology, 328-334.

Noctor, S.C., Flint, A.C., Weissman, T.A., Wong, W.S., Clinton, B.K., and Kriegstein, A.R. (2002). Dividing precursor cells of the embryonic cortical ventricular zone have morphological and molecular characteristics of radial glia. The Journal of neuroscience : the official journal of the Society for Neuroscience *22*, 3161-3173.

Noctor, S.C., Martínez-Cerdeño, V., Ivic, L., and Kriegstein, A.R. (2004). Cortical neurons arise in symmetric and asymmetric division zones and migrate through specific phases. Nature neuroscience *7*, 136-144.

Noctor, S.C., Martínez-Cerdeño, V., and Kriegstein, A.R. (2008). Distinct behaviors of neural stem and progenitor cells underlie cortical neurogenesis. The Journal of comparative neurology *508*, 28-44.

Nordström, U., Jessell, T.M., and Edlund, T. (2002). Progressive induction of caudal neural character by graded Wnt signaling. Nature neuroscience *5*, 525-532.

Oberg, C., Li, J., Pauley, A., Wolf, E., Gurney, M., and Lendahl, U. (2001). The Notch intracellular domain is ubiquitinated and negatively regulated by the mammalian Sel-10 homolog. The Journal of biological chemistry *276*, 35847-35853.

Ohata, S., Aoki, R., Kinoshita, S., Yamaguchi, M., Tsuruoka-Kinoshita, S., Tanaka, H., Wada, H., Watabe, S., Tsuboi, T., and Masai, I., et al. (2011). Dual roles of Notch in regulation of apically restricted mitosis and apicobasal polarity of neuroepithelial cells. Neuron *69*, 215-230.

Ohsako, S., Hyer, J., Panganiban, G., Oliver, I., and Caudy, M. (1994). Hairy function as a DNA-binding helix-loop-helix repressor of Drosophila sensory organ formation. Genes & development *8*, 2743-2755.

Ohtsuka, T., Sakamoto, M., Guillemot, F., and Kageyama, R. (2001). Roles of the basic helix-loop-helix genes Hes1 and Hes5 in expansion of neural stem cells of the developing brain. The Journal of biological chemistry *276*, 30467-30474.

Okajima, T., and Irvine, K.D. (2002). Regulation of Notch Signaling by O-Linked Fucose. Cell *111*, 893-904.

Okajima, T., Xu, A., and Irvine, K.D. (2003). Modulation of notch-ligand binding by protein O-fucosyltransferase 1 and fringe. The Journal of biological chemistry *278*, 42340-42345.

Parks, A.L., Klueg, K.M., Stout, J.R., and Muskavitch, M.A. (2000). Ligand endocytosis drives receptor dissociation and activation in the Notch pathway. Development (Cambridge, England) *127*, 1373-1385.

Pasternak, S.H., Bagshaw, R.D., Guiral, M., Zhang, S., Ackerley, C.A., Pak, B.J., Callahan, J.W., and Mahuran, D.J. (2003). Presenilin-1, nicastrin, amyloid precursor protein, and gamma-secretase activity are co-localized in the lysosomal membrane. The Journal of biological chemistry *278*, 26687-26694.

Pavlopoulos, E., Pitsouli, C., Klueg, K.M., Muskavitch, M.A.T., Moschonas, N.K., and Delidakis, C. (2001). neuralized Encodes a Peripheral Membrane Protein Involved in Delta Signaling and Endocytosis. Developmental Cell *1*, 807-816.

Peden, A.A., Oorschot, V., Hesser, B.A., Austin, C.D., Scheller, R.H., and Klumperman, J. (2004). Localization of the AP-3 adaptor complex defines a novel endosomal exit site for lysosomal membrane proteins. The Journal of cell biology *164*, 1065-1076.

Pei, Z., and Baker, N.E. (2008). Competition between Delta and the Abruptex domain of Notch. BMC developmental biology *8*, 4.

Pera, M.F., Andrade, J., Houssami, S., Reubinoff, B., Trounson, A., Stanley, E.G., Ward-van Oostwaard, D., and Mummery, C. (2004). Regulation of human embryonic stem cell differentiation by BMP-2 and its antagonist noggin. Journal of cell science *117*, 1269-1280.

Pereira-Leal, J.B., and Seabra, M.C. (2001). Evolution of the Rab family of small GTP-binding proteins. Journal of molecular biology *313*, 889-901.

Petcherski, A.G., and Kimble, J. (2000). Mastermind is a putative activator for Notch. Current Biology *10*, R471-R473.

Petersen, P.H., Zou, K., Hwang, J.K., Jan, Y.N., and Zhong, W. (2002). Progenitor cell maintenance requires numb and numblike during mouse neurogenesis. Nature *419*, 929-934.

Petersen, P.H., Zou, K., Krauss, S., and Zhong, W. (2004). Continuing role for mouse Numb and Numbl in maintaining progenitor cells during cortical neurogenesis. Nature neuroscience, 803-811.

Peyre, E., Jaouen, F., Saadaoui, M., Haren, L., Merdes, A., Durbec, P., and Morin, X. (2011). A lateral belt of cortical LGN and NuMA guides mitotic spindle movements and planar division in neuroepithelial cells. The Journal of cell biology, 141-154.

Piccolo, S., Agius, E., Leyns, L., Bhattacharyya, S., Grunz, H., Bouwmeester, T., and Robertis, E.M. de (1999). The head inducer Cerberus is a multifunctional antagonist of Nodal, BMP and Wnt signals. Nature *397*, 707-710.

Piccolo, S., Sasai, Y., Lu, B., and Robertis, E.M. de (1996). Dorsoventral Patterning in Xenopus: Inhibition of Ventral Signals by Direct Binding of Chordin to BMP-4. Cell *86*, 589-598.

Pilz, G.-A., Shitamukai, A., Reillo, I., Pacary, E., Schwausch, J., Stahl, R., Ninkovic, J., Snippert, H.J., Clevers, H., and Godinho, L., et al. (2013). Amplification of progenitors in the mammalian telencephalon includes a new radial glial cell type. Nature communications *4*, 2125.

Postiglione, M.P., Jüschke, C., Xie, Y., Haas, G.A., Charalambous, C., and Knoblich, J.A. (2011). Mouse inscuteable induces apical-basal spindle orientation to facilitate intermediate progenitor generation in the developing neocortex. Neuron *72*, 269-284.

Poulson, D.F. (1937). Chromosomal Deficiencies and the Embryonic Development of Drosophila Melanogaster. Proceedings of the National Academy of Sciences of the United States of America *23*, 133-137.

Pourcel, C., Salvignol, G., and Vergnaud, G. (2005). CRISPR elements in Yersinia pestis acquire new repeats by preferential uptake of bacteriophage DNA, and provide additional tools for evolutionary studies. Microbiology (Reading, England) *151*, 653-663.

Puca, L., Chastagner, P., Meas-Yedid, V., Israël, A., and Brou, C. (2013). A-arrestin 1 (ARRDC1) and β-arrestins cooperate to mediate Notch degradation in mammals. Journal of cell science *126*, 4457-4468.

Pui, J.C., Allman, D., Xu, L., DeRocco, S., Karnell, F.G., Bakkour, S., Lee, J.Y., Kadesch, T., Hardy, R.R., and Aster, J.C., et al. (1999). Notch1 Expression in Early Lymphopoiesis Influences B versus T Lineage Determination. Immunity *11*, 299-308.

Qi, H., Rand, M.D., Wu, X., Sestan, N., Wang, W., Rakic, P., Xu, T., and Artavanis-Tsakonas, S. (1999). Processing of the notch ligand delta by the metalloprotease Kuzbanian. Science (New York, N.Y.) *283*, 91-94.

Qian, X., Nguyen, H.N., Song, M.M., Hadiono, C., Ogden, S.C., Hammack, C., Yao, B., Hamersky, G.R., Jacob, F., and Zhong, C., et al. (2016). Brain-Region-Specific Organoids Using Mini-bioreactors for Modeling ZIKV Exposure. Cell, 1238-1254.

Radtke, F., Wilson, A., Stark, G., Bauer, M., van Meerwijk, J., MacDonald, H.R., and Aguet, M. (1999). Deficient T Cell Fate Specification in Mice with an Induced Inactivation of Notch1. Immunity *10*, 547-558.

Rao, S.K., Huynh, C., Proux-Gillardeaux, V., Galli, T., and Andrews, N.W. (2004). Identification of SNAREs involved in synaptotagmin VII-regulated lysosomal exocytosis. The Journal of biological chemistry *279*, 20471-20479.

Raposo, G., Nijman, H.W., Stoorvogel, W., Liejendekker, R., Harding, C.V., Melief, C.J., and Geuze, H.J. (1996). B lymphocytes secrete antigen-presenting vesicles. The Journal of experimental medicine *183*, 1161-1172.

Rasin, M.-R., Gazula, V.-R., Breunig, J.J., Kwan, K.Y., Johnson, M.B., Liu-Chen, S., Li, H.-S., Jan, L.Y., Jan, Y.-N., and Rakic, P., et al. (2007). Numb and Numbl are required for maintenance of cadherin-based adhesion and polarity of neural progenitors. Nature neuroscience, 819-827.

Rebay, I., Fleming, R.J., Fehon, R.G., Cherbas, L., Cherbas, P., and Artavanis-Tsakonas, S. (1991). Specific EGF repeats of Notch mediate interactions with Delta and Serrate: implications for Notch as a multifunctional receptor. Cell *67*, 687-699.

Reinhardt, P., Glatza, M., Hemmer, K., Tsytsyura, Y., Thiel, C.S., Höing, S., Moritz, S., Parga, J.A., Wagner, L., and Bruder, J.M., et al. (2013). Derivation and expansion using only small molecules of human neural progenitors for neurodegenerative disease modeling. PloS one *8*, e59252.

Renzis, S. de, Sönnichsen, B., and Zerial, M. (2002). Divalent Rab effectors regulate the sub-compartmental organization and sorting of early endosomes. Nature cell biology *4*, 124-133.

Rink, J., Ghigo, E., Kalaidzidis, Y., and Zerial, M. (2005). Rab conversion as a mechanism of progression from early to late endosomes. Cell *122*, 735-749.

Robinson, A., Escuin, S., Doudney, K., Vekemans, M., Stevenson, R.E., Greene, N.D.E., Copp, A.J., and Stanier, P. (2012). Mutations in the planar cell polarity genes CELSR1 and SCRIB are associated with the severe neural tube defect craniorachischisis. Human mutation, 440-447.

Rodríguez, A., Webster, P., Ortego, J., and Andrews, N.W. (1997). Lysosomes behave as Ca2+-regulated exocytic vesicles in fibroblasts and epithelial cells. The Journal of cell biology *137*, 93-104.

Roeth, J.F., Sawyer, J.K., Wilner, D.A., and Peifer, M. (2009). Rab11 helps maintain apical crumbs and adherens junctions in the Drosophila embryonic ectoderm. PloS one *4*, e7634.

Rogers, S., Wells, R., and Rechsteiner, M. (1986). Amino acid sequences common to rapidly degraded proteins: the PEST hypothesis. Science (New York, N.Y.) *234*, 364-368.

Rous, B.A., Reaves, B.J., Ihrke, G., Briggs, J.A.G., Gray, S.R., Stephens, D.J., Banting, G., and Luzio, J.P. (2002). Role of adaptor complex AP-3 in targeting wild-type and mutated CD63 to lysosomes. Molecular biology of the cell *13*, 1071-1082.

Roux, A., Koster, G., Lenz, M., Sorre, B., Manneville, J.-B., Nassoy, P., and Bassereau, P. (2010). Membrane curvature controls dynamin polymerization. Proceedings of the National Academy of Sciences of the United States of America *107*, 4141-4146.

Roux, A., Uyhazi, K., Frost, A., and Camilli, P. de (2006). GTP-dependent twisting of dynamin implicates constriction and tension in membrane fission. Nature *441*, 528-531.

Saftig, P., and Klumperman, J. (2009). Lysosome biogenesis and lysosomal membrane proteins: trafficking meets function. Nature reviews. Molecular cell biology *10*, 623-635.

Sagné, C., and Gasnier, B. (2008). Molecular physiology and pathophysiology of lysosomal membrane transporters. Journal of inherited metabolic disease *31*, 258-266.

Sahara, S., and O'Leary, D.D.M. (2009). Fgf10 regulates transition period of cortical stem cell differentiation to radial glia controlling generation of neurons and basal progenitors. Neuron *63*, 48-62.

Sahu, R., Kaushik, S., Clement, C.C., Cannizzo, E.S., Scharf, B., Follenzi, A., Potolicchio, I., Nieves, E., Cuervo, A.M., and Santambrogio, L. (2011). Microautophagy of cytosolic proteins by late endosomes. Developmental Cell *20*, 131-139.

Saito, T., Chiba, S., Ichikawa, M., Kunisato, A., Asai, T., Shimizu, K., Yamaguchi, T., Yamamoto, G., Seo, S., and Kumano, K., et al. (2003). Notch2 Is Preferentially Expressed in Mature B Cells and Indispensable for Marginal Zone B Lineage Development. Immunity *18*, 675-685.

Sakai, Y., Meno, C., Fujii, H., Nishino, J., Shiratori, H., Saijoh, Y., Rossant, J., and Hamada, H. (2001). The retinoic acid-inactivating enzyme CYP26 is essential for establishing an uneven distribution of retinoic acid along the anterio-posterior axis within the mouse embryo. Genes & development *15*, 213-225.

Sanalkumar, R., Indulekha, C.L., Divya, T.S., Divya, M.S., Anto, R.J., Vinod, B., Vidyanand, S., Jagatha, B., Venugopal, S., and James, J. (2010). ATF2 maintains a subset of neural progenitors through CBF1/Notch independent Hes-1 expression and synergistically activates the expression of Hes-1 in Notch-dependent neural progenitors. Journal of neurochemistry, 807-818.

Sancak, Y., Bar-Peled, L., Zoncu, R., Markhard, A.L., Nada, S., and Sabatini, D.M. (2010). Ragulator-Rag complex targets mTORC1 to the lysosomal surface and is necessary for its activation by amino acids. Cell *141*, 290-303.

Sanchez-Irizarry, C., Carpenter, A.C., Weng, A.P., Pear, W.S., Aster, J.C., and Blacklow, S.C. (2004). Notch subunit heterodimerization and prevention of ligand-independent proteolytic activation depend, respectively, on a novel domain and the LNR repeats. Molecular and cellular biology *24*, 9265-9273.

Sasai, Y., Kageyama, R., Tagawa, Y., Shigemoto, R., and Nakanishi, S. (1992). Two mammalian helix-loop-helix factors structurally related to Drosophila hairy and Enhancer of split. Genes & development *6*, 2620-2634.

Sato, T., Araki, I., and Nakamura, H. (2001). Inductive signal and tissue responsiveness defining the tectum and the cerebellum. Development (Cambridge, England) *128*, 2461-2469.

Sato, T., Shimazaki, T., Naka, H., Fukami, S.-I., Satoh, Y., Okano, H., Lax, I., Schlessinger, J., and Gotoh, N. (2010). FRS2α regulates Erk levels to control a self-renewal target Hes1 and proliferation of FGF-responsive neural stem/progenitor cells. Stem cells (Dayton, Ohio) *28*, 1661-1673.

Schaefer, M., Petronczki, M., Dorner, D., Forte, M., and Knoblich, J.A. (2001). Heterotrimeric G Proteins Direct Two Modes of Asymmetric Cell Division in the Drosophila Nervous System. Cell *107*, 183-194.

Schaefer, M., Shevchenko, A., Shevchenko, A., and Knoblich, J.A. (2000). A protein complex containing Inscuteable and the Gα-binding protein Pins orients asymmetric cell divisions in Drosophila. Current Biology *10*, 353-362.

Schmid, E.M., and McMahon, H.T. (2007). Integrating molecular and network biology to decode endocytosis. Nature *448*, 883-888.

Schmid-Burgk, J.L., Höning, K., Ebert, T.S., and Hornung, V. (2016). CRISPaint allows modular base-specific gene tagging using a ligase-4-dependent mechanism. Nature communications, 12338.

Schneider, M., Kumar, V., Nordstrøm, L.U., Feng, L., Takeuchi, H., Hao, H., Luca, V.C., Garcia, K.C., Stanley, P., and Wu, P., et al. (2018). Inhibition of Delta-induced Notch signaling using fucose analogs. Nature chemical biology *14*, 65-71.

Schneider, M., Troost, T., Grawe, F., Martinez-Arias, A., and Klein, T. (2013). Activation of Notch in lgd mutant cells requires the fusion of late endosomes with the lysosome. Journal of cell science *126*, 645-656.

Schröder, B.A., Wrocklage, C., Hasilik, A., and Saftig, P. (2010). The proteome of lysosomes. Proteomics *10*, 4053-4076.

Schroeter, E.H., Kisslinger, J.A., and Kopan, R. (1998). Notch-1 signalling requires ligand-induced proteolytic release of intracellular domain. Nature *393*, 382-386.

Schu, P.V., Takegawa, K., Fry, M.J., Stack, J.H., Waterfield, M.D., and Emr, S.D. (1993). Phosphatidylinositol 3-kinase encoded by yeast VPS34 gene essential for protein sorting. Science (New York, N.Y.) *260*, 88-91.

Seaman, M.N.J. (2004). Cargo-selective endosomal sorting for retrieval to the Golgi requires retromer. The Journal of cell biology *165*, 111-122.

Ségalen, M., Johnston, C.A., Martin, C.A., Dumortier, J.G., Prehoda, K.E., David, N.B., Doe, C.Q., and Bellaïche, Y. (2010). The Fz-Dsh planar cell polarity pathway induces oriented cell division via Mud/NuMA in Drosophila and zebrafish. Developmental Cell *19*, 740-752.

Seugnet, L., Simpson, P., and Haenlin, M. (1997). Requirement for dynamin during Notch signaling in Drosophila neurogenesis. Developmental biology *192*, 585-598.

Sever, S., Damke, H., and Schmid, S.L. (2000). Dynamin:GTP controls the formation of constricted coated pits, the rate limiting step in clathrin-mediated endocytosis. The Journal of cell biology *150*, 1137-1148.

Shaner, N.C., Campbell, R.E., Steinbach, P.A., Giepmans, B.N.G., Palmer, A.E., and Tsien, R.Y. (2004). Improved monomeric red, orange and yellow fluorescent proteins derived from Discosoma sp. red fluorescent protein. Nature biotechnology, 1567-1572.

Shanmugalingam, S., Houart, C., Picker, A., Reifers, F., Macdonald, R., Barth, A., Griffin, K., Brand, M., and Wilson, S.W. (2000). Ace/Fgf8 is required for forebrain commissure formation and patterning of the telencephalon. Development (Cambridge, England) *127*, 2549-2561.

Shapiro, J.L., Wen, X., Okamoto, C.T., Wang, H.J., Lyngstadaas, S.P., Goldberg, M., Snead, M.L., and Paine, M.L. (2007). Cellular uptake of amelogenin, and its localization to CD63, and Lamp1-positive vesicles. Cellular and molecular life sciences : CMLS *64*, 244-256.

Shearer, L.J., and Petersen, N.O. (2019). Distribution and Co-localization of endosome markers in cells. Heliyon, e02375.

Sheldon, H., Heikamp, E., Turley, H., Dragovic, R., Thomas, P., Oon, C.E., Leek, R., Edelmann, M., Kessler, B., and Sainson, R.C.A., et al. (2010). New mechanism for Notch signaling to endothelium at a distance by Delta-like 4 incorporation into exosomes. Blood, 2385-2394.

Shen, C.-P., Jan, L.Y., and Jan, Y.N. (1997). Miranda Is Required for the Asymmetric Localization of Prospero during Mitosis in Drosophila. Cell *90*, 449-458.

Shi, S.-H., Cheng, T., Jan, L.Y., and Jan, Y.-N. (2004). APC and GSK-3beta are involved in mPar3 targeting to the nascent axon and establishment of neuronal polarity. Current biology : CB *14*, 2025-2032.

Shimada, Y., Usui, T., Yanagawa, S.-i., Takeichi, M., and Uemura, T. (2001). Asymmetric colocalization of Flamingo, a seven-pass transmembrane cadherin, and Dishevelled in planar cell polarization. Current Biology *11*, 859-863.

Shimojo, H., Isomura, A., Ohtsuka, T., Kori, H., Miyachi, H., and Kageyama, R. (2016). Oscillatory control of Delta-like1 in cell interactions regulates dynamic gene expression and tissue morphogenesis. Genes & development *30*, 102-116.

Shimojo, H., Ohtsuka, T., and Kageyama, R. (2008). Oscillations in notch signaling regulate maintenance of neural progenitors. Neuron *58*, 52-64.

Shin, H.-W., Hayashi, M., Christoforidis, S., Lacas-Gervais, S., Hoepfner, S., Wenk, M.R., Modregger, J., Uttenweiler-Joseph, S., Wilm, M., and Nystuen, A., et al. (2005). An enzymatic cascade of Rab5 effectors regulates phosphoinositide turnover in the endocytic pathway. The Journal of cell biology *170*, 607-618.

Shitamukai, A., Konno, D., and Matsuzaki, F. (2011). Oblique radial glial divisions in the developing mouse neocortex induce self-renewing progenitors outside the germinal zone that resemble primate outer subventricular zone progenitors. The Journal of neuroscience : the official journal of the Society for Neuroscience *31*, 3683-3695.

Siegrist, S.E., and Doe, C.Q. (2006). Extrinsic cues orient the cell division axis in Drosophila embryonic neuroblasts. Development (Cambridge, England) *133*, 529-536.

Siller, K.H., Cabernard, C., and Doe, C.Q. (2006). The NuMA-related Mud protein binds Pins and regulates spindle orientation in Drosophila neuroblasts. Nature cell biology *8*, 594-600.

Simonsen, A., Lippé, R., Christoforidis, S., Gaullier, J.M., Brech, A., Callaghan, J., Toh, B.H., Murphy, C., Zerial, M., and Stenmark, H. (1998). EEA1 links PI(3)K function to Rab5 regulation of endosome fusion. Nature *394*, 494-498.

Sinha, S., and Chen, J.K. (2006). Purmorphamine activates the Hedgehog pathway by targeting Smoothened. Nature chemical biology, 29-30.

Sjöqvist, M., Antfolk, D., Ferraris, S., Rraklli, V., Haga, C., Antila, C., Mutvei, A., Imanishi, S.Y., Holmberg, J., and Jin, S., et al. (2014). PKCζ regulates Notch receptor routing and activity in a Notch signaling-dependent manner. Cell research *24*, 433-450.

Smith, C.A., Lau, K.M., Rahmani, Z., Dho, S.E., Brothers, G., She, Y.M., Berry, D.M., Bonneil, E., Thibault, P., and Schweisguth, F., et al. (2007). aPKC-mediated phosphorylation regulates asymmetric membrane localization of the cell fate determinant Numb. The EMBO journal *26*, 468-480.

Smith, J.C., Price, B.M., van Nimmen, K., and Huylebroeck, D. (1990). Identification of a potent Xenopus mesoderm-inducing factor as a homologue of activin A. Nature *345*, 729-731.

Snapp, E. (2005). Design and use of fluorescent fusion proteins in cell biology. Current protocols in cell biology *Chapter 21*, 21.4.1-21.4.13.

Spearman, C. (1904). The Proof and Measurement of Association between Two Things. The American Journal of Psychology *15*, 72.

Spemann, H., and Mangold, H. (1924). über Induktion von Embryonalanlagen durch Implantation artfremder Organisatoren. Archiv f mikr Anat u Entwicklungsmechanik *100*, 599-638.

Sprinzak, D., Lakhanpal, A., Lebon, L., Santat, L.A., Fontes, M.E., Anderson, G.A., Garcia-Ojalvo, J., and Elowitz, M.B. (2010). Cis-interactions between Notch and Delta generate mutually exclusive signalling states. Nature *465*, 86-90.

Stauffer, W., Sheng, H., and Lim, H.N. (2018). EzColocalization: An ImageJ plugin for visualizing and measuring colocalization in cells and organisms. Scientific reports, 15764.

Stenmark, H., Aasland, R., and Driscoll, P.C. (2002). The phosphatidylinositol 3-phosphate-binding FYVE finger. FEBS Letters *513*, 77-84.

Stenmark, H., Aasland, R., Toh, B.H., and D'Arrigo, A. (1996). Endosomal localization of the autoantigen EEA1 is mediated by a zinc-binding FYVE finger. The Journal of biological chemistry *271*, 24048-24054.

Stevenson, B.R., Siliciano, J.D., Mooseker, M.S., and Goodenough, D.A. (1986). Identification of ZO-1: a high molecular weight polypeptide associated with the tight junction (zonula occludens) in a variety of epithelia. The Journal of cell biology *103*, 755-766.

Stowell, M.H., Marks, B., Wigge, P., and McMahon, H.T. (1999). Nucleotide-dependent conformational changes in dynamin: evidence for a mechanochemical molecular spring. Nature cell biology *1*, 27-32.

Strooper, B. de, Annaert, W., Cupers, P., Saftig, P., Craessaerts, K., Mumm, J.S., Schroeter, E.H., Schrijvers, V., Wolfe, M.S., and Ray, W.J., et al. (1999). A presenilin-1-dependent gamma-secretase-like protease mediates release of Notch intracellular domain. Nature *398*, 518-522.

Struhl, G., and Adachi, A. (1998). Nuclear Access and Action of Notch In Vivo. Cell *93*, 649-660.

Sun, X., and Artavanis-Tsakonas, S. (1997). Secreted forms of DELTA and SERRATE define antagonists of Notch signaling in Drosophila. Development (Cambridge, England) *124*, 3439-3448.

Suzuki, I.K., Gacquer, D., van Heurck, R., Kumar, D., Wojno, M., Bilheu, A., Herpoel, A., Lambert, N., Cheron, J., and Polleux, F., et al. (2018). Human-Specific NOTCH2NL Genes Expand Cortical Neurogenesis through Delta/Notch Regulation. Cell *173*, 1370-1384.e16.

Syverud, B.C., Gumucio, J.P., Rodriguez, B.L., Wroblewski, O.M., Florida, S.E., Mendias, C.L., and Larkin, L.M. (2018). A Transgenic tdTomato Rat for Cell Migration and Tissue Engineering Applications. Tissue engineering. Part C, Methods *24*, 263-271.

Szymanski, C.J., Humphries, W.H., and Payne, C.K. (2011). Single particle tracking as a method to resolve differences in highly colocalized proteins. The Analyst *136*, 3527-3533.

Szymczak, A.L., and Vignali, D.A.A. (2005). Development of 2A peptide-based strategies in the design of multicistronic vectors. Expert opinion on biological therapy *5*, 627-638.

Tagami, S., Okochi, M., Yanagida, K., Ikuta, A., Fukumori, A., Matsumoto, N., Ishizuka-Katsura, Y., Nakayama, T., Itoh, N., and Jiang, J., et al. (2008). Regulation of Notch signaling by dynamic changes in the precision of S3 cleavage of Notch-1. Molecular and cellular biology *28*, 165-176.

Takahashi, K., Tanabe, K., Ohnuki, M., Narita, M., Ichisaka, T., Tomoda, K., and Yamanaka, S. (2007). Induction of pluripotent stem cells from adult human fibroblasts by defined factors. Cell *131*, 861-872.

Takahashi, K., and Yamanaka, S. (2006). Induction of pluripotent stem cells from mouse embryonic and adult fibroblast cultures by defined factors. Cell *126*, 663-676.

Takebayashi, K., Sasai, Y., Sakai, Y., Watanabe, T., Nakanishi, S., and Kageyama, R. (1994). Structure, chromosomal locus, and promoter analysis of the gene encoding the mouse helix-loop-helix factor HES-1. Negative autoregulation through the multiple N box elements. The Journal of biological chemistry *269*, 5150-5156.

Takekuni, K., Ikeda, W., Fujito, T., Morimoto, K., Takeuchi, M., Monden, M., and Takai, Y. (2003). Direct binding of cell polarity protein PAR-3 to cell-cell adhesion molecule nectin at neuroepithelial cells of developing mouse. The Journal of biological chemistry *278*, 5497-5500.

Tamura, K., Taniguchi, Y., Minoguchi, S., Sakai, T., Tun, T., Furukawa, T., and Honjo, T. (1995). Physical interaction between a novel domain of the receptor Notch and the transcription factor RBP-Jκ/Su(H). Current Biology *5*, 1416-1423.

Tanentzapf, G., and Tepass, U. (2003). Interactions between the crumbs, lethal giant larvae and bazooka pathways in epithelial polarization. Nature cell biology *5*, 46-52.

Tanigaki, K., Han, H., Yamamoto, N., Tashiro, K., Ikegawa, M., Kuroda, K., Suzuki, A., Nakano, T., and Honjo, T. (2002). Notch-RBP-J signaling is involved in cell fate determination of marginal zone B cells. Nature immunology *3*, 443-450.

Tao, Z., Li, T., Ma, H., Yang, Y., Zhang, C., Hai, L., Liu, P., Yuan, F., Li, J., and Yi, L., et al. (2018). Autophagy suppresses self-renewal ability and tumorigenicity of glioma-initiating cells and promotes Notch1 degradation. Cell death & disease *9*, 1063.

Tax, F.E., Yeargers, J.J., and Thomas, J.H. (1994). Sequence of C. elegans lag-2 reveals a cell-signalling domain shared with Delta and Serrate of Drosophila. Nature *368*, 150-154.

Teis, D., Saksena, S., and Emr, S.D. (2008). Ordered assembly of the ESCRT-III complex on endosomes is required to sequester cargo during MVB formation. Developmental Cell *15*, 578-589.

Thomson, J.A., Itskovitz-Eldor, J., Shapiro, S.S., Waknitz, M.A., Swiergiel, J.J., Marshall, V.S., and Jones, J.M. (1998). Embryonic stem cell lines derived from human blastocysts. Science (New York, N.Y.) *282*, 1145-1147.

Tiyanont, K., Wales, T.E., Aste-Amezaga, M., Aster, J.C., Engen, J.R., and Blacklow, S.C. (2011). Evidence for increased exposure of the Notch1 metalloprotease cleavage site upon conversion to an activated conformation. Structure (London, England : 1993) *19*, 546-554.

Tognon, E., Kobia, F., Busi, I., Fumagalli, A., Masi, F. de, and Vaccari, T. (2016). Control of lysosomal biogenesis and Notch-dependent tissue patterning by components of the TFEB-V-ATPase axis in Drosophila melanogaster. Autophagy *12*, 499-514.

Tojo, M., Hamashima, Y., Hanyu, A., Kajimoto, T., Saitoh, M., Miyazono, K., Node, M., and Imamura, T. (2005). The ALK-5 inhibitor A-83-01 inhibits Smad signaling and epithelial-to-mesenchymal transition by transforming growth factor-beta. Cancer science *96*, 791-800.

Trajkovic, K., Hsu, C., Chiantia, S., Rajendran, L., Wenzel, D., Wieland, F., Schwille, P., Brügger, B., and Simons, M. (2008). Ceramide triggers budding of exosome vesicles into multivesicular endosomes. Science (New York, N.Y.) *319*, 1244-1247.

Tree, D.R.P., Shulman, J.M., Rousset, R., Scott, M.P., Gubb, D., and Axelrod, J.D. (2002). Prickle Mediates Feedback Amplification to Generate Asymmetric Planar Cell Polarity Signaling. Cell *109*, 371-381.

Trombetta, E.S., Ebersold, M., Garrett, W., Pypaert, M., and Mellman, I. (2003). Activation of lysosomal function during dendritic cell maturation. Science (New York, N.Y.) *299*, 1400-1403.

Ullrich, O., Reinsch, S., Urbé, S., Zerial, M., and Parton, R.G. (1996). Rab11 regulates recycling through the pericentriolar recycling endosome. The Journal of cell biology *135*, 913-924.

Urs, S., Roudabush, A., O'Neill, C.F., Pinz, I., Prudovsky, I., Kacer, D., Tang, Y., Liaw, L., and Small, D. (2008). Soluble forms of the Notch ligands Delta1 and Jagged1 promote in vivo tumorigenicity in NIH3T3 fibroblasts with distinct phenotypes. The American journal of pathology *173*, 865-878.

Usui, T., Shima, Y., Shimada, Y., Hirano, S., Burgess, R.W., Schwarz, T.L., Takeichi, M., and Uemura, T. (1999). Flamingo, a Seven-Pass Transmembrane Cadherin, Regulates Planar Cell Polarity under the Control of Frizzled. Cell *98*, 585-595.

Vaccari, T., Lu, H., Kanwar, R., Fortini, M.E., and Bilder, D. (2008). Endosomal entry regulates Notch receptor activation in Drosophila melanogaster. The Journal of cell biology *180*, 755-762.

Valapala, M., Hose, S., Gongora, C., Dong, L., Wawrousek, E.F., Samuel Zigler, J., and Sinha, D. (2013). Impaired endolysosomal function disrupts Notch signalling in optic nerve astrocytes. Nature communications *4*, 1629.

van Es, J.H., van Gijn, M.E., Riccio, O., van den Born, M., Vooijs, M., Begthel, H., Cozijnsen, M., Robine, S., Winton, D.J., and Radtke, F., et al. (2005). Notch/gamma-secretase inhibition turns proliferative cells in intestinal crypts and adenomas into goblet cells. Nature *435*, 959-963.

van Niel, G., Charrin, S., Simoes, S., Romao, M., Rochin, L., Saftig, P., Marks, M.S., Rubinstein, E., and Raposo, G. (2011). The tetraspanin CD63 regulates ESCRT-independent and -dependent endosomal sorting during melanogenesis. Developmental Cell *21*, 708-721.

Varnum-Finney, B., Wu, L., Yu, M., Brashem-Stein, C., Staats, S., Flowers, D., Griffin, J.D., and Bernstein, I.D. (2000). Immobilization of Notch ligand, Delta-1, is required for induction of notch signaling. Journal of cell science *113 Pt 23*, 4313-4318.

Verkhusha, V.V., Kuznetsova, I.M., Stepanenko, O.V., Zaraisky, A.G., Shavlovsky, M.M., Turoverov, K.K., and Uversky, V.N. (2003). High stability of Discosoma DsRed as compared to Aequorea EGFP. Biochemistry *42*, 7879-7884.

Vessey, J.P., Amadei, G., Burns, S.E., Kiebler, M.A., Kaplan, D.R., and Miller, F.D. (2012). An asymmetrically localized Staufen2-dependent RNA complex regulates maintenance of mammalian neural stem cells. Cell stem cell, 517-528.

Vilas-Boas, F., Fior, R., Swedlow, J.R., Storey, K.G., and Henrique, D. (2011). A novel reporter of notch signalling indicates regulated and random Notch activation during vertebrate neurogenesis. BMC biology, 58.

Vinson, C.R., and Adler, P.N. (1987). Directional non-cell autonomy and the transmission of polarity information by the frizzled gene of Drosophila. Nature *329*, 549-551.

Vreede, G. de, Schoenfeld, J.D., Windler, S.L., Morrison, H., Lu, H., and Bilder, D. (2014). The Scribble module regulates retromer-dependent endocytic trafficking during epithelial polarization. Development (Cambridge, England) *141*, 2796-2802.

Walshe, J., and Mason, I. (2003). Unique and combinatorial functions of Fgf3 and Fgf8 during zebrafish forebrain development. Development (Cambridge, England) *130*, 4337-4349.

Waltzer, L., Bourillot, P.Y., Sergeant, A., and Manet, E. (1995). RBP-J kappa repression activity is mediated by a co-repressor and antagonized by the Epstein-Barr virus transcription factor EBNA2. Nucleic acids research *23*, 4939-4945.

Wang, H., Zang, C., Taing, L., Arnett, K.L., Wong, Y.J., Pear, W.S., Blacklow, S.C., Liu, X.S., and Aster, J.C. (2014). NOTCH1-RBPJ complexes drive target gene expression through dynamic interactions with superenhancers. Proceedings of the National Academy of Sciences of the United States of America *111*, 705-710.

Wang, J., Hamblet, N.S., Mark, S., Dickinson, M.E., Brinkman, B.C., Segil, N., Fraser, S.E., Chen, P., Wallingford, J.B., and Wynshaw-Boris, A. (2006). Dishevelled genes mediate a conserved mammalian PCP pathway to regulate convergent extension during neurulation. Development (Cambridge, England) *133*, 1767-1778.

Wang, W., and Struhl, G. (2004). Drosophila Epsin mediates a select endocytic pathway that DSL ligands must enter to activate Notch. Development (Cambridge, England) *131*, 5367-5380.

Watanabe, K., Kamiya, D., Nishiyama, A., Katayama, T., Nozaki, S., Kawasaki, H., Watanabe, Y., Mizuseki, K., and Sasai, Y. (2005). Directed differentiation of telencephalic precursors from embryonic stem cells. Nature neuroscience *8*, 288-296.

Weber, H., Holewa, B., Jones, E.A., and Ryffel, G.U. (1996). Mesoderm and endoderm differentiation in animal cap explants: identification of the HNF4-binding site as an activin A responsive element in the Xenopus HNF1alpha promoter. Development (Cambridge, England) *122*, 1975-1984.

Wharton, K.A., Johansen, K.M., Xu, T., and Artavanis-Tsakonas, S. (1985). Nucleotide sequence from the neurogenic locus notch implies a gene product that shares homology with proteins containing EGF-like repeats. Cell *43*, 567-581.

Wilkin, M., Tongngok, P., Gensch, N., Clemence, S., Motoki, M., Yamada, K., Hori, K., Taniguchi-Kanai, M., Franklin, E., and Matsuno, K., et al. (2008). Drosophila HOPS and AP-3 complex genes are required for a Deltex-regulated activation of notch in the endosomal trafficking pathway. Developmental Cell *15*, 762-772.

Windler, S.L., and Bilder, D. (2010). Endocytic internalization routes required for delta/notch signaling. Current biology : CB *20*, 538-543.

Winnard, P.T., Kluth, J.B., and Raman, V. (2006). Noninvasive optical tracking of red fluorescent protein-expressing cancer cells in a model of metastatic breast cancer. Neoplasia (New York, N.Y.) *8*, 796-806.

Wirtz-Peitz, F., Nishimura, T., and Knoblich, J.A. (2008). Linking cell cycle to asymmetric division: Aurora-A phosphorylates the Par complex to regulate Numb localization. Cell *135*, 161-173.

Wodarz, A., Ramrath, A., Grimm, A., and Knust, E. (2000). Drosophila atypical protein kinase C associates with Bazooka and controls polarity of epithelia and neuroblasts. The Journal of cell biology *150*, 1361-1374.

Wolfe, M.S. (2006). The gamma-secretase complex: membrane-embedded proteolytic ensemble. Biochemistry *45*, 7931-7939.

Woo, S.-M., Kim, J., Han, H.-W., Chae, J.-I., Son, M.-Y., Cho, S., Chung, H.-M., Han, Y.-M., and Kang, Y.-K. (2009). Notch signaling is required for maintaining stem-cell features of neuroprogenitor cells derived from human embryonic stem cells. BMC neuroscience *10*, 97.

Wu, L., Aster, J.C., Blacklow, S.C., Lake, R., Artavanis-Tsakonas, S., and Griffin, J.D. (2000). MAML1, a human homologue of Drosophila mastermind, is a transcriptional co-activator for NOTCH receptors. Nature genetics *26*, 484-489.

Wu, T., Hadjantonakis, A.-K., and Nowotschin, S. (2017). Visualizing endoderm cell populations and their dynamics in the mouse embryo with a Hex-tdTomato reporter. Biology open *6*, 678-687.

Wu, X., Fleming, A., Ricketts, T., Pavel, M., Virgin, H., Menzies, F.M., and Rubinsztein, D.C. (2016). Autophagy regulates Notch degradation and modulates stem cell development and neurogenesis. Nature communications *7*, 10533.

Xiang, Y., Tanaka, Y., Patterson, B., Kang, Y.-J., Govindaiah, G., Roselaar, N., Cakir, B., Kim, K.-Y., Lombroso, A.P., and Hwang, S.-M., et al. (2017). Fusion of Regionally Specified hPSC-Derived Organoids Models Human Brain Development and Interneuron Migration. Cell stem cell, 383-398.e7.

Yamada, K., Fuwa, T.J., Ayukawa, T., Tanaka, T., Nakamura, A., Wilkin, M.B., Baron, M., and Matsuno, K. (2011). Roles of Drosophila deltex in Notch receptor endocytic trafficking and activation. Genes to cells : devoted to molecular & cellular mechanisms *16*, 261-272.

Yan, Y., Denef, N., and Schüpbach, T. (2009). The vacuolar proton pump, V-ATPase, is required for notch signaling and endosomal trafficking in Drosophila. Developmental Cell *17*, 387-402.

Yatim, A., Benne, C., Sobhian, B., Laurent-Chabalier, S., Deas, O., Judde, J.-G., Lelievre, J.-D., Levy, Y., and Benkirane, M. (2012). NOTCH1 nuclear interactome reveals key regulators of its transcriptional activity and oncogenic function. Molecular Cell *48*, 445-458.

Yoon, K., Nery, S., Rutlin, M.L., Radtke, F., Fishell, G., and Gaiano, N. (2004). Fibroblast growth factor receptor signaling promotes radial glial identity and interacts with Notch1 signaling in telencephalic progenitors. The Journal of neuroscience : the official journal of the Society for Neuroscience *24*, 9497-9506.

Yu, X., Zou, J., Ye, Z., Hammond, H., Chen, G., Tokunaga, A., Mali, P., Li, Y.-M., Civin, C., and Gaiano, N., et al. (2008). Notch signaling activation in human embryonic stem cells is required for embryonic, but not trophoblastic, lineage commitment. Cell stem cell *2*, 461-471.

Zeltser, L.M., Larsen, C.W., and Lumsden, A. (2001). A new developmental compartment in the forebrain regulated by Lunatic fringe. Nature neuroscience *4*, 683-684.

Zhang, H., and Macara, I.G. (2008). The PAR-6 polarity protein regulates dendritic spine morphogenesis through p190 RhoGAP and the Rho GTPase. Developmental Cell *14*, 216-226.

Zhang, S.C., Wernig, M., Duncan, I.D., Brüstle, O., and Thomson, J.A. (2001). In vitro differentiation of transplantable neural precursors from human embryonic stem cells. Nature biotechnology *19*, 1129-1133.

Zhao, X., Tong, K., Chen, X., Yang, B., Li, Q., Dai, Z., Shi, X., Seiple, I.B., Huang, B., and Guo, S. (2020). Polarized endosome dynamics engage cytosolic Par-3 and dynein during asymmetric division.

Zhong, W., Feder, J.N., Jiang, M.-M., Jan, L.Y., and Jan, Y.N. (1996). Asymmetric Localization of a Mammalian Numb Homolog during Mouse Cortical Neurogenesis. Neuron *17*, 43-53.

Zhong, W., Jiang, M.M., Weinmaster, G., Jan, L.Y., and Jan, Y.N. (1997). Differential expression of mammalian Numb, Numblike and Notch1 suggests distinct roles during mouse cortical neurogenesis. Development (Cambridge, England) *124*, 1887-1897.

Zhou, W., He, Q., Zhang, C., He, X., Cui, Z., Liu, F., and Li, W. (2016). BLOS2 negatively regulates Notch signaling during neural and hematopoietic stem and progenitor cell development. eLife *5*.

Zhou, X., Sasaki, H., Lowe, L., Hogan, B.L., and Kuehn, M.R. (1993). Nodal is a novel TGF-beta-like gene expressed in the mouse node during gastrulation. Nature *361*, 543-547.

Zimmerman, L.B., Jesús-Escobar, J.M. de, and Harland, R.M. (1996). The Spemann organizer signal noggin binds and inactivates bone morphogenetic protein 4. Cell *86*, 599-606.

Zoncu, R., Bar-Peled, L., Efeyan, A., Wang, S., Sancak, Y., and Sabatini, D.M. (2011). mTORC1 senses lysosomal amino acids through an inside-out mechanism that requires the vacuolar H(+)-ATPase. Science (New York, N.Y.) *334*, 678-683.

Appendix

HES1 HDR-template:

5‘/3‘ homology arms with **HES1 exons**
T2A
tdTomato with **NLS** and *PEST*
AmpicillinR

```
1    - TAAATTCAATTCGCCCTATAGTGAGTCGTATTACAATTCACTGGCCGTCGTTTTACAACGTCGTGACTGGGAAAACCCTGGCGTTACCCAACTTAATCGC - 100
101  - CTTGCAGCACATCCCCCTTTCGCCAGCTGGCGTAATAGCGAAGAGGCCCGCACCGATCGCCCTTCCCAACAGTTGCGCAGCCTATACGTACGGCAGTTTA - 200
201  - AGGTTTACACCTATAAAAGAGAGAGCCGTTATCGTCTGTTTGTGGATGTACAGAGTGATATTATTGACACGCCGGGGCGACGGATGGTGATCCCCCTGGC - 300
301  - CAGTGCACGTCTGCTGTCAGATAAAGTCTCCCGTGAACTTTACCCGGTGGTGCATATCGGGGATGAAAGCTGGCGCATGATGACCACCGATATGGCCAGT - 400
401  - GTGCCGGTCTCCGTTATCGGGGAAGAAGTGGCTGATCTCAGCCACCGCGAAAATGACATCAAAAACGCCATTAACCTGATGTTCTGGGGAATATAAATGT - 500
501  - CAGGCATGAGATTATCAAAAAGGATCTTCACCTAGATCCTTTTCACGTAGAAAGCCAGTCCGCAGAAACGGTGCTGACCCCGGATGAATGTCAGCTACTG - 600
601  - GGCTATCTGGACAAGGGAAAACGCAAGCGCAAAGAGAAAGCAGGTAGCTTGCAGTGGGCTTACATGGCGATAGCTAGACTGGGCGGTTTTATGGACAGCA - 700
701  - AGCGAACCGGAATTGCCAGCTGGGGCGCCCTCTGGTAAGGTTGGGAAGCCCTGCAAAGTAAACTGGATGGCTTTCTTGCCGCCAAGGATCTGATGGCGCA - 800
801  - GGGGATCAAGCTCTGATCAAGAGACAGGATGAGGATCGTTTCGCATGATTGAACAAGATGGATTGCACGCAGGTTCTCCGGCCGCTTGGGTGGAGAGGCT - 900
901  - ATTCGGCTATGACTGGGCACAACAGACAATCGGCTGCTCTGATGCCGCCGTGTTCCGGCTGTCAGCGCAGGGGCGCCCGGTTCTTTTTGTCAAGACCGAC - 1000
1001 - CTGTCCGGTGCCCTGAATGAACTGCAAGACGAGGCAGCGCGGCTATCGTGGCTGGCCACGACGGGCGTTCCTTGCGCAGCTGTGCTCGACGTTGTCACTG - 1100
1101 - AAGCGGGAAGGGACTGGCTGCTATTGGGCGAAGTGCCGGGGCAGGATCTCCTGTCATCTCACCTTGCTCCTGCCGAGAAAGTATCCATCATGGCTGATGC - 1200
1201 - AATGCGGCGGCTGCATACGCTTGATCCGGCTACCTGCCCATTCGACCACCAAGCGAAACATCGCATCGAGCGAGCACGTACTCGGATGGAAGCCGGTCTT - 1300
1301 - GTCGATCAGGATGATCTGGACGAAGAGCATCAGGGGCTCGCGCCAGCCGAACTGTTCGCCAGGCTCAAGGCGAGCATGCCCGACGGCGAGGATCTCGTCG - 1400
1401 - TGACCCATGGCGATGCCTGCTTGCCGAATATCATGGTGGAAAATGGCCGCTTTTCTGGATTCATCGACTGTGGCCGGCTGGGTGTGGCGGACCGCTATCA - 1500
1501 - GGACATAGCGTTGGCTACCCGTGATATTGCTGAAGAGCTTGGCGGCGAATGGGCTGACCGCTTCCTCGTGCTTTACGGTATCGCCGCTCCCGATTCGCAG - 1600
1601 - CGCATCGCCTTCTATCGCCTTCTTGACGAGTTCTTCTGAATTATTAACGCTTACAATTTCCTGATGCGGTATTTTCTCCTTACGCATCTGTGCGGTATTT - 1700
1701 - CACACCGCATCAGGTGGCACTTTTCGGGGAAATGTGCGCGGAACCCCTATTTGTTTATTTTTCTAAATACATTCAAATATGTATCCGCTCATGAGATTAT - 1800
1801 - CAAAAAGGATCTTCACCTAGATCCTTTTAAATTAAAAATGAAGTTTTAAATCAATCTAAAGTATATATGAGTAAACTTGGTCTGACAGTTACCAATGCTT - 1900
1901 - AATCAGTGAGGCACCTATCTCAGCGATCTGTCTATTTCGTTCATCCATAGTTGCCTGACTCCCCGTCGTGTAGATAACTACGATACGGGAGGGCTTACCA - 2000
2001 - TCTGGCCCCAGTGCTGCAATGATACCGCGAGACCCACGCTCACCGGCTCCAGATTTATCAGCAATAAACCAGCCAGCCGGAAGGGCCGAGCGCAGAAGTG - 2100
2101 - GTCCTGCAACTTTATCCGCCTCCATCCAGTCTATTAATTGTTGCCGGGAAGCTAGAGTAAGTAGTTCGCCAGTTAATAGTTTGCGCAACGTTGTTGCCAT - 2200
2201 - TGCTACAGGCATCGTGGTGTCACGCTCGTCGTTTGGTATGGCTTCATTCAGCTCCGGTTCCCAACGATCAAGGCGAGTTACATGATCCCCCATGTTGTGC - 2300
2301 - AAAAAAGCGGTTAGCTCCTTCGGTCCTCCGATCGTTGTCAGAAGTAAGTTGGCCGCAGTGTTATCACTCATGGTTATGGCAGCACTGCATAATTCTCTTA - 2400
2401 - CTGTCATGCCATCCGTAAGATGCTTTTCTGTGACTGGTGAGTACTCAACCAAGTCATTCTGAGAATAGTGTATGCGGCGACCGAGTTGCTCTTGCCCGGC - 2500
2501 - GTCAATACGGGATAATACCGCGCCACATAGCAGAACTTTAAAAGTGCTCATCATTGGAAAACGTTCTTCGGGGCGAAAACTCTCAAGGATCTTACCGCTG - 2600
2601 - TTGAGATCCAGTTCGATGTAACCCACTCGTGCACCCAACTGATCTTCAGCATCTTTTACTTTCACCAGCGTTTCTGGGTGAGCAAAAACAGGAAGGCAAA - 2700
2701 - ATGCCGCAAAAAAGGGAATAAGGGCGACACGGAAATGTTGAATACTCATACTCTTCCTTTTTCAATATTATTGAAGCATTTATCAGGGTTATTGTCTCAT - 2800
2801 - GACCAAAATCCCTTAACGTGAGTTTTCGTTCCACTGAGCGTCAGACCCCGTAGAAAAGATCAAAGGATCTTCTTGAGATCCTTTTTTTCTGCGCGTAATC - 2900
2901 - TGCTGCTTGCAAACAAAAAAACCACCGCTACCAGCGGTGGTTTGTTTGCCGGATCAAGAGCTACCAACTCTTTTTCCGAAGGTAACTGGCTTCAGCAGAG - 3000
3001 - CGCAGATACCAAATACTGTTCTTCTAGTGTAGCCGTAGTTAGGCCACCACTTCAAGAACTCTGTAGCACCGCCTACATACCTCGCTCTGCTAATCCTGTT - 3100
3101 - ACCAGTGGCTGCTGCCAGTGGCGATAAGTCGTGTCTTACCGGGTTGGACTCAAGACGATAGTTACCGGATAAGGCGCAGCGGTCGGGCTGAACGGGGGGT - 3200
3201 - TCGTGCACACAGCCCAGCTTGGAGCGAACGACCTACACCGAACTGAGATACCTACAGCGTGAGCTATGAGAAAGCGCCACGCTTCCCGAAGGGAGAAAGG - 3300
3301 - CGGACAGGTATCCGGTAAGCGGCAGGGTCGGAACAGGAGAGCGCACGAGGGAGCTTCCAGGGGGAAACGCCTGGTATCTTTATAGTCCTGTCGGGTTTCG - 3400
3401 - CCACCTCTGACTTGAGCGTCGATTTTTGTGATGCTCGTCAGGGGGGCGGAGCCTATGGAAAAACGCCAGCAACGCGGCCTTTTTACGGTTCCTGGCCTTT - 3500
3501 - TGCTGGCCTTTTGCTCACATGTTCTTTCCTGCGTTATCCCCTGATTCTGTGGATAACCGTATTACCGCCTTTGAGTGAGCTGATACCGCTCGCCGCAGCC - 3600
3601 - GAACGACCGAGCGCAGCGAGTCAGTGAGCGAGGAAGCGGAAGAGCGCCCAATACGCAAACCGCCTCTCCCCGCGCGTTGGCCGATTCATTAATGCAGCTG - 3700
3701 - GCACGACAGGTTTCCCGACTGGAAAGCGGGCAGTGAGCGCAACGCAATTAATGTGAGTTAGCTCACTCATTAGGCACCCCAGGCTTTACACTTTATGCTT - 3800
3801 - CCGGCTCGTATGTTGTGTGGAATTGTGAGCGGATAACAATTTCACACAGGAAACAGCTATGACCATGATTACGCCAAGCTCAGAATTAACCCTCACTAAA - 3900
3901 - GGGACTAGTCCTGCAGGTTTAAACGAATTCCTGGGGGTCACTGGTTTAGCACTCCTTCCCGTTGCAGAAGGGGAAATGAGGCTTGGATGATGGATTGGGA - 4000
4001 - GGCATTGTCCAAGGTCACATCGCGCGCGGGGGTGGGGGTGACAGATCTGGGGCTGAGATAGGTTTAAATGCAGCTACAGGGAATCGGGAAGGAGTGGCTG - 4100
4101 - GGCTTTTGGCAGCAACGCTAGTGTGGAGAGGTGGCTGGTTTTTTCTAAACCCATCTCACCCTCCCTGCCGGAGGCAGTTTCACGGGCGCATGGTCAGGGA - 4200
4201 - GGCGCGCCACAGGGACCTCCCAGGGCGGAGGCAGTGGCCACGGGGCCAGGGCCGTTCGGTGACCCGTCTGTCTCTTTCTGGCCCGCAG**CTGCGCTGAGCA** - 4300
4301 - **CAGACCCAAGTGTGCTGGGGAAGTACCGAGCCGGCTTCAGCGAGTGCATGAACGAGGTGACCCGCTTCCTGTCCACGTGCGAGGGCGTTAATACCGAGGT** - 4400
4401 - **GCGCACTCGGCTGCTCGGCCACCTGGCCAACTGCATGACCCAGATCAATGCCATGACCTACCCCGGGCAGCCGCACCCCGCCTTGCAGGCGCCGCCACCG** - 4500
4501 - **CCCCCACCGGGACCCGGCGGCCCCCAGCACGCGCCGTTCGCGCCCGCCGCCGCCACTCGTGCCCATCCCCGGGGCGCGGCGCCCCCTCCCGGCGGCGCCC** - 4600
4601 - **CCTGCAAGCTGGGCAGCCAGGCTGGAGAGGCGGCTAAGGTGTTTGGAGGCTTCCAGGTGGTACCGGCTCCCGATGGCCAGTTTGCTTTCCTCATTCCCAA** - 4700
4701 - **CGGGGCCTTCGCGCACAGCGGCCCTGTCATCCCCGTCTACACCAGCAACAGCGGCACCTCCGTGGGCCCCAACGCAGTGTCACCTTCCAGCGGCCCCTCG** - 4800
4801 - **CTTACGGCGGACTCCATGTGGAGGCCGTGGCGGAAC**GTCGACGAGGGCAGAGGAAGTCTTCTAACATGCGGTGACGTGGAGGAGAATCCCGGCCCTACCG - 4900
4901 - GTATGGTGAGCAAGGGCGAGGAGGTCATCAAAGAGTTCATGCGCTTCAAGGTGCGGATGGAGGGCTCCATGAACGGCCACGAGTTCGAGATCGAGGGCGA - 5000
5001 - GGGCGAGGGCCGCCCCTACGAGGGCACCCAGACCGCCAAGCTGAAGGTGACCAAGGGCGGCCCCCTGCCCTTCGCCTGGGACATCCTGTCCCCCCAGTTC - 5100
5101 - ATGTACGGCTCCAAGGCGTACGTGAAGCACCCCGCCGACATCCCCGATTACAAGAAGCTGTCCTTCCCCGAGGGCTTCAAGTGGGAGCGCGTGATGAACT - 5200
5201 - TCGAGGACGGCGGTCTGGTGACCGTGACCCAGGACTCCTCCCTCCAGGACGGCACGCTGATCTACAAGGTGAAGATGCGCGGCACCAACTTCCCCCCCGA - 5300
5301 - CGGCCCCGTAATGCAGAAGAAGACGATGGGCTGGGAGGCCTCCACCGAGCGCCTGTACCCCCGCGACGGCGTGCTGAAGGGCGAGATCCACCAGGCCCTG - 5400
5401 - AAGCTGAAGGACGGCGGCCACTACCTGGTGGAGTTCAAGACCATCTACATGGCCAAGAAGCCCGTGCAACTGCCCGGCTACTACTACGTGGACACCAAGC - 5500
5501 - TGGACATCACCTCCCACAACGAGGACTACACCATCGTGGAACAGTACGAGCGCTCCGAGGGCCGCCACCACCTGTTCCTGGGGCATGGCACCGGCAGCAG - 5600
5601 - CGGCAGCGGCAGCTCCGGCACCGCCTCCTCCGAGGACAACAACATGGCCGTCATCAAAGAGTTCATGCGCTTCAAGGTGCGGATGGAGGGCTCCATGAAC - 5700
5701 - GGCCACGAGTTCGAGATCGAGGGCGAGGGCGAGGGCCGCCCCTACGAGGGCACCCAGACCGCCAAGCTGAAGGTGACCAAGGGCGGCCCCCTGCCCTTCG - 5800
5801 - CCTGGGACATCCTGTCCCCCCAGTTCATGTACGGCTCCAAGGCGTACGTGAAGCACCCCGCCGACATCCCCGATTACAAGAAGCTGTCCTTCCCCGAGGG - 5900
5901 - CTTCAAGTGGGAGCGCGTGATGAACTTCGAGGACGGCGGTCTGGTGACCGTGACCCAGGACTCCTCCCTCCAGGACGGCACGCTGATCTACAAGGTGAAG - 6000
6001 - ATGCGCGGCACCAACTTCCCCCCCGACGGCCCCGTAATGCAGAAGAAGACGATGGGCTGGGAGGCCTCCACCGAGCGCCTGTACCCCCGCGACGGCGTGC - 6100
6101 - TGAAGGGCGAGATCCACCAGGCCCTGAAGCTGAAGGACGGCGGCCACTACCTGGTGGAGTTCAAGACCATCTACATGGCCAAGAAGCCCGTGCAACTGCC - 6200
6201 - CGGCTACTACTACGTGGACACCAAGCTGGACATCACCTCCCACAACGAGGACTACACCATCGTGGAACAGTACGAGCGCTCCGAGGGCCGCCACCACCTG - 6300
6301 - TTCCTGTACGGCATGGACGAGCTGTACAAGACGCGT**CCTCCAAAAAAGAAGAGAAAGGTAGAAGACCCCT**TGTACA*AGAGCCATGGCTTCCCGCCGGCTG* - 6400
6401 - *TGGCTGCTCAGGATGATGGCACGCTGCCCATGTCCTGTGCCCAGGAGAGCGGGATGGACCGTCACCCTGCAGCCTGTGCTCCTGCTAGGATCAATGTGTA* - 6500
6501 - GGAGCTC**CACCTCTCTTCCCTCCGGACTCTAAACAGGAACTTGAATACTGGGAGAGAAGAGGACTTTTTTGATTAAGTGGTTACTTTGTGTTTTTTTAAT** - 6600
6601 - **TTCTAAGAAGTTACTTTTTGTAGAGAGAGCTGTATTAAGTGACTGACCATGCACTATATTTGTATATATTTTATATGTTCATATTGGATTGCGCCTTTGT** - 6700
6701 - **ATTATAAAAGCTCAGATGACATTTCGTTTTTTACACGAGATTTCTTTTTTATGTGATGCCAAAGATGTTTGAAAATGCTCTTAAAATATCTTCCTTTGGG** - 6800
6801 - **GAAGTTTATTTGAGAAAATATAATAAAAGAAAAAAGTAAAGGCTTTTA**TGTCTTCGAACTGATTCTTCCAGAATATGTAAAAAGGCTTTTGGTGGAATTT - 6900
6901 - GAATTACATGTAATTGGTAATTCAGGAATTGACTCTTTTGTTATTAAAAGAACATTTGTAAAAATCCATCAAACTTTTCACCAATCCTCCATGAACTAAA - 7000
7001 - AAGACTAAATTCCATTTACTTTACAAGCAGCCATCTGGTAAGGCTTCCCTGATAAACTTGTGGTCAGTCTCTTAAAGGATTTCCAAAAAAAATGTTTTTA - 7100
7101 - AGTTGCAGTCGGGTAAGTCTGCAGCCCTTGTTCTTCTAGCTCCTCCTGAGGAAGATTGAACAGGACTAAATTCACGAAGCTAATGGATCCAATCCTATTG - 7200
7201 - CCCATTGCACGTTAAGGGTGGTTCCTGCAGCTCTCCTCTCAGGGTAGCTCACCAGCATCCAAAGCAAAAACACTTCCAACTGCTGCGCCTCCTTCAAGAC - 7300
7301 - TTGGGGTCTTCATTAATTAGCCAATCCTTTGGTTCAAATAAGACGTTCCCTAGCACCCAAAAGTTTCCTCTCCGCACCCTCTTAAAGCAAGCGGCCGC - 7398
```

HES1 gRNA-plasmid:

U6 promoter
gRNA with scaffold
CMV promoter
hSpCas9 with *FLAG-tag* and **NLS**
T2A
PuromycinR
AmpicillinR with *promoter*

```
1    - GAGGGCCTATTTCCCATGATTCCTTCATATTTGCATATACGATACAAGGCTGTTAGAGAGATAATTGGAATTAATTTGACTGTAAACACAAAGATATTAG - 100
101  - TACAAAATACGTGACGTAGAAAGTAATAATTTCTTGGGTAGTTTGCAGTTTTAAAATTATGTTTTAAAATGGACTATCATATGCTTACCGTAACTTGAAA - 200
201  - GTATTTCGATTTCTTGGCTTTATATATCTTGTGGAAAGGACGAAACACCGggaggccgtggcggaactgaGTTTTAGAGCTAGAAATAGCAAGTTAAAAT - 300
301  - AAGGCTAGTCCGTTATCAACTTGAAAAAGTGGCACCGAGTCGGTGCTTTTTTGTTTTAGAGCTAGAAATAGCAAGTTAAAATAAGGCTAGTCCGTTTTTA - 400
401  - GCGCGTGCGCCAATTCTGCAGACAAATGGCTCTAGAGGTACCCGTTACATAACTTACGGTAAATGGCCCGCCTGGCTGACCGCCCAACGACCCCCGCCCA - 500
501  - TTGACGTCAATAGTAACGCCAATAGGGACTTTCCATTGACGTCAATGGGTGGAGTATTTACGGTAAACTGCCCACTTGGCAGTACATCAAGTGTATCATA - 600
601  - TGCCAAGTACGCCCCCTATTGACGTCAATGACGGTAAATGGCCCGCCTGGCATTGTGCCCAGTACATGACCTTATGGGACTTTCCTACTTGGCAGTACAT - 700
701  - CTACGTATTAGTCATCGCTATTACCATGGTCGAGGTGAGCCCCACGTTCTGCTTCACTCTCCCCATCTCCCCCCCCTCCCCACCCCCAATTTTGTATTTA - 800
801  - TTTATTTTTTAATTATTTTGTGCAGCGATGGGGGCGGGGGGGGGGGGGGGCGCGCGCCAGGCGGGGCGGGGCGGGGCGAGGGGCGGGGCGGGGCGAGGC - 900
901  - GGAGAGGTGCGGCGGCAGCCAATCAGAGCGGCGCGCTCCGAAAGTTTCCTTTTATGGCGAGGCGGCGGCGGCGGCGCCCTATAAAAAGCGAAGCGCGCG - 1000
1001 - GCGGGCGGGAGTCGCTGCGCGCTGCCTTCGCCCCGTGCCCCGCTCCGCCGCCGCCTCGCGCCGCCCGCCCCGGCTCTGACTGACCGCGTTACTCCCACAG - 1100
1101 - GTGAGCGGGCGGGACGGCCCTTCTCCTCCGGGCTGTAATTAGCTGAGCAAGAGGTAAGGGTTTAAGGGATGGTTGGTTGGTGGGGTATTAATGTTTAATT - 1200
1201 - ACCTGGAGCACCTGCCTGAAATCACTTTTTTTCAGGTTGGACCGGTGCCACCATGGACTATAAGGACCACGACGGAGACTACAAGGATCATGATATTGAT - 1300
1301 - TACAAAGACGATGACGATAAGATGGCCCCAAAGAAGAAGCGGAAGGTCGGTATCCACGGAGTCCCAGCAGCCGACAAGAAGTACAGCATCGGCCTGGACA - 1400
1401 - TCGGCACCAACTCTGTGGGCTGGGCCGTGATCACCGACGAGTACAAGGTGCCCAGCAAGAAATTCAAGGTGCTGGGCAACACCGACCGGCACAGCATCAA - 1500
1501 - GAAGAACCTGATCGGAGCCCTGCTGTTCGACAGCGGCGAAACAGCCGAGGCCACCCGGCTGAAGAGAACCGCCAGAAGAAGATACACCAGACGGAAGAAC - 1600
1601 - CGGATCTGCTATCTGCAAGAGATCTTCAGCAACGAGATGGCCAAGGTGGACGACAGCTTCTTCCACAGACTGGAAGAGTCCTTCCTGGTGGAAGAGGATA - 1700
1701 - AGAAGCACGAGCGGCACCCCATCTTCGGCAACATCGTGGACGAGGTGGCCTACCACGAGAAGTACCCCACCATCTACCACCTGAGAAAGAAACTGGTGGA - 1800
1801 - CAGCACCGACAAGGCCGACCTGCGGCTGATCTATCTGGCCCTGGCCCACATGATCAAGTTCCGGGGCCACTTCCTGATCGAGGGCGACCTGAACCCCGAC - 1900
1901 - AACAGCGACGTGGACAAGCTGTTCATCCAGCTGGTGCAGACCTACAACCAGCTGTTCGAGGAAAACCCCATCAACGCCAGCGGCGTGGACGCCAAGGCCA - 2000
2001 - TCCTGTCTGCCAGACTGAGCAAGAGCAGACGGCTGGAAAATCTGATCGCCCAGCTGCCCGGCGAGAAGAAGAATGGCCTGTTCGGAAACCTGATTGCCCT - 2100
2101 - GAGCCTGGGCCTGACCCCCAACTTCAAGAGCAACTTCGACCTGGCCGAGGATGCCAAACTGCAGCTGAGCAAGGACACCTACGACGACGACCTGGACAAC - 2200
2201 - CTGCTGGCCCAGATCGGCGACCAGTACGCCGACCTGTTTCTGGCCGCCAAGAACCTGTCCGACGCCATCCTGCTGAGCGACATCCTGAGAGTGAACACCG - 2300
2301 - AGATCACCAAGGCCCCCCTGAGCGCCTCTATGATCAAGAGATACGACGAGCACCACCAGGACCTGACCCTGCTGAAAGCTCTCGTGCGGCAGCAGCTGCC - 2400
2401 - TGAGAAGTACAAAGAGATTTTCTTCGACCAGAGCAAGAACGGCTACGCCGGCTACATTGACGGCGGAGCCAGCCAGGAAGAGTTCTACAAGTTCATCAAG - 2500
2501 - CCCATCCTGGAAAAGATGGACGGCACCGAGGAACTGCTCGTGAAGCTGAACAGAGAGGACCTGCTGCGGAAGCAGCGGACCTTCGACAACGGCAGCATCC - 2600
2601 - CCCACCAGATCCACCTGGGAGAGCTGCACGCCATTCTGCGGCGGCAGGAAGATTTTTACCCATTCCTGAAGGACAACCGGGAAAAGATCGAGAAGATCCT - 2700
2701 - GACCTTCCGCATCCCCTACTACGTGGGCCCTCTGGCCAGGGGAAACAGCAGATTCGCCTGGATGACCAGAAAGAGCGAGGAAACCATCACCCCCTGGAAC - 2800
2801 - TTCGAGGAAGTGGTGGACAAGGGCGCTTCCGCCCAGAGCTTCATCGAGCGGATGACCAACTTCGATAAGAACCTGCCCAACGAGAAGGTGCTGCCCAAGC - 2900
2901 - ACAGCCTGCTGTACGAGTACTTCACCGTGTATAACGAGCTGACCAAAGTGAAATACGTGACCGAGGGAATGAGAAAGCCCGCCTTCCTGAGCGGCGAGCA - 3000
3001 - GAAAAAGGCCATCGTGGACCTGCTGTTCAAGACCAACCGGAAAGTGACCGTGAAGCAGCTGAAAGAGGACTACTTCAAGAAAATCGAGTGCTTCGACTCC - 3100
3101 - GTGGAAATCTCCGGCGTGGAAGATCGGTTCAACGCCTCCCTGGGCACATACCACGATCTGCTGAAAATTATCAAGGACAAGGACTTCCTGGACAATGAGG - 3200
3201 - AAAACGAGGACATTCTGGAAGATATCGTGCTGACCCTGACACTGTTTGAGGACAGAGAGATGATCGAGGAACGGCTGAAAACCTATGCCCACCTGTTCGA - 3300
3301 - CGACAAAGTGATGAAGCAGCTGAAGCGGCGGAGATACACCGGCTGGGGCAGGCTGAGCCGGAAGCTGATCAACGGCATCCGGGACAAGCAGTCCGGCAAG - 3400
3401 - ACAATCCTGGATTTCCTGAAGTCCGACGGCTTCGCCAACAGAAACTTCATGCAGCTGATCCACGACGACAGCCTGACCTTTAAAGAGGACATCCAGAAAG - 3500
3501 - CCCAGGTGTCCGGCCAGGGCGATAGCCTGCACGAGCACATTGCCAATCTGGCCGGCAGCCCCGCCATTAAGAAGGGCATCCTGCAGACAGTGAAGGTGGT - 3600
3601 - GGACGAGCTCGTGAAAGTGATGGGCCGGCACAAGCCCGAGAACATCGTGATCGAAATGGCCAGAGAGAACCAGACCACCCAGAAGGGACAGAAGAACAGC - 3700
3701 - CGCGAGAGAATGAAGCGGATCGAAGAGGGCATCAAAGAGCTGGGCAGCCAGATCCTGAAAGAACACCCCGTGGAAAACACCCAGCTGCAGAACGAGAAGC - 3800
3801 - TGTACCTGTACTACCTGCAGAATGGGCGGGATATGTACGTGGACCAGGAACTGGACATCAACCGGCTGTCCGACTACGATGTGGACCATATCGTGCCTCA - 3900
3901 - GAGCTTTCTGAAGGACGACTCCATCGACAACAAGGTGCTGACCAGAAGCGACAAGAACCGGGGCAAGAGCGACAACGTGCCCTCCGAAGAGGTCGTGAAG - 4000
4001 - AAGATGAAGAACTACTGGCGGCAGCTGCTGAACGCCAAGCTGATTACCCAGAGAAAGTTCGACAATCTGACCAAGGCCGAGAGAGGCGGCCTGAGCGAAC - 4100
4101 - TGGATAAGGCCGGCTTCATCAAGAGACAGCTGGTGGAAACCCGGCAGATCACAAAGCACGTGGCACAGATCCTGGACTCCCGGATGAACACTAAGTACGA - 4200
4201 - CGAGAATGACAAGCTGATCCGGGAAGTGAAAGTGATCACCCTGAAGTCCAAGCTGGTGTCCGATTTCCGGAAGGATTTCCAGTTTTACAAAGTGCGCGAG - 4300
4301 - ATCAACAACTACCACCACGCCCACGACGCCTACCTGAACGCCGTCGTGGGAACCGCCCTGATCAAAAAGTACCCTAAGCTGGAAAGCGAGTTCGTGTACG - 4400
4401 - GCGACTACAAGGTGTACGACGTGCGGAAGATGATCGCCAAGAGCGAGCAGGAAATCGGCAAGGCTACCGCCAAGTACTTCTTCTACAGCAACATCATGAA - 4500
4501 - CTTTTTCAAGACCGAGATTACCCTGGCCAACGGCGAGATCCGGAAGCGGCCTCTGATCGAGACAAACGGCGAAACCGGGGAGATCGTGTGGGATAAGGGC - 4600
4601 - CGGGATTTTGCCACCGTGCGGAAAGTGCTGAGCATGCCCCAAGTGAATATCGTGAAAAAGACCGAGGTGCAGACAGGCGGCTTCAGCAAAGAGTCTATCC - 4700
4701 - TGCCCAAGAGGAACAGCGATAAGCTGATCGCCAGAAAGAAGGACTGGGACCCTAAGAAGTACGGCGGCTTCGACAGCCCCACCGTGGCCTATTCTGTGCT - 4800
4801 - GGTGGTGGCCAAAGTGGAAAAGGGCAAGTCCAAGAAACTGAAGAGTGTGAAAGAGCTGCTGGGGATCACCATCATGGAAAGAAGCAGCTTCGAGAAGAAT - 4900
4901 - CCCATCGACTTTCTGGAAGCCAAGGGCTACAAAGAAGTGAAAAAGGACCTGATCATCAAGCTGCCTAAGTACTCCCTGTTCGAGCTGGAAAACGGCCGGA - 5000
5001 - AGAGAATGCTGGCCTCTGCCGGCGAACTGCAGAAGGGAAACGAACTGGCCCTGCCCTCCAAATATGTGAACTTCCTGTACCTGGCCAGCCACTATGAGAA - 5100
5101 - GCTGAAGGGCTCCCCCGAGGATAATGAGCAGAAACAGCTGTTTGTGGAACAGCACAAGCACTACCTGGACGAGATCATCGAGCAGATCAGCGAGTTCTCC - 5200
5201 - AAGAGAGTGATCCTGGCCGACGCTAATCTGGACAAAGTGCTGTCCGCCTACAACAAGCACCGGGATAAGCCCATCAGAGAGCAGGCCGAGAATATCATCC - 5300
5301 - ACCTGTTTACCCTGACCAATCTGGGAGCCCCTGCCGCCTTCAAGTACTTTGACACCACCATCGACCGGAAGAGGTACACCAGCACCAAAGAGGTGCTGGA - 5400
5401 - CGCCACCCTGATCCACCAGAGCATCACCGGCCTGTACGAGACACGGATCGACCTGTCTCAGCTGGGAGGCGACAAAAGGCCGGCGGCCACGAAAAAGGCC - 5500
5501 - GGCCAGGCAAAAAAGAAAAAGGAATTCGGCAGTGGAGAGGGCAGAGGAAGTCTGCTAACATGCGGTGACGTCGAGGAGAATCCTGGCCCAATGACCGAGT - 5600
5601 - ACAAGCCCACGGTGCGCCTCGCCACCCGCGACGACGTCCCCAGGGCCGTACGCACCCTCGCCGCCGCGTTCGCCGACTACCCCGCCACGCGCCACACCGT - 5700
5701 - CGATCCGGACCGCCACATCGAGCGGGTCACCGAGCTGCAAGAACTCTTCCTCACGCGCGTCGGGCTCGACATCGGCAAGGTGTGGGTCGCGGACGACGGC - 5800
5801 - GCCGCGGTGGCGGTCTGGACCACGCCGGAGAGCGTCGAAGCGGGGGCGGTGTTCGCCGAGATCGGCCCGCGCATGGCCGAGTTGAGCGGTTCCCGGCTGG - 5900
5901 - CCGCGCAGCAACAGATGGAAGGCCTCCTGGCGCCGCACCGGCCCAAGGAGCCCGCGTGGTTCCTGGCCACCGTCGGAGTCTCGCCCGACCACCAGGGCAA - 6000
6001 - GGGTCTGGGCAGCGCCGTCGTGCTCCCCGGAGTGGAGGCGGCCGAGCGCGCCGGGGTGCCCGCCTTCCTGGAGACCTCCGCGCCCCGCAACCTCCCCTTC - 6100
6101 - TACGAGCGGCTCGGCTTCACCGTCACCGCCGACGTCGAGGTGCCCGAAGGACCGCGCACCTGGTGCATGACCCGCAAGCCCGGTGCCTGAGAATTCTAAC - 6200
6201 - TAGAGCTCGCTGATCAGCCTCGACTGTGCCTTCTAGTTGCCAGCCATCTGTTGTTTGCCCCTCCCCCGTGCCTTCCTTGACCCTGGAAGGTGCCACTCCC - 6300
6301 - ACTGTCCTTTCCTAATAAAATGAGGAAATTGCATCGCATTGTCTGAGTAGGTGTCATTCTATTCTGGGGGGTGGGGTGGGGCAGGACAGCAAGGGGGAGG - 6400
6401 - ATTGGGAAGAGAATAGCAGGCATGCTGGGGAGCGGCCGCAGGAACCCCTAGTGATGGAGTTGGCCACTCCCTCTCTGCGCGCTCGCTCGCTCACTGAGGC - 6500
6501 - CGGGCGACCAAAGGTCGCCCGACGCCCGGGCTTTGCCCGGGCGGCCTCAGTGAGCGAGCGAGCGCGCAGCTGCCTGCAGGGGCGCCTGATGCGGTATTTT - 6600
6601 - CTCCTTACGCATCTGTGCGGTATTTCACACCGCATACGTCAAAGCAACCATAGTACGCGCCCTGTAGCGGCGCATTAAGCGCGGCGGGTGTGGTGGTTAC - 6700
6701 - GCGCAGCGTGACCGCTACACTTGCCAGCGCCTTAGCGCCCGCTCCTTTCGCTTTCTTCCCTTCCTTTCTCGCCACGTTCGCCGGCTTTCCCCGTCAAGCT - 6800
6801 - CTAAATCGGGGGCTCCCTTTAGGGTTCCGATTTAGTGCTTTACGGCACCTCGACCCCAAAAAACTTGATTTGGGTGATGGTTCACGTAGTGGGCCATCGC - 6900
6901 - CCTGATAGACGGTTTTTCGCCCTTTGACGTTGGAGTCCACGTTCTTTAATAGTGGACTCTTGTTCCAAACTGGAACAACACTCAACTCTATCTCGGGCTA - 7000
7001 - TTCTTTTGATTTATAAGGGATTTTGCCGATTTCGGTCTATTGGTTAAAAAATGAGCTGATTTAACAAAAATTTAACGCGAATTTTAACAAAATATTAACG - 7100
7101 - TTTACAATTTTATGGTGCACTCTCAGTACAATCTGCTCTGATGCCGCATAGTTAAGCCAGCCCCGACACCCGCCAACACCCGCTGACGCGCCCTGACGGG - 7200
7201 - CTTGTCTGCTCCCGGCATCCGCTTACAGACAAGCTGTGACCGTCTCCGGGAGCTGCATGTGTCAGAGGTTTTCACCGTCATCACCGAAACGCGCGAGACG - 7300
7301 - AAAGGGCCTCGTGATACGCCTATTTTTATAGGTTAATGTCATGATAATAATGGTTTCTTAGACGTCAGGTGGCACTTTTCGGGGAAATGTGCGCGGAACCC - 7400
7401 - CCTATTTGTTTATTTTTCTAAATACATTCAAATATGTATCCGCTCATGAGACAATAACCCTGATAAATGCTTCAATAATATTGAAAAAGGAAGAGTATGA - 7500
7501 - GTATTCAACATTTCCGTGTCGCCCTTATTCCCTTTTTTGCGGCATTTTGCCTTCCTGTTTTTGCTCACCCAGAAACGCTGGTGAAAGTAAAAGATGCTGA - 7600
```

```
7601 - AGATCAGTTGGGTGCACGAGTGGGTTACATCGAACTGGATCTCAACAGCGGTAAGATCCTTGAGAGTTTTCGCCCCGAAGAACGTTTTCCAATGATGAGC - 7700
7701 - ACTTTTAAAGTTCTGCTATGTGGCGCGGTATTATCCCGTATTGACGCCGGGCAAGAGCAACTCGGTCGCCGCATACACTATTCTCAGAATGACTTGGTTG - 7800
7801 - AGTACTCACCAGTCACAGAAAAGCATCTTACGGATGGCATGACAGTAAGAGAATTATGCAGTGCTGCCATAACCATGAGTGATAACACTGCGGCCAACTT - 7900
7901 - ACTTCTGACAACGATCGGAGGACCGAAGGAGCTAACCGCTTTTTTGCACAACATGGGGGATCATGTAACTCGCCTTGATCGTTGGGAACCGGAGCTGAAT - 8000
8001 - GAAGCCATACCAAACGACGAGCGTGACACCACGATGCCTGTAGCAATGGCAACAACGTTGCGCAAACTATTAACTGGCGAACTACTTACTCTAGCTTCCC - 8100
8101 - GGCAACAATTAATAGACTGGATGGAGGCGGATAAAGTTGCAGGACCACTTCTGCGCTCGGCCCTTCCGGCTGGCTGGTTTATTGCTGATAAATCTGGAGC - 8200
8201 - CGGTGAGCGTGGAAGCCGCGGTATCATTGCAGCACTGGGGCCAGATGGTAAGCCCTCCCGTATCGTAGTTATCTACACGACGGGGAGTCAGGCAACTATG - 8300
8301 - GATGAACGAAATAGACAGATCGCTGAGATAGGTGCCTCACTGATTAAGCATTGGTAACTGTCAGACCAAGTTTACTCATATATACTTTAGATTGATTTAA - 8400
8401 - AACTTCATTTTTAATTTAAAAGGATCTAGGTGAAGATCCTTTTTGATAATCTCATGACCAAAATCCCTTAACGTGAGTTTTCGTTCCACTGAGCGTCAGA - 8500
8501 - CCCCGTAGAAAAGATCAAAGGATCTTCTTGAGATCCTTTTTTTCTGCGCGTAATCTGCTGCTTGCAAACAAAAAAACCACCGCTACCAGCGGTGGTTTGT - 8600
8601 - TTGCCGGATCAAGAGCTACCAACTCTTTTTCCGAAGGTAACTGGCTTCAGCAGAGCGCAGATACCAAATACTGTTCTTCTAGTGTAGCCGTAGTTAGGCC - 8700
8701 - ACCACTTCAAGAACTCTGTAGCACCGCCTACATACCTCGCTCTGCTAATCCTGTTACCAGTGGCTGCTGCCAGTGGCGATAAGTCGTGTCTTACCGGGTT - 8800
8801 - GGACTCAAGACGATAGTTACCGGATAAGGCGCAGCGGTCGGGCTGAACGGGGGGTTCGTGCACACAGCCCAGCTTGGAGCGAACGACCTACACCGAACTG - 8900
8901 - AGATACCTACAGCGTGAGCTATGAGAAAGCGCCACGCTTCCCGAAGGGAGAAAGGCGGACAGGTATCCGGTAAGCGGCAGGGTCGGAACAGGAGAGCGCA - 9000
9001 - CGAGGGAGCTTCCAGGGGGAAACGCCTGGTATCTTTATAGTCCTGTCGGGTTTCGCCACCTCTGACTTGAGCGTCGATTTTTGTGATGCTCGTCAGGGGG - 9100
9101 - GCGGAGCCTATGGAAAAACGCCAGCAACGCGGCCTTTTTACGGTTCCTGGCCTTTTGCTGGCCTTTTGCTCACATGT - 9177
```

Declaration of Authorship

Affidavit according to § 8 of the doctoral degree regulations of the Combined Faculty of Natural Sciences and Mathematics of the Ruperto Carola University Heidelberg.

1. The thesis I have submitted entitled “Deciphering a regulatory function of endolysosomes in asymmetric cell division of human neural stem cells via the Notch signalling pathway” is my own work.
2. I have only used the sources indicated and have not made unauthorized use of services of a third party. Where the work of others has been quoted or reproduced, the source is always given.
3. I have not yet presented this thesis or parts thereof to a university as part of an examination or degree.
4. I confirm that the declarations made above are correct.
5. I am aware of the importance of a sworn affidavit and the criminal prosecution in case of a false or incomplete affidavit.

I affirm that the above is the absolute truth to the best of my knowledge and that I have not concealed anything.

_____ _____

Place and date Signature

Danksagungen

Prof. Dr. Philipp Koch möchte ich zunächst für die Themenstellung und für die Möglichkeit danken, meine Promotion am Hector Institut für translationale Hirnforschung durchzuführen. Im Besonderen danke ich für das entgegengebrachte Vertrauen, die Freiheit dieses Projekt nach eigenen Vorstellungen zu gestalten und die fachliche Betreuung.

Bei Prof. Dr. Gudrun Rappold möchte ich mich für die Begutachtung dieser Arbeit und die konstruktive Diskussion der Zwischenergebnisse während der TAC-Meetings bedanken.

Prof. Dr. Francesca Ciccolini und Prof. Dr. Ingrid Lohmann danke ich dafür, dass sie sich bereiterklärt haben mein Prüfungskomitee zu vervollständigen.

Allen aktuellen und ehemaligen Mitarbeitern der Arbeitsgruppen Koch und Ladewig danke ich für den tollen Gruppenzusammenhalt und eine entspannte Arbeitsatmosphäre. Besonders, möchte ich Ruven und Ammar danken, die mich die längste Zeit begleitet haben und die ich jederzeit um Rat fragen konnte. Danke für eure offenen Ohren und die gemeinsame Zeit auch außerhalb des Labors. Für die praktische, als auch mentale Unterstützung möchte ich außerdem besonders Isa, Marko, Anne und Andrea danken.

Außerdem möchte ich den beiden anderen Engeln und Sven danken. Ihr habt mir regelmäßig klargemacht, dass man sich diesen Titel egal wo in Deutschland und der Welt hart erarbeiten muss und man auf dem Weg nicht den Mut verlieren darf.

Nicht zuletzt danke ich meiner Familie für alles, die bedingungslose Unterstützung, die große Geduld und Verständnis. Ohne euch wäre das alles nicht möglich gewesen.

Alles Liebe, alles Gute…